ANALYSES OF THERMAL AND SPECTRAL CHARACTERISTICS OF ARTIFICIAL TURF AND NATURAL GRASS IN LAS VEGAS VALLEY

By

Tarannum Kalam Khandoker

Bachelor of Science in Civil Engineering
Ahsanullah University of Science and Technology
2019

A thesis submitted in partial fulfillment
of the requirements for the

Master of Science in Engineering - Civil and Environmental Engineering

Department of Civil and Environmental Engineering and Construction
Howard R. Hughes College of Engineering
The Graduate College

University of Nevada, Las Vegas
May 2024

UNLV | GRADUATE COLLEGE

Thesis Approval

The Graduate College
The University of Nevada, Las Vegas

April 1, 2024

This thesis prepared by

Tarannum Kalam Khandoker

entitled

Analyses of Thermal and Spectral Characteristics of Artificial Turf and Natural Grass in Las Vegas Valley

is approved in partial fulfillment of the requirements for the degree of

Master of Science in Engineering - Civil and Environmental Engineering
Department of Civil and Environmental Engineering and Construction

Sajjad Ahmad, Ph.D.
Examination Committee Co-Chair

Haroon Stephen, Ph.D.
Examination Committee Co-Chair

Marie-Odile Fortier, Ph.D.
Examination Committee Member

Ashok Singh, Ph.D.
Graduate College Faculty Representative

Alyssa Crittenden, Ph.D.
Vice Provost for Graduate Education & Dean of the Graduate College

ABSTRACT

This thesis presents a comprehensive analysis of the thermal and spectral characteristics of Las Vegas Valley (LVV). The first objective examines the effects of artificial turf on the urban thermal environment in the LVV by analyzing the impact of Land Surface Temperature (LST) and surface albedo at 26 ROIs that transitioned from natural to artificial turf, alongside another 26 ROIs that remained unchanged between 2018 and 2022 utilizing available Landsat 8 satellite images for the respective years. In the comprehensive comparison of ROIs over the two years in question, it was observed that transitioning to artificial turf correlated with elevated surface temperatures, but only during the warmer months. Two series of paired T-Tests results, taking the combined annual and seasonal data, revealed significant differences on the LST of the transitioned ROIs indicating turf transition had substantial impact on LST for these ROIs. The albedo values for sites with natural grass remained relatively unchanged between the two years. Conversely, a notable decrease in albedo was observed in most sites that transitioned to artificial turf. The T-Tests revealed significant differences in albedo between 2018 and 2022 for these transitioned sites.

The second objective examined the spectral signatures of 26 transitioned ROIs in both 2018 and 2022 by creating spectral signature curves and analyzed Normalized Difference Vegetation Index (NDVI) at both transitioned and non-transitioned ROIs in both years by creating the NDVI maps. For the spectral signatures, the 2018 curves had features indicative of natural grass, while the 2022 curves did not show these traits. The most evident distinction was in the SWIR1 region's reflectance, with opposing slope directions in the two years. Interestingly, despite being plastic, the synthetic turf exhibited increased reflectance in the SWIR1 region, possibly due to surface temperature effects. Average reflectance values of all 26 ROIs of each month of 2018 and 2022 at each wavelength displayed distinct curves for each year. Two sets of paired T-Test results, one for

each month and the other for each ROI, presented significant differences in the reflectance values between 2018 and 2022 due to the turf transition. Distinct NDVI values and curves were obtained for artificial turf. T-Test results confirmed the significant differences on NDVI due to the turf transition as well. The entire analysis for the first and second objectives was conducted using GEE and ArcGIS Pro, with statistical assessments carried out in R-Studio.

This thesis includes an additional chapter that examines the health and environmental effects of artificial turf. It covers issues such as the use of recycled tire crumb as infill, the presence of microplastics in turf components, and the composition of turf fibers. It also addresses health risks like Methicillin-Resistant Staphylococcus Aureus (MRSA) infections, heat-related illnesses, and various injuries that athletes might suffer on artificial playing surfaces. On the environmental side, the focus is on the higher temperatures of turf surfaces, ecological damage from toxic substances, and a greater risk of flooding. The thesis suggests that the decision to install artificial turf should be tailored to the unique conditions and requirements of each location.

Studying the impact of artificial turf on the urban thermal environment of LVV can be helpful for informed urban planning and policymaking, aimed at creating a healthy and comfortable urban environment, especially considering the unique climate challenges of the region.

ACKNOWLEDGEMENT

I want to express my deepest gratitude to my committee members for their invaluable guidance and support. Special thanks to Dr. Sajjad Ahmad and Dr. Haroon Sahotra, my supervisors, for steering this research with their expertise and insights. My gratitude also goes to Dr. Marie-Odile Fortier and Dr. Ashok Singh, who served as my Advisory Committee Member and the Graduate College Representative, respectively. Their thoughtful insights and rigorous reviews have greatly enhanced the quality of my work.

I would also like to acknowledge my peers in the research group, with whom I've shared the highs and lows of the past two and a half years. Your unwavering support and companionship have been a cornerstone of my journey. The memories we've created will be treasured forever.

Finally, my heartfelt thanks go to my family, the foundation of my success. Particularly, my deepest thanks to my father, whose belief in my potential never wavered. His encouragement to pursue further education and his consent for my studies in the US have been pivotal in making my dream a reality. My mother, with her boundless love and prayers, has been my silent pillar, bravely overcoming her apprehension to let her younger daughter venture afar for education. Her quiet strength and hidden sacrifices have allowed me to pursue opportunities beyond our shores. A special mention to my sister and brother-in-law, whose motivation and guidance were instrumental in my decision to advance my education in the US and who continue to be my pillars of support.

TABLE OF CONTENTS

ABSTRACT iii

ACKNOWLEDGEMENT v

TABLE OF CONTENTS vi

LIST OF TABLES xii

LIST OF FIGURES xv

LIST OF ABBREVIATIONS xx

CHAPTER 1: INTRODUCTION 1

1.1 Research Background 1

1.2 Research Motivation 6

1.3 Research Objectives 8

1.4 Research Tasks 10

CHAPTER 2: ARTIFICIAL TURF AND URBAN THERMAL ENVIRONMENT: ANALYSES OF THE CHANGES IN LAND SURFACE TEMPERATURE AND SURFACE ALBEDO IN LAS VEGAS VALLEY 12

2.1 Introduction 12

2.2 Literature Review 15

2.3 Study Area 20

2.4 Materials and Methods 23

2.5 Results and Discussions 44
2.5.1 Land Surface Temperature (LST) 45
2.5.1.1 Comparison of the LST for each ROI across various dates within the years 2018 and 2022 45
2.5.1.2 Comparison of the average LST for each ROI between 2018 and 2022 46
2.5.1.3 Comparison of the annual average LST of all ROIs between 2018 and 2022 51
2.5.1.4 Comparison of the seasonal variabilities 55
2.5.1.5 T-Tests 62
2.5.2 Surface Albedo 71
2.5.2.1 Comparison of the surface albedo for each ROI across various dates within the years 2018 and 2022 72
2.5.2.2 Comparison of the average surface albedo for each ROI between 2018 and 2022 .. 73
2.5.2.3 Comparison of the annual average albedo values of all ROIs between 2018 and 2022 77
2.5.2.4 Comparison of the seasonal variabilities 79
2.5.2.5 T-Tests 87
2.5.3 LST-Albedo Relationship for the Transitioned ROIs in 2022 91
2.6 Conclusions 96
2.7 Limitations and Recommendations 100
2.7.1 Limitations 100

2.7.2 Recommendations for the Future Studies 101

2.7.3 Recommendations for the Policy Makers and Urban Planners 102

REFERENCES 106

CHAPTER 3: DETECTION AND ANALYSES OF THE SPECTRAL SIGNATURES AND NDVI OF ARTIFICIAL TURF AND NATURAL GRASS IN LAS VEGAS VALLEY 113

3.1 Introduction 113

3.2 Study Area 121

3.3 Materials and Methods 123

3.4 Results and Discussions 137

3.4.1 Spectral Signature 137

3.4.2 Normalized Difference Vegetation Index (NDVI) 155

3.4.2.1 Comparison of the NDVI of all ROIs between 2018 and 2022 156

3.4.2.2 Comparison of the seasonal variabilities among the transitioned ROIs 159

3.4.2.3 NDVI Time Sequence Curve 164

3.4.2.4 T-Tests 167

3.5 Conclusions 170

3.6 Limitations and Recommendations 173

3.6.1 Limitations 173

3.6.2 Recommendations for the Future Studies 174

3.6.3 Recommendations for the Policy Makers and Urban Planners 175

REFERENCES 177

CHAPTER 4: HEALTH AND ENVIRONMENTAL IMPLICATIONS OF ARTIFICIAL TURF 182

4.1 Introduction 182

4.2 Health Impacts of Artificial Turf 186

4.2.1 Use of recycled tire crumb as infill material 186

4.2.2 Incorporation of microplastics in artificial playing surfaces 188

4.2.3 Dye and material composition of synthetic turf fibers 189

4.2.4 Release of reproductive toxins from tire crumb leachate 189

4.2.5 Risk of MRSA infection among athletes 189

4.2.6 Increased likelihood of heat-related illness 190

4.2.7 Athletic injuries sustained 190

4.3 Environmental Impacts 192

4.3.1 Elevated temperatures of playing surface 192

4.3.2 Concerns about the environment stemming from tire crumbs 193

4.3.3 Release of heavy metals into the environment 195

4.3.4 Harm to ecosystems caused by toxic substances 195

4.3.5 Increased potential for flooding 196

4.3.6 Contribution to plastic pollution in the environment 196

4.4 Appropriateness for Artificial Turf Usage 197

4.5 Conclusions 198

4.5.1 Challenges 199

4.5.2 Opportunities 200

REFERENCES 202

CHAPTER 5: CONTRIBUTIONS AND RECOMMENDATIONS 207

5.1 Summary 207

5.2 Contributions 211

5.3 Limitations 212

5.4 Recommendations for the Future Studies 213

5.5 Recommendations for the Policy Makers and Urban Planners 215

APPENDIX A 218

Appendix A.1: Comparative Analysis of LST for 26 transitioned ROIs in 2018 (Blue) and 2022 (Orange) 218

Appendix A.2: Comparative Analysis of LST for 26 non-transitioned ROIs in 2018 (Blue) and 2022 (Orange) 223

Appendix A.3: Comparative Analysis of Surface Albedo for 26 transitioned ROIs in 2018 (Blue) and 2022 (Orange) 228

Appendix A.4: Comparative Analysis of Surface Albedo for 26 non-transitioned ROIs in 2018 (Blue) and 2022 (Orange) 233

Appendix A.5: LST 18 Inverse Distance Row 238

Appendix A.6: LST 18 KNN Row 8 240

Appendix A.7: LST 22 Inverse Distance Row 242

Appendix A.8: LST 22 KNN Row 8 244

REFERENCES 246

CURRICULUM VITAE 260

LIST OF TABLES

Table 2.1: Low-high- average air temperature, and precipitation (Source: Weather Underground) and the cloud covers of the obtained satellite images of 2018 (Source: Earth Explorer) 26

Table 2.2: Low-high- average air temperature, and precipitation (Source: Weather Underground) and the cloud covers of the obtained satellite images of 2022 (Source: Earth Explorer) 27

Table 2.3: USGS Landsat 8 Level 2, Collection 2, Tier 1 bands used in measuring the Surface Albedo 41

Table 2.4: Summary of the types of paired T-Tests applied, the count of tests conducted in both transitioned and non-transitioned categories and the corresponding threshold values. 43

Table 2.5: Average LST values and standard deviation of all ROIs in 2018 and 2022 52

Table 2.6: The median values in LST noted in different seasons for both transitioned and non-transitioned ROIs and the differences in the median values between 2018 and 2022. 58

Table 2.7: P-Values for the annual Paired T-Tests considering all LST values from all ROIs (Threshold P-Value = 0.002) 62

Table 2.8: P-Values for the Paired T-Tests at individual ROI performed by taking all the data from the available dates (Threshold P-Value = 0.05) 63

Table 2.9: P-Values for the seasonal Paired T-Tests performed separately for each ROI and for each season (Threshold P-Value = 0.05) 64

Table 2.10: P-Values for Combined seasonal Paired T-Tests performed by taking all data from all ROIs for each season (Threshold P-Value = 0.002) 65

Table 2.11: Summary of Spatial Autocorrelation Tests using the LST values of 2018 and 2022. 67

Table 2.12: Average albedo values of all ROIs for 2018 and 2022 77

Table 2.13: The median values in Surface Albedo noted in different seasons for both transitioned and non-transitioned ROIs and the differences in the median values between 2018 and 2022. 83

Table 2.14: P-Values for the annual Paired T-Tests considering all LST values from all ROIs (Threshold P-Value = 0.002) 87

Table 2.15: P -Values for the Paired T-Tests at individual ROI performed by taking all the data from the available dates (Threshold P-Value = 0.05) 88

Table 2.16: P-Values for the seasonal Paired T-Tests performed separately for each ROI and for each season (Threshold P-Value = 0.05) 89

Table 2.17: P-Values for Combined seasonal Paired T-Tests performed by taking all data from all ROIs for each season (Threshold P-Value = 0.002) 90

Table 3.1: Dates of Spectral Signature Map Generation and Corresponding Cloud Cover 124

Table 3.2: Landsat 8 Collection 2 Tier 1 Bands used to plot spectral signature curves. 127

Table 3.3: Summary of the types of paired T-Tests applied, the count of tests conducted in both transitioned and non-transitioned categories and the corresponding threshold values. 136

Table 3.4: Median and Mean Reflectance Values for Various Spectral Bands in 2018 and 2022 with Corresponding Differences 140

Table 3.5: P Values of the T-Tests of each month of the transitioned ROI (Threshold P-Value = 0.05) 152

Table 3.6: P-values for the T-Tests of each ROI (Threshold P-Value = 0.05) 153

Table 3.7: The median values in NDVI noted in different seasons for both transitioned and non-transitioned ROIs and the differences in the median values between 2018 and 2022. 163

Table 3.8: P-Values for the annual Paired T-Tests considering all LST values from all ROIs (Threshold P-Value = 0.002) 167

Table 3.9: P-Values for the Paired T-Tests at individual ROI performed by taking all the data from the available dates (Threshold P-Value = 0.05)..... 168

Table 3.10: P-Values for Combined seasonal Paired T-Tests performed by taking all data from all ROIs for each season (Threshold P-Value = 0.002) 169

Table 4.1: Artificial Turf Materials and their associated health impacts..... 185

Table 4.2: Artificial Turf Materials and their associated Environmental Impacts..... 186

Table 4.3: Appropriateness for artificial turf usage 197

LIST OF FIGURES

Figure 2.1: Study Area: Las Vegas Valley, Nevada 22

Figure 2.2: Distribution of the dates of the obtained satellite images in 2018 and 2022 25

Figure 2.3: Distribution of average day temperatures for 2018 and 2022 28

Figure 2.4: Comparison of 10 am air temperatures with the peak temperatures recorded each day for the years (a) 2018 and (b) 2022 (Source: Weather Underground) 30

Figure 2.5: Schematic of workflow to retrieve the LST from Landsat 8 Satellite images. 32

Figure 2.6: Steps involved to retrieve LST in GEE and ArcGIS Pro 33

Figure 2.7: Representation of selected ROIs for analysis. (a) Depicts two fully contained pixels within the confines of Desert Pines High School football field, identified as a transitioned ROI, with the left displaying a grayscale image and the right showcasing the true-color image. (b) Illustrates three fully contained pixels situated within the Las Vegas Golf Club grounds, identified as a non-transitioned ROI, where the left image is grayscale, and the right reveals the natural coloration. 36

Figure 2.8: Yellow dots represent the ROIs converted from natural grass to artificial turf between 2018 and 2022 and green dots represent the ROIs that did not go through any conversion. 37

Figure 2.9: Steps to retrieve Surface Albedo of selected ROIs in GEE and ArcGIS Pro..... 39

Figure 2.10: Average LST differences for each ROI between 2018 and 2022 for transitioned ROIs 47

Figure 2.11: Average LST differences for each ROI between 2018 and 2022 for non-transitioned ROIs 48

Figure 2.12: Distribution of the average LST for football fields that transitioned from natural to artificial turf, comparing data from 2018 (blue) and 2022 (orange)..... 49

Figure 2.13: Distribution of the average LST for Golf Courses that maintained the natural grass surfaces, comparing data from 2018 (blue) and 2022 (orange)..... 50

Figure 2.14: Comparative analysis of average LST for Transitioned and Non-Transitioned ROIs between 2018 and 2022 53

Figure 2.15: Distribution of the average seasonal LST values at each transitioned ROI switched from Natural grass to Artificial turf between 2018 and 2022. 56

Figure 2.16: Distribution of the average seasonal LST values at each non-transitioned ROI that maintained only natural grass between 2018 and 2022. 57

Figure 2.17: Seasonal LST changes for the transitioned ROIs..... 60

Figure 2.18: Seasonal LST changes for the non-transitioned ROIs 61

Figure 2.19: Average albedo differences at each transitioned ROI between 2018 and 2022..... 74

Figure 2.20: Average albedo differences at each non-transitioned ROI between 2018 and 2022 75

Figure 2.21: Distribution of the average albedo for Football fields (Transitioned ROIs) and Golf Courses (Non-transitioned ROIs), comparing data from 2018 and 2022. 76

Figure 2.22: (a) Average seasonal albedo values for Transitioned ROIs; (b) Average seasonal albedo values for non-transitioned ROIs 81

Figure 2.23: Seasonal albedo changes for the transitioned ROIs 85

Figure 2.24: Seasonal albedo changes for the non-transitioned ROIs..... 86

Figure 2.25: Scatter plots showing the LST-Albedo relationships for each transitioned ROI at each season in 2018. 92

Figure 2.26: Scatter plots showing the LST-Albedo relationships for each transitioned ROI at each season in 2022. 93

Figure 3.1: Study Area: Las Vegas Valley, Nevada 122

Figure 3.2: Distribution of the dates of the obtained satellite images in 2018 and 2022 125

Figure 3.3: Visual representation of the methodology to plot the spectral signature curves..... 126

Figure 3.4: Yellow regions represent the ROIs converted from natural grass to artificial turf between 2018 and 2022. 129

Figure 3.5: Steps involved to retrieve NDVI values from ROIs in GEE and ArcGIS Pro..... 131

Figure 3.6: Representation of selected ROIs for analysis. (a) Depicts two fully contained pixels within the confines of Desert Pines High School football field, identified as a transitioned ROI, with the left displaying a grayscale image and the right showcasing the true-color image. (b) Illustrates three fully contained pixels situated within the Las Vegas Golf Club grounds, identified as a non-transitioned ROI, where the left image is grayscale, and the right reveals the natural coloration. 133

Figure 3.7: Sky Blue dots represent the ROIs converted from natural grass to artificial turf between 2018 and 2022 and green dots represent the ROIs that did not go through any conversion. 134

Figure 3.8: Distribution of the reflectance values from all the ROIs at each wavelength in 2018 and 2022..... 138

Figure 3.9: Average annual reflectance values of all 26 ROIs at each wavelength in 2018 and 2022..... 142

Figure 3.10: Average reflectance values of each ROI at each wavelength for 2018 and 2022. The black lines represent the spectral signatures of 26 ROIs in 2018, while the red represent the curves from 2022. 143

Figure 3.11: Average reflectance values of each wavelength at each month of 2018 and 2022. The black lines represent the average reflectance values for the months of 2018, while the red represent the curves from 2022. 144

Figure 3.12: Average reflectance values at each wavelength in January 2018 and February 2018 146

Figure 3.13: Spectral signatures of artificial turf on April 2022, May 2022 and November 2022 showing very slight reflectance values in the NIR region. 147

Figure 3.14: Average reflectance at the NIR, SWIR1 and SWIR2 regions in each month of 2018 and 2022 149

Figure 3.15: Average reflectance at the blue, green, and red regions in each month of 2018 and 2022 150

Figure 3.16: Distribution of the NDVI values from all ROIs at Transitioned (Football Fields) and non-transitioned (Golf Courses) ROIs in 2018 and 2022 157

Figure 3.17: Annual average NDVI values at each transitioned and non-transitioned ROIs 158

Figure 3.18: Distribution of average NDVI Values of each transitioned ROI at each season of 2018 and 2022 160

Figure 3.19: Distribution of average NDVI Values of each non-transitioned ROI at each season of 2018 and 2022 161

Figure 3.20: Average NDVI values for each month of 2018 and 2022 for (a) football fields and (b) golf courses 165

Figure 4.1: Schematic illustrations of the makeup of a typical artificial turf field: (a) the major components of artificial turf, and (b) the built-in drainage system (Cheng et al., 2014) 184

Figure 4.2: The routes and corresponding quantities of rubber granulate used as infill for an artificial turf football field (adapted from Kole et al., 2023) 194

Figure A.1: Comparative Analysis of LST for 26 transitioned ROIs in 2018 (Blue) and 2022 (Orange) 222

Figure A.2: Comparative Analysis of LST for 26 non-transitioned ROIs in 2018 (Blue) and 2022 (Orange) 227

Figure A.3: Comparative Analysis of Surface Albedo for 26 transitioned ROIs in 2018 (Blue) and 2022 (Orange) 232

Figure A.4: Comparative Analysis of Surface Albedo for 26 non-transitioned ROIs in 2018 (Blue) and 2022 (Orange) 237

LIST OF ABBREVIATIONS

SNWA	- Southern Nevada Water Authority
WSL	- Water Smart Landscapes
LVV	- Las Vegas Valley
LST	- Land Surface Temperature
ROI	- Regions of Interests
GEE	- Google Earth Engine
NDVI	- Normalized Difference Vegetation Index
IR	- Infrared
SWIR1	- Shortwave Infrared 1
SWIR2	- Shortwave Infrared 2
EM Spectrum	- Electromagnetic Spectrum
MRSA	- Methicillin-Resistant Staphylococcus Aureus
TPE	- Thermoplastic Elastomer
SBR	- Styrene-Butadiene Rubber

CHAPTER 1: INTRODUCTION

1.1 Research Background

Artificial turf, also known as synthetic grass, is a man-made surface created to resemble natural grass, first used in the 1960s primarily for sports fields. Its use has expanded to various athletic and recreational areas due to its affordability and low maintenance nature. In environments where sustaining natural grass is impractical due to severe snow or lack of water, artificial grass offers a more resilient option. A key benefit in dry and semi-dry regions is its ability to conserve water by eliminating the need for irrigation (Kanaan et al., 2020). According to the studies by Cheng et al. (2014) and Lavorgna et al. (2011), a field of artificial turf could conserve as much as 1 million gallons of water each year. Besides conserving water and reduced maintenance costs, artificial turf is adaptable to various climates and multi-purpose stadiums. Its application has extended beyond sports venues to include residential and commercial landscaping in regions where maintaining natural grass is difficult and resource intensive. Constructed from synthetic plastic and chemical fibers, artificial turf is noted for its excellent drainage capabilities. Technological advancements have continually enhanced its manufacture, with the latest, sixth-generation turf closely mirroring natural grass in aspects like shock absorbency and ball interaction, even surpassing natural grass in some traits (Xiao & Cao 2013). The broad applicability of artificial turf is further enriched by its uniformity, the option for varied colors, and its resistance to wear.

The arid southwestern U.S. is experiencing an increasing demand on its water resources due to its expanding growth, especially in extensive urban areas where water predominantly supports urban greenery (Wynne & Devitt, 2020). Las Vegas, Nevada, with a current population over 2.2 million, stands out as one of the rapidly expanding cities in the United States, tripling its population from 1990 to 2018. The residential area, encompassing both single-family houses and

multi-unit apartment complexes, accounts for 60 percent of Southern Nevada's yearly water consumption. Outdoor usage, particularly for landscape watering, dominates residential water use. This water, once used outside, is lost to evaporation and is not reclaimable for recycling (Southern Nevada Water Authority (SNWA), 2023). Therefore, water agencies, including SNWA, have prioritized the reduction of outdoor water consumption to ensure a sustainable balance between water availability and its usage (Wynne & Devitt, 2020).

Ensuring a consistent and safe drinking water supply for Southern Nevada depends on effective water conservation (Water Smart Landscape Rebate Program). Beginning in 1991, SNWA and its associated agencies launched one of the most extensive water conservation initiatives of the US in response to the persistent drought conditions in the Colorado River Basin, which posed risks to water resources and distribution systems. The SNWA engages in both immediate and future-oriented strategies to maintain high quality water and dependable service for its users. To encourage conservation and minimize water consumption, it employs a variety of demand management strategies such as pricing strategies, incentives, rules, and awareness programs. These approaches are designed to complement each other in fostering responsible water usage. Through these conservation initiatives, there has been a 58 percent reduction in water usage per person from 2002 to 2023, despite a population growth of over 786,000 in the same period. (Joint Water Conservation Plan, 2019)

The SNWA has created a comprehensive set of resources to assist customers within its jurisdiction in enhancing water efficiency and curbing wastage.

- A standout initiative is the Water Smart Landscape Rebate Program, which has proven to be highly effective in cutting down water use outdoors. Since its launch

in 1999, the program has seen over 60,500 conversions by residents and businesses, removing close to 190 million square feet of grass and saving around 130 billion gallons of water. In 2018, the rebate was increased to $3.00 for each square foot of turf replaced with desert-friendly landscaping for the first 10,000 square feet, and $1.50 per square foot for any additional area. The highest annual reward for a property is set at $500,000. To date, more than 223 million square feet of turf have been removed, conserving over 176 billion gallons of water. (Joint Water Conservation Plan, 2019). By 2007, homeowners had replaced approximately 535 acres of turf, equivalent to about 1% of the total residential land (Brelsford & Abbott, 2017).

- Switching from cool-season to warm-season grass varieties in areas designated for active use, which substantially lowers water needed for irrigation. Warm-season grasses are more suited to hot environments and can withstand heavy use.
- The Water Efficient Technologies Rebate Program, which has enabled participating businesses to save over 19 billion gallons of water since its inception in 2001.
- The provision of various instant coupons and rebates for homeowners, such as the Water Smart Car Wash Coupons, rebates for Smart Irrigation Controllers, and Pool Cover Rebates. Before the conclusion of the program in June 2020, more than 45,000 coupons had been issued, leading to an estimated saving of 5.6 billion gallons of water. (Joint Water Conservation Plan, 2019)

The SNWA is also implementing or considering several key water efficiency strategies, including:

- Eliminating Nonfunctional Turf: Targeting the removal of nonfunctional turf, such as in medians and traffic circles, which consumes significant water resources without providing utility. With around 5,000 acres of such turf remaining, focusing on its replacement is crucial. Although not all turf was removed, the emphasis is on retaining it only where it serves a functional purpose. In 2021, the Nevada Legislature passed a new law which will restrict the use of Colorado River water supplied by Water Authority member agencies for irrigating non-functional grass starting from 2027 (Joint Water Conservation Plan, 2019). Single-family residential property owners can either undertake the project themselves or hire a contractor and receive $3 per square foot for the first 10,000 square feet of grass they replace, followed by $1.50 per square foot for any additional area, within each fiscal year running from July 1 to June 30. An estimated water savings of 825,000 gallons annually is expected for an average conversion of 15,000 square feet to water-efficient landscaping. (What We're Doing to Conserve, 2024)
- Banning New Grass Installations: This measure will prohibit grass in new developments, anticipated to conserve around 27,000 acre-feet of water in the future.
- Limiting Residential Pool Sizes: In the middle of 2022, the board of the Las Vegas Valley Water District enacted new regulations, capping the surface area of new residential pools and spas at 600 square feet for each property. On average, residential pools in the region measure approximately 475 square feet. The new restriction aims to curb the emergence of extremely large residential pools — with some exceeding 3,000 square feet — which are notably water-intensive. Over the

coming decade, this policy is projected to conserve more than 32 million gallons of water (Drought and Conservation Measures, 2024).

Additional measures like a moratorium on evaporative cooling and a voluntary septic conversion program are also part of the comprehensive water efficiency plan.

However, there is an ongoing debate regarding the environmental friendliness of replacing natural grass with artificial turf. A significant concern with artificial turfgrass is the elevated surface temperatures it can reach during daylight hours (Devitt et al., 2007). Buskirk et al. (1971) noted that on warm, sunny days, artificial turf temperatures could surpass those of natural grass by 30°C to 65°C, posing serious concerns. This increase in temperature can adversely affect player comfort and health, especially when surface temperatures rise above the 45°C threshold for heat pain, as discussed by Kandelin et al. (1976). Lee et al. (2018) found that in urban areas like Seoul, Korea, artificial turf fails to cool surface temperatures and often records higher temperatures compared to other urban materials. Xiao and Cao (2013) pointed out that the thermal performance difference between natural and artificial turf materials could alter the local thermal and humidity conditions on sports fields, potentially impacting athletes' thermal comfort and performance. Jim (2016) argued that the shift from natural to artificial turf reduces urban cooling effects and heightens heat-stress health hazards. Despite ongoing advancements to make artificial turf more similar to natural grass in look and feel, Villacañas et al. (2017) assert that these modifications have not successfully addressed the issue of heat accumulation, leading to user dissatisfaction, performance drops, and an increased risk of heat-related injuries. The thermal characteristics of artificial turf, which can contribute to elevated local temperatures, present significant environmental challenges and represent one of the critical disadvantages associated with its use.

The Las Vegas Valley (LVV) has been chosen as the focal point of this study due to its extensive use of artificial turf. While artificial turf can save water in arid regions such as LVV, it might compromise thermal comfort due to elevated surface temperatures. Elevated Land Surface Temperature (LST) can have cascading effects on the local urban environment and can have direct health impacts on residents.

Understanding the trade-offs between water conservation and thermal comfort is essential for informed urban planning. Also, changes in albedo due to the transition from natural to artificial grass can influence local energy balances, potentially affecting the local climates. By measuring how albedo changes with the transition to artificial turf, urban planners can understand its broader climatic implications. Therefore, the first objective of this study is to evaluate the impact of artificial turf on the urban thermal environment by measuring the LST and Surface Albedo through remote sensing techniques.

Measuring the total amount of natural grass surfaces within the valley is crucial to evaluate the effectiveness of different lawn conversion programs. With such information, conversion efforts can be more strategically directed towards the areas with higher concentrations of natural grass which would benefit the most from such conversions, thus optimizing the impact of the program (Brandt, 2008). Therefore, another objective of this study is to differentiate and characterize the spectral signatures and NDVI of artificial turf and natural grass within the LVV.

1.2 Research Motivation

The comprehensive review of existing literature on the surface temperatures of artificial turf reveals a predominant focus on evaluating extreme conditions during sunny, clear summer days. While this approach has provided valuable insights, it overlooks the nuanced variations

across different seasons and diverse geographical landscapes. Researchers such as Aoki (2009) and Loveday (2019) have made strides in incorporating winter measurements, yet there remains a significant gap in our understanding of how artificial turf behaves across the full spectrum of seasonal changes.

Furthermore, the geographic scope of these studies has largely been confined to temperate regions, with a notable concentration of research emanating from the United States and a few other countries. This regional focus raises questions about the applicability of findings across varied climatic conditions, particularly in areas with extreme climates that may exhibit distinct thermal behaviors.

Another critical gap lies in the methodology of data collection. Existing studies have predominantly relied on infrared thermometers, thermocouples, and albedo meters for surface temperature and albedo measurements, with thermal imaging used to a lesser extent. These methods, while effective, are limited by the need for physical presence on-site and do not offer a comprehensive overview of large geographical areas.

Moreover, the temporal scope of previous studies has been relatively narrow, often spanning only a couple of days. This short duration fails to capture the dynamic and fluctuating nature of surface temperatures and albedo over longer periods, thereby providing a snapshot rather than a complete picture of the thermal impact of artificial turf.

The rapid expansion of urban landscapes has intensified the need for effective urban planning and development strategies. Traditional ground measurement techniques for identifying and differentiating between natural and artificial grass cover over large areas are often labor-intensive, time-consuming, and may not be feasible for continuous monitoring. The capability to accurately classify these land covers through remote sensing techniques could revolutionize urban

ecological assessments, offering a high-resolution, cost-effective, and efficient tool for urban planners. This research seeks to harness advanced remote sensing technologies to discern natural from artificial grass over expansive regions.

In light of these gaps, this research aims to leverage the capabilities of Google Earth Engine (GEE) and ArcGIS Pro to examine the Land Surface Temperature (LST), surface albedo, spectral signatures and Normalized Difference Vegetation Index (NDVI) of natural grass and artificial turf across the Las Vegas Valley (LVV). By employing these advanced tools, this study offers a novel, cost-effective approach to data collection, eliminating the dependency on sophisticated field equipment and expensive satellite imagery. This research stands out by extending the analysis beyond the summer months to include all seasons of the years 2018 and 2022, thereby providing a more holistic understanding of seasonal variations in surface temperatures, surface albedo, spectral signatures, and NDVI of artificial turf.

By analyzing 45 Landsat 8 satellite images from 2018 and 2022 and focusing on 26 Regions of Interest (ROIs) that transitioned from natural to artificial turf, along with a control group of natural grass areas, this study not only broadens the temporal and geographical scope of the research but also introduces a unique comparative dimension to the analysis. This comprehensive approach addresses the previously identified knowledge gaps and contributes significantly to the body of knowledge on the environmental impacts of artificial turf.

1.3 Research Objectives

Las Vegas, a city experiencing rapid growth in the United States, faces escalating pressures on its water supply. In response, the 1999 Water Smart Landscapes (WSL) program was launched to encourage residents to switch from traditional grass lawns to water-efficient xeriscaping,

particularly during the drought in 2004. This initiative resulted in the removal of approximately 535 acres of turf by 2007, as part of efforts to ensure a stable and safe drinking water source for Southern Nevada. However, the ecological consequences of substituting natural grass with artificial turf remain a point of contention. This is largely because artificial turf can attain significantly higher surface temperatures due to its low reflectivity, minimal heat capacity, and water-repellent materials, which enhance heat absorption and retention, potentially leading to adverse environmental impacts. Therefore, the first objective of this research is to evaluate the impact of artificial turf on the urban thermal environment by measuring the Land Surface Temperature (LST) and Surface Albedo through remote sensing techniques. This objective aims to answer the following research questions:

1. What is the impact of turf conversions on LST?
2. What is the impact of turf conversions on Surface Albedo?
3. How do the LST and Albedo changes in areas with turf conversion compared to areas that maintained the same natural grass?

Given the research suggesting artificial turf could raise surface temperatures, identifying locations with artificial and natural grass coverage in the valley becomes crucial. Recognizing the unique spectral signatures of each turf type can aid in their identification. In the past, identifying these signatures depended on advanced and expensive techniques like commercial satellite imagery, hyperspectral imaging, or spectroradiometers, which are not easily accessible to the general public or educational institutions. Therefore, the second objective of this study is to differentiate and characterize the spectral signatures and Normalized Difference Vegetation Index

(NDVI) of artificial turf and natural grass within the LVV. This objective aims to answer the following research questions:

1. What are the distinct spectral signatures of natural and artificial turf?
2. Which wavelengths show the most significant differences between natural grass and artificial turf spectral signatures?
3. How does the NDVI of artificial turf differ from those of natural grass?

1.4 Research Tasks

The tasks are organized in the format of manuscripts. The first chapter provides an introduction and outlines the research questions guiding the study. The second chapter, titled "Artificial Turf and Urban Thermal Environment: Analyses of the Changes in Land Surface Temperature and Surface Albedo in Las Vegas Valley," addresses the first set of research questions by investigating the impact of artificial turf on the urban thermal environment within the LVV. This investigation involved analyzing LST and surface albedo at 26 ROIs that switched from natural grass to artificial turf, compared to 26 ROIs that did not change during the period from 2018 to 2022. The ROIs that underwent the transition were mainly high school football fields, whereas the unchanged ROIs, predominantly golf courses, acted as a baseline for the study. Analysis was performed using GEE and ArcGIS Pro, with statistical evaluations conducted in R-Studio. The third chapter, "Detection and Analysis of the Spectral Signatures and NDVI of Artificial Turf and Natural Grass in Las Vegas Valley," addresses the second set of research questions. It focuses on 26 high school football fields in the valley that were converted from natural grass to artificial turf between 2018 and 2022, A total of 45 charts, detailing the spectral signature curves for all the selected regions, were produced, and analyzed. Chapter 4 delves into the health

and environmental implications of artificial turf. The use of artificial turf has raised concerns about health and environmental issues due to the materials used to produce artificial turf. The issues have been studied and discussed in numerous papers which have been reviewed in this section. The fifth chapter offers a summary of the objectives of the study, key findings, and limitations, and proposes directions for future research.

CHAPTER 2: ARTIFICIAL TURF AND URBAN THERMAL ENVIRONMENT: ANALYSES OF THE CHANGES IN LAND SURFACE TEMPERATURE AND SURFACE ALBEDO IN LAS VEGAS VALLEY

2.1 Introduction

Artificial turf, often known as synthetic turf or artificial grass, is a man-made material made from synthetic fibers designed to mimic the appearance of natural grass. Since the 1960s, it has been utilized as a substitute for real grass (Jastifer et al., 2019). Originally conceived as an option for indoor baseball fields, its usage gradually expanded to encompass various athletic purposes, gaining popularity in the 1970s across fields, stadiums, and indoor/outdoor athletic facilities (Jastifer et al., 2019). The challenges associated with maintaining natural grass in regions with heavy snowfall have led to an increased adoption of artificial turf. In dry climates, one of the major arguments in favor of artificial turf is its potential for water conservation; replacing water-intensive grass with a non-irrigated option (Kanaan et al., 2020). According to Cheng et al. (2014) and Lavorgna et al. (2011), a typical synthetic turf football field can conserve from 0.5 to 1 million gallons of water annually. Some other advantages include lower maintenance costs, suitability for cold and arid regions, and its versatility for use in stadiums with multiple purposes. Although initially designed for sports fields, artificial turf has found wider applications in residential lawns and commercial properties due to its benefits. In regions with extreme climates, where the upkeep of high-quality natural grass fields requires chemical treatments and substantial amounts of water, artificial turf serves as a viable alternative.

The arid southwest of the U.S., particularly in rapidly growing urban areas like Las Vegas, Nevada, is facing increased pressure on water resources, largely due to the need to maintain urban

green spaces (Wynne & Devitt, 2020). Las Vegas has seen its population surge to over 2.2 million, more than tripling since 1990. In Southern Nevada, residential areas, which include both single-family homes and apartment complexes, are responsible for 60% of the annual water use. Most of this residential water is used outdoors for landscaping and is not recoverable for reuse due to evaporation (Southern Nevada Water Authority (SNWA), 2023). Consequently, water management organizations, such as the Southern Nevada Water Authority, are focusing efforts on reducing outdoor water use to maintain a sustainable balance between water supply and demand (Wynne & Devitt, 2020).

In 1999, Las Vegas introduced the Water Smart Landscapes (WSL) initiative, a program incentivizing homeowner to replace turf grass with xeric landscaping that would save the use of water. With the help of the Water Smart Landscapes rebate program, the community has successfully transformed over 223 million square feet of lawns into water-efficient landscapes, resulting in a savings of over 176 billion gallons of water (Joint Water Conservation Plan, 2019). In 2021, the Nevada Legislature passed a new law which will restrict the use of Colorado River water supplied by Water Authority member agencies for irrigating non-functional grass starting from 2027. This regulation targets commercial, multi-family, governmental, and other properties in Southern Nevada.

However, there is an ongoing debate regarding the environmental friendliness of replacing natural grass with artificial turf. A significant concern with artificial turfgrass is the elevated surface temperatures it can reach during daylight hours (Devitt et al., 2007). Lavorgna et al. (2011) highlighted that these synthetic turf fields can have temperatures ranging between 60°C and 80°C. As a result, they often require watering systems, including drainage, to regulate and maintain them

at a comfortable temperature, approximately 37.7°C, for usage. The thermal characteristics of artificial turf, which can contribute to elevated local temperatures, present significant environmental challenges and represent one of the critical disadvantages associated with its use. An estimated water savings of 825,000 gallons annually is expected for an average conversion of 15,000 square feet to water-efficient landscaping (Water Smart Landscapes Rebate, n.d.-b).

The Las Vegas Valley (LVV) has been chosen as the focal point of this study due to its extensive use of artificial turf. While artificial turf can save water in arid regions such as LVV, it might compromise thermal comfort due to elevated surface temperatures. Elevated LST can have cascading effects on the local urban environment and can have direct health impacts on residents.

Understanding the trade-offs between water conservation and thermal comfort is essential for informed urban planning. Also, changes in albedo due to the transition from natural to artificial grass can influence local energy balances, potentially affecting the local climates. By measuring how albedo changes with the transition to artificial turf, urban planners can understand its broader climatic implications. Therefore, the following objective has been undertaken:

Research Objective: To evaluate the impact of artificial turf on the urban thermal environment by measuring the Land Surface Temperature and Surface Albedo through remote sensing techniques.

Research Questions:

1. What is the impact of turf conversions on LST?
2. What is the impact of turf conversions on Surface Albedo?

3. How do the LST and Albedo changes in areas with turf conversion compared to areas that maintained the same natural grass?

Research Hypothesis: The transformation of 26 ROIs from natural grass to artificial turf over the period from 2018 to 2022 has resulted in notable changes in both Land Surface Temperature and Surface Albedo.

Both LST and Surface Albedo have been measured through remote sensing technologies. Improved spatial, temporal, and spectral resolutions of sensors have made it possible to identify surface materials with greater precision due to recent developments in remote sensing technology. The most notable advancement has been found in the spatial resolution of the satellite optical sensor, and Google Earth has made the resulting very high-resolution photos widely accessible (Hara et al., 2013).

2.2 Literature Review

An extensive review of research on LST and surface albedo was undertaken, focusing predominantly on studies from countries with temperate climates. In the United States, notable investigations include those into the surface temperatures of artificial turfs, conducted in various locations such as Pennsylvania by Buskirk et al. (1971), Texas by Ramsey (1982) and Carvalho et al. (2021), Hawaii by Kandelin et al. (1976), Las Vegas by Devitt et al. (2007), and Southern California by Yaghoobian et al. (2010). Internationally, significant contributions have been made by Aoki (2009) in Japan, Loveday et al. (2019) and Petrass et al. (2014) in Australia, Jim (2016) in Hong Kong, Gustin et al. (2018) in the UK, and Lee et al. (2018) in Seoul, Korea.

In every study reviewed, the surface temperatures recorded on artificial turf were consistently higher than those of natural grass or any other surface elements. The initial comparisons between artificial turf and natural grass, conducted by Buskirk et al. (1971), Kandelin et al. (1976), and Ramsay (1982), all confirmed that artificial turf fields exhibited higher surface temperatures than their natural grass counterparts. Gustin et al. (2018) noted in their study of a third-generation artificial turf pitch, that the surface temperature of the pitch could rise or fall rapidly, by approximately 2.5–3.0 °C per minute. Additionally, the research by Xiao and Chao (2013) into the thermal properties of natural and artificial turfs revealed that both the foliar surface temperature and the average air temperature were significantly higher on artificial turf compared to natural grass during the early summer period.

Several studies, including those by Carvalho et al. (2021), Garai and Kleissl (2011), Gustin et al. (2018), and Aoki (2009), also investigated the albedo of artificial turf in addition to surface temperature, consistently finding that artificial turf exhibits lower albedo. Aoki (2009) specifically noted an inverse correlation between surface temperatures and albedo values. Measurements of temperatures below the surface or of the underlying layers were rare, with only Carvalho et al. (2021) and Jim (2017) reporting on subsurface and substrate temperatures of artificial turf fields, respectively.

To measure surface temperatures, most researchers employed infrared thermometers or thermocouples, whereas albedo values were typically measured using albedo meters. Loveday et al. (2019) and Lee et al. (2018) utilized thermal images as a method for assessing surface temperatures.

Most of the research was carried out during summer days characterized by clear skies and intense sunlight to assess the most extreme conditions. Typically, data collection spanned over two days. Aoki (2009) and Loveday et al. (2019) expanded their investigations to include seasonal temperature fluctuations of artificial turf, recording temperatures in both the winter and summer seasons. Aoki (2009) observed elevated temperatures on artificial turf in both seasons but noted that the temperature differences between artificial and natural grass surfaces was more pronounced during the summer months.

Studies by Devitt et al. (2007), Lee et al. (2018), Loveday et al. (2019), Carvalho et al. (2021), and Williams and Pulley (2002) compared the surface temperatures of artificial turf to those of other urban surfaces or elements. Williams and Pulley (2002) evaluated two types of artificial turf against natural grass, concrete, and soil, discovering that artificial turf could reach temperatures as high as 69.4°C, significantly hotter than the maximum of 31.4°C recorded for natural grass on the same day. Lee et al. (2018) examined the thermal behavior of various urban street elements, observing notably higher temperatures on artificial turf and wooden decks during the day, which then significantly decreased at night. Carvalho et al. (2021) compared the surface temperatures of natural grass, artificial turf, decomposed granite, and hardwood mulch, finding artificial turf to have the highest surface temperatures, the lowest albedo, and the highest net radiation among the materials tested. Loveday et al. (2019) assessed the surface temperatures of 19 different landscape elements across all four seasons in a single day, noting that despite similar colors, artificial and natural grass differed significantly in thermal behavior. On average, artificial turf was 11.2°C warmer than natural grass during the summer measurement period.

Various researchers have identified multiple factors contributing to the increased surface temperatures observed on artificial turf fields. Aoki (2009) and Gustin et al. (2018) attributed the temperature rise primarily to the absorption of solar radiation. Petrass et al. (2014) expanded on this by noting that ambient temperature and relative humidity also play significant roles in influencing the temperature of artificial turf surfaces. Their comparison across 34 synthetic turf products revealed that not only environmental factors but also specific components of the synthetic turf system, such as the type of infill material and the presence of a shock pad, markedly affect surface temperatures. Twomey et al. (2014) conducted measurements of ambient and surface temperatures, relative humidity, wind speed, and cloud cover on a third generation (3G) artificial turf and two natural grass surfaces nearby. Their findings highlighted that the artificial turf consistently registered higher surface temperatures than the natural grass, with cloud cover being a significant determinant of the temperatures recorded. Jim (2016) examined six factors related to the radiant-energy environment on both natural and artificial turf sports fields and found that artificial turf absorbed intense shortwave and longwave radiation more readily, leading to surface temperatures as high as 70.2°C, compared to less than 40°C for natural turf. This absorption initiated a warming effect that started with the low albedo and high net solar irradiance of artificial turf materials, combined with their low specific heat capacity, resulting in elevated material temperatures, increased ground-thermal radiation, and the transfer of heat to the air above the ground through conduction and convection. The study by Devitt et al. (2007) revealed that the key factors contributing to the increase in temperature of artificial turf surfaces were the intensity of the sunlight hitting the surface and the angle of the sun above the horizon.

While most studies adopted the empirical field experiment approach, Yaghoobian et al. (2010) and Gustin et al. (2018) employed quantitative modeling or simulation methods to

investigate their hypotheses. Gustin et al. (2018) constructed a numerical model that, informed by empirical data, accurately estimated surface temperatures, and demonstrated that higher surface albedos could lead to a notable decrease in peak surface temperatures. Yaghoobian et al. (2010) introduced the Temperatures of Urban Facets in 3D (TUF3D) model and, through integrating a basic offline convection model that substituted grass with artificial turf, discovered this change could contribute an additional 2.3 kW h m^{-2} day^{-1} of heat to the surrounding air, potentially raising urban air temperatures by as much as 48°C.

Jim (2017) conducted detailed observations on four types of radiant energy (direct solar, reflected solar, sky thermal, and ground thermal) across five different heights (150 cm, 50 cm, 15 cm, the surface of the turf, and the substrate layer) under three distinct summer weather patterns (sunny, cloudy, overcast). On a clear, sunny day, the surface of the artificial turf reached temperatures as high as 72.4°C, in contrast to natural turf, which peaked at 36.6°C. The artificial turf dissipated this heat through conduction and convection to the air just above the ground and via significant ground-thermal radiation. During cloudy conditions, the artificial turf's temperature increase was less intense, facilitating earlier cooling in the late afternoon. On overcast days, temperatures at both the artificial and natural turf sites remained within safe limits.

Aoki (2009), Petrass et al. (2015), Villacañas et al. (2017), and Devitt et al. (2007) conducted investigations into the surface temperatures on various artificial turf fields and products. Aoki (2009) assessed the surface temperature and albedo of five different outdoor sports surfaces, including three with artificial turf (a field, a track, and a tennis court with sand-filled artificial turf), one with natural grass, and a clay track. Among the artificial surfaces, the turf field recorded the highest temperatures in the summer, whereas the turf track was warmer in the winter. Petrass et al.

(2015) compared the surface temperatures of two artificial turf types against natural grass, noting that surface temperatures were influenced by the ambient air temperature and that both artificial surfaces were significantly hotter than natural grass at the same location, with differences of 12.46°C and 22.15°C at metropolitan and regional venues, respectively. Villacañas et al. (2017) explored how structural elements like fiber type, infill type, turf age, and usage hours affect the temperature of artificial turf football fields. Their findings indicated that fields made with Styrene-Butadiene Rubber (SBR) and fibrillated fibers exhibited higher temperatures, highlighting the impact of infill and fiber types on third-generation artificial turf field temperatures, with thermoplastic rubber and monofilament fibers contributing to temperature reduction. Devitt et al. (2007) gathered data on surface temperature, spectral reflectance, solar radiation, and air temperature related to various landscape coverings and artificial turf components. Their analysis showed that the surface temperature of green artificial turf with black rubber infill was significantly higher than that of white artificial turf, asphalt, bare soil, concrete, and natural grass, concluding that the addition of rubber beads, regardless of color, raised the temperature of the artificial turf grass system.

2.3 Study Area

LVV has been chosen as the focal point of this study due to its extensive use of artificial turf. Located in southern Nevada, LVV is one of the largest metropolitan areas in the Southwestern U.S. This area lies in a higher-altitude segment of the Mojave Desert, specifically in the central-western region of Clark County, Nevada. It's encircled by several mountain ranges, with the tallest peak reaching up to 11,918 feet (Morris et al., 1997). The climate of Las Vegas is characterized as a subtropical hot desert (Koppen climate classification: BWh), which is common in the Mojave

Desert. This entails prolonged, intensely hot summers, brief mild winters, and transitional seasons that are warm (NOAA's National Weather Service, n.d.). Rain is infrequent, averaging about 4.2 inches annually (Weather Averages Las Vegas, Nevada, n.d.). Among North American cities, Las Vegas stands out for its sunshine, dryness, and exceptionally low humidity levels, often dropping below 10% (Cities with Low Humidity in US - Current Results, n.d.). The period from June to September is notably hot due to the low humidity. July stands as the hottest month, with average daytime highs reaching 104.5°F. The yearly average high temperature is around 80°F (Weather Averages Las Vegas, Nevada, n.d.).

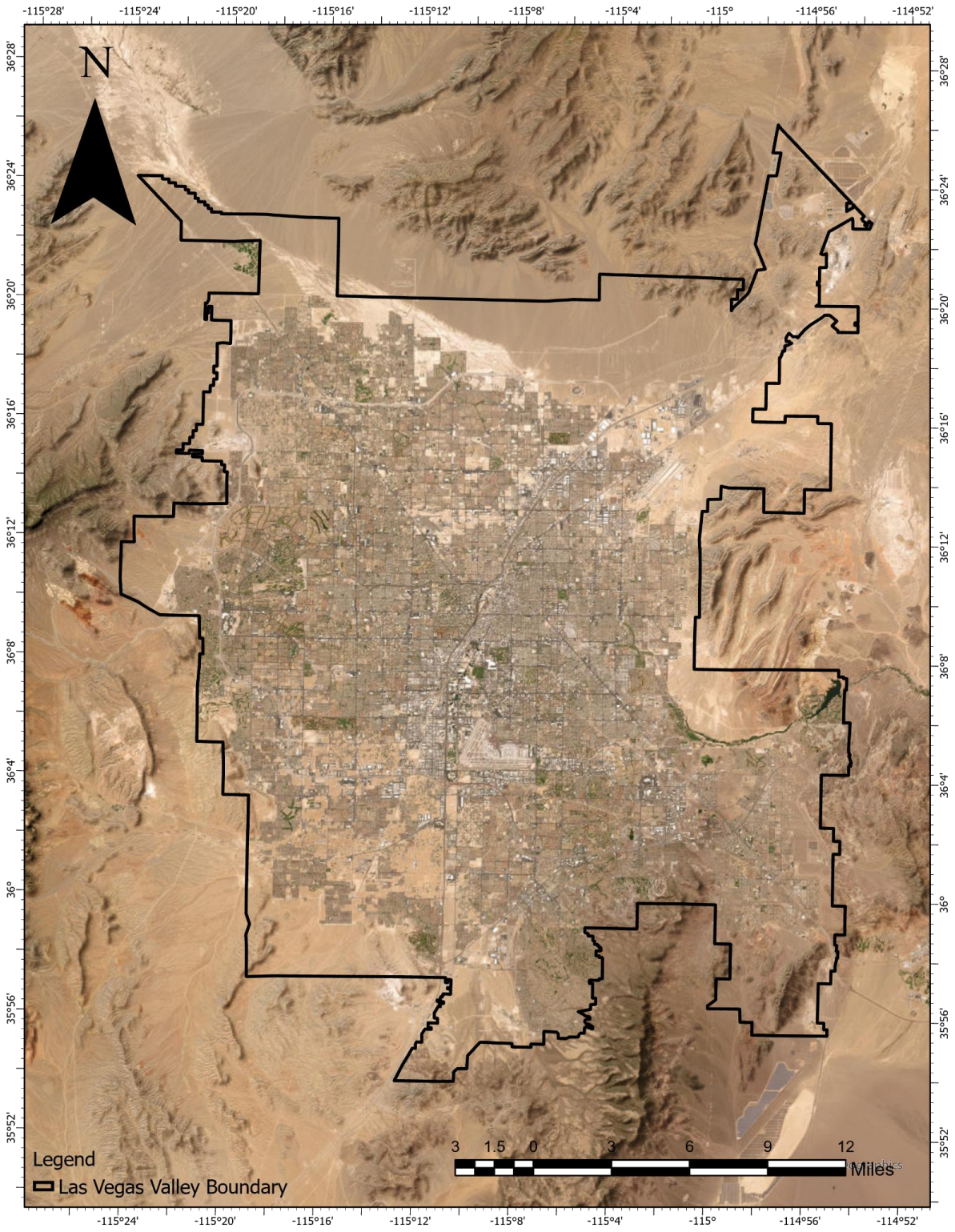

Figure 2.1: Study Area: Las Vegas Valley, Nevada

2.4 Materials and Methods

In this research, the goal is to assess the impact of artificial turf on the urban thermal environment by measuring the LST and Surface Albedo using remote sensing technologies.

Satellite remote sensing offers a direct and consistent approach to assess the thermal contrast between urban and rural regions. Extensive research has been carried out on the utilization of remotely sensed data to identify thermal characteristics of urban surfaces (Xian & Crane, 2006). Temperature images acquired through satellite data enable the estimation of LST, which represents the temperature of the land surface directly interacting with the atmosphere. LST can be influenced by various factors, including solar radiation, vegetation cover, and soil moisture (Black et al., 2019). The study of urban climates heavily relies on LST as it modifies the air temperature within the atmospheric boundary layer and serves as a vital parameter for surface energy and water balance at local and global scales (Yu et al., 2018). It is important to note that LST differs from the air temperature reported in daily weather forecasts. Changes in urban LST can significantly impact local weather and climate (Xian & Crane, 2006).

Thermal bands on remote sensing satellites play a crucial role in determining LST. Multiple satellites such as Landsat, Aster, AVHRR, MODIS, etc., possess thermal bands for this purpose. Due to the greater heterogeneity in urban areas, a finer spatial resolution is necessary to study LST variations in these regions (Bala et al., 2018).

Most of this project was carried out using Google Earth Engine (GEE), with some tasks completed in ArcGIS Pro by Environmental Systems Research Institutes (ESRI), California. GEE is a cloud computing platform renowned for offering robust computing capabilities, especially when handling massive geospatial datasets (Gorelick et al., 2017). It is engineered to manage and

analyze vast (petabyte-scale) datasets to aid decision-making (Mutanga & Kumar, 2019). The efficiency of Google's computing combined with data mining capabilities has captivated numerous professionals and scholars due to its rapid information access, as highlighted by Becker et al. (2021).

The study focused on the analysis between 2018 and 2022. During 2020-21, 29 football fields in Southern Nevada public schools transitioned from natural grass to synthetic turf (Seeman, 2020). Therefore, all these fields had natural grass in 2018, and have artificial turf at present. Out of these 29 fields, 26 fields have been designated as the Regions of interest (ROIs) for this study, while the remaining three are outside the designated study zone. Additionally, 26 ROIs were chosen that did not undergo the transition process from natural to artificial turf. Among these 26 ROIs, 1 ROI belongs to a sports complex, 4 ROIs are in 4 parks, and the rest of the ROIs are in golf courses. These non-transitioned ROIs worked as a control group. This control group served as an important benchmark. The temperature difference in the football fields due to the alteration from natural to artificial turf was analyzed with respect to the temperature difference in the non-transitioned ROIs between 2018 and 2022. The comparison between the football fields and golf courses can help isolate the effects of turf transition from other environmental changes.

All the Landsat 8 satellite images available for 2018 and 2022 were downloaded and used for this study. Table 2.1 and Table 2.2 display the dates on which satellite images were obtained for the years 2018 and 2022, respectively, along with corresponding information on low, high, and average temperatures, precipitation, and cloud cover for each image. Figure 2.2 illustrates the frequency of satellite images obtained for each day over the course of a year, comparing the data between 2018 and 2022. The blue bars represent the count of images for 2018, and the red bars

represent the count for 2022. Figure 2.3 displays the distribution of average day temperature for each date on which a satellite image was obtained, across 2018 and 2022.

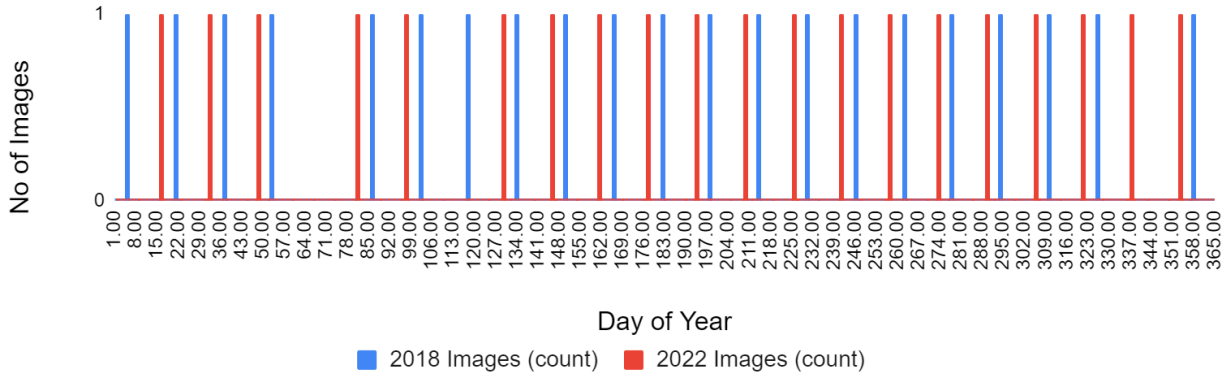

Figure 2.2: Distribution of the dates of the obtained satellite images in 2018 and 2022

Table 2.1: Low-high- average air temperature, and precipitation (Source: Weather Underground) and the cloud covers of the obtained satellite images of 2018 (Source: Earth Explorer)

Dates	Low Temperature (°C)	High Temperature (°C)	Average Day Temperature (°C)	Precipitation (mm)	Cloud Cover (CC) (%)
5-Jan-18	5	19	11.83	0	0.58
21-Jan-18	3	12	7.29	0	1.9
6-Feb-18	13	22	17.17	0	0.2
22-Feb-18	-1	13	6.96	0	46.62
10-March-18	12	19	14.7	0	100
26-Mar-18	9	17	13.24	0	5.79
11-Apr-18	23	33	27.07	0	0.07
27-April-18	20	34	28.2	0	0.09
13-May-18	18	28	23.46	0	12.7
29-May-18	22	35	29.5	0	4.54
14-Jun-18	26	40	34.41	0	0.45
30-Jun-18	25	38	32.4	0	0.35
16-Jul-18	31	42	36.17	0	11.76
1-Aug-18	31	43	38.03	0	4.3
17-Aug-18	28	38	33.81	0	6.12
2-Sep-18	23	37	30.79	0	4.71
18-Sep-18	20	37	29	0	0
4-Oct-18	17	27	21.17	4.06	17.67
20-Oct-18	15	27	21.58	0	14.96
5-Nov-18	12	24	17.38	0	0.03
21-Nov-18	5	18	12.33	0	2.31
7-Dec-18	7	13	10	2.29	86.51
23-Dec-18	6	16	10.17	0	4.53

Table 2.2: Low-high- average air temperature, and precipitation (Source: Weather Underground) and the cloud covers of the obtained satellite images of 2022 (Source: Earth Explorer)

Dates	Low Temperature (°C)	High Temperature (°C)	Average Day Temperature (°C)	Precipitation (mm)	Cloud Cover (CC) (%)
16-Jan-22	3	17	9.71	0	33.03
1-Feb-22	6	16	10.88	0	38.72
17-Feb-22	8	17	11.58	0	0.37
5-Mar-22	7	13	11.16	0	36.98
21-Mar-22	11	23	16.5	0	1.83
6-Apr-22	16	26	21.13	0	0.23
22-April-22	11	22	16	0	80.84
8-May-22	18	29	24.21	0	0.08
24-May-22	21	33	27.63	0	0.24
9-Jun-22	27	42	35.84	0	1.36
25-Jun-22	25	40	34.21	0	1.07
11-Jul-22	29	44	38.04	0	0.9
27-Jul-22	26	38	31.41	0	31.06
12-Aug-22	27	37	30.86	20.57	46.23
28-Aug-22	27	40	34.29	0	0.82
13-Sep-22	23	33	28.47	2.03	75.96
29-Sep-22	23	36	29.42	1.02	1.93
15-Oct-22	19	31	23.88	0	43.17
31-Oct-22	13	24	18.13	0	0.17
16-Nov-22	7	17	11.3	0	0.47
2-Dec-22	9	17	13.83	0	35.85
18-Dec-22	-1	11	4.63	0	31.51

Four images, two from 2018 and two from 2022, were omitted from the research because they exhibited substantial cloud cover. Specifically, the excluded images from 2018 were dated February 22nd (with 46.62% cloud cover) and December 7th (with 86.51% cloud cover). From 2022, the dates of the omitted images were April 22nd (with 80.84% cloud cover) and September 13th (with 75.96% cloud cover). The extensive cloudiness in these images resulted in the inability to derive LST or surface albedo measurements for most of the ROIs on these dates.

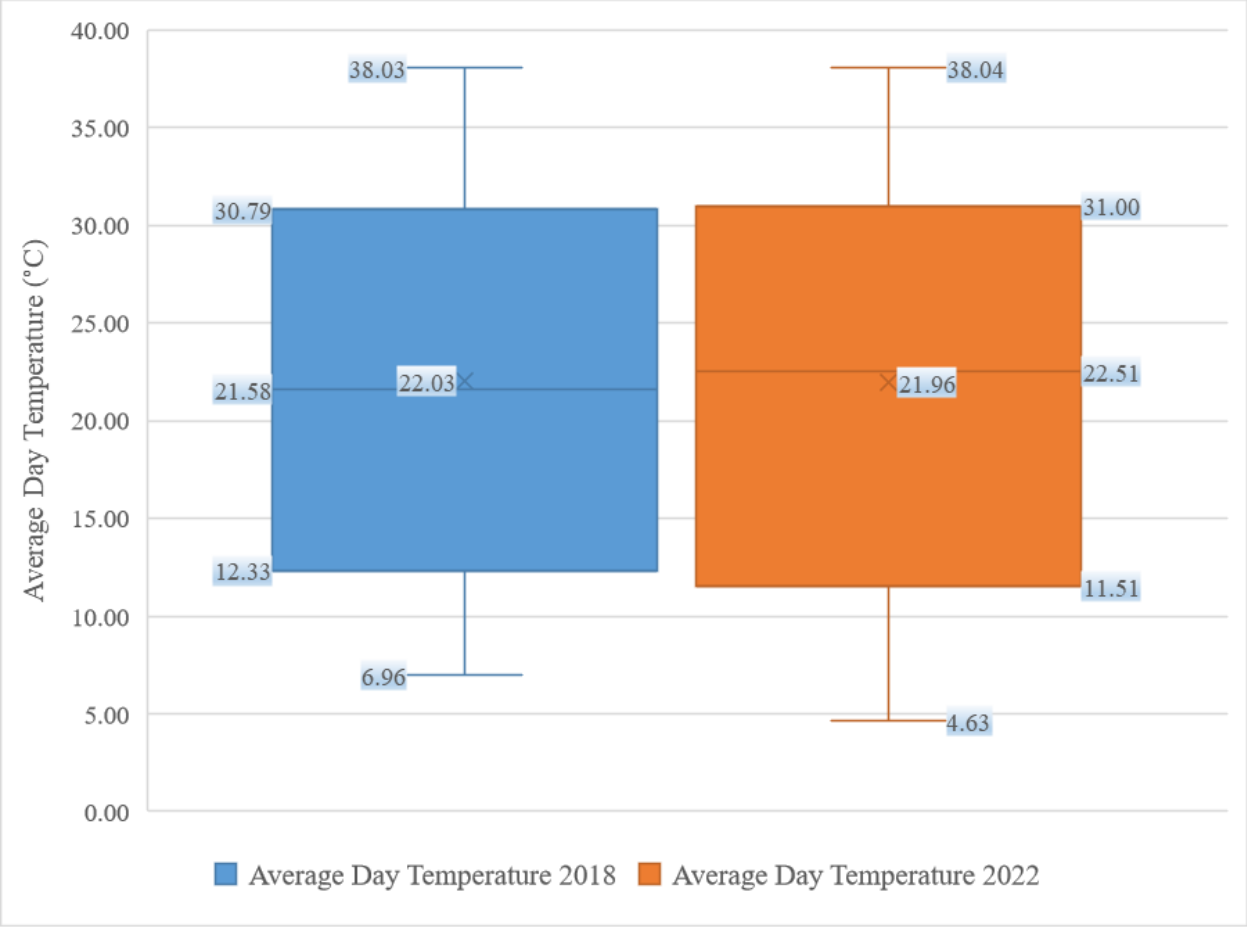

Figure 2.3: Distribution of average day temperatures for 2018 and 2022

Figure 2.3 represents the distribution of average day temperatures for two different years, with blue representing 2018 and orange representing 2022. Both years have a similar median temperature, indicated by the line inside each box, which suggests that the central tendency of temperatures has remained relatively consistent from 2018 to 2022. The range of temperatures appears to be wider for 2022, suggesting there was greater variability in daily temperatures during that year. The interquartile range, which shows the middle 50% of the data, also seems wider for 2022, further supporting the idea of greater variability in temperatures compared to 2018. The distribution for 2018 appears more symmetrical around the median, while 2022's distribution seems slightly skewed upwards, with the median closer to the bottom of the box. This suggests that more of the 2022 data is spread towards higher temperatures. The average day temperatures for these two years seem to be relatively comparable, with potentially less variability in 2018 compared to 2022.

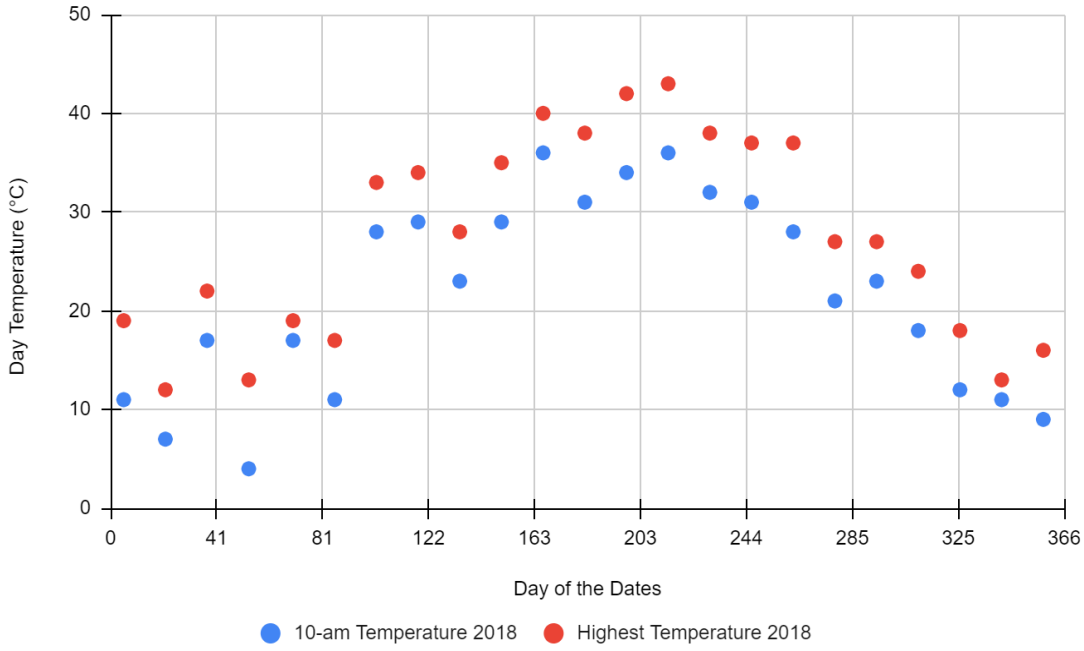

(a)

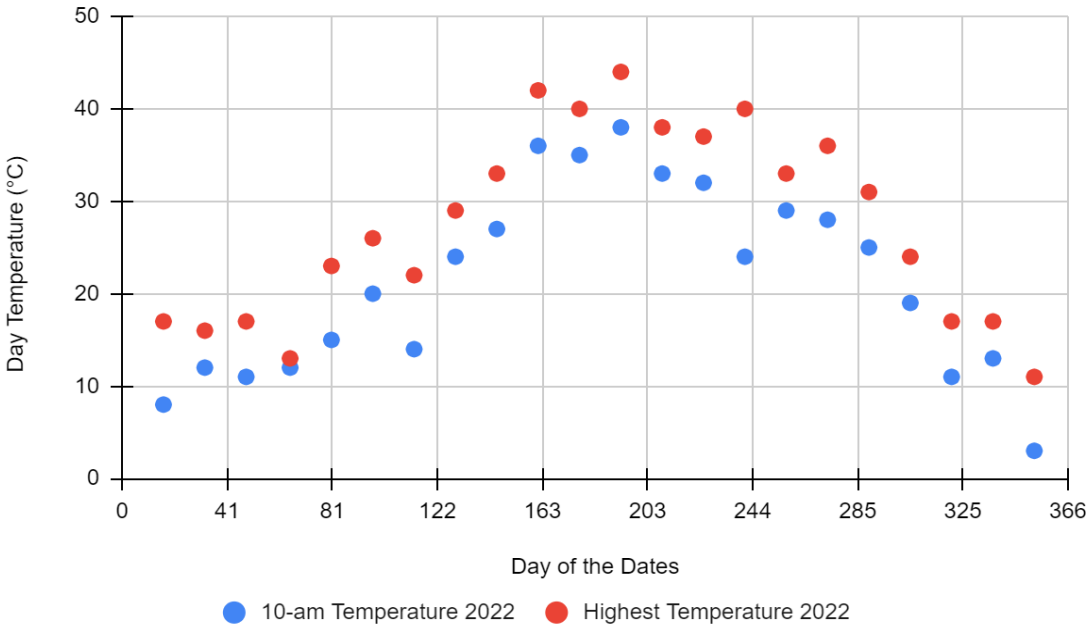

(b)

Figure 2.4: Comparison of 10 am air temperatures with the peak temperatures recorded each day for the years (a) 2018 and (b) 2022 (Source: Weather Underground)

Figure 2.4 presents a side-by-side analysis of air temperatures at 10 am and the maximum day temperatures for the years 2018 and 2022. It was observed that the temperatures at 10 am were consistently lower than the daily peaks for both years. On average, the temperature difference at these times was 5.83°C in 2018 and increased slightly to 6.23°C in 2022. This particular time of 10 am was chosen for comparison as it aligns with the overpass time of the Landsat 8 satellite, which is approximately 10:00 am +/- 15 minutes (European Space Agency, 2022). As such, the satellite imagery, captured at local 10 am, offers a specific snapshot of surface conditions at that moment (Black et al., 2019). It's important to note that the highest LST values might occur later in the day, typically in the afternoon.

Figure 2.5 represents the schematic workflow to calculate the LST for the study area. Figure 2.6 shows the visual representation of the methodology to calculate the LST.

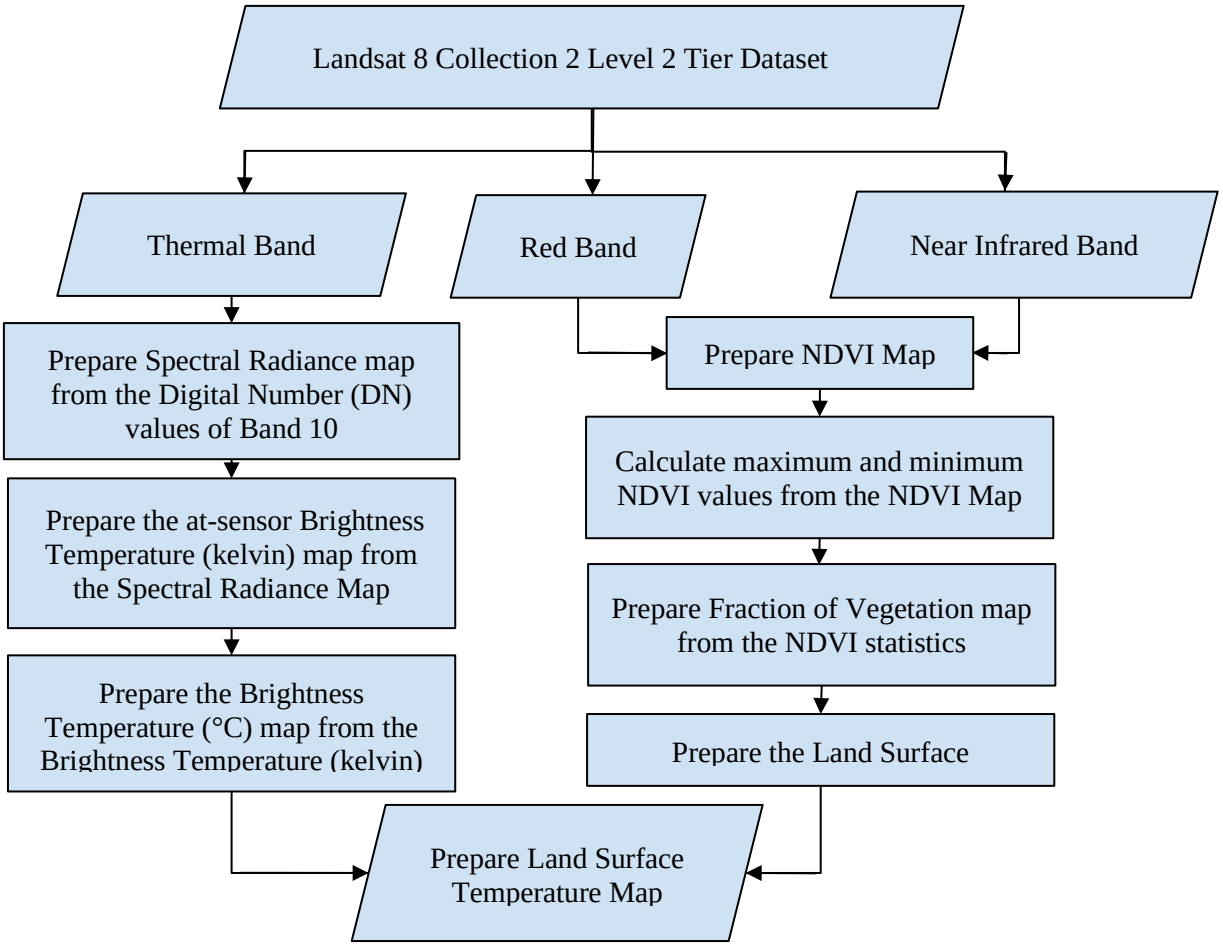

Figure 2.5: Schematic of workflow to retrieve the LST from Landsat 8 Satellite images.

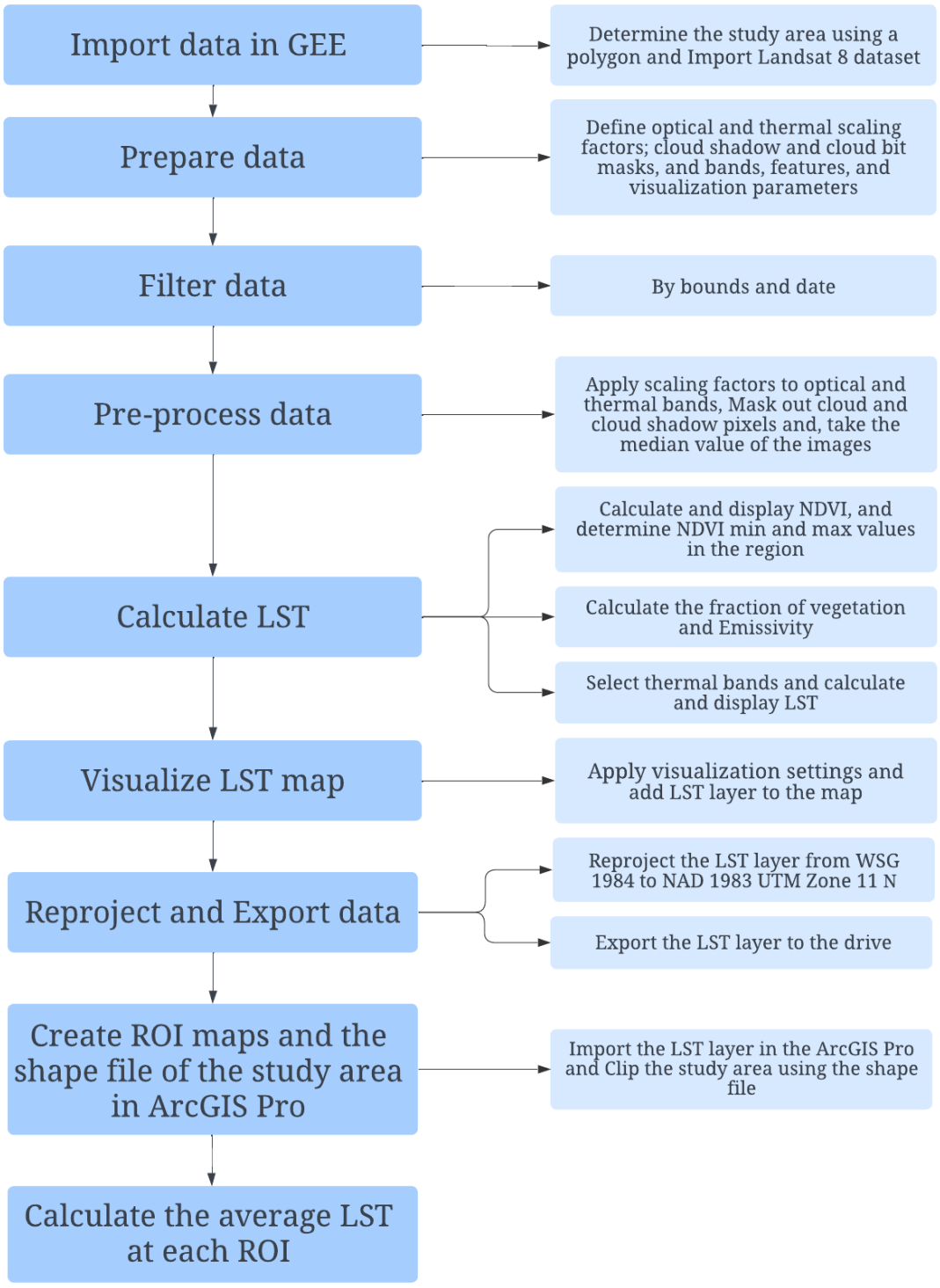

Figure 2.6: Steps involved to retrieve LST in GEE and ArcGIS Pro

For LST, the Landsat 8 Collection 2 Level 2 Tier 1 dataset was initially imported into the code editor, and a study area polygon was delineated. During the data initialization phase, first, optical and thermal scaling factors were defined, cloud shadow and cloud bit masks were then established, and finally various bands, features, and visual parameters were determined. The Landsat 8 image collection was narrowed down based on specific dates and the selected region.

In the data pre-processing stage, first, the scaling factors were applied to the optical and thermal bands of the image employing the “applyScaleFactors” function to convert the raw digital numbers (DN) into reflectance and brightness temperatures, respectively. Secondly, the 'maskL8sr' function was utilized to exclude cloud-covered and shadowed pixels based on the pixel quality assessment (QA) band. Finally, the median values of the processed image were extracted.

Subsequently, the data was visualized on the map and relevant calculations were performed. A true color composition of the imagery was rendered. Normalized Difference Vegetation Index (NDVI) of the study area was determined using the near-infrared (NIR) and red bands of the filtered image and displayed on the map. This process enabled the derivation of minimum and maximum NDVI values, from which vegetation fraction was computed. Using the fraction of vegetation, the emissivity was computed. Finally, with the emissivity and the thermal band 10, the LST was calculated for the study area. A visualization palette for LST was provided, and the LST layer was added to the map. The LST layer's coordinate system was subsequently reprojected from WSG 1984 to NAD 1983 UTM Zone 11 N to align with the coordinates of LVV. Finally, the images for each date were exported as a Tiff file. The cloud computations were done following the paper by Waleed and Sajjad (2022).

Following that, the subsequent phase involved defining the ROIs in ArcGIS Pro to examine temperature fluctuations within each ROI across the four-year period. As mentioned earlier, 26 ROIs transitioned from natural to artificial turf between 2018 and 2022, and 26 ROIs did not go through any transition and served as a control group. For the purposes of this research, two separate ROI maps were created for two cases: transitioned ROIs and non-transitioned ROIs. Two to three complete pixels located within the boundaries of the football fields and other land types were selected as the ROIs (Figure 2.7). The selection of complete pixels is aimed at minimizing the influence of mixed pixels that contain multiple land classes. A ROI map was then created showing all the transitioned and non-transitioned ROIs (Figure 2.8). The LST layer exported from GEE was retrieved from Google Drive and displayed on the Arc map. The LST layer was clipped using the shape file of the study area. The shape file of the LVV was created in ArcGIS Pro utilizing the political boundary of the area. Finally, temperature data was collected from each ROI using the "Zonal Statistics as Table" tool in ArcGIS Pro. This produced standalone tables with ROI-specific values for subsequent analyses. The gathered data was then compiled into a separate Excel sheet for further analysis.

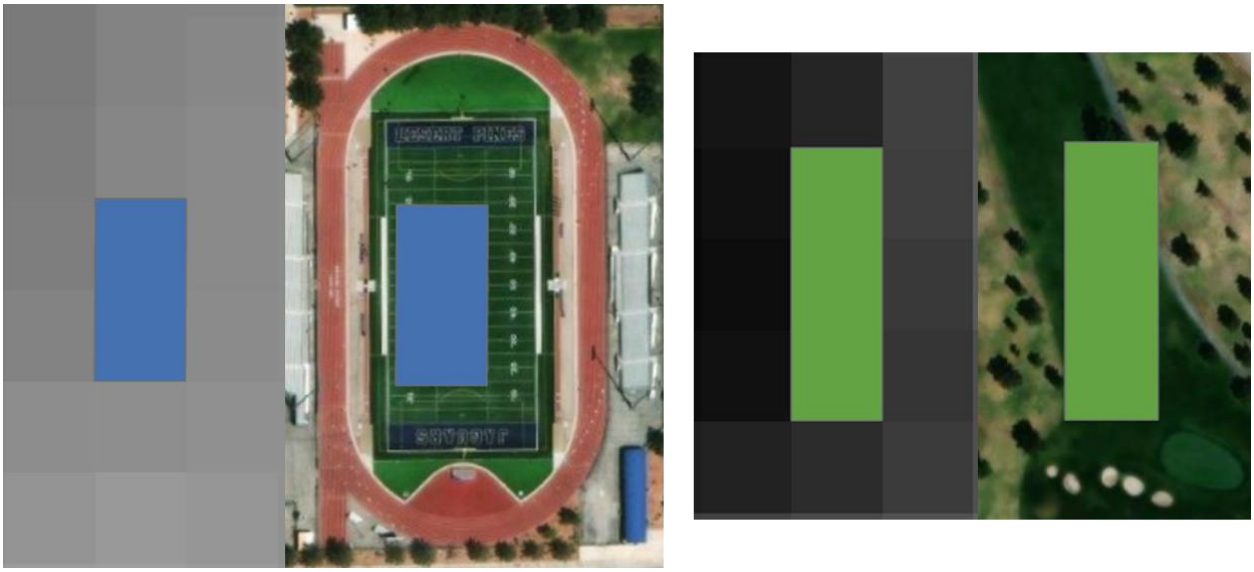

(a) (b)

Figure 2.7: Representation of selected ROIs for analysis. (a) Depicts two fully contained pixels within the confines of Desert Pines High School football field, identified as a transitioned ROI, with the left displaying a grayscale image and the right showcasing the true-color image. (b) Illustrates three fully contained pixels situated within the Las Vegas Golf Club grounds, identified as a non-transitioned ROI, where the left image is grayscale, and the right reveals the natural coloration.

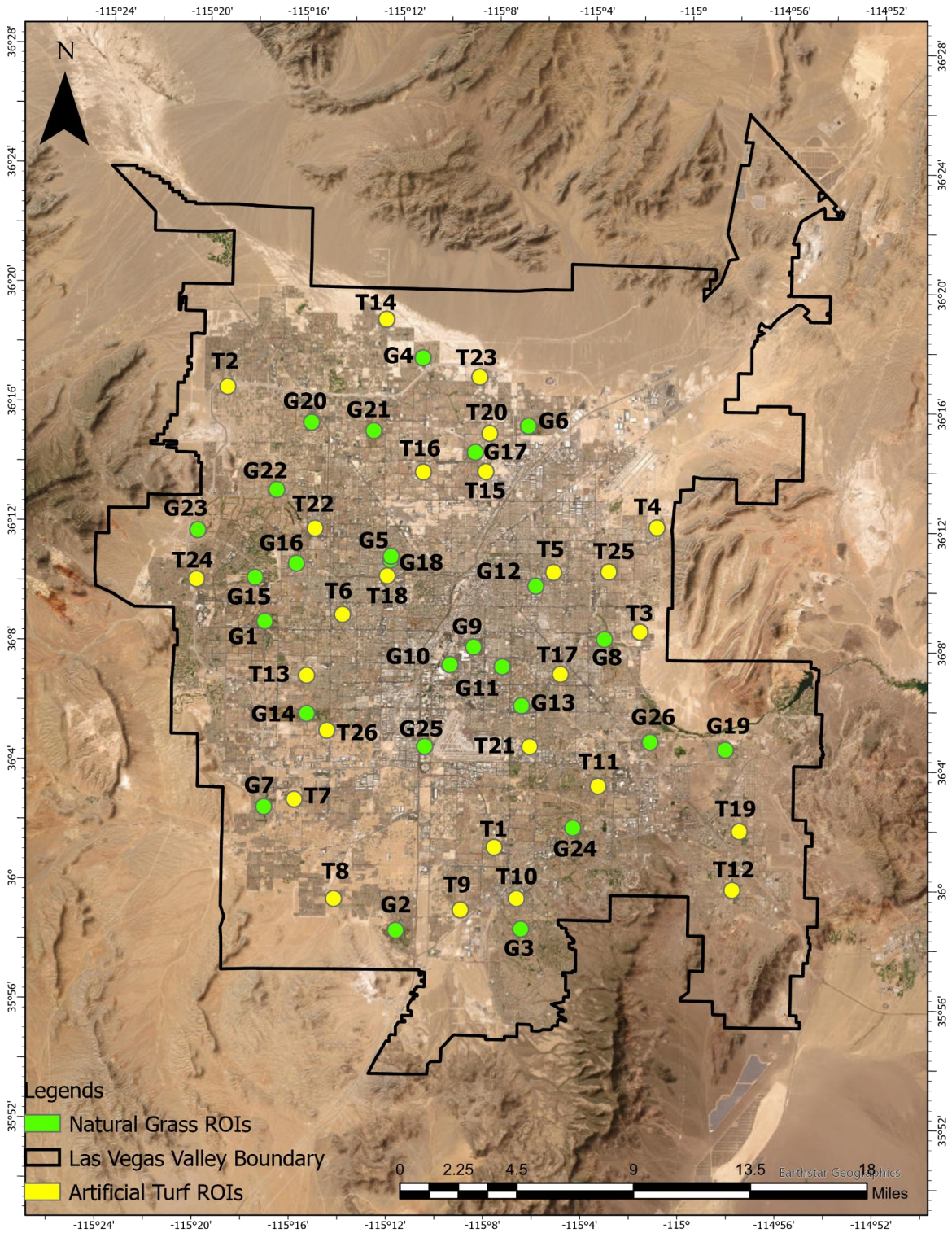

Figure 2.8: Yellow dots represent the ROIs converted from natural grass to artificial turf between 2018 and 2022 and green dots represent the ROIs that did not go through any conversion.

Surface Albedo:

The Surface Albedo is a measure of reflectivity in all directions above the surface which integrates across the entire spectrum of the wavelengths that the surface is exposed to. Surface albedo maps were generated for 2018 and 2022 in GEE for all the months. Figure 2.9 shows the steps to calculate albedo values using GEE and ArcGIS pro.

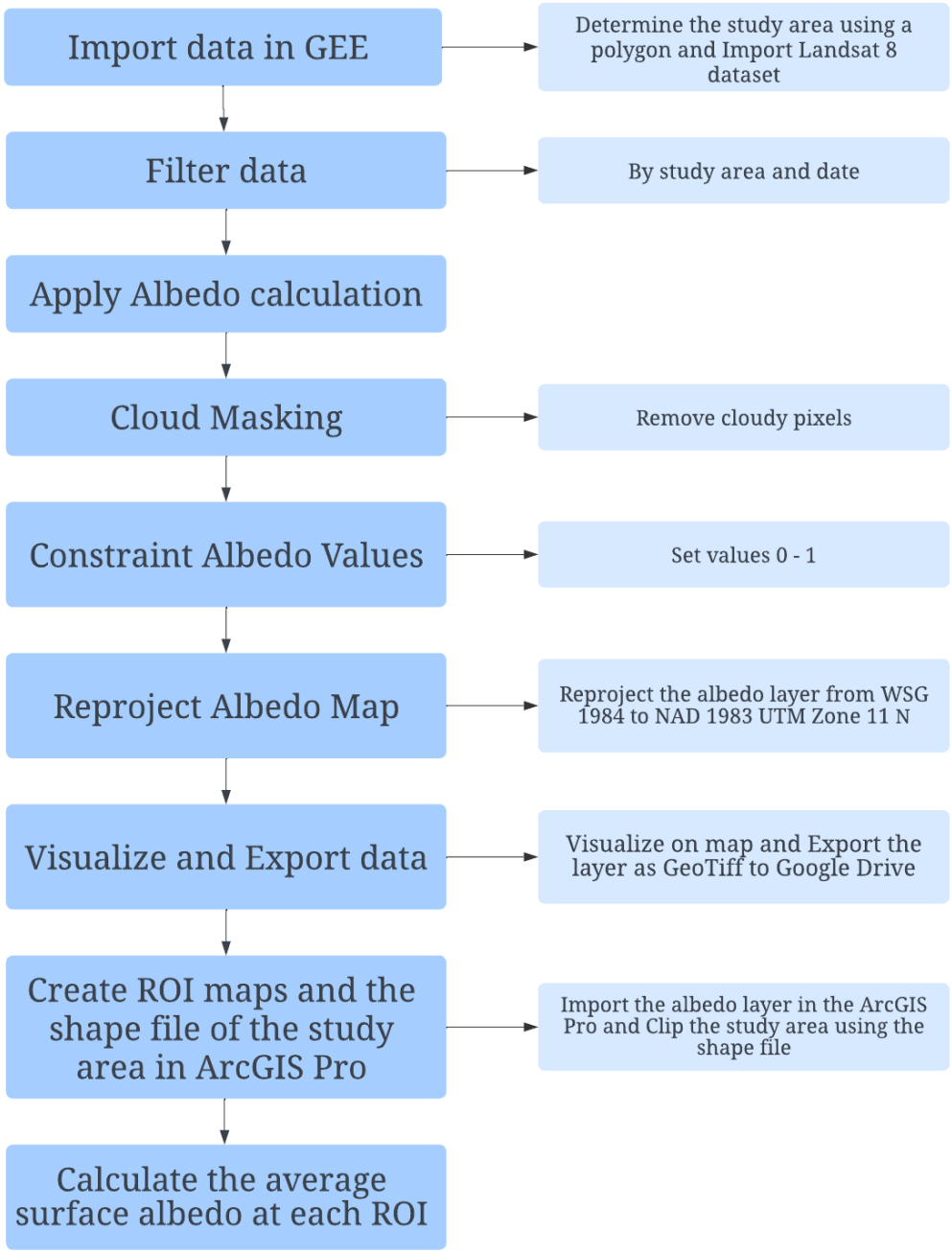

Figure 2.9: Steps to retrieve Surface Albedo of selected ROIs in GEE and ArcGIS Pro

At first, the study area was defined using a polygon and the Landsat 8 data was imported. This study employed the USGS Landsat 8 Level 2, Collection 2, Tier 1 dataset, which contains atmospherically corrected surface reflectance and land surface temperature derived from the data produced by the Landsat 8 OLI/TIRS sensors. Out of the 17 bands in this image collection, this study focused on 5. (USGS Landsat 8 Level 2, Collection 2, Tier 1, n.d.) Table 2.3 provides details on the selected bands and their respective attributes.

In the next step, a Landsat image was used as an input using the “image” function. The image was then modified by applying new bands which involved applying mathematical transformation to adjust the values. Next step was to calculate the surface albedo of the study area using a formula that involves different bands. Coefficients used in the formula are weights assigned to each band to calculate albedo. Next, some filters were applied such as date and boundary to get images for the study area. The “albedo” function was applied to each image in the collection. The “maskLandsat” function was used to remove cloudy pixels from each image. Next step was to add the median albedo data as a layer on the map, with a specified range of albedo values (0 - 0.4).

Next, the “bitwiseExtract” function was used to extract specific bits from a value which is used to interpret the "QA_Pixel" band to identify cloud free pixels. The typical range of albedo is 0 to 1. More than 1 and less than 0 come due to the noise in the data and errors in the calculation. Therefore, constraints were applied to the data in the GEE script to ensure that all albedo values are within the physically meaningful range of 0-1. Reprojection of the coordinates from WGS 1984 to NAD 1983 UTM Zone 11N was done. This was done to match the coordinate system of Las Vegas. Reprojected images were added to the map. Finally, the images were exported as a Tiff

file. The images were downloaded from Google Drive and were opened on ArcGIS pro for further analysis.

In ArcGIS Pro, these images were retrieved from Google Drive and displayed on the Arc map. Two existing ROI maps, showing 26 ROIs where turf transitioned from natural to artificial between 2018 and 2022, and 26 ROIs which did not go through any alteration, were used in measuring the average surface albedo for each ROI using the "Zonal Statistics as Table" tool. This produced standalone tables with ROI-specific values for subsequent analyses. The data was gathered on an excel sheet for further analyses. The study's final step involved clipping the polygon using the area's shapefile.

Table 2.3: USGS Landsat 8 Level 2, Collection 2, Tier 1 bands used in measuring the Surface Albedo

Band Names	Band Description	Resolution (Meters)	Wavelength (μm)
SR_B2	Band 2 (Blue) Surface Reflectance	30	0.452 - 0.512
SR_B4	Band 4 (Red) Surface Reflectance	30	0.636 - 0.673
SR_B5	Band 5 (Near Infrared) Surface Reflectance	30	0.851 - 0.879
SR_B6	Band 6 (Shortwave Infrared 1) Surface Reflectance	30	1.566 - 1.651
SR_B7	Band 7 (Shortwave Infrared 2) Surface Reflectance	30	2.107 - 2.294

In this study, the codes for retrieving surface albedo values from the GEE were set up to work with any land cover class, as it did not include specific constraints that would limit it to a particular land class type. The formula used for calculating albedo was generic and can be applied to any land surface type. It was based on a weighted sum of reflectance from various spectral bands. While the code was generalized in terms of albedo calculation, the specific parameters, like the date range, area of interest (polygon), and reprojection CRS, imply that the code is tailored to a specific dataset or study area rather than a specific land class type.

A comprehensive series of Paired T-Tests was conducted to assess the impact of transitioning from natural to artificial turf on both LST and Surface Albedo. The T-Tests were conducted for both transitioned and non-transitioned ROIs. In this research, paired sample T-Tests were utilized due to their relevance in comparing two sets of variables from identical subjects. Typically, this form of analysis is apt when the variables are differentiated by time. For the purposes of our investigation, this was particularly applicable as the measurements for LST, or surface albedo were recorded from the same geographical locations at two distinct time points. Table 2.4 gives an overview of four series of Paired T-Tests conducted for LST and Surface Albedo Analysis. The table summarizes the types of T-Tests applied, including annual, seasonal, and individual ROI assessments for both transitioned and non-transitioned ROIs, along with the count of tests conducted per category and the corresponding threshold P-values.

Table 2.4: Summary of the types of paired T-Tests applied, the count of tests conducted in both transitioned and non-transitioned categories and the corresponding threshold values.

Paired T-Tests	Description	No of pair of T-Tests for Transitioned ROIs	No of pair of T-Tests for Non-Transitioned ROIs	P-Values
Annual T-Test	All data from all ROIs for the entire year were combined	1	1	0.05/26 = 0.002
Individual ROI	T-Tests were performed for each ROI taking all the data from the available dates	26	26	0.05 for each ROI
Seasonal T-Tests for each ROI	The data were categorized into four seasons, Winter, Spring, Summer, and Fall and T-Tests were performed separately for each ROI and for each season	26 * 4 = 104	26 * 4 = 104	0.05 for each ROI
Combined Seasonal T-Tests	All data from all ROIs were pooled for each season to conduct T-Tests	4	4	0.05/26 = 0.002 for each season

An alpha level of 0.05 was established as the threshold for statistical significance for the second and third series of T-Tests, indicating that any differences observed would need to be statistically significant to be considered meaningful. In the context of statistical significance, if the p-value is above a predefined threshold (commonly 0.05), it is generally interpreted that there is not enough statistical evidence to reject the null hypothesis. Thus, it would be concluded that the differences between the paired samples are not statistically significant.

Bonferroni adjustment was considered for the other two series of T-Tests by adjusting the alpha level to avoid multiple testing problems. The Bonferroni adjustment is a method to control Type I errors (false positives) when conducting multiple tests. It reduces the alpha level to account for the number of tests being performed which is done by dividing the original alpha level by the number of tests. Bonferroni Adjustment reduces the probability of obtaining a significant result by chance alone across all the tests.

The null hypothesis (H0) of this study posits that there are no significant differences in LST/ Albedo resulting from the turf type change between the years 2018 and 2022. Conversely, the alternative hypothesis (H1) contends that there are significant differences in the LST/ Albedo between the years 2018 and 2022 attributable to the conversion from natural to artificial turf.

R Studio was utilized to perform these statistical tests. In the R studio, each data set was first subjected to normality testing to determine if it follows a normal distribution. For data sets that do not pass the normality test, indicated by an alpha value of less than the actual alpha value, the Mann-Whitney U test was applied.

2.5 Results and Discussions

This study aims to discuss the following topics:

1. The variation in LST of 26 selected ROIs that transitioned from natural to artificial turf between the years 2018 and 2022.
2. The alterations in Surface Albedo values across the same 26 ROIs, consequent to the replacement of natural grass with artificial turf within the same timeframe.

3. A comparative analysis of LST and albedo modifications in the ROIs that underwent the transition from natural to artificial grass against those ROIs which retained their natural grass cover, thereby assessing the direct impacts of this land cover transition.

2.5.1 Land Surface Temperature (LST)

23 LST maps for 2018 and 22 LST maps for 2022 were generated using GEE platforms. Landsat 8 satellite was used to generate maps. The maps were then imported to ArcGIS pro, where they were clipped according to the shapefile of LVV. A ROI map showing 26 ROIs that have been switched from natural to artificial grass between 2018 and 2022, and 26 ROIs that did not go through any transition between the time, was used to measure the average LST values at these ROIs. The data were gathered on an excel sheet for further analysis. Two cases were made for the ease of the analysis:

a. Case I: 2018 (NG) vs 2022 (AT), the ROIs transitioned from natural grass to artificial turf.

b. Case II: 2018 (NG) vs 2022 (NG), the ROIs did not go through any alteration and maintained natural grass in both years.

2.5.1.1 Comparison of the LST for each ROI across various dates within the years 2018 and 2022

a. Case I: 2018 (NG) vs 2022 (AT)

For the ROIs that underwent a transition from natural to artificial turf between pre (2018) and post-conversion (2022), the data indicate a rise in LST during the months of June, July, and August across all such ROIs. During the remaining months, most of the transitioned ROIs did not exhibit a significant increase in LST.

b. Case II: 2018 (NG) vs 2022 (NG)

Conversely, for the ROIs that did not undergo any transition, a noticeable increase in LST was observed only in a few ROIs during the summer months, while for the rest of the year, LST remained largely unchanged in 2022 compared to 2018.

The distribution of LST Values for 26 transitioned and 26 non-transitioned ROIs are provided in Appendix A.1 and A.2, respectively. Blue boxes represent LST data for the year 2018, and orange boxes show LST data for the year 2022. Each box plot illustrates the variation in LST readings across multiple dates within the respective years. The Y-axis indicates the LST range in degrees Celsius.

For transitioned ROIs, the post-conversion data (2022) exhibits increased variability, as suggested by the wider range of the box plots for that year. Except for one ROI (T26), median LST values for 2022 decreased across all ROIs. Non-transitioned ROIs reveal a similar trend of heightened variability in 2022 for the ROIs that did not undergo transition. The median LST for these ROIs decreased, with an average reduction of 6.1°C per ROI. In contrast, the average decline in median LST among the transitioned ROIs was 5.17°C.

2.5.1.2 Comparison of the average LST for each ROI between 2018 and 2022

The average LST for each ROI was calculated for the years 2018 and 2022, and comparisons were drawn by subtracting the average LST of 2018 from that of 2022. Subsequently, scatter plots were generated to visualize the data where blue dots represent the average LST for each ROI in 2018, and red dots for 2022.

a. Case I: 2018 (NG) vs 2022 (AT)

The analysis revealed an increase in average LST for 7 ROIs, while a decrease was noted in the remaining ROIs. The most substantial rise in temperature was recorded at the football field

of Durango High School (T26), with an increase of 2.33°C. Figure 2.10 illustrates the LST differences for each transitioned ROI between 2018 and 2022.

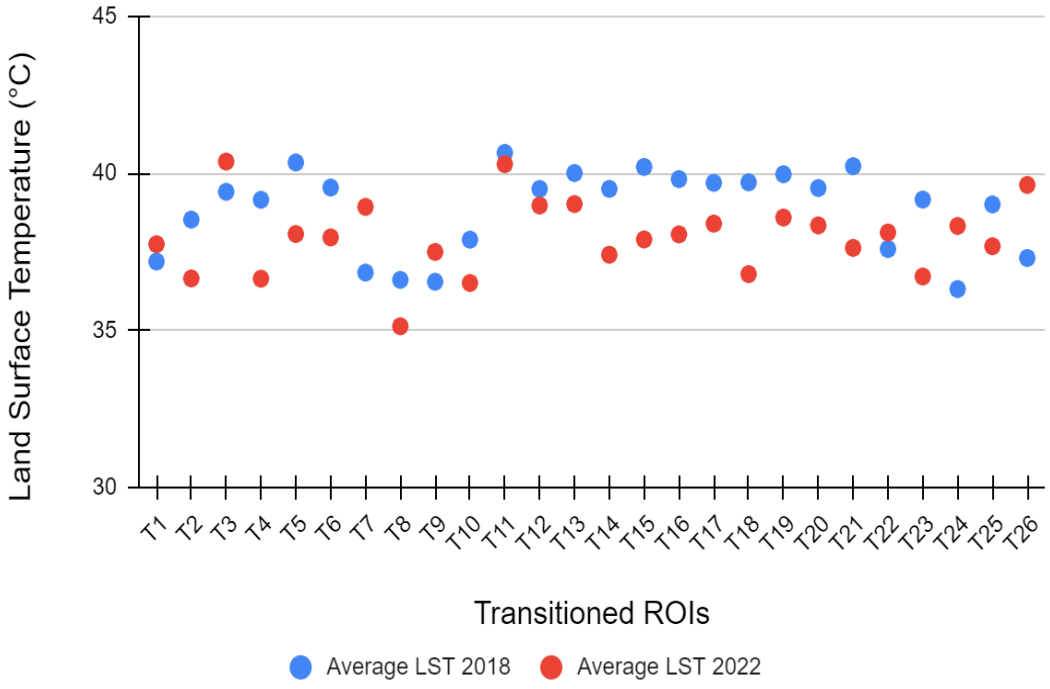

Figure 2.10: Average LST differences for each ROI between 2018 and 2022 for transitioned ROIs

b. Case II: 2018 (NG) vs 2022 (NG)

An increase in average LST was observed in only one ROI, specifically at Rhodes Ranch Golf Club (G7), by 0.72°C. Conversely, the average LST decreased in 2022 for the other ROIs. Figure 2.11 presents the LST differences for each ROI between 2018 and 2022.

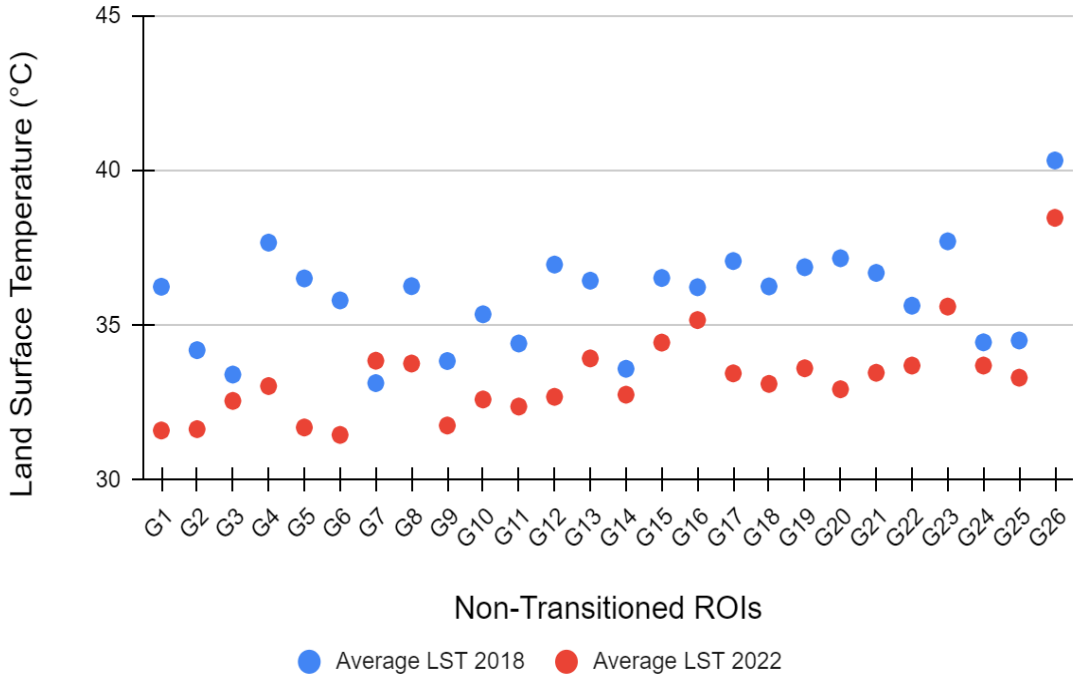

Figure 2.11: Average LST differences for each ROI between 2018 and 2022 for non-transitioned ROIs

Figure 2.12 shows a comparison of LST for football fields that transitioned from natural to artificial turf between 2018 and 2022. The box plots compare average LSTs from two different years, providing insight into whether the change in turf material had an impact on the surface temperature of the fields. From the box plots, it seems that there is a noticeable difference in average LSTs between the two years. Figure 2.13 presents a comparison of average LSTs for golf courses that have maintained natural grass surfaces between the same years. This comparison could serve as a control to understand the natural variability in LST over time without the influence of changing the surface material.

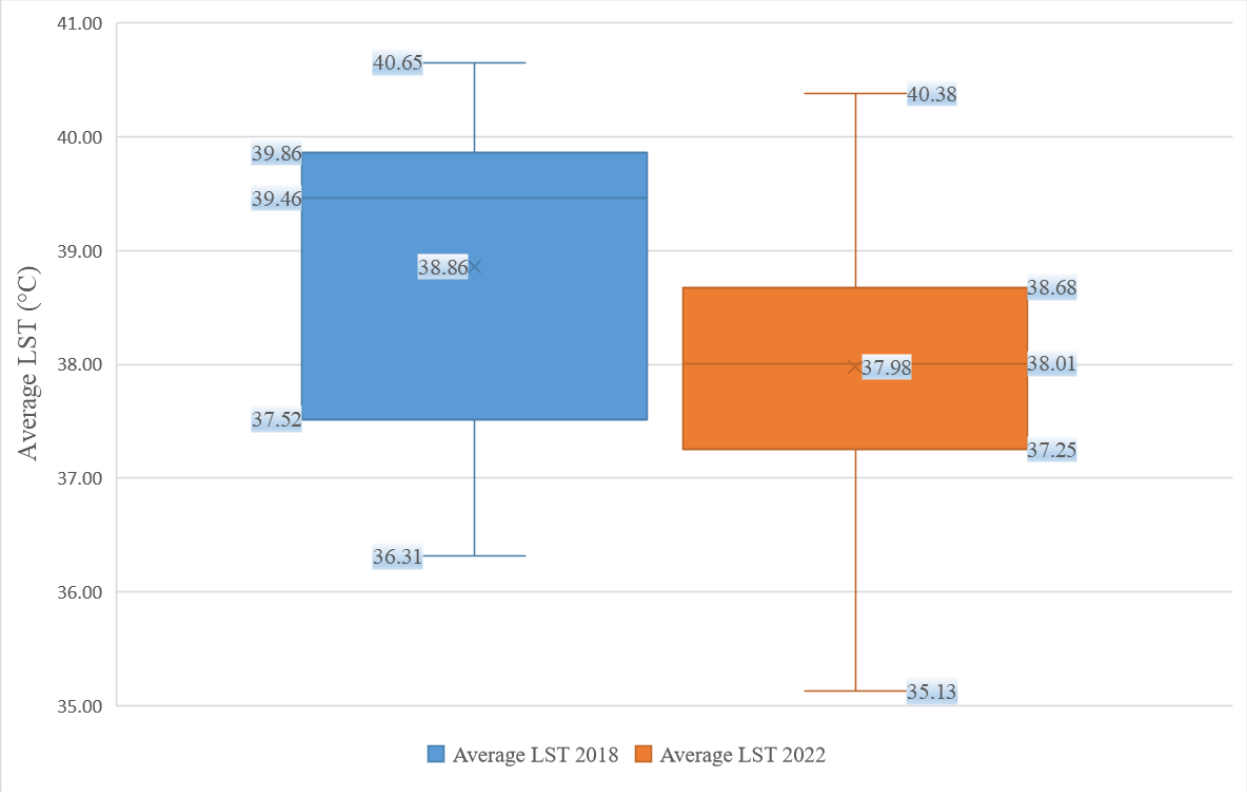

Figure 2.12: Distribution of the average LST for football fields that transitioned from natural to artificial turf, comparing data from 2018 (blue) and 2022 (orange)

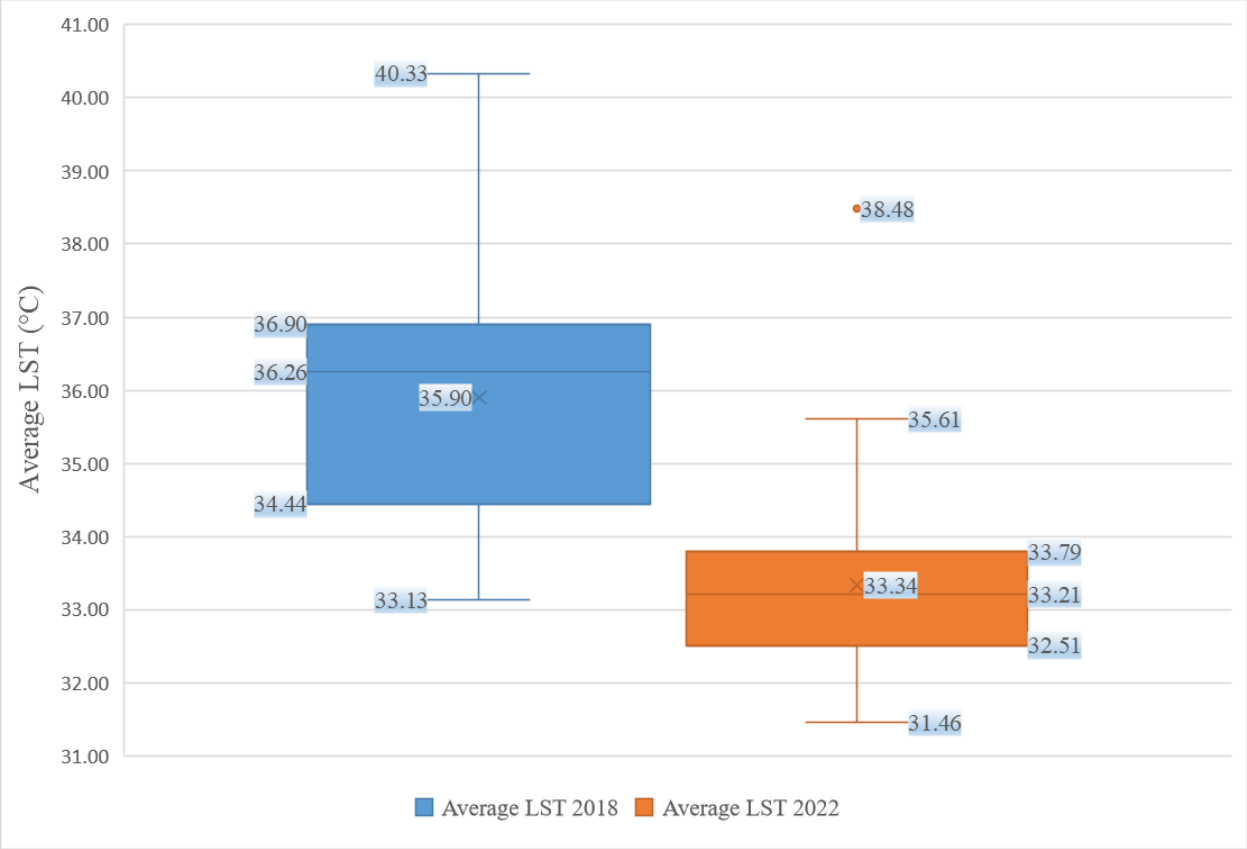

Figure 2.13: Distribution of the average LST for Golf Courses that maintained the natural grass surfaces, comparing data from 2018 (blue) and 2022 (orange)

In Figure 2.12, the median LST appears to be slightly lower in 2022 (orange) compared to 2018 (blue), indicating a small decrease in the central tendency of the LST after the transition to artificial turf. The range of LST values, denoted by the whiskers, has a slight downward shift in 2022. This suggests that the highest temperatures recorded in 2022 are lower than those recorded in 2018. The interquartile range (IQR), which is the height of the boxes, is narrower for the 2022 data compared to the 2018 data. This suggests that the middle 50% of LST values in 2022 were closer together than in 2018, indicating less variability in LST in 2022. In summary, the transition

from natural to artificial turf seems to be associated with a slight decrease in the median LST and a decrease in temperature variability, as well as a reduction in extreme temperature values.

In Figure 2.13, the average LST for the golf courses, which maintained their natural grass surfaces, has decreased from 2018 to 2022. This is indicated by the median value which has shifted downward in 2022 (orange) compared to 2018 (blue). The variability of LST, as represented by the range of the boxes and the whiskers, has also decreased from 2018 to 2022. This suggests a narrower range of temperature fluctuations in 2022. The upper extreme values and the maximum values have also decreased, showing that the highest temperatures recorded were lower in 2022 compared to 2018. Overall, these observations could suggest a general cooling trend over the four years.

The figures indicate that due to the general cooling trend in 2022, the LST reduced for both transitioned and non-transitioned ROIs. The average LST reduction might not be as pronounced for transitioned ROIs as non-transitioned ROIs due to the impact of turf transition. But other factors such as changes in irrigation practices, urban development, or microclimate variations could also affect the LST of these transitioned ROIs.

2.5.1.3 Comparison of the annual average LST of all ROIs between 2018 and 2022

The average LST values of all ROIs were obtained for 2018 and 2022, and then were compared. The mean, median, and standard deviation values of each type of ROI for both years are provided in Table 2.5.

Table 2.5: Average LST values and standard deviation of all ROIs in 2018 and 2022

Transitioned ROIs (Football Fields)		**2018 Natural Grass**	**2022 Artificial Turf**
	Average LST (°C)	38.857	37.975
	Median	39.459	38.008
	Standard Deviation	1.345	1.19
Non-Transitioned ROIs (Golf Courses)		**2018 Natural Grass**	**2022 Natural Grass**
	Average LST (°C)	35.9	33.336
	Median	36.256	33.208
	Standard Deviation	1.629	1.484

Contrary to the common findings in literature, there was no significant increase in average LST for the football fields in 2022 despite the transition to artificial turf. The data shows that the average LST for ROIs that transitioned from natural grass to artificial turf (football fields) was slightly cooler in 2022 compared to 2018. Similarly, non-transitioned areas (golf courses) also recorded a cooler average LST in 2022 than in 2018. This could suggest a general cooling trend in the climate between these years, which may have influenced the lower LST readings in 2022. The average LST difference was higher for the golf courses (2.546°C) than the football fields (0.882°C) (Figure 2.14).

The median LST values declined from 2018 to 2022 for both transitioned (football fields) and non-transitioned (golf courses) ROIs. The decrease was more pronounced in the non-transitioned ROIs, where the median LST dropped by over 3°C.

In comparing the LST values for the years 2018 and 2022, it was observed that the standard deviation, which indicates how spread out the numbers are, decreased for both transitioned and non-transitioned ROIs. This reduction in standard deviation indicates that the LST readings in 2022 were more consistent and less spread out than in 2018. This could suggest that the variability in temperature conditions at each ROI became more uniform over the study period, regardless of the transition from natural to artificial surfaces.

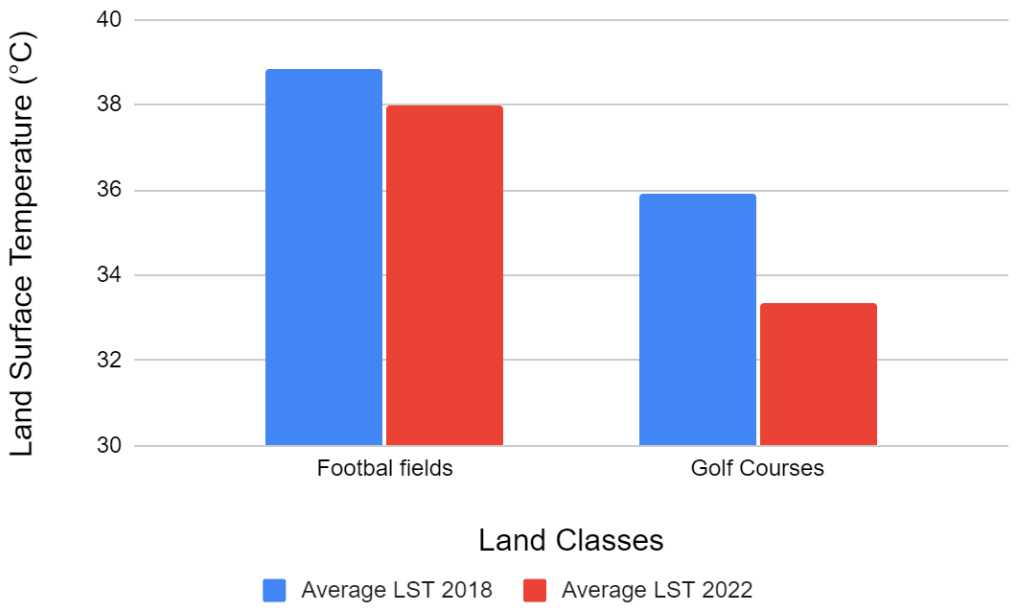

Figure 2.14: Comparative analysis of average LST for Transitioned and Non-Transitioned ROIs between 2018 and 2022

Figure 2.14 shows the comparative analysis of the average LST for transitioned (Football Fields) and non-transitioned ROIs (Golf Courses) between 2018 and 2022. The blue bars indicate the average LST for the year 2018, while the red bars show the average for 2022, facilitating a direct comparison of temperature changes over the four-year span for each land class. It shows that even though both football fields and golf courses had natural grass in 2018, the average LST of the football fields is much higher than the average LST of the golf courses. In 2018, the average LST of the football fields has been found to be 38.857°C and the average LST of golf courses has been found to be 35.9°C. This 2.957°C discrepancy between the average LST of two different types of land classes, despite all the ROIs being natural grass sites in 2018 can be due to the following reasons:

1. Different types of grasses have different thermal properties. Golf courses are typically made of cool season grasses which have higher evapotranspiration rate (3 to 8 millimeters per day) (Huang, 2008). This can affect the surface temperature due to the cooling effect through evapotranspiration.
2. Football fields and golf courses may have different lengths of grass. Longer grasses have increased growth rate, contain higher amounts of chlorophyll and consume greater amounts of water as indicated by Biran et al. (1981) which may contribute to an increased rate of evapotranspiration.
3. The amount and frequency of watering the grass can affect surface temperature. More frequent watering can lower the temperature due to increased evaporation.
4. The level of activity in the fields can impact surface temperature. School football fields may experience more compaction due to regular use, which can reduce the ability of soil to retain moisture, leading to decreased evapotranspiration rate.

5. Intense activity can damage the grass, reducing its overall health and vigor. Damaged or stressed grass may have a reduced transpiration rate which can result in increased surface temperature.
6. The local environment, including the amount of shade, wind patterns, and proximity to buildings or other structures, can influence the temperature. Golf courses typically have varied landscapes having more trees, natural shade, or water bodies nearby, which can contribute to the cooler surface temperatures.

2.5.1.4 Comparison of the seasonal variabilities

LST data for each ROI were categorized and averaged by season—winter, spring, summer, and fall—and subsequently compared between the years 2018 and 2022 for both cases. Box plots were made to show the distribution of the average seasonal LST values at each transitioned and non-transitioned ROI across all seasons (Figure 2.15 and 2.16). The LST values from 2018 were subtracted from those of 2022 to determine the changes. Seasonal LST variation maps were generated for each ROI, illustrating the differences for both cases (Figure 2.17 and 2.18).

a. Case I: 2018 (NG) vs 2022 (AT)

For the ROIs that transitioned from natural grass to artificial turf, a significant increase in LST was observed during the summer season across all ROIs. The most substantial rise was 8.96°C at the football field of Las Vegas High School (T3). During the other seasons, only two ROIs in the winter season exhibited an LST increase of less than 1°C (T3 and T7). Figure 2.15 illustrates the average LST values for each season across the studied ROIs, which transitioned from natural grass to artificial turf between 2018 and 2022.

b. Case II: 2018 (NG) vs 2022 (NG)

For the ROIs that retained natural grass, the LST during the summer season of 2022 increased for 17 ROIs, while a decrease was noted for the remaining ROIs. The greatest increase recorded was 5.86°C at Paradise Park (G13). In the other seasons, LST increase was observed at only one ROI during the winter season. Figure 2.16 shows the average seasonal LST values for each non-transitioned ROIs, which maintained natural grass surfaces between 2018 and 2022.

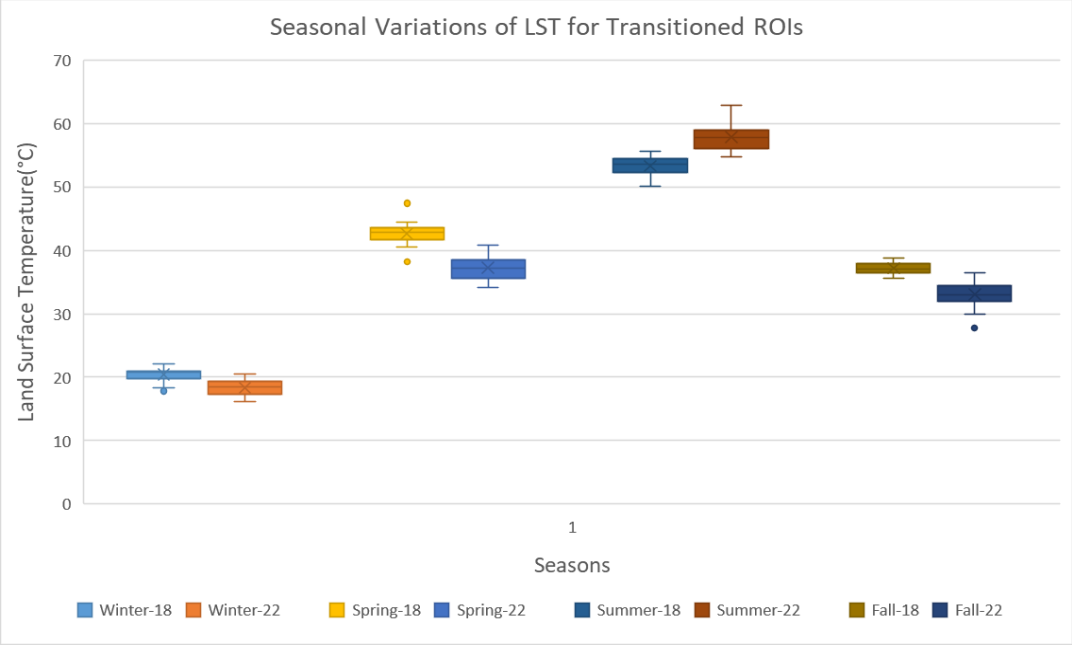

Figure 2.15: Distribution of the average seasonal LST values at each transitioned ROI switched from Natural grass to Artificial turf between 2018 and 2022.

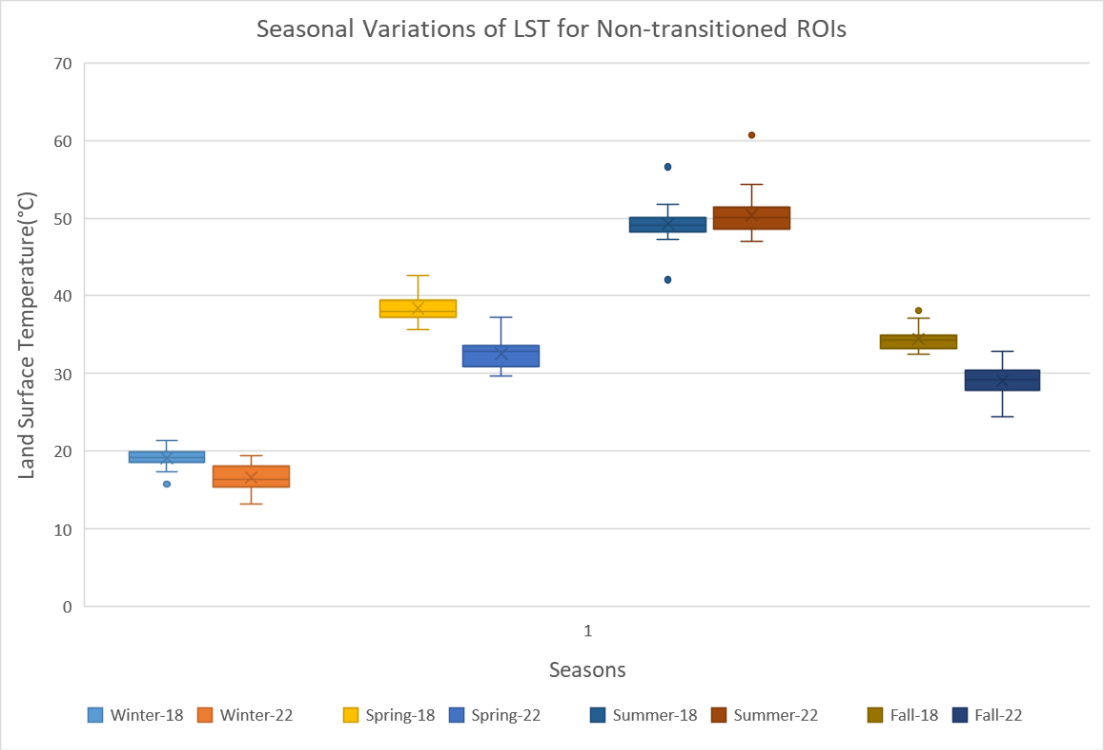

Figure 2.16: Distribution of the average seasonal LST values at each non-transitioned ROI that maintained only natural grass between 2018 and 2022.

From Figures 2.15 and 2.16, a clear seasonal variation in LST can be found for both observed years. The figures show a consistency in the LST patterns indicating that seasonal factors affecting LST are consistent over the years. In Figure 2.15, the transition from natural grass to artificial turf seems to notably affect LST only in the summer, with other seasons not showing significant LST increases. Conversely, Figure 2.16 presents higher LST readings for most non-transitioned ROIs during winter, spring, and fall, with varied results for the summer of 2022 compared to 2018. Some variability in LST was found at each season for both years indicated by the spread of the dots may be due to the locations of the ROIs, type of turf materials and local weather conditions. The transitioned ROIs exhibit a larger temperature disparity in the summer

compared to the non-transitioned ROIs, with the smallest temperature differences observed in winter for both scenarios.

Table 2.6: The median values in LST noted in different seasons for both transitioned and non-transitioned ROIs and the differences in the median values between 2018 and 2022.

Transitioned ROIs			Non-Transitioned ROIs		
Seasons	LST (°C)	2022 - 2018	Seasons	LST (°C)	2022 - 2018
Winter-18	20.79	-2.38	Winter-18	19.23	-2.85
Winter-22	18.41		Winter-22	16.36	
Spring-18	42.83	-5.62	Spring-18	37.99	-5.18
Spring-22	37.21		Spring-22	32.81	
Summer-18	53.52	4.19	Summer-18	49.13	0.97
Summer-22	57.71		Summer-22	50.09	
Fall-18	37.08	-4.04	Fall-18	34.34	-5.16
Fall-22	33.05		Fall-22	29.19	

Table 2.6 shows the median LST values for transitioned and non-transitioned ROIs during various seasons of 2018 and 2022, and the corresponding differences. Positive differences indicate an increase in median LST, while negative values denote a decrease.

There are observable changes in the median LST values from 2018 to 2022 for both transitioned and non-transitioned ROIs across all seasons. LST values vary with seasons, with higher temperatures in the summer months and lower temperatures during the other months. For

transitioned ROIs, the LST values in 2022 have generally increased during the summer and decreased during winter, spring, and fall when compared to 2018. For non-transitioned ROIs, there was a similar pattern of decrease in winter, spring, and fall, but the change in summer is minimal. Transitioned ROIs show a notable increase in summer temperatures from 2018 to 2022, whereas there was a slight increase in LST during summer in non-transitioned ROIs. The transitioning from natural to artificial turf may have influenced the LST values, potentially leading to higher LST in transitioned areas compared to non-transitioned ones, particularly during the summer.

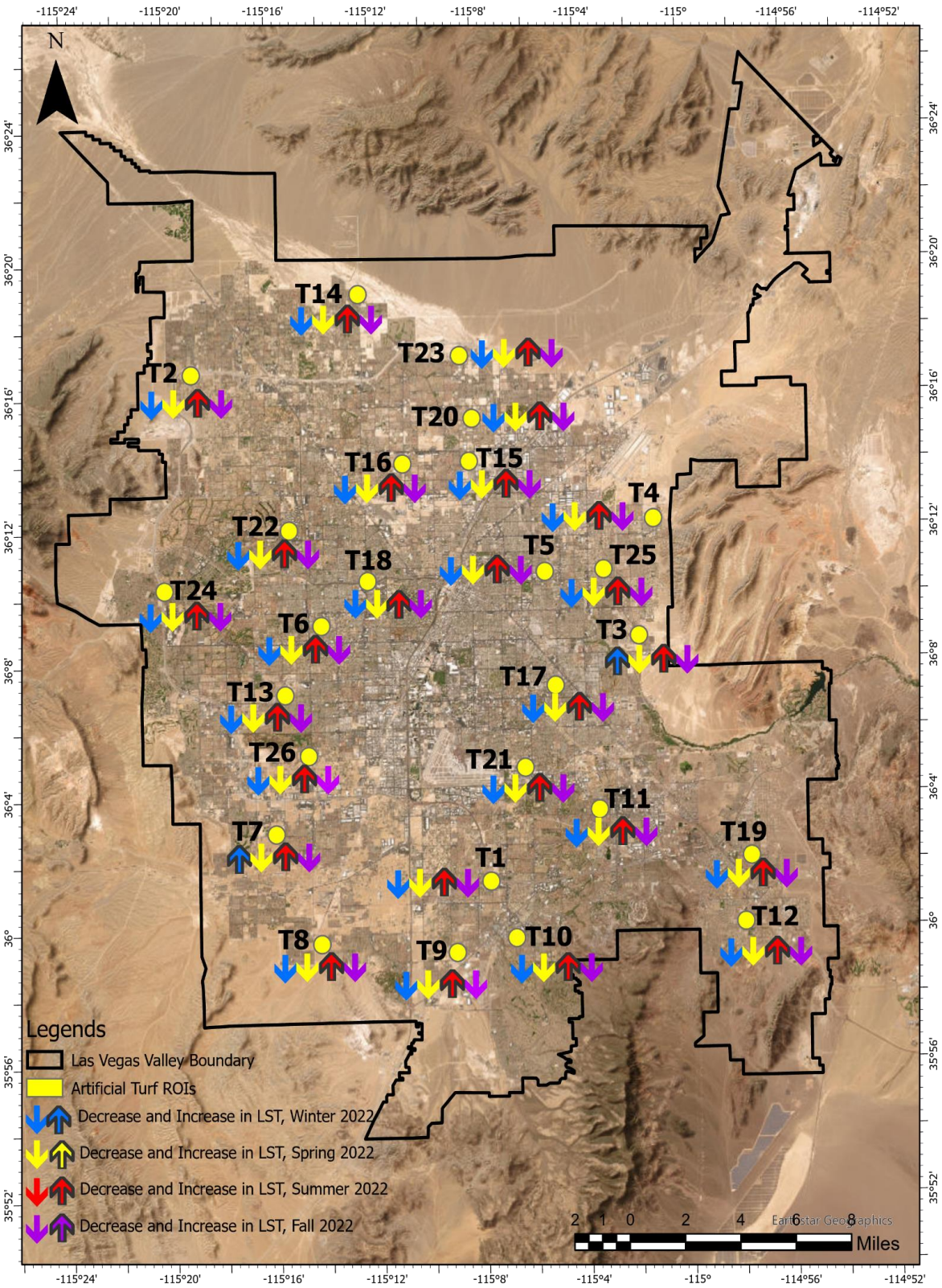

Figure 2.17: Seasonal LST changes for the transitioned ROIs

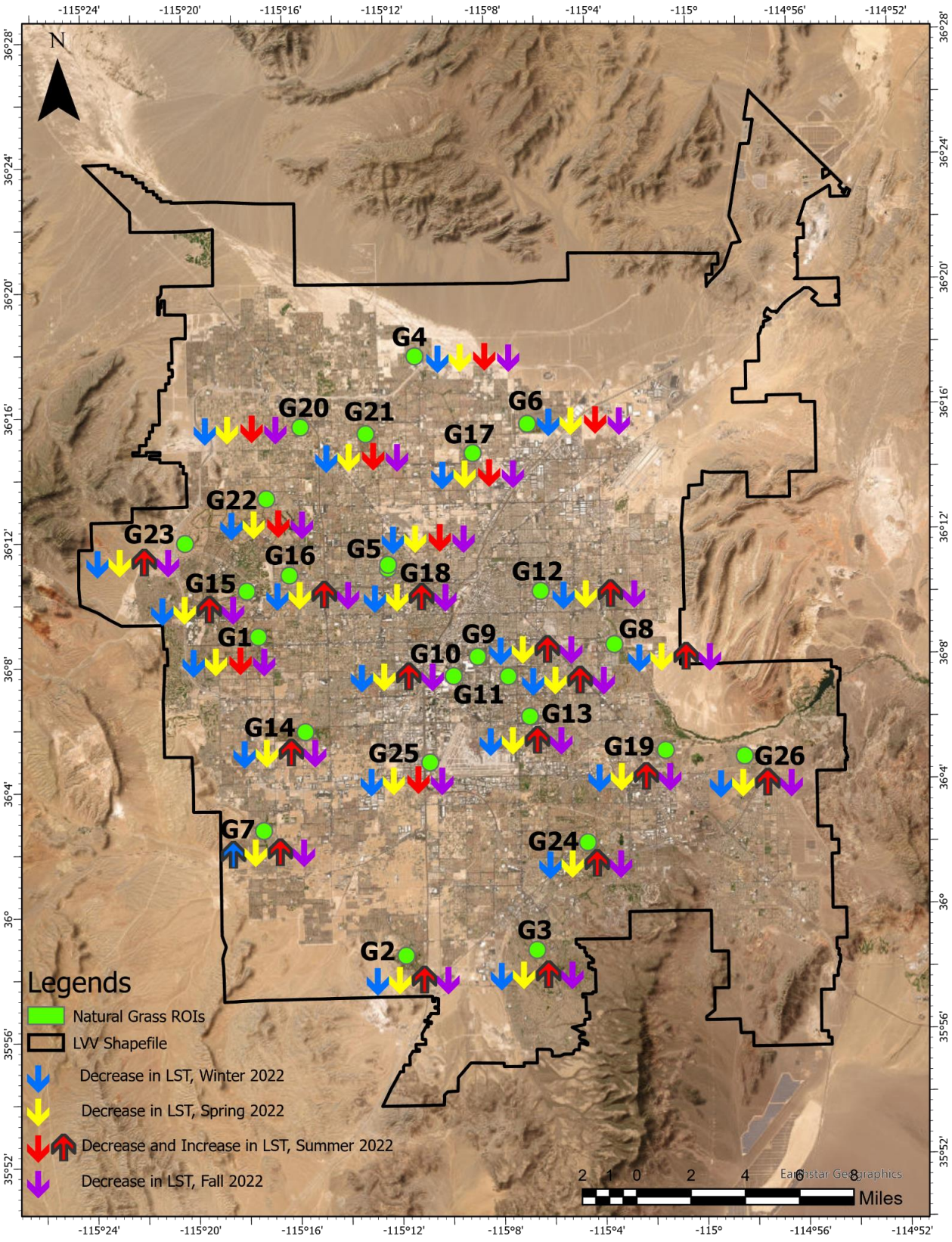

Figure 2.18: Seasonal LST changes for the non-transitioned ROIs

2.5.1.5 T-Tests

The T-Test is utilized in statistics to determine if there are significant differences between two distinct groups. These tests were carried out using R-Studio. For every pair of data, normality checks were conducted. If the data did not meet the normality criteria, Mann-Whitney U Tests were applied. Table 2.4 provides an outline of the paired T-Test varieties executed, the number of tests for transitioned and non-transitioned ROIs, and their respective threshold values. The resulting p-values for each paired T-Test executed in this investigation are presented in Tables 2.7, 2.8, 2.9, and 2.10.

Table 2.7: P-Values for the annual Paired T-Tests considering all LST values from all ROIs (Threshold P-Value = 0.002)

Transitioned ROIs	Non-Transitioned ROIs
1.169e-05*	< 2.2e-16*

Table 2.8: P-Values for the Paired T-Tests at individual ROI performed by taking all the data from the available dates (Threshold P-Value = 0.05)

Land Surface Temperature							
Transitioned ROIs				Non-Transitioned ROIs			
ROIs	P Values	ROIs	P Values	ROIs	P Values	ROIs	P Values
T1	0.62	T14	0.16	G1	0.0006*	G14	0.32
T2	0.41	T15	0.10	G2	0.06	G15	0.04*
T3	0.6	T16	0.14	G3	0.17	G16	0.28
T4	0.11	T17	0.2	G4	0.11	G17	0.01*
T5	0.14	T18	0.06	G5	0.0002*	G18	0.049*
T6	0.12	T19	0.35	G6	0.002*	G19	0.017*
T7	0.60	T20	0.27	G7	0.78	G20	0.01*
T8	0.18	T21	0.22	G8	0.03*	G21	0.01*
T9	0.96	T22	0.83	G9	0.24	G22	0.01*
T10	0.35	T23	0.046*	G10	0.006*	G23	0.04*
T11	0.54	T24	0.63	G11	0.11	G24	0.31
T12	0.64	T25	0.20	G12	0.001*	G25	0.1
T13	0.32	T26	0.51	G13	0.15	G26	0.23

Table 2.9: P-Values for the seasonal Paired T-Tests performed separately for each ROI and for each season (Threshold P-Value = 0.05)

	Transitioned ROIs					Non-Transitioned ROIs			
ROIs	Winter	Spring	Summer	Fall	ROIs	Winter	Spring	Summer	Fall
T1	0.64	0.03*	0.0005*	0.56	G1	0.04	0.0097*	0.73	0.06
T2	0.25	0.10	0.08	0.58	G2	0.26	0.0187*	0.31	0.35
T3	0.56	0.05	0.02*	0.29	G3	0.27	0.10	0.19	0.17
T4	0.07	0.01*	0.008*	0.10	G4	0.17	0.08	0.63	0.17
T5	0.38	0.03*	0.63	0.16	G5	0.008*	0.008*	0.32	0.09
T6	0.17	0.14	0.50	0.09	G6	0.03*	0.01*	0.81	0.12
T7	0.40	0.06	0.06	0.50	G7	0.29	0.04*	0.05	0.58
T8	0.30	0.03*	0.12	0.40	G8	0.21	0.02*	0.07	0.04*
T9	0.49	0.20	0.02*	0.38	G9	0.009*	0.02*	0.33	0.06
T10	0.40	0.25	0.02*	0.37	G10	0.02*	0.008*	0.23	0.07
T11	0.56	0.047*	0.0004*	0.16	G11	0.10	0.01*	0.11	0.04*
T12	0.17	0.07	0.04*	0.26	G12	0.08	0.02*	0.27	0.03*
T13	0.37	0.10	0.53	0.56	G13	0.30	0.03*	0.12	0.05
T14	0.12	0.13	0.003*	0.48	G14	0.37	0.03*	0.17	0.11
T15	0.02*	0.041*	0.20	0.06	G15	0.04*	0.01*	0.77	0.36
T16	0.005*	0.06	0.009*	0.37	G16	0.04*	0.01*	0.24	0.25
T17	0.46	0.03*	0.009*	0.12	G17	0.032*	0.03*	0.87	0.07
T18	0.03*	0.02*	0.84	0.47	G18	0.002*	0.03*	0.63	0.22
T19	0.40	0.19	0.016*	0.13	G19	0.30	0.07	0.65	0.008*
T20	0.09	0.04*	0.29	0.27	G20	0.009*	0.08	0.73	0.38
T21	0.36	0.02*	0.01*	0.08	G21	0.02*	0.11	0.81	0.27
T22	0.04*	0.13	0.06	0.40	G22	0.04*	0.09	0.63	0.32
T23	0.10	0.13	0.03*	0.26	G23	0.05*	0.03*	0.18	0.30
T24	0.91	0.11	0.18	0.51	G24	0.90	0.07	0.09	0.13
T25	0.31	0.002*	0.002*	0.22	G25	0.98	0.03*	0.73	0.16
T26	0.28	0.25	0.08	0.09	G26	0.38	0.12	0.09	0.04*

Table 2.10: P-Values for Combined seasonal Paired T-Tests performed by taking all data from all ROIs for each season (Threshold P-Value = 0.002)

Transitioned ROIs				Non-Transitioned ROIs			
Winter	Spring	Summer	Fall	Winter	Spring	Summer	Fall
0.0007811*	9.518e-12*	6.134e-16*	< 2.2e-16*	1.128e-07*	< 2.2e-16*	1.44e-06*	< 2.2e-16*

The first series of paired T-Test, which aggregated all data from all 26 ROIs throughout the entire year, indicated notable differences in LST for both categories of ROIs, with p-values falling beneath the 0.002 significance level.

In the second series of T-Tests, which analyzed each ROI individually considering all LST data across all available dates, only one transitioned ROI had notable LST differences. However, 14 non-transitioned ROIs exhibited significant LST differences, with p-values dipping below the 0.05 mark. The marked variations in LST for certain non-transitioned ROIs, despite consistent turf types, could be attributed to inherent weather pattern changes over the years. Factors such as temperature shifts, precipitation variances, and cloudiness between 2018 and 2022 might have influenced the LST of these areas. Moreover, fluctuations in soil moisture over time could also contribute to the LST changes.

The third series of paired T-Tests, categorized by the four seasons and conducted for each ROI within each season, showed that only a few transitioned and non-transitioned ROIs at each season experienced a significant LST variation between the years 2018 and 2022, with p-values smaller than 0.05. These results suggest that while there were observable temperature increases

during summer in the transitioned ROIs, they were not statistically significant across the ROIs outside of this season.

Lastly, the combined seasonal T-Tests, which pooled data across all 26 ROIs for each individual season, found significant LST variances for both transitioned and non-transitioned ROIs, as reflected by p-values below 0.002.

According to the first and fourth series of T-Tests, the alternative hypothesis can not be rejected for the transitioned ROIs since significant differences between the pre (2018) and post (2022) conversion were found. These results indicated that the turf conversion has affected LST in these specific areas.

According to the second and third series of T-Tests, the null hypothesis cannot be rejected for the transitioned ROIs, as most of the ROIs did not show any significant differences. These results suggest that the transition from natural to artificial surfaces in these ROIs did not markedly impact LST for transitioned areas.

Moran's I is an index used to determine the degree of spatial correlation which assesses the similarity of observations based on the locations at which they were recorded. Moran's I tests were conducted in ArcGIS Pro to determine if there were any spatial correlations in the LST values for the transitioned ROIs in 2018 and 2022. Table 2.11 presents the conceptualization of spatial relationships, standardization options, the number of neighbors used, Moran's I index values, corresponding P-values, and the resulting pattern classification (Clustered or Random) for each spatial autocorrelation test scenario. Comprehensive reports were generated for each case through ArcGIS Pro and have been added to the appendix (Appendix A.5, A.6, A.7, and A.8).

Table 2.11: Summary of Spatial Autocorrelation Tests using the LST values of 2018 and 2022.

	Conceptualization of spatial relationship	Standardization	Number of Neighbors	Moran's Index	P-Value	Outcome
LST_18	Inverse Distance	Row		0.4247	0.00116	Clustered
LST_18	K Nearest Neighbors	Row	8	0.2262	0.000390	Clustered
LST_22	Inverse Distance	Row		0.0514	0.511432	Random
LST_22	K Nearest Neighbors	Row	8	0.01322	0.466378	Random

The table compares two methods of conceptualizing spatial relationships, "Inverse Distance" and "K Nearest Neighbors". These methods are used to define the weight of influence one observation has on another based on their spatial proximity. For both years, the spatial relationships are standardized using the "Row" option. Standardization can affect the interpretation of spatial relationships by adjusting weights according to some criteria. Moran's I index is a measure of spatial autocorrelation. Positive values close to 1 indicate a clustered pattern (similar values are close together), while values close to 0 indicate a random pattern (no discernible pattern). For LST_18, both tests show significant positive Moran's I value (ranging from 0.2262 to 0.4247), suggesting a clustered pattern of LST. For LST_22, the Moran's I values are low (0.0514 and 0.01322), indicating that the pattern of LST is more random or dispersed. The P-value tests the hypothesis that the observed spatial pattern is generated by a random process. A low P-value (typically <0.05) indicates that the observed spatial pattern is statistically significantly different from random. For LST_18, both tests yield P-values much lower than 0.05, which means

the clustered patterns are statistically significant. For LST_22, the high P-values suggest that the observed pattern cannot be distinguished from random; thus, the hypothesis of random distribution cannot be rejected.

Based on Moran's I Index and p-values, LST_18 shows a statistically significant clustered pattern regardless of the method of conceptualization of spatial relationships or standardization. In contrast, LST_22 shows a random pattern, indicating that the temperatures are randomly distributed in space, or at least, the analysis cannot detect a significant pattern. This information could be used to understand changes in the spatial distribution of temperatures over time.

In the comparative analysis of all the ROIs between the two years studied, it was found that the conversion to artificial turf was associated with higher surface temperatures during warmer months. Conversely, a decrease in the LST was observed during the cooler months. This aligns with research that artificial turf can become much hotter than natural grass under intense sunlight and high temperatures (Jim, 2016). Among the transitioned ROIs, an increase in average LST was recorded in only seven ROIs, while a decrease was noted in the rest. Seasonally, the summer months exhibited a notable surge in LST across all ROIs. In contrast, no other ROI showed any increase in LST during any other seasons except two ROIs which experienced a marginal LST rise of less than 1°C during winter. Two types of T-Tests showed significant changes in LST between 2018 and 2022 where combined data were considered. Other two types of T-Tests results did not reflect significant changes in any ROI.

The components used for infill in artificial turf have low albedo and lower specific heat which induces heat absorption and retention (Liu & Jim, 2021). Additionally, artificial turf exhibits lower volumetric heat capacity (Carvalho et al., 2021) and lower water retaining capacity causing them to heat up more quickly (Liu & Jim, 2021). The hydrophobic nature (Jim, 2016) of artificial

turf materials, along with their limited ability to hold water (Liu & Jim, 2021), prevents them from evaporating moisture. These thermal properties can cause a significant rise in both the surface and the ambient air temperatures near the ground (Liu & Jim, 2021), leading to adverse environmental impacts. This is considered as one of the major disadvantages of using artificial turf.

As shown in Figure 2.4, the average discrepancy between the 10 am temperatures and the daily peaks for specific dates rose marginally from 5.83°C in 2018 to 6.23°C in 2022. The LST readings taken at 10 am are likely a few degrees Celsius below the true peak LST, which could be captured during the hottest part of the day. To obtain the actual peak LST, an on-site infrared radiometer can be employed, rather than relying on satellite-based remote sensing data.

Kanaan et al. (2020) and McNitt et al. (2008) explored strategies for lowering the temperature of artificial turf surfaces. Kanaan et al. (2020) developed a mathematical model to determine the necessary water volume to keep artificial turf temperatures comparable with those of natural grass. The study took place from August 2017 through June 2018 at a baseball field located at New Mexico State University in Las Cruces, New Mexico. Their research indicated that cooling a 100 m^2 artificial turf field with a density of 12.59 kg/m^2 from 60°C to 30°C requires 430,000 liters of 25°C water. They inferred that the choice of artificial turf over natural Bermuda grass in dry climates for saving water is a complex decision. McNitt et al. (2008) investigated different techniques to cool synthetic turf, including various watering and covering strategies, or using infill mixed with calcined clay to boost moisture retention. They found that irrigation had the most prolonged cooling effect on synthetic turf surfaces.

Duble (1993) discussed about natural grass irrigation and suggested that irrigation schedules ought to be determined by factors such as the total evapotranspiration loss, the capacity

of the soil to hold moisture, the depth to which roots effectively grow, the rate at which water penetrates the soil, and the specific variety of turfgrass for natural turfgrass water use to be most efficient. Intense upkeep of areas like sports fields and golf course fairways in the southern states requires irrigation compensates for about half of the turf's water requirements, as natural rainfall is insufficient. Consequently, to maintain warm season turfgrasses, it's necessary to apply 20 to 30 inches of water annually in the South, and 40 to 50 inches in the West. These amounts translate to roughly 0.5 to 1.5 million gallons per acre, or 12 to 36 thousand gallons for every 1,000 square feet of turf, signifying a substantial financial cost due to the volume of water utilized (Duble, 1993). The study was done in Texas.

To compare the water requirements of cooling artificial turf versus maintaining natural grass according to Kannan et al. (2020) and Duble (1993) studies, specific contexts need to be considered in which water is being used for each.

For artificial turf, Kannan et al. (2020) found that to cool a 100 m^2 Artificial turf field with a density of 12.59 kg/m^2 from 60°C down to 30°C, it takes 430,000 liters (113593.983 gallons) of water at a temperature of 25°C. This is a large amount of water required for a significant cooling effect, reflecting a single intensive cooling event.

In contrast, for natural grass, the water usage is spread throughout the year to maintain the turf. In the South, warm season turfgrasses require 20 to 30 inches of water per year, and in the West, they require 40 to 50 inches. These figures amount to approximately 0.5 to 1.5 million gallons per acre annually, or 12 to 36 thousand gallons for every 1,000 square feet (93 m^2). This water use is for regular maintenance and sustenance of the grass, rather than for cooling.

This suggests that the immediate water requirement for cooling artificial turf is similar to the annual water requirement for sustaining a slightly smaller area of natural grass, underlining the high immediate water demand for cooling artificial turf surfaces. However, it's important to note that the artificial turf may not require such intense cooling on a regular basis, whereas natural grass needs consistent watering throughout the growing season to remain healthy.

2.5.2 Surface Albedo

According to the literature review, artificial turf absorbs most of the solar radiation (Jim, 2017; Carvalho et al., 2021) due to having lower surface albedo (Yaghoobian et al., 2010; Carvalho et al., 2021; Jim, 2017) which is directly associated with the surface temperature. The lower surface albedo of the artificial turf leads to significant heat absorption and retention, due to the heat-absorbing characteristics of different artificial turf materials, such as plastic fibers and rubber infill materials (Jim, 2016). Artificial turf surfaces radiate thermal radiation after absorbing the solar radiation which increases the ambient temperature (Jim, 2017).

To measure the impact of artificial turf on the surface albedo, 45 surface albedo maps were generated for 2018 and 2022 using the GEE platform. Landsat 8 satellite was used to generate maps. The maps were then imported to ArcGIS pro, where they were clipped according to the shapefile of LVV. A ROI map showing 26 ROIs that have been switched from natural to artificial grass between 2018 and 2022, and 26 ROIs that did not go through any transition between the time period, was used to measure the average albedo values at these ROIs. The data were gathered in an excel sheet for further analysis.

Areas with lower albedo values such as closer to 0 are darker on the map, indicating that they reflect a smaller portion of the incoming sunlight. These areas are covered with darker

surfaces such as water bodies or dense forests. Areas with higher albedo values such as closer to 0.4 are lighter on the map, indicating that they reflect a higher portion of the incoming sunlight. These areas are covered with lighter surfaces, such as snow, ice, or urban areas with many buildings.

2.5.2.1 Comparison of the surface albedo for each ROI across various dates within the years 2018 and 2022

a. Case I: 2018 (NG) vs 2022 (AT)

Between 2018 and 2022, selected ROIs within high school football fields have undergone a shift from natural grass to artificial turf. In 2018, when the ROIs featured natural grass, albedo measurements fluctuated between 0.032 and 0.219. Conversely, in 2022, following the transition to artificial turf, the range is between 0.007 and 0.143.

b. Case II: 2018 (NG) vs 2022 (NG)

The ROIs that have remained unchanged are predominantly golf courses. Albedo measurements in 2018 varied between 0.045 and 0.198, whereas in 2022, they spanned from 0.024 to 0.242. The pattern of albedo values over the two years exhibited some consistency, with certain values rising in 2022 and others decreasing.

The distribution of albedo values for 26 transitioned and non-transitioned ROIs are provided in Appendix A.3 and Appendix A.4, respectively. Blue boxes represent the albedo values for the year 2018, and orange boxes show albedo values for the year 2022. Each box plot illustrates the variation in albedo readings across multiple dates within the respective years. The Y-axis indicates the Albedo range.

After the turf conversion (2022), the albedo measurements for all the transitioned ROIs, as depicted in Appendix A.3, were reduced compared to those in 2018, with the newer data also exhibiting less fluctuation. Conversely, Appendix A.4 presented a varied set of outcomes.

2.5.2.2 Comparison of the average surface albedo for each ROI between 2018 and 2022

The average surface albedo values for each ROI were calculated for the years 2018 and 2022, and comparisons were drawn by subtracting the average albedo of 2018 from that of 2022. Subsequently, scatter plots were generated to visualize the data where blue dots represent the average albedo for each ROI in 2018, and red dots for 2022.

a. Case I: 2018 (NG) vs 2022 (AT)

Figure 2.19 shows the average albedo at each ROI for the transitioned ROIs. The plot clearly shows that the albedo values in 2022 at all the ROIs are lower than the albedo at 2018. The value ranged from -0.024 to -0.076.

b. Case II: 2018 (NG) vs 2022 (NG)

Figure 2.20 shows the average albedo at each ROI for the non-transitioned ROIs. The plot shows that the albedo values in 2022 decreased at 8 ROIs and increased in the rest of the ROIs. The value ranged from 0.026 to -0.0008.

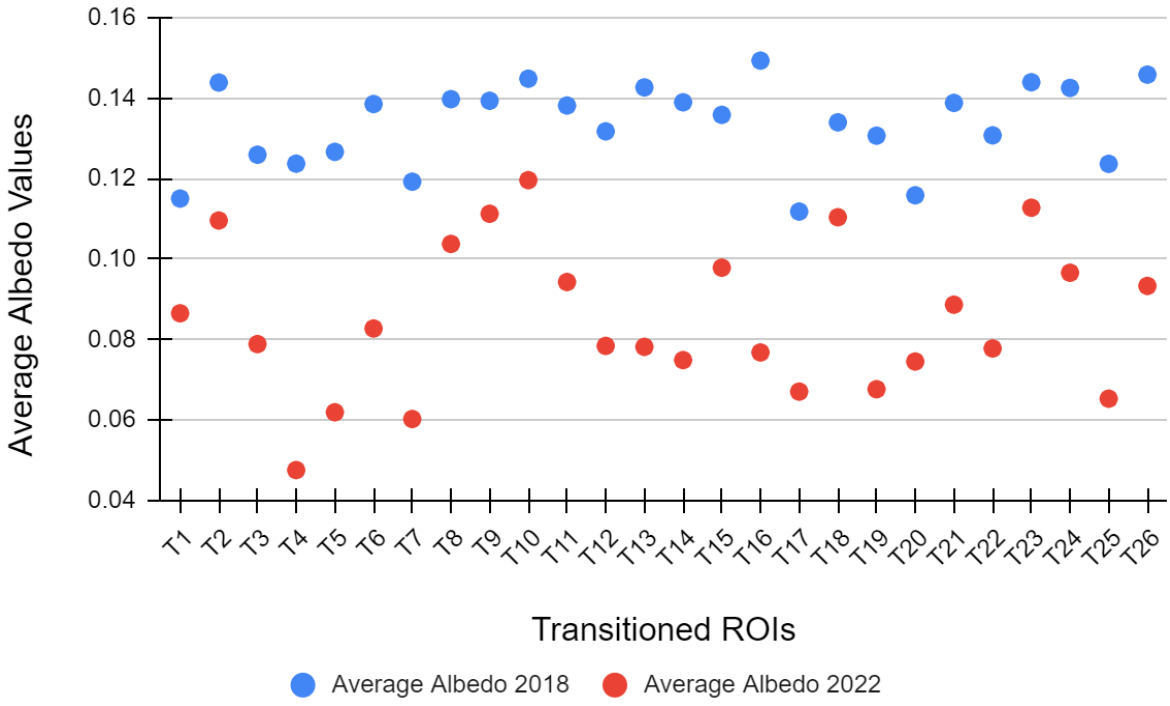

Figure 2.19: Average albedo differences at each transitioned ROI between 2018 and 2022

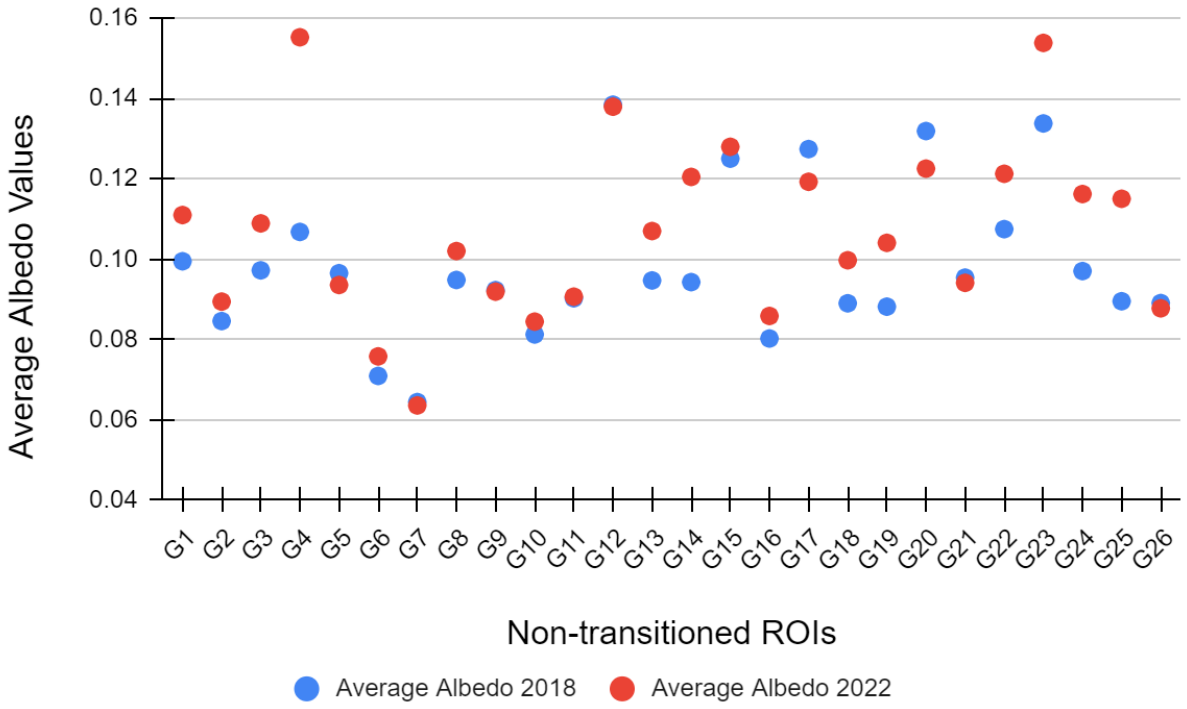

Figure 2.20: Average albedo differences at each non-transitioned ROI between 2018 and 2022

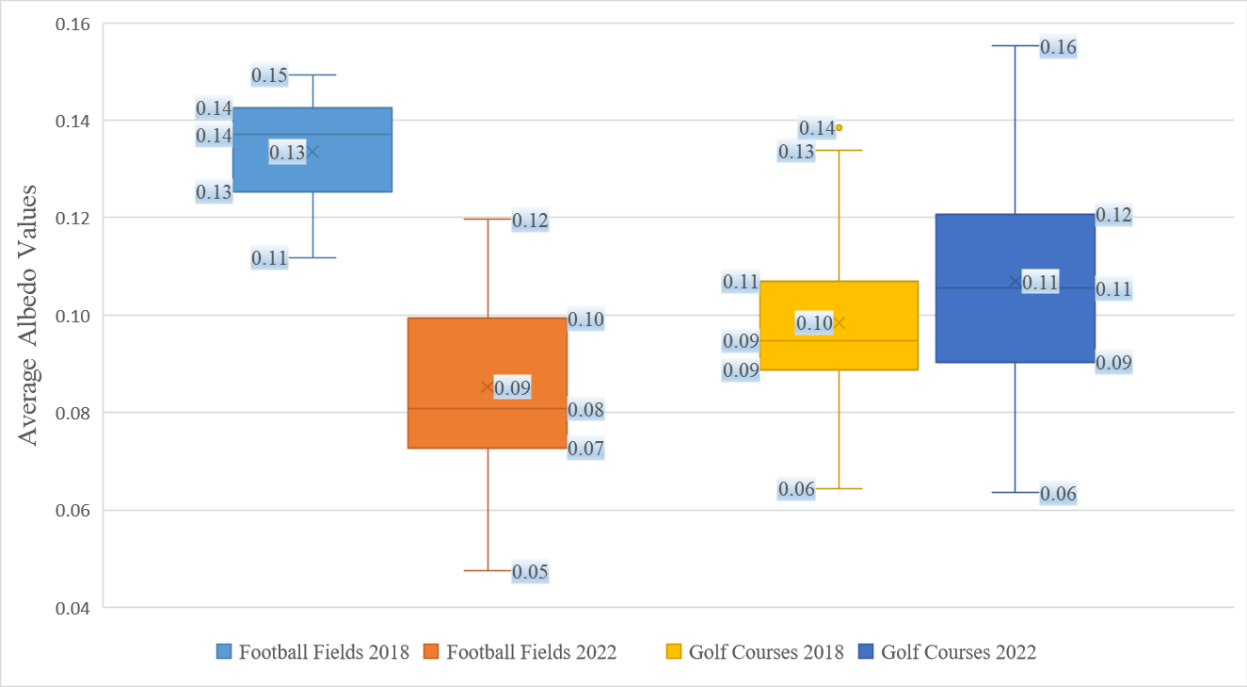

Figure 2.21: Distribution of the average albedo for Football fields (Transitioned ROIs) and Golf Courses (Non-transitioned ROIs), comparing data from 2018 and 2022.

Figure 2.21 presents a comparison of the average surface albedo values for football fields and golf courses. It highlights the change in median albedo values for football fields between 2018 and 2022, reflecting the effects of shifting from natural to artificial turf with a noticeable median decrease of 0.049 in albedo post-conversion. In contrast, the median albedo values for golf courses over the same period show a minimal difference of 0.009, suggesting that the preservation of natural grass surfaces has little to no significant impact on albedo values over time.

2.5.2.3 Comparison of the annual average albedo values of all ROIs between 2018 and 2022

The annual average albedo values of all ROIs were obtained for 2018 and 2022, and then were compared. The mean values of each type of ROI for both years are provided in Table 2.12.

Table 2.12: Average albedo values of all ROIs for 2018 and 2022

Transitioned ROIs (Football Fields)		**2018 Natural Grass**	**2022 Artificial Turf**
	Average Albedo	0.134	0.085
	Median	0.137	0.081
Non-Transitioned ROIs (Golf Courses)		**2018 Natural Grass**	**2022 Natural Grass**
	Average Albedo	0.098	0.107
	Median	0.095	0.106

In 2018, the average albedo value for the football fields was 0.134 when it had natural grass surfaces, while in 2022, it was 0.085 for the artificial turf surfaces. This average albedo value for the artificial turf ROIs closely aligns with the findings of C.Y. Jim in his 2016 study, where he reported an average albedo value of 0.073 from an artificial turf field. Additionally, for the non-transitioned ROIs, the average albedo values for natural grass were 0.098 in 2018 and slightly higher at 0.107 in 2022 which indicates that maintaining natural grass did not significantly change the albedo over time. The average albedo decreased by 0.049 for the transitioned ROIs and increased by 0.009 for the non-transitioned ROIs in 2022.

Even though they are composed of the same natural grass surfaces, the golf courses showed less seasonal fluctuation in albedo compared to the football fields during the year 2018. 1n 2018, the average albedo for the football fields and the golf courses were 0.134 and 0.098 respectively. Despite having the same type of surfaces, golf courses had 0.036 lower albedo than the football fields. The discrepancy between the albedo values of the football fields and the golf courses, despite having the same turf type in 2018, can be attributed to the following reasons:

1. Different land types may have different species of grass having various surface characteristics such as different leaf sizes, shapes, colors and textures that, in turn, can affect albedo.
2. The density of the grass can influence the albedo. Denser grass has decreased surface albedo (Tian et al, 2014). Denser grass might retain more moisture content contributing to lower albedo.
3. Since dry soil has more albedo values than wet soil (Ponce et al., 1997), if the football fields have dryer soil conditions than the golf courses, it can contribute to the higher albedo values for the football fields.
4. Different maintenance methods, such as mowing, watering or fertilizations, can influence the surface characteristics of the grass, thereby affecting their reflective properties.
5. The presence of tall trees in the golf courses can cast shadows, reducing the amount of sunlight that reaches the grass, and can contribute to the lower albedo values for the golf courses.

6. Usage patterns of the surfaces can influence the albedo values. Golf courses are not used at the same level as football fields, potentially resulting in less seasonal damage to the grass.

2.5.2.4 Comparison of the seasonal variabilities

Albedo values for each ROI were categorized and averaged by season—winter, spring, summer, and fall—and subsequently compared between the years 2018 and 2022 for both cases. Box plots were made to show the distribution of the average seasonal LST values at each transitioned and non-transitioned ROI across all seasons (Figure 2.22). The albedo values from 2018 were subtracted from those of 2022 to determine the seasonal changes. Seasonal albedo variation maps were generated for each ROI, illustrating the differences for both cases (Figure 2.23 and 2.24).

a. Case I: 2018 (NG) vs 2022 (AT)

For the ROIs that underwent a change from natural grass to artificial turf, a slight increase in albedo values was observed during the summer season for only two ROIs. Conversely, the albedo values decreased for each ROI during the rest of the year. Figure 2.22(a) showcases the changes in surface albedos for these transitioned ROIs across the different seasons, highlighting the environmental impact of altering the surface materials.

b. Case II: 2018 (NG) vs 2022 (NG)

The ROIs that maintained their natural grass surfaces displayed varying albedo results seasonally. In winter, albedo values decreased for four ROIs and rose for the remainder. In spring, six ROIs showed a decrease, while the others showed an increase. The trend continued into summer, with thirteen ROIs experiencing a decrease, and in fall, eighteen out of twenty-six ROIs had lower albedo values. This suggests a seasonal pattern with a general decrease in surface albedo

from winter to fall. Notably, Craig Ranch Regional Park (G17) and Painted Desert Golf Club (G20), both situated in northern Las Vegas, saw albedo reductions in all seasons. These changes are detailed in Figure 2.22(b), which presents seasonal albedo shifts for the non-transitioned ROIs.

ROIs that underwent a transition exhibited persistently reduced albedo levels throughout all seasons in 2022, with the most significant differences occurring during the winter. In contrast, ROIs that did not transition displayed fluctuating albedo measurements across all seasons. Some variability in albedo was found for both transitioned and non-transitioned ROIs that could be attributed to factors such as their specific geographic locations, the local weather patterns, and other environmental conditions.

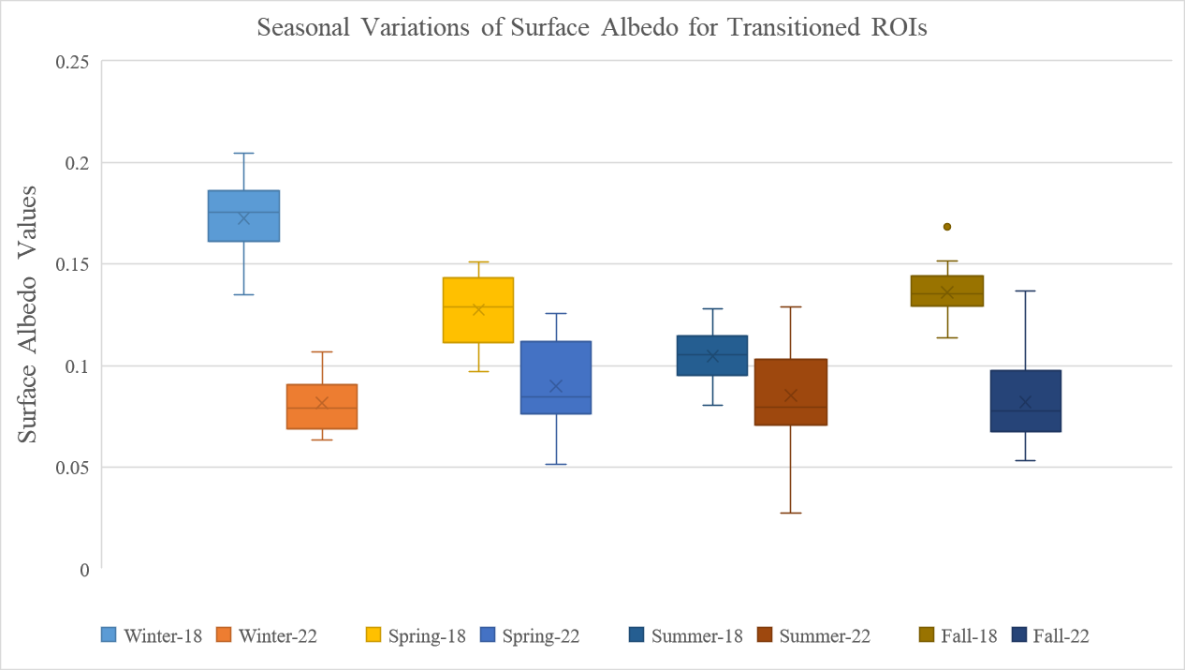

(a)

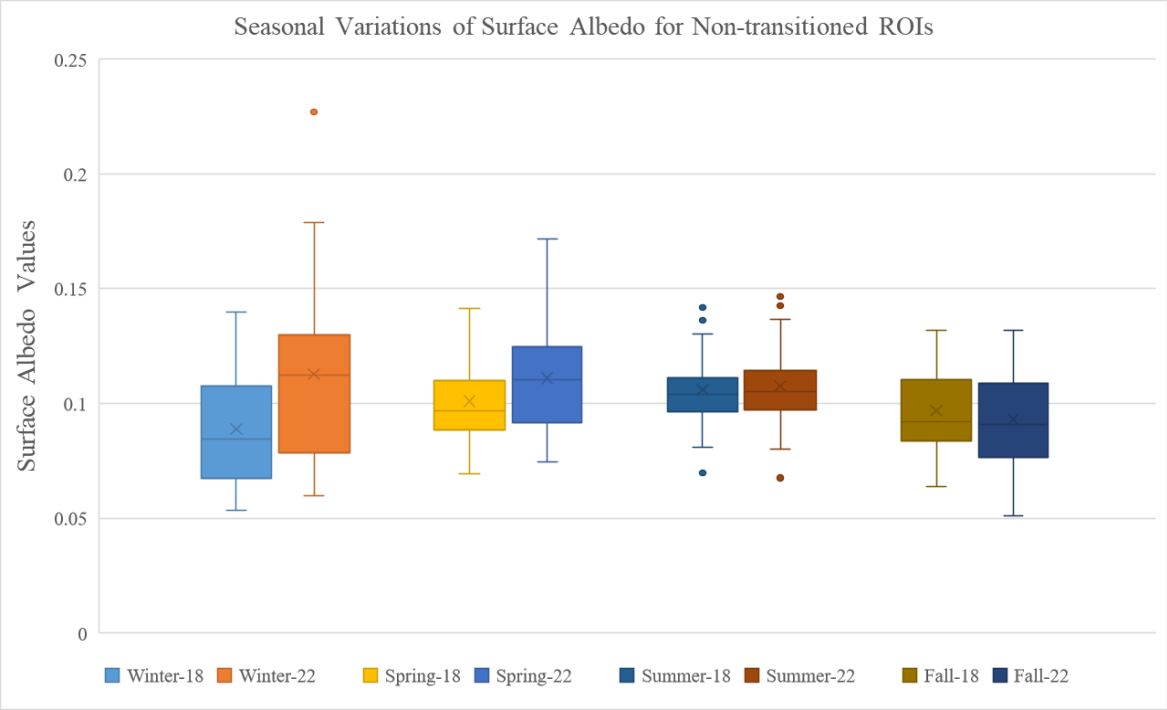

(b)

Figure 2.22: (a) Average seasonal albedo values for Transitioned ROIs; (b) Average seasonal albedo values for non-transitioned ROIs

There was a noticeable reduction in albedo values across most ROIs in 2022, with the readings displaying uniformity across the seasons. Several variables have been identified by Ponce et al. (1997) as key determinants of surface albedo, which include: (1) the solar elevation or zenith angle at different times of the day; (2) the seasonality of the year; (3) the landscape's topography; (4) the type and density of vegetation; (5) the roughness and the texture of the surface; (6) the composition and color of the soil and rocks; (7) the level of moisture present in the soil; and (8) the presence of snow which generally has a high albedo. Human activities are noted to have the potential to modify factors such as vegetative cover, surface roughness, and soil moisture.

The artificial turf, composed of synthetic fibers, lacks the natural capacity for seasonal adaptation, remaining unaffected by diverse weather conditions such as rain, growth, or trimming, which typically influence natural grass, leading to consistent albedo readings for artificial turf surfaces. The differing maintenance requirements between the two surface types also contribute to the variation in albedo. The application of various fertilizers, pesticides, and chemicals can affect the color and density of both types of turfs, thereby influencing the albedos differently. As for artificial turf, the infill materials used can vary in color and size, which directly impacts the albedo. When these infill materials are replenished, it can lead to a shift in the reflective properties of the artificial surfaces. Research by Myers and Allen (1968) established that an increase in the particle's diameter typically leads to a reduction in reflectance.

On the other hand, the albedo values in 2018 exhibited distinct seasonal trends, with higher reflectivity in the winter and reduced albedo during the summer months. This seasonal behavior is attributed to the natural cycle of grass, which becomes dormant and less green during winter, and can be covered by snow which can increase their reflectivity. While in the summer season, as the vegetation absorbs more sunlight for photosynthesis, grasses are healthier and greener which

results in a lower albedo value. According to Way et al. (2017), photosynthetic capacity of vegetation increases in the early summer with peak in mid-summer and then declines over the late summer and autumn. Also, the moisture content can vary greatly during different seasons affecting the albedo values. Vegetation needs more water during summer months than winter months. Wet soils tend to have lower albedo than dry soils due to the absorption characteristics of water (Ponce et al., 1997). Dickinson (1983) noted that soil moisture can substantially reduce albedo, often by around half.

Table 2.13: The median values in Surface Albedo noted in different seasons for both transitioned and non-transitioned ROIs and the differences in the median values between 2018 and 2022.

Transitioned ROIs			Non-Transitioned ROIs		
Seasons	Surface Albedo	2022 - 2018	Seasons	Surface Albedo	2022 - 2018
Winter-18	0.18	-0.10	Winter-18	0.08	0.03
Winter-22	0.08		Winter-22	0.11	
Spring-18	0.13	-0.04	Spring-18	0.10	0.01
Spring-22	0.08		Spring-22	0.11	
Summer-18	0.11	-0.03	Summer-18	0.10	0.001
Summer-22	0.08		Summer-22	0.10	
Fall-18	0.14	-0.06	Fall-18	0.09	-0.0009
Fall-22	0.08		Fall-22	0.09	

Table 2.13 shows the median albedo values for transitioned and non-transitioned ROIs during various seasons of 2018 and 2022, and the corresponding differences. Positive differences indicate an increase in median LST, while negative values denote a decrease.

The football fields, which are the transitioned ROIs that shifted from natural to artificial turf between 2018 and 2022, experienced a decrease in surface albedo during all seasons. The decreased albedo values in the post conversion during all seasons suggest that the artificial turf has a lower albedo than the natural turf. For the non-transitioned ROIs, which are the golf courses that maintained their natural grass surfaces, the changes in albedo are very slight in all seasons suggesting that the albedo for natural grass surfaces remains relatively stable year over year. The greater changes in albedo values for the transitioned ROIs compared to the non-transitioned ones could be due to the difference in surface materials and how they interact with solar radiation across different seasons. The data indicates that converting to artificial turf can have a noticeable impact on the reflective properties of the surface.

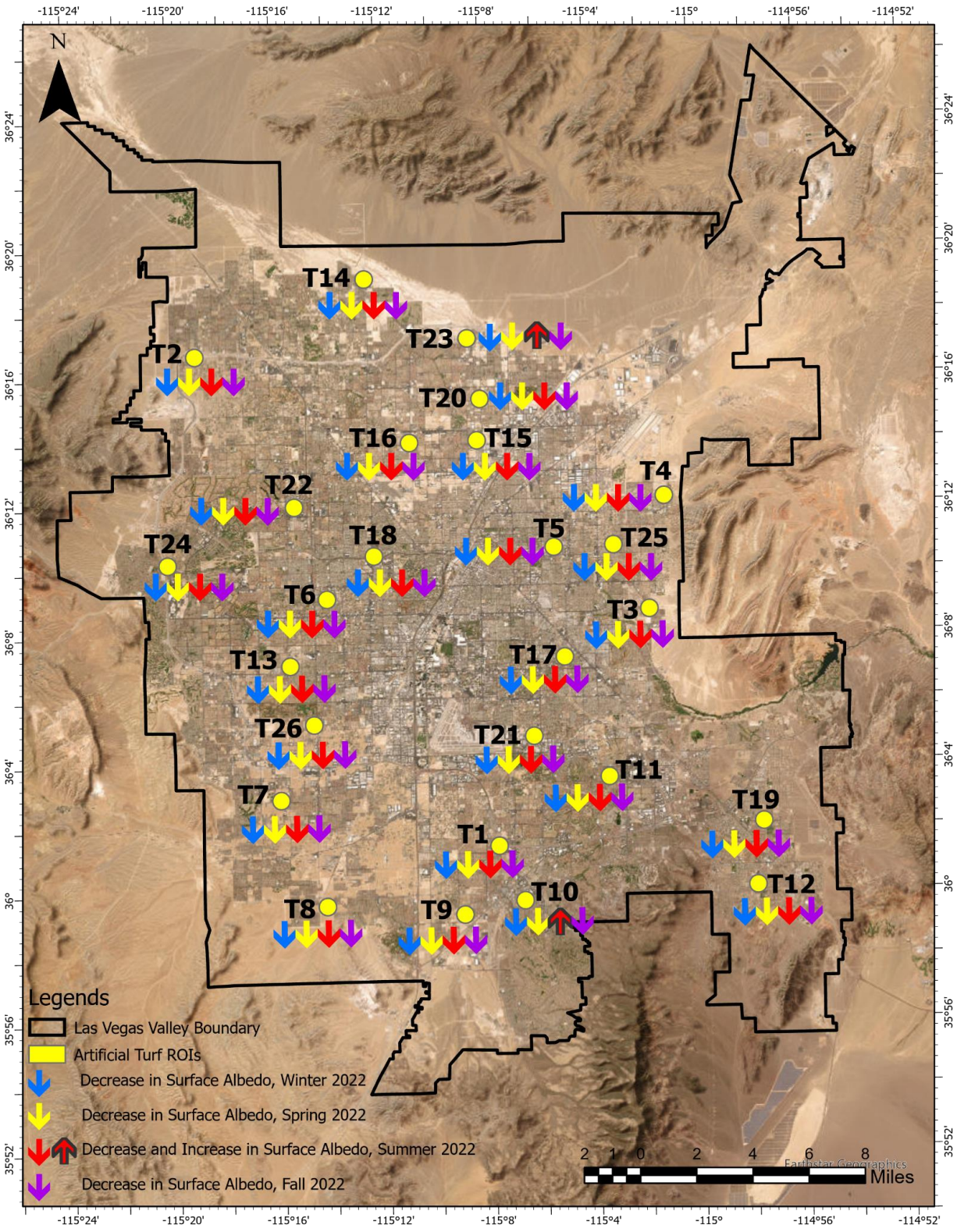

Figure 2.23: Seasonal albedo changes for the transitioned ROIs

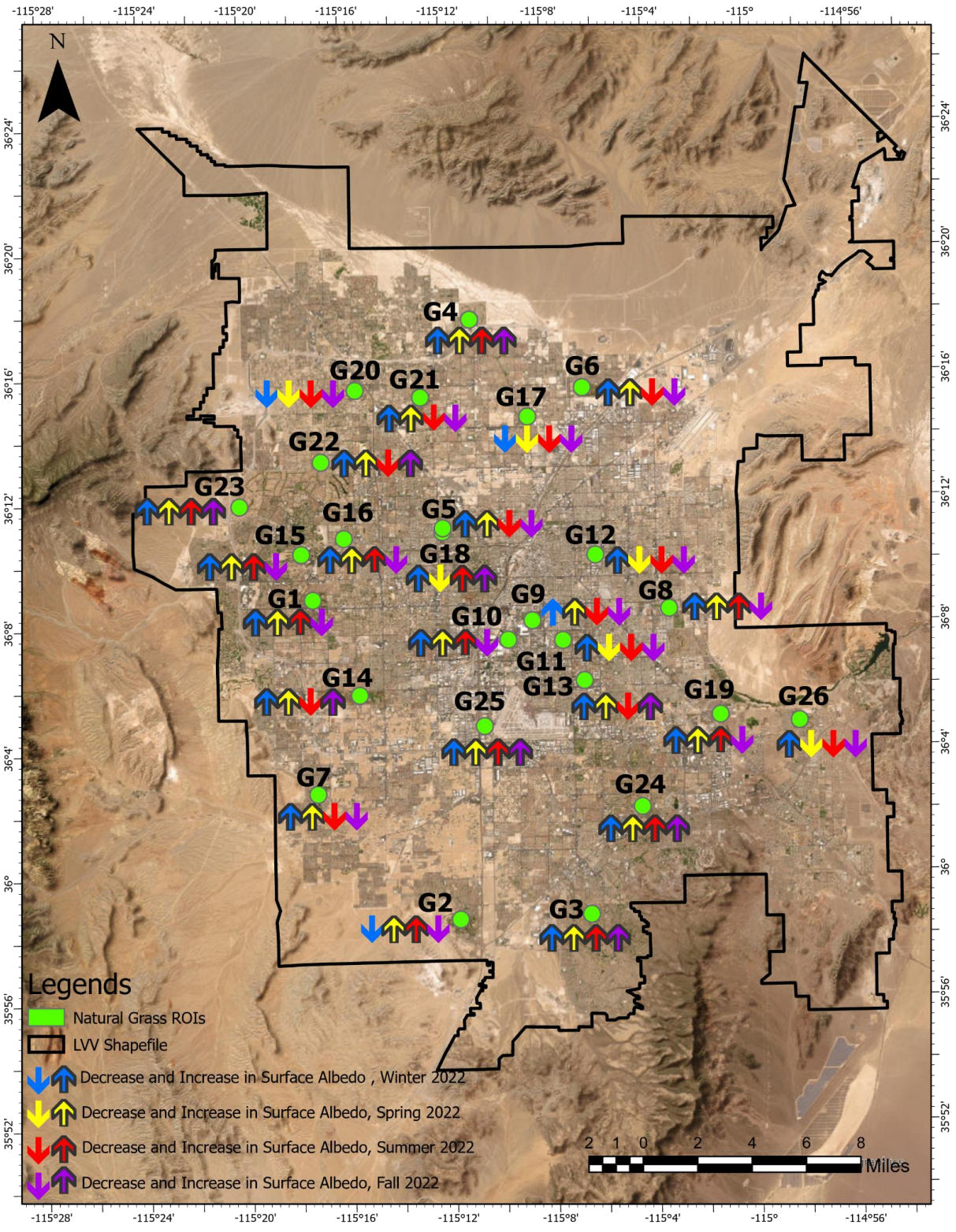

Figure 2.24: Seasonal albedo changes for the non-transitioned ROIs

2.5.2.5 T-Tests

Four series of paired T-Tests were conducted to find any significant differences in the surface albedo values between 2018 and 2022 for both transitioned and non-transitioned ROIs. The tests were performed in R-Studio. Normality tests were done for all pairs of data. Mann Whitney U Tests were performed for the pairs that did not pass the normality tests. Table 2.4 provides an outline of the paired T-Test varieties executed, the number of tests for transitioned and non-transitioned ROIs, and their respective threshold values. The resulting p-values for each paired T-Test executed in this investigation are presented in Tables 2.14, 2.15, 2.16, and 2.17.

Table 2.14: P-Values for the annual Paired T-Tests considering all LST values from all ROIs (Threshold P-Value = 0.002)

Transitioned ROIs	Non-Transitioned ROIs
< 2.2e-16*	1.143e-10*

Table 2.15: P -Values for the Paired T-Tests at individual ROI performed by taking all the data from the available dates (Threshold P-Value = 0.05)

Surface Albedo							
Transitioned ROIs				Non-Transitioned ROIs			
ROIs	P Values	ROIs	P Values	ROIs	P Values	ROIs	P Values
T1	0.0002*	T14	1.526e-05*	G1	0.07	G14	0.009*
T2	1.144e-05*	T15	1.907e-05*	G2	0.95	G15	0.42
T3	3.815e-06*	T16	4.584e-07*	G3	0.0007*	G16	0.2
T4	4.726e-08*	T17	1.841e-07*	G4	0.001*	G17	0.05*
T5	3.815e-06*	T18	0.0002*	G5	0.31	G18	0.27
T6	1.526e-05*	T19	7.629e-06*	G6	0.49	G19	0.06
T7	3.052e-05*	T20	0.0003701*	G7	0.9	G20	0.009*
T8	0.0005*	T21	2.168e-07*	G8	0.06	G21	0.42
T9	0.001*	T22	0.0001*	G9	0.38	G22	0.16
T10	0.0002*	T23	0.0001*	G10	0.85	G23	0.002*
T11	3.797e-05*	T24	3.052e-05*	G11	0.72	G24	0.0003*
T12	2.508e-05*	T25	7.629e-06*	G12	0.97	G25	0.002*
T13	3.577e-06*	T26	0.002*	G13	0.02293*	G26	0.18

Table 2.16: P-Values for the seasonal Paired T-Tests performed separately for each ROI and for each season (Threshold P-Value = 0.05)

	Transitioned ROIs					Non-Transitioned ROIs			
ROIs	Winter	Spring	Summer	Fall	ROIs	Winter	Spring	Summer	Fall
T1	0.003*	0.03*	0.73	0.01*	G1	0.03*	0.16	0.58	0.88
T2	0.01*	0.01*	0.13	0.20	G2	0.77	0.24	0.95	0.5
T3	0.002*	0.06	0.002*	0.04*	G3	0.25	0.7	0.07	1
T4	0.003*	0.06	0.01*	0.01*	G4	0.001*	0.01*	0.2	0.53
T5	0.001*	0.003*	0.01*	0.02*	G5	0.004*	0.96	0.05	0.32
T6	0.13	0.04*	0.06	0.05	G6	0.46	0.19	0.76	0.86
T7	0.13	0.10	0.06	0.25	G7	0.63	0.25	0.63	0.25
T8	0.003*	0.48	0.45	0.01*	G8	0.72	0.4	0.33	0.82
T9	0.21	0.13	0.46	0.04*	G9	0.14	0.43	0.63	0.45
T10	0.01*	0.29	0.91	0.08	G10	0.19	0.14	0.48	0.1
T11	0.01*	0.06	0.31	0.06	G11	0.15	1	0.1	0.57
T12	0.25	0.005*	0.03*	0.03*	G12	0.70	0.59	0.63	0.33
T13	0.003*	0.004*	0.002*	0.01*	G13	0.04*	0.06	0.69	0.49
T14	0.002*	0.03*	0.003*	0.001*	G14	0.001*	0.13	0.93	0.89
T15	0.02*	0.003*	0.26	0.05*	G15	0.49	0.71	1	0.88
T16	0.12	0.01*	0.004*	0.02*	G16	0.04*	0.19	0.13	0.16
T17	0.01*	0.005*	0.004*	0.25	G17	0.96	0.46	0.25	0.02
T18	0.05*	0.25	1	0.19	G18	0.31	0.63	0.3	0.79
T19	0.03*	0.03*	0.0002*	0.01*	G19	0.13	0.04*	0.01*	0.40
T20	0.10	0.18	0.44	0.13	G20	1	0.06	0.01*	0.12
T21	0.98	0.001*	0.06	0.08	G21	0.10	0.7	0.13	0.09
T22	0.02*	0.02*	0.002*	0.09	G22	0.09	0.81	0.84	0.6
T23	0.04*	0.09	0.02	0.13	G23	0.02*	0.13	0.06	0.9
T24	0.02*	0.13	0.84	0.03*	G24	0.11	0.1	0.16	0.84
T25	0.003*	0.03*	0.14	0.06	G25	0.16	0.11	0.1	0.32
T26	0.002*	0.09	0.001*	0.63	G26	0.93	0.37	0.43	0.27

Table 2.17: P-Values for Combined seasonal Paired T-Tests performed by taking all data from all ROIs for each season (Threshold P-Value = 0.002)

Transitioned ROIs				Non-Transitioned ROIs			
Winter	Spring	Summer	Fall	Winter	Spring	Summer	Fall
2.55e-15*	< 2.2e-16*	< 2.2e-16*	8.131e-16*	6.684e-11*	1.42e-06*	0.37	0.009*

The first series of paired T-Test, which pooled all yearly data from all 26 ROIs, uncovered notable albedo differences for both transitioned and non-transitioned ROIs, with p-values falling beneath the 0.002 significance level.

The second series of T-Tests, which examined each ROI individually across all collected data points, indicated significant albedo variations for all transitioned ROIs and for nine non-transitioned ROIs, achieving p-values below the 0.05 threshold. The findings from these T-Tests suggest that the shift from natural to artificial turf had a significant impact on the albedo of the transitioned ROIs during the study period.

The third set of paired T-Tests, organized by the four seasons, and executed for each ROI within those seasons, showed significant albedo alteration for 19, 14, 11, and 13 transitioned ROIs during Winter, Spring, Summer, and Fall, respectively, with p-values smaller than 0.05. Only a few non-transitioned ROIs showed significant differences in albedo between 2018 and 2022 at various seasons.

Lastly, the combined Seasonal T-Tests, which aggregated data from all ROIs by season, indicated substantial albedo differences for both transitioned and non-transitioned ROIs, with p-values below the 0.002 threshold.

According to the first, second and fourth series of T-Tests, the findings consistently demonstrate significant albedo differentiation for ROIs that transitioned from natural grass to artificial turf, underscoring the profound influence that turf conversion has on surface albedo. For these T-Tests, the alternative hypothesis cannot be rejected for the transitioned ROIs since significant differences between the pre (2018) and post (2002) conversion were found. According to the third series of T-Tests, the null hypothesis cannot be rejected for the transitioned ROIs, as no significant differences were found. This implies that the conversion did not result in statistically significant changes in albedo for these areas.

2.5.3 LST-Albedo Relationship for the Transitioned ROIs in 2022

Aoki (2009) indicates that the surface albedos play a crucial role in determining its temperature. Dark or vegetated surfaces, with their lower albedo, tend to absorb more sunlight, which increases their temperature. On the other hand, light-colored or snow-covered surfaces have a higher albedo and therefore reflect more sunlight, keeping temperatures lower. This study involved creating four separate scatter plots to analyze the relationship between LST and albedo across 26 transitioned ROIs throughout all the seasons in 2022. The scatter plots for each season in Figure 2.29 depict LST on the x-axis and albedo values on the y-axis for each of the transitioned ROI.

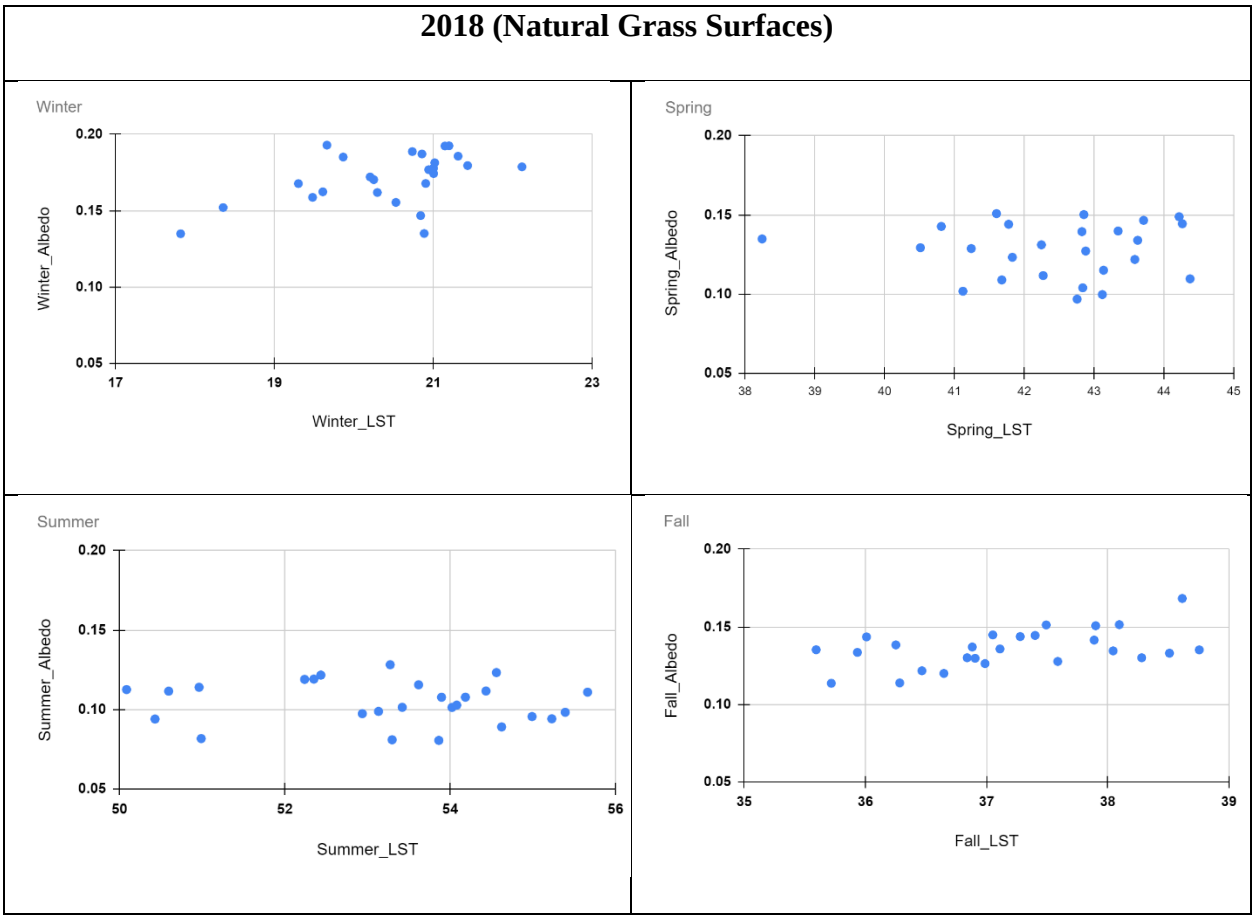

Figure 2.25: Scatter plots showing the LST-Albedo relationships for each transitioned ROI at each season in 2018.

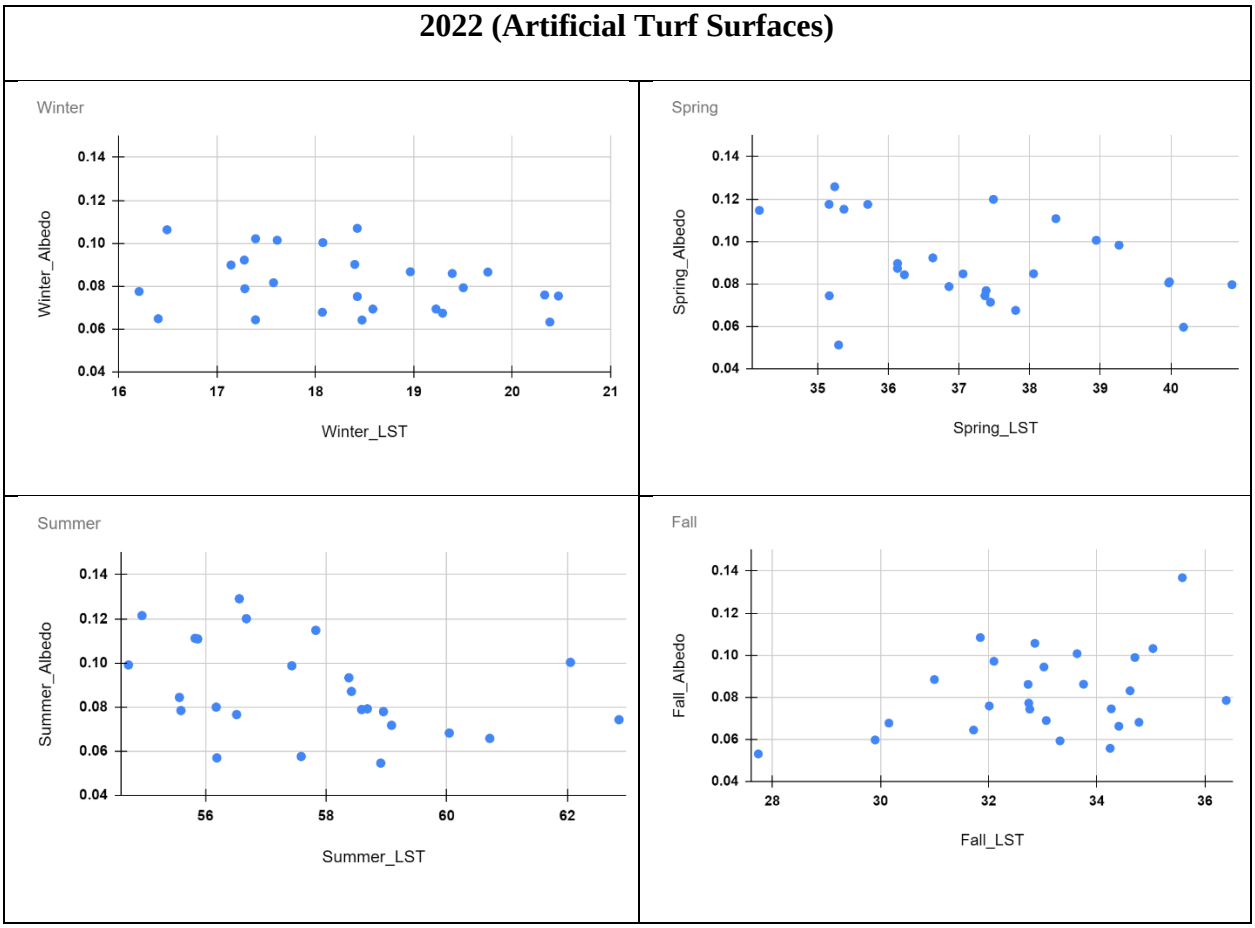

Figure 2.26: Scatter plots showing the LST-Albedo relationships for each transitioned ROI at each season in 2022.

The scattered plots do not show any clear trend or pattern between the two variables in 2018 and 2022 indicating that the changes in albedo do not consistently relate to the changes in LST.

The correlation coefficient is a numerical indicator that quantifies the strength of a linear relationship between two variables, with its value ranging from -1 to +1. A value of -1 signifies a perfect negative correlation, +1 signifies a perfect positive correlation, and 0 means there is no

correlation. In this study, correlation coefficients were calculated for different pairs of data across the seasons for both 2018 and 2022. The coefficients obtained were -0.2793 for winter, -0.3422 for spring, -0.3815 for summer, and 0.3758 for fall in 2022, corresponding to the ROIs that transitioned from natural to artificial surfaces. These results suggest a weak to moderate negative correlation between LST and albedo values for winter, spring, and summer, implying that LST tends to rise as albedo decreases. However, the positive correlation observed in fall indicates an increase in LST with an increase in albedo, which is contrary to the expected trend based on existing literature that associates artificial turf with higher temperatures and reduced albedo. The correlation coefficients obtained in 2018 for winter, spring, summer and fall were 0.542, -0.003, -0.107, and 0.48 respectively. The coefficients for winter and fall suggest a positive correlation between the LST and Surface Albedo indicating LST increases with the increase in Albedo. While the correlation coefficients for Spring and Summer suggest a “No Correlation” or a very weak correlation between the two variables.

Aoki (2009) conducted an analysis on the surface temperature and albedo of five different outdoor sports surfaces, finding that surface temperatures tend to decrease as albedo increases. Based on this inverse correlation, the author suggested that, given consistent material composition and structure, one can predict surface temperature based on albedo. Ponce et al. (1997) and Bonfils et al. (2001) noted that surface albedo is subject to significant variation, influenced by the specific characteristics and state of the surface material.

This LST-albedo relationship is crucial in understanding and managing urban heat islands, climate change impacts, and the design of sustainable environments. By altering surface albedo through the choice of materials or vegetation, one can influence the LST and thereby affect local microclimates, energy use, and overall comfort levels.

Gustin et al. (2018) highlighted the potential for significant decreases in surface temperatures through the enhancement of surface albedo. Similarly, Elhinnawy (2004) emphasized the role of high albedo values in urban design as an effective method to mitigate urban heat islands, noting a 3°C drop in surface temperature for each 0.05 increase in albedo during peak heat times at 9:00 am. Gustin et al. (2018) developed a numerical model indicating that substituting the black crumb rubber in an artificial 3rd generation turf field with a higher albedo and more conductive material could reduce peak surface temperatures by 14–20°C. Lopez-Cabeza et al. (2022) applied the ENVI-met simulation tool to assess how varying albedo levels affect the thermal efficiency and comfort within a courtyard, finding that high-albedo surfaces could lower temperatures by up to 25°C compared to their low-albedo counterparts due to reduced heat accumulation from solar radiation. The adoption of materials with high reflectivity not only offers local temperature moderation but also contributes to lower energy use and cooling demands in the summer, enhancing overall thermal comfort (Konopacki and Akbari, 2001). Lee et al. (2018) further advocated for the use of building materials with high reflectivity or emissivity, particularly at lower building levels, to improve urban environmental conditions.

High albedo materials minimize the amount of energy by reflecting more sunlight that is absorbed as heat. This is significant because absorbed solar radiation can significantly increase the temperature of a material, leading to higher temperatures in the surrounding environment. The increase in surface temperature increases the intensity of longwave radiation (Taha, 1997), leading to a higher temperature. Artificial turf has a high emissivity property which, in turns, increases the longwave radiation from the artificial turf surfaces (Kanaan et al., 2020)

This study supported the literature and showed that the surface albedo in natural grass ROIs were similar in both years. In most of the transitioned ROIs, albedo has reduced since artificial

turf has replaced natural grass in those ROIs. The Paired T-Tests results also showed significant differences among transitioned ROIs between 2018 and 2022, while it did not show any significant differences among non-transitioned ROIs. J. Wickham et al. (2016) studied that land cover change does not always affect albedo significantly. In this research, though albedo got reduced in 2022 after the land cover change occurred, the difference between albedo values of 2018 and 2022 were not significant enough.

While selecting the components of artificial turf, the albedo, or the reflective properties of the materials of the components should also be considered wisely to achieve certain thermal performance goals. Since plant development, chemical reactions, and the activity of soil-dwelling microbes are all affected by temperature, grasping the typical temperature trends within the soil of artificial turf fields is also crucial. This knowledge aids in determining the optimal timing for watering, fertilizing, and applying treatments to maximize effectiveness. It's also critical for forecasting the likelihood of problems such as weed growth, disease outbreaks, and insect infestations, which are often temperature-sensitive (Li, 2008).

2.6 Conclusions

This study examines the effects of artificial turf on the urban thermal environment in the LVV. To assess this impact, LST and surface albedo were analyzed at 26 ROIs that transitioned from natural to artificial turf, alongside another 26 ROIs that remained unchanged between 2018 and 2022. The data for this analysis was obtained from all available Landsat 8 satellite imagery for the respective years. The transitioned ROIs are high school football fields, while the non-transitioned ROIs, primarily golf courses, served as a control group in this research. The entire

analysis was conducted using GEE and ArcGIS Pro, with statistical assessments carried out in R-Studio.

This study investigated the effect of artificial turf on LST in the LVV from 2018 to 2022, focusing on 26 ROIs where turf transitioned from natural to artificial. These were compared with 26 control ROIs that retained their natural turf. Initial analyses involved comparing LST for each ROI across the two years, revealing that artificial turf tended to elevate surface temperatures during warmer months, while cooler months saw a reduction in LST for transitioned ROIs. The control group, however, showed minimal changes, with a slight increase in LST during summer in a few ROIs. Further analysis examined average LST changes per ROI, identifying an increase in 7 transitioned ROIs but a decrease or no change in the rest. Conversely, the control ROIs largely maintained their average LST, with only one showing an increase. Annual average comparisons indicated a general decrease in surface temperature for both groups in 2022. Seasonal variability was also assessed, showing a significant summer LST increase in all transitioned ROIs, whereas the control ROIs presented mixed results. T-Tests were conducted to assess the significance of these changes. The T-Tests results which combined the data revealed substantial impact of turf transition on LST for transitioned ROIs, and stability within the control group across the study period.

The average discrepancy between the 10 am temperatures and the daily peaks for specific dates rose marginally from 5.83°C in 2018 to 6.23°C in 2022. The LST readings taken at 10 am using Landsat 8 satellites are likely a few degrees Celsius below the true peak LST, which could be captured during the hottest part of the day. To obtain the actual peak LST, an on-site infrared radiometer can be employed, rather than relying on satellite-based remote sensing data.

Several analyses were performed to assess the effect of switching to artificial turf on the surface albedo within the LVV over the period from 2018 to 2022, focusing on 26 ROIs that underwent this transition. These findings were then compared with those from another 26 ROIs that maintained their natural turf, serving as a control group for this investigation. Initial assessments involved comparing the surface albedo for each ROI across the two years through box plots. A significant decline in albedo values was noted in 2022 for the ROIs that had transitioned, with these values remaining relatively stable throughout the year, in contrast to the seasonal variability observed in 2018. The average albedo for all transitioned ROIs decreased in 2022 where the albedo values decreased at 8 non-transitioned ROIs and increased in the rest. Seasonal analysis indicated a reduction in albedo for nearly all transitioned ROIs during the summer, except for two. In contrast, the non-transitioned ROIs in the controlled group displayed a seasonal trend of decreasing albedo from winter to fall. The T-Tests revealed marked differences in surface albedo between 2018 and 2022 for the transitioned ROIs, whereas the non-transitioned ROIs mostly showed no significant change.

In the comprehensive comparison of ROIs over the two years in question, it was observed that transitioning to artificial turf correlated with elevated surface temperatures, but only during the warmer months. The T-Tests also confirm these changes. The albedo values for ROIs with natural grass remained relatively unchanged between the two years. Conversely, a notable decrease in albedo was observed in most ROIs that transitioned to artificial turf. The T-Tests revealed significant differences in albedo between 2018 and 2022 for these transitioned ROIs, whereas the non-transitioned ROIs showed no significant changes.

The relationship between LST and albedo for ROIs that transitioned from natural to artificial turf in 2018 and 2022 was evaluated across different seasons, but the scatter plots did not show a definitive pattern. The calculated correlation coefficients showed weak inverse correlations for the winter, spring, and summer seasons in 2022, suggesting that LST tends to rise as albedo decreases. However, an unexpected positive correlation was observed for the fall season, contradicting the commonly held view in existing studies that artificial turf leads to increased temperatures and lower albedo. For 2018, the coefficients for winter and fall suggested a positive correlation between the LST and Surface Albedo indicating LST increases with the increase in Albedo. While the correlation coefficients for Spring and Summer suggested a "No Correlation" or a very weak correlation between the two variables.

Artificial turf is often utilized as a water-saving substitute for natural grass in arid regions like the LVV, where water conservation is a major concern. Artificial turf can raise local temperatures, therefore it's important to balance the advantages of water conservation against any potential thermal effects. Elevated surface temperatures have the potential to negatively impact public health, cause discomfort, and raise the risk of heat-related illnesses. Artificial turf should not be considered as a full replacement for natural grass. Its suitability varies with different weather conditions. Shi and Jim (2021) suggested avoiding artificial turf in areas that receive direct sunlight, as it can increase the risk of heat stress, and particularly in situations involving intense physical activities under direct sun exposure. Therefore, studying the impact of artificial turf on the urban thermal environment of LVV is essential for informed urban planning and policymaking, aimed at creating a healthy and comfortable urban environment, especially considering the unique climate challenges of the region.

2.7 Limitations and Recommendations

2.7.1 Limitations

- Since the equatorial crossing time of Landsat 8 satellite is 10:00 am +/- 15 minutes (European Space Agency, 2022), the remote sensing images are taken at 10am local time. Hence, the recorded temperature gives a snapshot of the surface conditions specifically at that time (Black et al., 2019). The LST might not be the peak at this time.
- Some external factors, such as changes in surrounding infrastructure, shade availability, irrigation practices, and other management changes can affect the LST readings.
- The temporal resolution of the Landsat 8 satellite is 16 days. So only one or two images were found each month. The data from this one image can be impacted by several factors, such as,
    - ➢ The 4 Oct 2018, 7 Dec 2018, 12 Aug 2022, 13 September 2022, and 29 September 2022 data might have been affected by different amounts of precipitation that occurred that day. (NORTH LAS VEGAS, NV Weather History | Weather Underground)
    - ➢ 6 Feb 2018 and 11 April 2018 both were much hotter than the average temperature which might have affected the result.
    - ➢ Cloud cover is also an important factor that can influence the result. In this study, several data had a considerable amount of cloud cover which may have affected the data. (Table 2.1 and 2.2)
- Freely available Landsat 8 dataset was used in this study, which has coarser spatial resolution. Finer resolution data could give better results.

- The study solely focused on the football fields which comes up with some limitations, such as,
    - ➢ Since football fields represent a specific type of land use, therefore, the result obtained from this study cannot be generalized for other land uses such as residential lawn or public parks etc.
    - ➢ The uniformity in the size and shape of the football fields can limit the understanding on how LST varies with different sizes and configurations of land areas.
    - ➢ The materials and methods used in constructing the artificial turf for the football fields might differ from other applications, leading to different thermal properties and LST responses.

2.7.2 Recommendations for the Future Studies

- Subsequent research could employ high-resolution satellite imagery from commercial satellites. Companies like Maxar Technologies, Planet Labs, 21st Century Aerospace Technology, and Airbus Defense and Space, which operate in the commercial satellite sector, provide the public with access to some of the most detailed satellite imagery. They supply images with resolutions reaching up to 30 centimeters (about 11.8 inches) per pixel, allowing for the identification of ground objects as small as 30 centimeters in the imagery. (GeoWGS, 2024)
- Investigating the LST and surface albedo across various natural grass types (such as Bermuda, Bent, and Rye) and artificial turfs made from diverse materials like polyethylene, polypropylene, and nylon would facilitate a comparative study.

- Given that temperature fluctuations are natural from year to year, extending the analysis over multiple years would enhance the comparative aspect of the study.
- To mitigate the limitations of solely focusing on football fields, it might be beneficial to include a more diverse range of sites and consider additional variables that could influence LST for future studies.
- Future studies could extend to measuring the night-time temperatures of artificial turf in addition to daytime readings. Monitoring the 24-hour diurnal cycle could reveal nocturnal heat exchanges, which play a crucial role in the overall energy balance.
- Verifying the outcomes of this study through ground truthing with suitable measurement tools can help ascertain the accuracy of the findings.
- The study compared the LST/ Albedo differences in football fields with the golf courses which have varying topography, grass characteristics, surrounding structures etc. For enhanced accuracy, a comparison should be made between football fields that have transitioned and those that have remained unchanged.

2.7.3 Recommendations for the Policy Makers and Urban Planners

- The study indicates that artificial turf elevates surface temperatures in the summer, highlighting the need for policymakers and urban planners to consider this factor in their summer construction and landscaping plans.
- Given the substantial water required to lower temperatures on artificial turf fields during hotter months, water resource management should be tailored to accommodate this demand.

- The strategic placement of artificial turf is essential to prevent any single area from having an excessive concentration, which could result in elevated surface temperatures compared to other locations.
- In areas with artificial turf, adding shade structures, water features, or incorporating cooling materials into the surrounding landscapes are some examples of heat mitigation measures that can be used to mitigate the increase of heat during summer season.
- Since artificial turf has been found to have lower surface albedo values, identifying ways to make these surfaces more reflective, or incorporating higher albedo materials in the vicinity can reduce the overall thermal effect.
- Promoting a variety of landscaping options, such as artificial turf and drought-tolerant native plants, could offer a balanced approach to urban green space, promoting ecological sustainability and biodiversity while effectively controlling heat and water use.
- Continuous monitoring of urban areas with artificial turf is recommended to further understand long-term impacts on local microclimates and to assess whether adjustments in urban planning policies might be needed.
- Alternatives to traditional recycled crumb rubber, such as organic or natural infill materials derived from coconut shells, walnut shells, rice husks, and renewable corks, could offer a solution, albeit at a higher cost.
- The choice of fiber height and density, along with the type of infill used in artificial turf, can impact water drainage and retention, as highlighted by Simpson and Francis (2021). These elements should be meticulously considered during the selection process prior to installing artificial turf to ensure optimal hydrological performance. In their research, Petrass et al. (2014) found that products using Thermoplastic Elastomer (TPE) as infill

exhibited significantly cooler surface temperatures compared to those using organic or Styrene-butadiene Rubber (SBR) infill. Villacañas et al. (2017) suggested the use of thermoplastic rubber and monofilament fibers to reduce the turf surface temperature.

- Given that increased surface albedo can significantly lower maximum surface temperatures (Gustin et al., 2018), urban planners are advised to incorporate urban elements with higher albedo values to help reduce surface temperatures.
- Urban planners should understand the factors responsible for the potential heat stress from high-temperature surfaces like artificial turf in public spaces, particularly in areas with extreme summer temperatures.
- The development and use of more sustainable and environmentally friendly artificial turf alternatives that closely mimic the thermal properties of natural grass should be encouraged.
- Integration of remote sensing data into climate adaptation strategies would help to create cooler urban environments.
- Policies should be developed that require the consideration of spectral and thermal characteristics in the selection of urban materials.
- Henderson et al. (2003) mentioned modifying the infill material, such as utilizing organic, dyed, sand-coated, rubber-coated, or cryogenically chilled rubber, alongside the installation of below-ground water systems designed to retain moisture and ensure the cooling of the turf fibers, thus reducing the surface temperature of artificial turf.
- Villacañas et al. (2017) noted that the temperature of synthetic turf fields can reflect their level of usage and deterioration, finding that surface temperatures fluctuate based on weekly activity. According to their study, fields that experience over 35 hours of weekly

play and have SBR infill tend to exhibit elevated temperatures in comparison to less frequently used fields. On the other hand, fields utilizing TPE demonstrate a contrasting pattern, where temperatures remain lower despite higher levels of activity. Urban policymakers can adopt this approach as part of the maintenance strategy for artificial turf installations.

- Wardenaar et al. (2023) discussed the "cool" turf technology, which has gained popularity in the US. It works using the evaporation of water from its organic infill, providing significant cooling benefits, especially during peak heat periods (Hydrochill | Shaw Sports Turf, n.d.). The authors mentioned a drawback of such turf technology which is mirroring the same surface and ambient temperatures as conventional artificial turf types when there is insufficient amount of moisture in the infill. Consequently, it becomes essential for sports field managers to ensure the "HydroChill" turf is adequately irrigated. In the dry climates of the southwestern U.S., the infill's moisture might quickly evaporate (Guyer et al., 2021), whereas in regions with higher humidity and moisture, the infill retains water longer, slowing down the evaporation process and thereby helping to cool both the surface and the surrounding air more effectively.
- According to the SNWA conservation plan 2019 existing building regulations limit the installation of turf in new developments. It should be maintained strictly by the urban planners to prevent water wastage on non-functional turf. (Joint Water Conservation Plan, 2019)

REFERENCES

Aoki, T. (2009). Effect of solar illuminance and albedo on surface temperature of outdoor sport surfaces. Nat. Environ., 11, 40–48.

Bala, R., Prasad, R., Yadav, V. P., & Sharma, J. (2018). A Comparative Study of Land Surface Temperature With Different Indices on Heterogeneous Land Cover Using Landsat 8 Data. *International Archives of the Photogrammetry, Remote Sensing and Spatial Information Sciences.*, *XLII-5*, 389–394. https://doi.org/10.5194/isprs-archives-XLII-5-389-2018

Becker, W. R., Ló, T. B., Johann, J. A., & Mercante, E. (2021). Statistical features for land use and land cover classification in Google Earth Engine. *Remote Sensing Applications, 21, 100459.* https://doi.org/10.1016/j.rsase.2020.100459

Biran, I., Bravdo, B., Bushkin-Harav, I., & Rawitz, E. (1981). Water consumption and growth rate of 11 turfgrasses as affected by mowing height, irrigation frequency, and soil moisture 1. *Agronomy Journal*, *73*(1), 85-90. https://doi.org/10.2134/agronj1981.00021962007300010020x

Black, A., Ahmad, S., & Stephen, H. (2019). Urban heat island intensity mapping of Las Vegas using Landsat thermal infrared data. *World Environmental and Water Resources Congress 2019: Groundwater, Sustainability, Hydro-Climate/Climate Change, and Environmental Engineering - Selected Papers from the World Environmental and Water Resources Congress 2019, 397–409.* https://doi.org/10.1061/9780784482346.040

Bonfils, C., de Noblet-Ducoudré, N., Braconnot, P., & Joussaume, S. (2001). Hot Desert Albedo and Climate Change: Mid-Holocene Monsoon in North Africa. *Journal of Climate, 14*(17), 3724–3737. https://doi.org/10.1175/1520-0442(2001)014<3724:HDAACC>2.0.CO;2

Brelsford, C., & Abbott, J. K. (2017). Growing into Water Conservation? Decomposing the Drivers of Reduced Water Consumption in Las Vegas, NV. *Ecological Economics, 133*, 99–110. https://doi.org/10.1016/j.ecolecon.2016.10.012

Buskirk, E. R., McLaughlin, E. R., & Loomis, J. L. (1971). Microclimate over Artificial Turf. Journal of Health, Physical Education, Recreation., 42(9), 29–30. https://doi.org/10.1080/00221473.1971.10617177

Carvalho, H. D. R., Chang, B., McInnes, K. J., Heilman, J. L., Wherley, B., & Aitkenhead-Peterson, J. A. (2021). Energy balance and temperature regime of different materials used in urban landscaping. *Urban Climate*, *37*, 100854. https://doi.org/10.1016/j.uclim.2021.100854

Cheng, H., Hu, Y., & Reinhard, M. (2014). Environmental and Health Impacts of Artificial Turf: A Review. *Environmental Science & Technology*, *48*(4), 2114–2129. https://doi.org/10.1021/es4044193

Cities with low humidity in US - current results. (n.d.). https://www.currentresults.com/Weather-Extremes/US/low-humidity-cities.php

Devitt, D. A., Young, M. H., Baghzouz, M., Bird, B. M., & Devittl, B. D. A. (2007). Surface temperature, heat loading and spectral reflectance of artificial turfgrass. *J Turfgrass Sports Surf Sci*, *83*, 68-82.

Dickinson, R. E. (1983). Land Surface Processes and Climate—Surface Albedos and Energy Balance. In *Advances in Geophysics* (Vol. 25, pp. 305–353). Elsevier Science & Technology. https://doi.org/10.1016/S0065-2687(08)60176-4

Elhinnawy, T. S. (2004). Tools To Investigate Building Envelope Thermal Behaviour For Urban Heat Island Mitigation (UHIM). Eng. Res. J.

European Space Agency. (2022, December 6). *Landsat-8*. Earth Online. https://earth.esa.int/eogateway/missions/landsat-8

Garai, A., & Kleissi, J. (2011). Air and Surface Temperature Coupling in the Convective Atmospheric Boundary Layer. *Journal of the Atmospheric Sciences*, *68*(12), 2945–2954. https://doi.org/10.1175/JAS-D-11-057.1

GeoWGS. (2024, January 19). What is the highest resolution satellite imagery available? *GeoWGS84*. https://www.geowgs84.com/post/what-is-the-highest-resolution-satellite-imageryavailable#:~:text=As%20of%20January%202024%2C%20commercial,imagery%20available%20to%20the%20public .

Gorelick, N., Hancher, M., Dixon, M., Ilyushchenko, S., Thau, D., & Moore, R. (2017). Google Earth Engine: Planetary-scale geospatial analysis for everyone. *Remote Sensing of Environment*, *202*, 18–27. https://doi.org/10.1016/j.rse.2017.06.031

Gustin, M., P. R. Fleming, D. Allinson, and S. Watson. 2018. "Modeling surface temperatures on 3G." Proceedings 2 (6): 279. https://doi-org.ezproxy.library.unlv.edu/10.3390/proceedings2060279.

Guyer, H., Georgescu, M., Hondula, D. M., Wardenaar, F., & Vanos, J. (2021). Identifying the need for locally-observed wet bulb globe temperature across outdoor athletic venues for current and future climates in a desert environment. Environmental Research Letters, 16(12), 124042. https://doi.org/10.1088/1748-9326/ac32fb

Hara, K., Liu, W., Yamazaki, F., Suzuki, K., & Maruyama, Y. (2013). Spectral Characteristics And Classification Of Urban Land-Cover Based On Airborne Hyperspectral Data. *Proceedings of ACRS* 2013 http://ares.tu.chiba-u.jp/yamazaki/pdf/proceeding/2013ACRS_Hara.pdf

Henderson, J. J., Rogers III, J. N., & Crum, J. R. (2003). Athletic Field Systems Study 2000-2003.

Huang, B. (2008). Turfgrass water requirements and factors affecting water usage. *Water quality and quantity issues for turfgrass in urban landscapes. Council Agr. Sci. Technol. Spec. Publ*, *27*, 193-205.

Hydrochill | Shaw Sports Turf. (n.d.). https://www.shawsportsturf.com/hydrochill/

Jastifer, J. R., McNitt, A. S., Mack, C. D., Kent, R. W., McCullough, K. A., Coughlin, M. J., & Anderson, R. B. (2019). Synthetic Turf: History, Design, Maintenance, and Athlete Safety. *Sports Health*, *11*(1), 84–90. https://doi.org/10.1177/1941738118793378

Jim, C. Y. (2016). Solar–terrestrial radiant-energy regimes and temperature anomalies of natural and artificial turfs. *Applied Energy*, *173*, 520–534. https://doi.org/10.1016/j.apenergy.2016.04.072

Jim, C. Y. (2017). Intense summer heat fluxes in artificial turf harm people and environment. *Landscape and Urban Planning*, *157*, 561–576. https://doi.org/10.1016/j.landurbplan.2016.09.012

Kanaan, A., Sevostianova, E., Leinauer, B., & Sevostianov, I. (2020). Water Requirements for Cooling Artificial Turf. *Journal of Irrigation and Drainage Engineering*, *146*(10). https://doi.org/10.1061/(ASCE)IR.1943-4774.0001506

Kandelin, W. W. (1976). Athletic field microclimates and heat stress. Journal of Safety Research, 8(3), 106–111.

Konopacki, S. J., & Akbari, H. (2001). *Measured energy savings and demand reduction from a reflective roof membrane on a large retail store in Austin*.

Kirkpatrick, M., Stewart, D., Bridges, C., Crear, C., Gibson, J., Jones, J., & Lee, J. (2019). Joint Water Conservation Plan. https://www.snwa.com/assets/pdf/reports-conservation-plan-2019.pdf

Loveday, J., Loveday, G., Byrne, J. J., Boon-lay Ong, & Morrison, G. M. (2019). Seasonal and diurnal surface temperatures of urban landscape elements. *Sustainability*, *11*(19), 5280. doi:https://doi.org/10.3390/su11195280

Lavorgna, J., Song, J., Beattie, W., Riley, M., Beil, C., Levchenko, K., & Shofar, S. (2011). A Review of Benefits and Issues Associated with Natural Grass and Artificial Turf Rectangular Stadium Fields Final Report. *Montgomery County Council: Rockville, MD*.

Lee, S., Moon, H., Choi, Y., & Yoon, D. K. (2018). Analyzing thermal characteristics of urban streets using a thermal imaging camera: A case study on commercial streets in Seoul, Korea. Sustainability (Basel, Switzerland), 10(2), 519. https://doi.org/10.3390/su10020519

Liu, Z., & Jim, C. Y. (2021). Playing on natural or artificial turf sports field? Assessing heat stress of children, young athletes, and adults in Hong Kong. *Sustainable Cities and Society*, *75*, 103271. https://doi.org/10.1016/j.scs.2021.103271

Li, D. (2008). Managing field surface temperature. In *FIELD SCIENCE* [Journal-article]. https://sturf.lib.msu.edu/article/2008apr14.pdf

Lopez-Cabeza, V. P., Alzate-Gaviria, S., Diz-Mellado, E., Rivera-Gomez, C., & Galan-Marin, C. (2022). Albedo influence on the microclimate and thermal comfort of courtyards under Mediterranean hot summer climate conditions. *Sustainable Cities and Society*, *81*, 103872. https://doi.org/10.1016/j.scs.2022.103872

McNitt, A., Petrunak, D., & Serensits, T. (2008). Temperature Amelioration Of Synthetic Turf Surfaces Through Irrigation. *Acta Horticulturae, 783(Jun)*, 573–582. https://doi.org/10.17660/ActaHortic.2008.783.59

Mediterranean hot summer climate conditions. *Sustainable Cities and Society*, *81*, 103872. https://doi.org/10.1016/j.scs.2022.103872

Morris, R. L., Devitt, D. A., Crites, A. M., Borden, G., & Allen, L. N. (1997). Urbanization and Water Conservation in Las Vegas Valley, Nevada. *Journal of Water Resources Planning and Management*, *123*(3), 189–195. https://doi.org/10.1061/(ASCE)0733-9496(1997)123:3(189)

Mutanga, O., & Kumar, L. (2019). Google Earth Engine Applications. *Remote Sensing (Basel, Switzerland)*, *11*(5), 591. https://doi.org/10.3390/rs11050591

Myers, V. I., & Allen, W. A. (1968). Electro Optical remote sensing methods as nondestructive testing and measuring techniques in agriculture. *Applied Optics (2004)*, *7*(9), 1819–1838. https://doi.org/10.1364/AO.7.001819

NOAA's National Weather Service. (n.d.). *Climate*. https://www.weather.gov/wrh/climate?wfo=vef

NORTH LAS VEGAS, NV Weather History | Weather Underground. (n.d.). https://www.wunderground.com/history/monthly/us/nv/north-las vegas/KVGT/date/2018-4

Petrass, L. A., Twomey, D. M., & Harvey, J. T. (2014). Understanding how the Components of a Synthetic Turf System Contribute to Increased Surface Temperature. *Procedia Engineering*, *72*, 943–948. https://doi.org/10.1016/j.proeng.2014.06.159

Petrass, L. A., Twomey, D. M., Harvey, J. T., Otago, L., & LeRossignol, P. (2015). Comparison of surface temperatures of different synthetic turf systems and natural grass: Have advances in synthetic turf technology made a difference. *Proceedings of the Institution of*

Mechanical Engineers, Part P: Journal of Sports Engineering and Technology, *229*(1), 10-16.

Ponce, V. M., Lohani, A. K., & Huston, P. T. (1997). Surface Albedo and Water Resources: Hydroclimatological Impact of Human Activities. *Journal of Hydrologic Engineering*, *2*(4), 197–203. https://doi.org/10.1061/(ASCE)1084-0699(1997)2:4(197)

Ramsey, J. D. (1982). Environmental Heat from Synthetic and Natural Turf. Research Quarterly for Exercise and Sport, 53(1), 82–85. https://doi.org/10.1080/02701367.1982.10605230

Seeman, M. (2020, July 16). Artificial turf to replace grass fields at 29 Southern Nevada schools. KSNV. https://news3lv.com/news/local/artificial-turf-to-replace-grass-fields-at-29-southern-nevada-schools

Shi, Y., & Jim, C. Y. (2022). Developing a thermal suitability index to assess artificial turf applications for various site-weather and user-activity scenarios. *Landscape and Urban Planning*, *217*, 104276. https://doi.org/10.1016/j.landurbplan.2021.104276

Simpson, T. J., & Francis, R. A. (2021). Artificial lawns exhibit increased runoff and decreased water retention compared to living lawns following controlled rainfall experiments. *Urban Forestry & Urban Greening*, *63*, 127232. https://doi.org/10.1016/j.ufug.2021.127232

Southern Nevada Water Authority. (n.d.). https://www.snwa.com/water-resources/conservation-initiatives/index.html

Tian, L., Zhang, Y., & Zhu, J. (2014). Decreased surface albedo driven by denser vegetation on the Tibetan Plateau. *Environmental Research Letters*, *9*(10), 104001. https://doi.org/10.1088/1748-9326/9/10/104001

Twomey, D., Petrass, L., Harvey, J., Otago, L., & LeRossignol, P. (2014). Heat experienced on synthetic turf surfaces: An inevitable or preventable risk? *Journal of Science and Medicine in Sport, Suppl.Supplement 1, 18,* e119-e120. doi:https://doi.org/10.1016/j.jsams.2014.11.086

Understand laws & ordinances. (n.d.). https://www.snwa.com/conservation/understand-laws-ordinances/index.html#:~:text=Grass%20restrictions&text=A%20law%20enacted%20by%20the,nonfunctional%20grass%2C%20beginning%20in%202027

USGS Landsat 8 Level 2, Collection 2, Tier 1. (n.d.). Google for Developers. https://developers.google.com/earth-engine/datasets/catalog/LANDSAT_LC08_C02_T1_L2#:~:text=These%20images%20contain%205%20visible,processed%20to%20orthorectified%20surface%20temperature

Villacañas, V., Sánchez-Sánchez, J., García-Unanue, J., López, J., & Gallardo, L. (2017). The influence of various types of artificial turfs on football fields and their effects on the thermal profile of surfaces. *Proceedings of the Institution of Mechanical Engineers, Part P: Journal of Sports Engineering and Technology*, *231*(1), 21-32.

Waleed, M., & Sajjad, M. (2022). Leveraging cloud-based computing and spatial modeling approaches for land surface temperature disparities in response to land cover change: Evidence from Pakistan. *Remote Sensing Applications*, *25*, 100665. https://doi.org/10.1016/j.rsase.2021.100665

Water Smart Landscapes Rebate. (n.d.-b). https://www.snwa.com/rebates/wsl/index.html#process

Water Smart Landscapes Rebate Program https://www.usbr.gov/watersmart/weeg/docs/2022/Southern_Nevada_Water_Authority_FGII_FY22WEEG_508.pdf

Way, D. A., Stinziano, J. R., Berghoff, H., & Oren, R. (2017). How well do growing season dynamics of photosynthetic capacity correlate with leaf biochemistry and climate fluctuations? *Tree Physiology*, 37(7), 879–888. https://doi.org/10.1093/treephys/tpx086

Wynne, T., & Devitt, D. (2020). Evapotranspiration of Urban Landscape Trees and Turfgrass in an Arid Environment: Potential Trade-offs in the Landscape. *HortScience, 55*(10), 1558–1566. https://doi.org/10.21273/HORTSCI15027-20

Weather averages Las Vegas, Nevada. (n.d.). US Climate Data. https://www.usclimatedata.com/climate/las-vegas/nevada/united-states/usnv0049

Wickham, J., Nash, M. S., & Barnes, C. A. (2016). Effect of land cover change on snow free surface albedo across the continental United States. *Global and Planetary Change, 146, 1–9.* https://doi.org/10.1016/j.gloplacha.2016.09.005

Williams, C. F., & Pulley, G. E. (2002). Synthetic surface heat studies. Brigham Young University.

Xian, G. and Crane, M. (2006). An analysis of urban thermal characteristics and associated land cover in Tampa Bay and Las Vegas using Landsat satellite data. *Remote Sensing of Environment*, 104(2), 147–156. https://doi.org/10.1016/j.rse.2005.09.023

Xiao, Y. Q., & Cao, Y. X. (2013). Study on thermal environment of sports field in different materials. *Applied Mechanics and Materials, 361-363*, 538. doi:https://doi.org/10.4028/www.scientific.net/AMM.361-363.538

Yaghoobian, N., Kleissl, J., & Krayenhoff, E. S. (2010). Modeling the Thermal Effects of Artificial Turf on the Urban Environment. *Journal of Applied Meteorology and Climatology*, *49*(3), 332–345. https://doi.org/10.1175/2009JAMC2198.1

Yu, Y., Liu, Y., Yu, P., Liu, Y., & Yu, P. (2018). 5.12 - Land Surface Temperature Product Development for JPSS and GOES-R Missions. In *Comprehensive Remote Sensing* (pp. 284–303). Elsevier Inc. https://doi.org/10.1016/B978-0-12-409548-9.10522-6

CHAPTER 3: DETECTION AND ANALYSES OF THE SPECTRAL SIGNATURES AND NDVI OF ARTIFICIAL TURF AND NATURAL GRASS IN LAS VEGAS VALLEY

3.1 Introduction

Artificial turf has been used instead of natural grass since the 1960s (Jastifer et al., 2019). Its water conservation potentiality, low maintenance costs, climate independent nature and its versatility to use for different purposes increased the use of artificial turf over the years. According to Cheng et al. (2014) and Lavorgna et al. (2011), a typical artificial turf football field can conserve from 0.5 to 1 million gallons of water annually.

However, there are growing concerns about substituting natural grass with artificial turf, originating from an ongoing debate regarding the environmental sustainability of artificial turf. A major concern comes from the elevated surface temperature it can reach during daylight hours (Devitt et al., 2007). The infill materials of artificial turf have low specific heat and low albedo, which promotes heat absorption and retention (Liu & Jim, 2021). Furthermore, artificial turf warms up more quickly due to its reduced water-holding capacity and reduced volumetric heat capacity (Carvalho et al., 2021; Liu & Jim, 2021). Artificial turf materials are unable to remove moisture due to their hydrophobic properties (Jim, 2016) and low water-holding capacity (Liu & Jim, 2021). These thermal characteristics have the potential to drastically raise both the ground's surface temperature and surrounding air temperature (Liu & Jim, 2021), which would be detrimental to the environment. This is one of the biggest disadvantages of artificial turf.

Due to its rapid growth, the arid southwestern United States is seeing an increase in demand for its water resources, particularly in large urban centers where water is mostly used to support urban greenery (Wynne & Devitt, 2020). With a population of about 2.2 million as of right now,

Las Vegas, Nevada, stands out as one of the American cities that is growing the fastest, tripling in size between 1990 and 2018. Sixty percent of Southern Nevada's annual water use is in the residential region. Residential water use is mostly dominated by outdoor use, especially landscape irrigation. According to the Southern Nevada Water Authority (SNWA), 2023, once this water is consumed outside, it evaporates and cannot be recovered for recycling. In order to maintain a sustainable balance between the supply and use of water, water agencies, such as SNWA, have made reducing outdoor water consumption a top priority (Wynne & Devitt, 2020).

The Water Smart Landscapes (WSL) initiative was launched in 1999 in Las Vegas as a way to encourage homeowners to switch from turf grass to water-saving xeric landscaping. This initiative became a vital part of SNWA's strategy to secure water supplies during the 2004 drought. About 535 acres of grass, or 1% of all residential land, had been replaced by homeowners by 2007 (Brelsford & Abbott, 2017). The community has successfully converted over 223 million square feet of lawns into water-efficient landscaping with the aid of the Water Smart landscaping rebate program, saving over 176 billion gallons of water (Joint Water Conservation Plan, 2019). A new law passed by the Nevada Legislature in 2021 limits the use of Colorado River water provided by member agencies of the Water Authority for irrigating non-functional grass beginning in 2027 (Understand laws & ordinances). An average conversion of 15,000 square feet to water-efficient landscaping is predicted to result in yearly water savings of 825,000 gallons (Water Smart Landscapes Rebate, n.d.-b).

In this study, we differentiated and characterized the spectral signatures of artificial turf and natural grass within the LVV. This study focuses on LVV for its significant usage of artificial turf. Measuring the total amount of natural grass surfaces within the valley is crucial to evaluate

the effectiveness of different lawn conversion programs. With such information, conversion efforts can be more strategically directed towards the areas with higher concentrations of natural grass which would benefit the most from such conversions, thus optimizing the impact of the program (Brandt, 2008).

Remote Sensing (RS) is a crucial method for obtaining data on Land Use and Land Cover (LULC), and it's indispensable for monitoring on a large scale. When analyzing ground covers through RS, they exhibit specific spectral signatures, also known as spectral reflectance patterns (Becker et al., 2021). A spectral signature represents how a material reflects or emits across different wavelengths of the EM spectrum. It is the ratio of reflected radiation energy to incident radiation energy on an object and is a function of wavelength (Gupta et al., 2022). Every substance on the surface of the planet has a unique value for its spectral reflectance characteristics because the reflectance value varies with the wavelength and topography features (Gupta et al., 2022). The color and tone of an object in an image are directly correlated with its reflectivity (Jensen, 2009).

Spectral signatures comprise not only the spectral values but also the spectral curve shape (Chen et al., 2016). The spectral response of an object is represented graphically by spectral reflectance curves, which display the reflectance values (Y-Axis) at various EM spectrum wavelengths (X-Axis). The curves show the various spectral properties of various objects. The curve displays "Peak and Valley" configurations, where the valley denotes a lower reflection or predominant absorption in the energy while the peak denotes a strong reflection of incident light from any wavelength. The substance's physical and chemical state, surface roughness, and geometric conditions—such as the sunlight's incidence angle—all affect the reflectance qualities of the material.

This signature is pivotal in analyzing the Landsat dataset because it helps in distinguishing and differentiating various Earth features (Kachhwaha, 1983). Such spectral data can identify differences among vegetative surfaces and other land covers, highlighting variations between vegetation types and states (Becker et al., 2021). Important qualitative and quantitative information for image classification is provided by the spectral signature. Consequently, the foundation for classifying remotely sensed data is spectral signatures (Chen et al., 2016). The majority of remote sensing applications process digital images to extract spectral signatures at each pixel, which are then used in various ways to divide the image into groups of related pixels. In the final stage, they compare each group's spectral signature with a known class (classification).

The spectral signatures of an object can be detected in various ways. In the past, hyperspectral or multispectral satellite imagery was the primary means for capturing spectral signatures. The vast amount of data produced by hyperspectral imaging, stemming from its many spectral bands, poses challenges in storage, processing, and analysis. Kim et al. (2016), Akwensi et al. (2023), Priem and Canters, (2016) and Kruse et al. (2016) used hyperspectral images in their studies. Another method involves using a spectroradiometer, an instrument that quantifies light intensity across an extensive wavelength range, to determine an object's spectral reflectance. This instrument offers a comprehensive spectral profile, showcasing light intensity at each distinct wavelength. Mei et al. (2016) and Salvador et al. (2014) used spectroradiometers in their research. Some researchers have employed data fusion techniques for capturing spectral signatures, necessitating a profound understanding of advanced machine learning algorithms.

Devitt et al. (2007) used a spectroradiometer to measure the spectral reflectance across a range of landscape surfaces, including various artificial turf types—green and white—as well as asphalt, bare soil, concrete, and natural grass. They found that artificial turf exhibited the lowest

reflectance across the entire EM spectrum, leading to the highest surface temperatures among the tested surfaces. The study revealed a significant correlation between average reflectance in the near-infrared (NIR) region (701 - 1300 nm) and surface temperature for the different landscape coverings, with a P-value of less than 0.05, indicating statistical significance. Spectral reflectance was measured using a spectroradiometer.

In this research, the potential of GEE was explored to ascertain the spectral signatures of natural grass and artificial turf across 26 regions of interest (ROIs) in the LVV. GEE is a cloud-powered tool designed for large-scale geospatial analyses, leveraging Google's vast computational resources to address significant societal challenges like deforestation, drought, disease, and more (Gorelick et al., 2017). Currently, approved users can access GEE and its extensive data catalog via two web platforms: GEE Explorer and Code Editor. The GEE Explorer web application provides access to a vast collection of public remote sensing images, complete with a suite of pre-built analytical tools. In contrast, the GEE Code Editor offers users the flexibility to tailor their analyses using common programming languages like JavaScript and Python (Liss et al., 2017; Tamiminia et al., 2020). These primary functionalities empower users to explore, process, and visualize large geospatial datasets without the need for high-end computing resources or deep coding knowledge. The introduction of GEE has sparked significant interest and involvement in the fields of remote sensing and geospatial data science (Tamiminia et al., 2020).

This method will help researchers to get the spectral signature of any object from a larger area at completely free of cost, without using any powerful tool or expensive satellite. Urban planners can locate artificial turf in LVV with the aid of spectral signature identification. It will be possible to measure the transition from natural grass to artificial turf and ascertain how the two types of turf impact the water use of the area by examining the spectral signatures of the two types

of turf. The negative environmental effects of artificial turf can be minimized by monitoring its location and size. By separating artificial turf that doesn't require watering from natural vegetation that does, municipalities may more effectively plan their use of water. When planning the construction of recreational facilities within a city, it can be helpful to identify regions with a high density of artificial turf.

In addition to identifying the spectral signatures of artificial turf, the Normalized Difference Vegetation Index (NDVI) was calculated using GEE and ArcGIS pro. NDVI serves as a reliable indicator of vegetative health by assessing the disparity between the NIR and red-light reflectance. Healthy vegetation typically reflects ample NIR and green light, but they absorb more of the red and blue spectrum, leading to the green appearance that human eyes can observe. A high NDVI value, resulting from low red reflectance and high NIR reflectance, suggests robust plant health.

The NDVI is a versatile analytical tool that serves a broad spectrum of ecological and agricultural applications (Kriegler et al., 1969). It is used to estimate the Leaf Area Index (LAI), a key component in crop growth modeling. NDVI also helps calculate the biomass of herbaceous and other vegetation types in terms of tons per hectare. It's valuable for assessing the photosynthetic activity within vegetation, as well as for determining the percentage of ground cover. NDVI measurements can be used to evaluate the cumulative effect of rainfall on vegetation over time, ascertain the carrying capacity of rangelands, and forecast yields for different crop types. Moreover, NDVI is useful for assessing the quality of the environment, particularly in terms of its suitability as a habitat for animals and its potential for harboring pests and diseases.

Various methodologies have been implemented by researchers to assess NDVI for different types of vegetation. Kwan et al. (2020) utilized land cover classification and machine learning to

distinguish artificial turf from natural grass, ultimately categorizing it as non-vegetation despite their visual similarities. Spadoni et al. (2020) computed NDVI using Sentinel-2 multispectral images within GEE to aid in creating forest cartography, underscoring the expectation of varied NDVI patterns across different vegetation types. Hashim et al. (2019) leveraged NDVI alongside very high-resolution satellite imagery, such as from Pleiades, to differentiate between vegetated and non-vegetated areas in urban settings, proving NDVI to be a vital tool for urban vegetation detection. Additionally, Wetherly et al. (2017) applied the Airborne Visible Infrared Imaging Spectrometer for detailed urban analysis, asserting that such high-resolution spectral data enhances the distinction between similar-looking materials like turfgrass and trees.

Chen et al. (2018) developed a classification system for urban land cover mapping using high-resolution hyperspectral data, observing that even shaded vegetation displays high NDVI values akin to those in direct sunlight, and sparse grass-covered soils can also show high NDVI readings. Their approach initially misclassified artificial turf as vegetation due to high NDVI readings, which was later corrected. Wang et al. (2022) introduced a monitoring method for non-agricultural land activities utilizing domestic satellite imagery and deep learning, selecting optimal observation periods for different crops through NDVI time sequence analysis. Their technique, too, initially recorded high NDVI values for artificial turf. These studies illustrate the versatility and complexities of using NDVI in classifying and monitoring vegetation and highlight the importance of context and calibration in interpreting NDVI data.

Identifying the NDVI for artificial turf and natural grass in LVV can be helpful in several ways, particularly given the region's arid climate and water scarcity issues. NDVI measurements can help in assessing the vitality and health of natural grass areas, which require significant water for maintenance. By comparing NDVI values of natural grass with those of artificial turf, urban

planners and water conservationists can better understand the effectiveness of artificial turf in reducing water usage and can strategize water conservation efforts more effectively. NDVI can indicate the presence and health of vegetation, which plays a crucial role in mitigating urban heat island effects. By analyzing the NDVI of natural grass and comparing it with artificial turf, researchers can evaluate the potential of these surfaces to reduce urban temperatures, which is particularly relevant in a desert city like Las Vegas. Understanding the distribution and health of green spaces through NDVI can aid in urban planning, especially in optimizing the use of available land for recreational, residential, or commercial purposes while ensuring sustainability and environmental quality. Policymakers can use NDVI data to make informed decisions regarding the installation of artificial turf versus the maintenance of natural grass areas, considering the trade-offs between water use, ecological impacts, and recreational needs of the community.

Therefore, the research objective of this study is to detect and analyze the spectral signatures and NDVI of artificial turf and natural grass in Las Vegas Valley.

Research Questions:

1. What are the distinct spectral signatures of natural and artificial turf?
2. Which wavelengths show the most significant differences between natural grass and artificial turf spectral signatures?
3. How does the NDVI of artificial turf differ from those of natural grass?

Research Hypothesis: There are significant differences on the spectral signature and NDVI due to the conversion from natural to artificial turf between 2018 and 2022 on 26 transitioned ROIs.

3.2 Study Area

Since LVV uses a lot of artificial turf, it has been selected as the primary focus of the research. One of the biggest metropolitan regions in the Southwestern United States is the LVV, which is situated in Southern Nevada. This area is in the central-western part of Clark County, Nevada, which is a higher-altitude segment of the Mojave Desert. It is surrounded by multiple mountain ranges, the highest of which is 11,918 feet high (Morris et al., 1997). As is typical of the Mojave Desert, Las Vegas' climate is classified as a subtropical hot desert (Koppen climatic classification: BWh). This means long, scorching summers, short, moderate winters, and warm transitional seasons (National Weather Service, NOAA, n.d.). The yearly average amount of rain is rather low, averaging about 4.2 inches (Weather Averages Las Vegas, Nevada, n.d.). Las Vegas is a city that is unique in North America due to its high amounts of sunshine, dryness, and unusually low humidity—which frequently falls below 10% (Cities with Low Humidity in US - Current Results, n.d.). Because of the low humidity, June through September is a particularly hot month. The hottest month is July when daytime highs typically exceed 104.5°F. The annual average high temperature is approximately 80°F (Weather Averages Las Vegas, Nevada, n.d.).

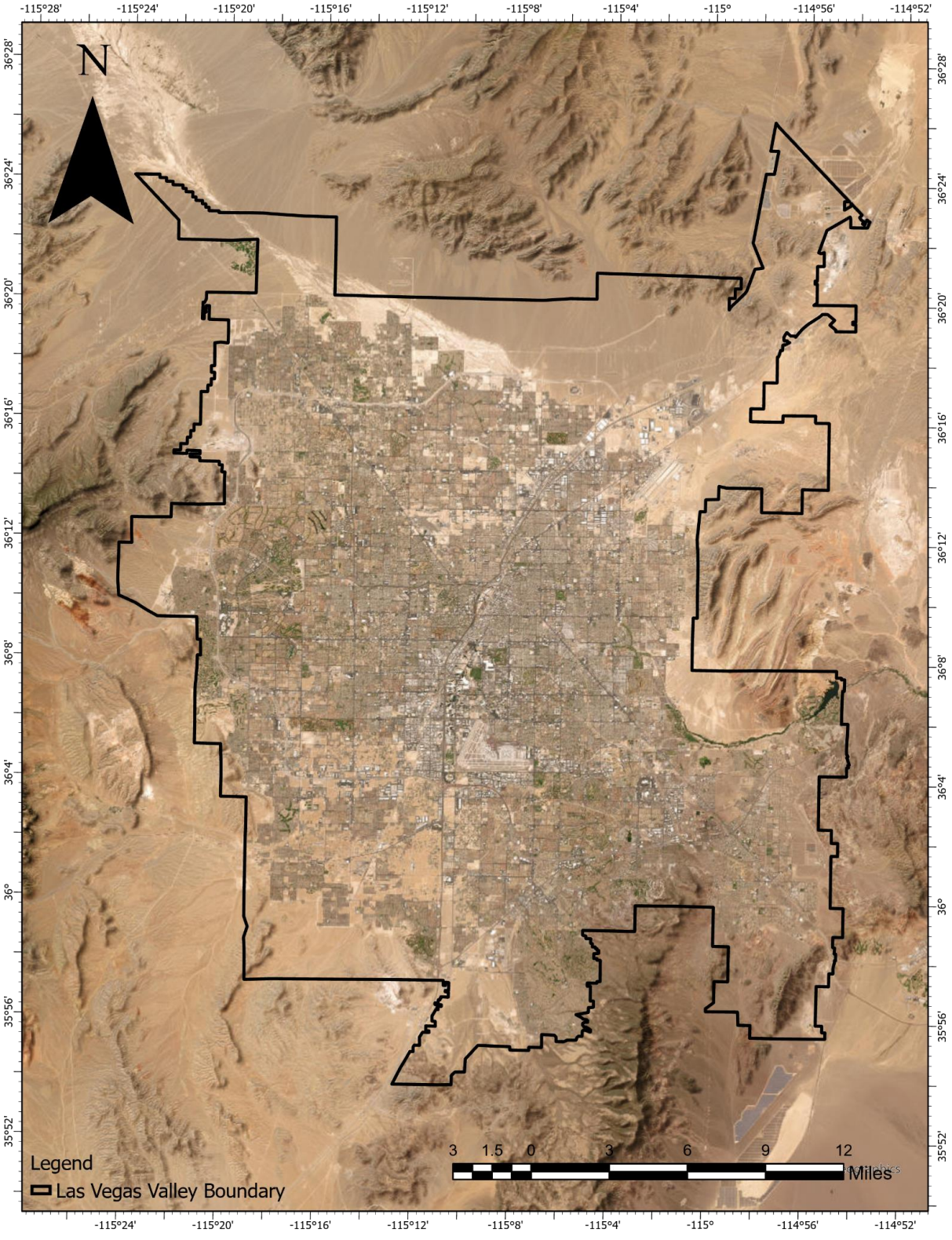

Figure 3.1: Study Area: Las Vegas Valley, Nevada

3.3 Materials and Methods

In this research, the objective is to compare the spectral reflectance curves of 26 ROIs switched from natural to artificial turf between 2018 and 2022 in the LVV utilizing GEE.

GEE cloud computing platform enables large-scale analysis of environmental data and with ample computational resources, as it uses Google servers for processing and storage. (Gorelick et al., 2017) The GEE Code Editor was utilized instead of the GEE Explorer due to the versatility and functionality of the program. GEE compiles over four decades of both historical and contemporary global satellite data, equipped with the analytical tools and computational strength to process this extensive dataset. (*Google Earth Engine*, n.d.) Pre-processed Landsat 8 satellite images were used in this study for 2018 and 2022 which was available through GEE. One tile having path and row 039 and 035 respectively, was required to cover the entire study area. A total of 26 spectral signature maps were generated for the LVV.

All the Landsat 8 satellite images available for 2018 and 2022 were downloaded and used for this study. Table 3.1 presents the dates on which the spectral signature maps were generated, accompanied by the corresponding cloud cover percentages for each date.

Table 3.1: Dates of Spectral Signature Map Generation and Corresponding Cloud Cover

2018		2022	
Dates	Cloud Cover (%)	Dates	Cloud Cover (%)
5-Jan-18	0.58	16-Jan-22	33.03
21-Jan-18	1.9	1-Feb-22	38.72
6-Feb-18	0.2	17-Feb-22	0.37
22-Feb-18	46.62	5-Mar-22	36.98
10-March-18	100	21-Mar-22	1.83
26-Mar-18	5.79	6-Apr-22	0.23
11-Apr-18	0.07	22-April-22	80.84
27-April-18	0.09	8-May-22	0.08
13-May-18	12.7	24-May-22	0.24
29-May-18	4.54	9-Jun-22	1.36
14-Jun-18	0.45	25-Jun-22	1.07
30-Jun-18	0.35	11-Jul-22	0.9
16-Jul-18	11.76	27-Jul-22	31.06
1-Aug-18	4.3	12-Aug-22	46.23
17-Aug-18	6.12	28-Aug-22	0.82
2-Sep-18	4.71	13-Sep-22	75.96
18-Sep-18	0	29-Sep-22	1.93
4-Oct-18	17.67	15-Oct-22	43.17
20-Oct-18	14.96	31-Oct-22	0.17
5-Nov-18	0.03	16-Nov-22	0.47
21-Nov-18	2.31	2-Dec-22	35.85
7-Dec-18	86.51	18-Dec-22	31.51
23-Dec-18	4.53		

Figure 3.2 presents the frequency of Landsat 8 satellite imagery acquisition dates for the years 2018 and 2022. Given Landsat 8's temporal resolution of 16 days, the imagery is spaced 16 days apart annually. The X-axis indicates the day of the year, and the Y-axis shows the count of images captured on specific days. The imagery from 2018 is depicted by blue bars, while the imagery from 2022 is shown with red bars.

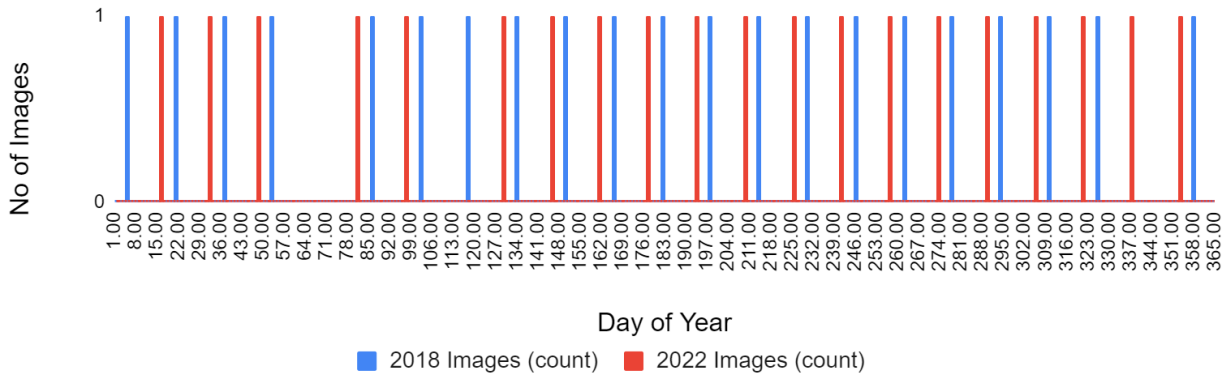

Figure 3.2: Distribution of the dates of the obtained satellite images in 2018 and 2022

The framework of this study is delineated in Figure 3.3. This chart offers a structured visual representation of the sequential steps and processes undertaken throughout the research.

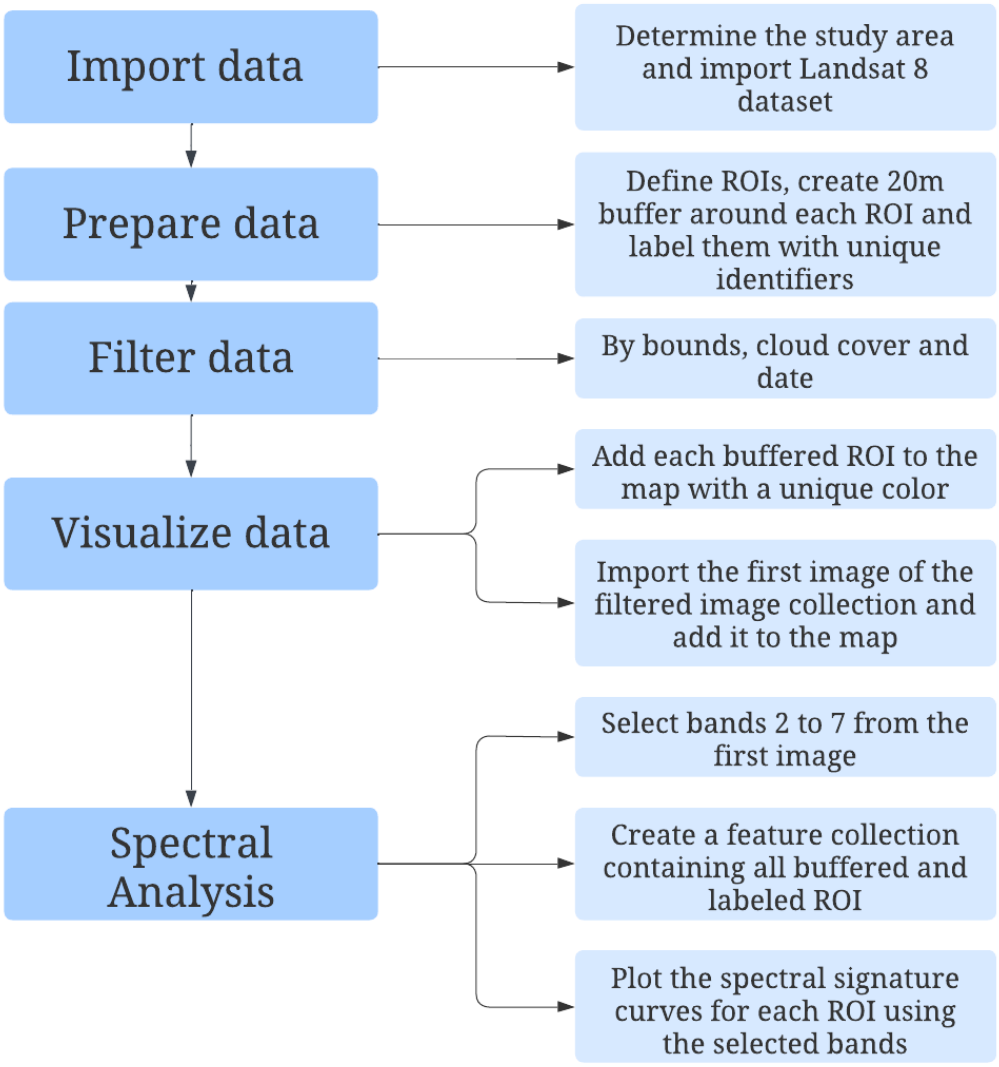

Figure 3.3: Visual representation of the methodology to plot the spectral signature curves.

Initially, a polygon was utilized to determine the study area, followed by the importation of satellite imagery. This research employed the Landsat 8 Collection 2 Tier 1 datasets, which feature calibrated top-of-atmosphere (TOA) reflectance. The highest quality Landsat scenes are categorized into Tier 1 and are deemed appropriate for time-series analytical processes. Tier 1

encompasses Level-1 Precision Terrain (L1TP) processed data, known for their consistent radiometry and inter-calibration across various Landsat sensors (Crawford et al., 2023). Out of the 17 bands in this image collection, this study focused on 6. Table 3.2 provides details on the selected bands and their respective attributes.

Table 3.2: Landsat 8 Collection 2 Tier 1 Bands used to plot spectral signature curves.

Name	Description	Resolution (Meters)	Wavelength (nm)
B2	Blue	30	450 - 510
B3	Red	30	530 - 590
B4	Green	30	640 - 670
B5	Near Infrared (NIR)	30	850 - 880
B6	Shortwave Infrared 1 (SWIR 1)	30	1570 - 1650
B7	Shortwave Infrared 2 (SWIR 2)	30	2110 - 2290

The ROIs were developed in the next stage. In Southern Nevada public schools, 29 football fields switched from natural grass to synthetic turf in 2020–21 (Seeman, 2020). Three of them were beyond the approved study zone, and 26 of these were identified as the focal sites for this investigation. These ROIs were first identified within GEE by means of point features. Then, a 20-meter buffer was built around each point. Each of these buffered zones were subsequently integrated into the map using the “Map.addLayer” function. Several filters were applied in the

following stage. The polygon-defined study area was set as the boundary, and date filters were ensured so that only a single image is accessible. The first image from the collection was then chosen and incorporated into the map.

To chart the spectral signature curve for each month of 2018 and 2022, specific plotting parameters were set. These charts are linear graphs, with the X-axis denoting the bands and the Y-axis indicating the reflectance from each band. The “Reduce.region” function was employed to obtain the mean value from each buffered zone. Alongside each spectral signature curve, a CSV file was generated and preserved post-execution for subsequent analysis. Figure 3.4 illustrates the ROIs where spectral signature curves from 2018 and 2022 were created and analyzed for comparison. This study area map was prepared in ArcGIS Pro.

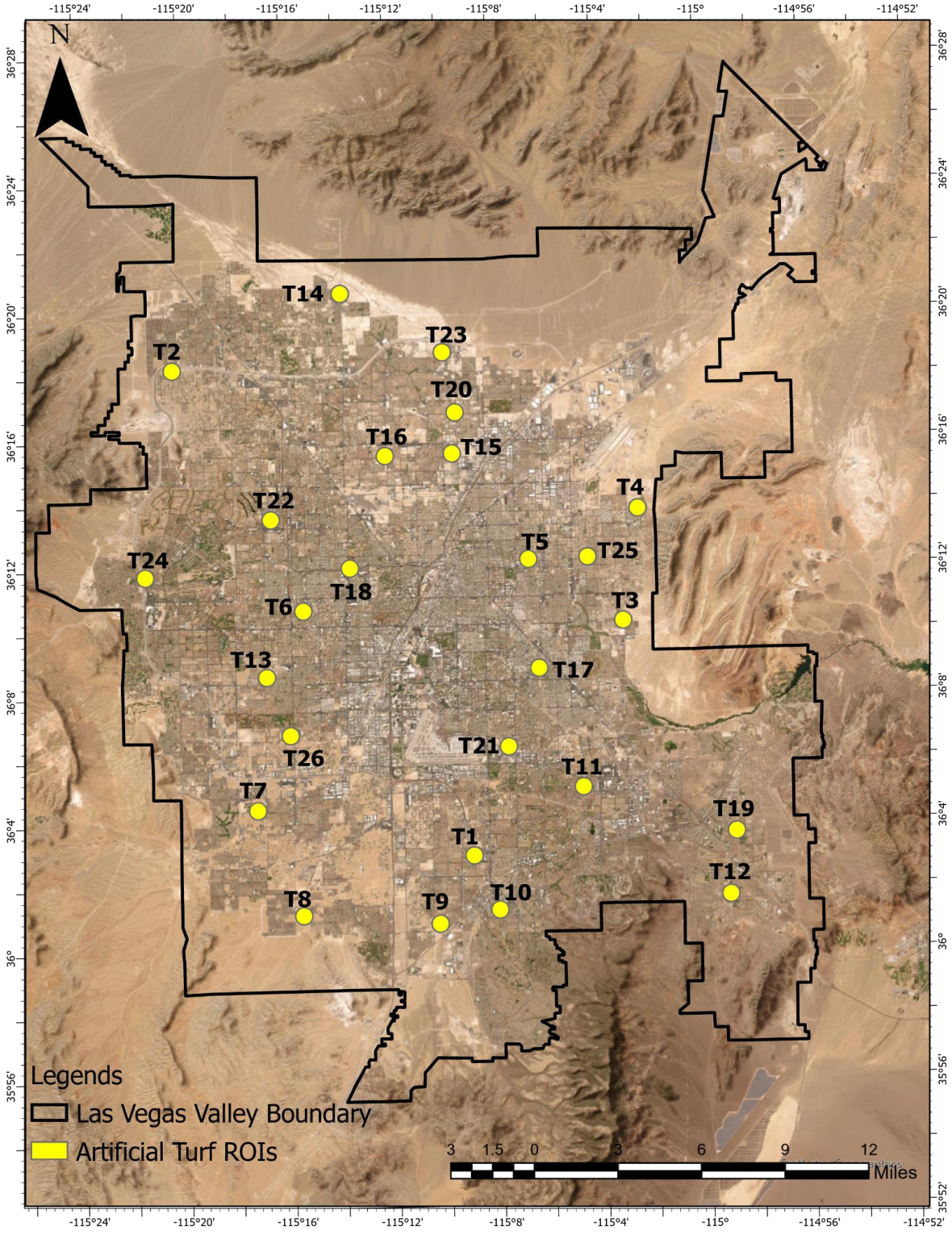

Figure 3.4: Yellow regions represent the ROIs converted from natural grass to artificial turf between 2018 and 2022.

Additionally, the NDVI was calculated for two sets of ROIs. The first set is the transitioned ROIs, that transitioned from natural to artificial turfs between 2018 and 2022. These ROIs are the football fields as mentioned earlier. The second set is the non-transitioned ROIs that maintained natural grass surface over the years. These ROIs are mostly the golf courses around the LVV. Figure 3.5 shows the visual representation of the methodology to calculate the NDVI.

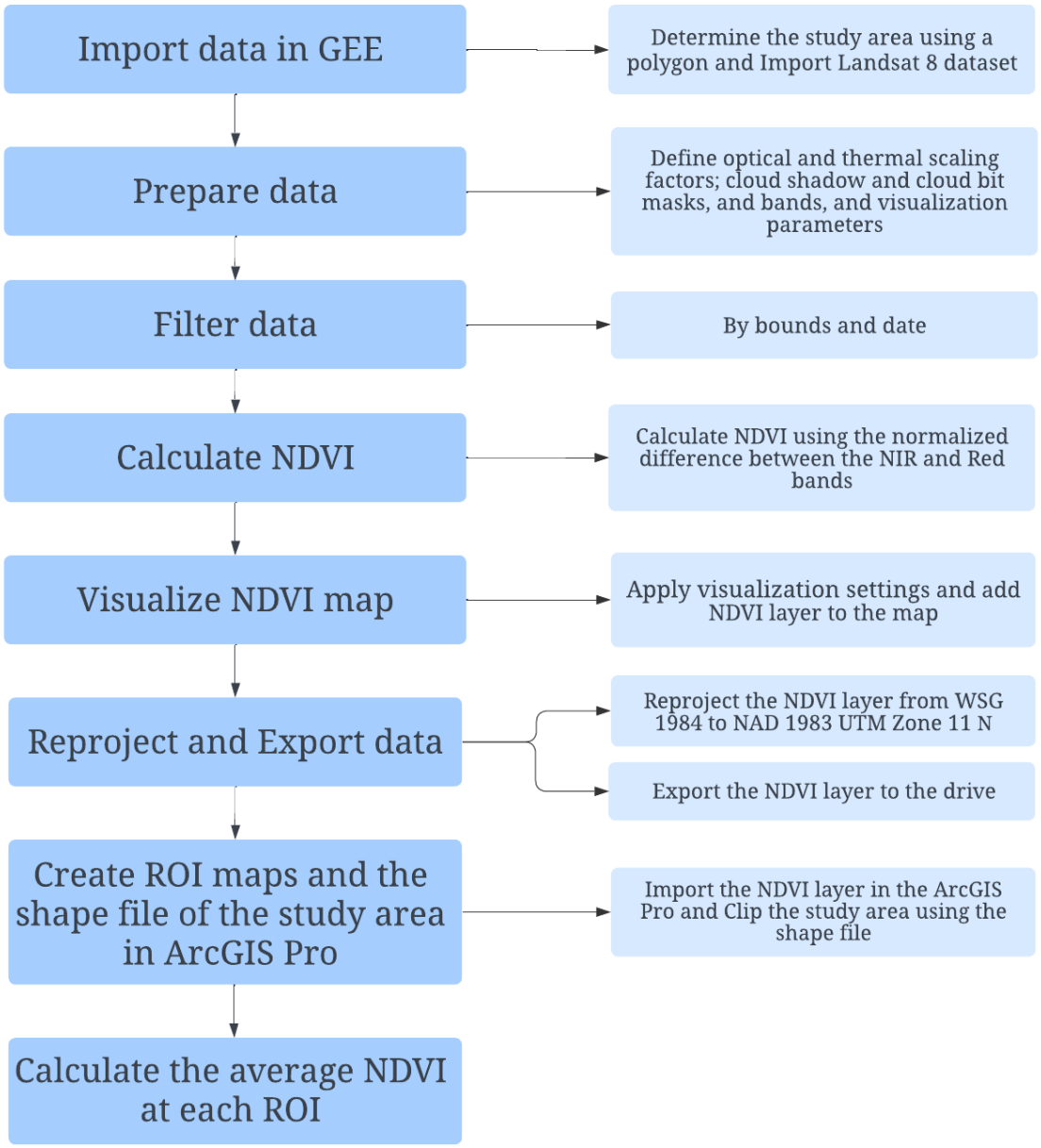

Figure 3.5: Steps involved to retrieve NDVI values from ROIs in GEE and ArcGIS Pro.

During the data initialization phase, the Landsat 8 Collection 2 Level 2 Tier 1 dataset was initially imported into the GEE code editor, and a study area polygon was delineated. In the data pre-processing stage, first, optical, and thermal scaling factors were defined using the 'applyScaleFactors' function. After that, the 'maskL8sr' function was used to remove cloud and cloud shadow from the images by using the 'QA_Pixel' band to identify and exclude these pixels. Finally, the Landsat 8 image collection was narrowed down based on specific dates and the selected region.

Subsequently, the data was visualized on the map and relevant calculations were performed. A true color composition of the imagery was added to the map by defining a visualization parameter for the true color image. Then, the NDVI of the study area was determined using the NIR and red bands of the filtered image and displayed on the map.

The coordinate system of the NDVI layer was subsequently reprojected from WSG 1984 to NAD 1983 UTM Zone 11 N to align with the coordinates of LVV. Finally, the images for each date were exported as a Tiff file.

Following that, the subsequent phase involved defining the ROIs in ArcGIS Pro to examine the NDVI values within each ROI across the four-year period. As mentioned earlier, 26 ROIs transitioned from natural to artificial turf between 2018 and 2022, and 26 ROIs did not go through any transition and served as a control group. For the purposes of this research, two separate ROI maps were created for two cases: transitioned ROIs and non-transitioned ROIs. Two to three complete pixels located within the boundaries of the football fields and other land types were selected as the ROIs (Figure 3.6). The selection of complete pixels is aimed at minimizing the influence of mixed pixels that contain multiple land classes. A ROI map was then created showing

all the transitioned and non-transitioned ROIs (Figure 3.7). The NDVI layers exported from GEE were retrieved from Google Drive and displayed on the Arc map. The NDVI layer was clipped using the shape file of the study area. The shape file of the LVV was created in ArcGIS Pro utilizing the political boundary of the area. Finally, data was collected from each ROI using the "Zonal Statistics as Table" tool in ArcGIS Pro. This produced standalone tables with ROI-specific values for subsequent analyses. The gathered data were then compiled into a separate Excel sheet for further analysis.

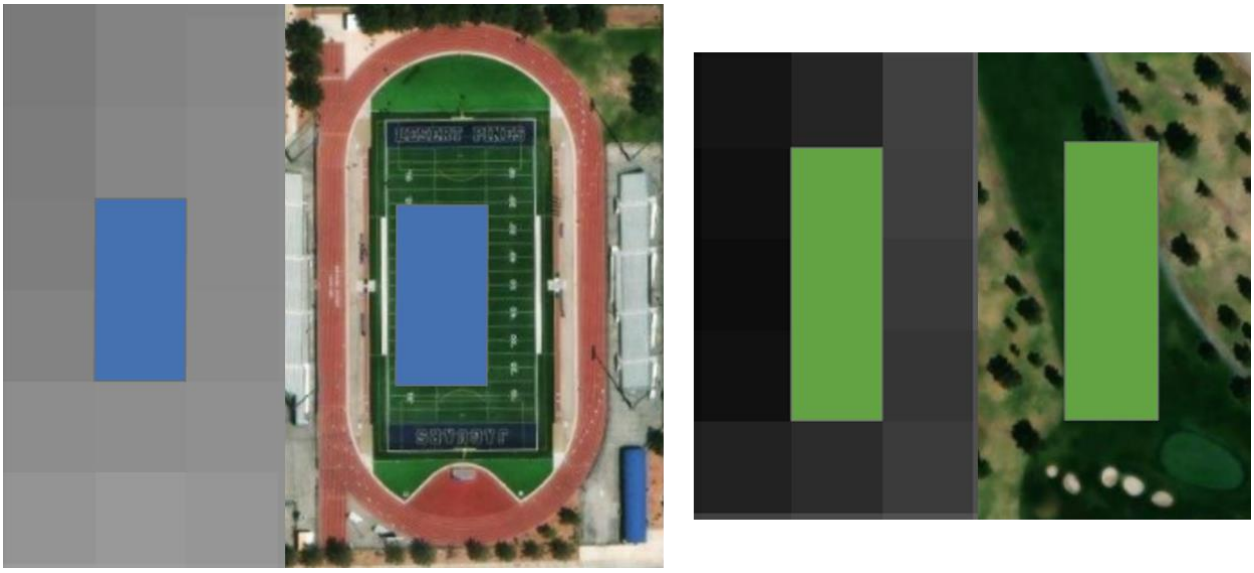

(a) (b)

Figure 3.6: Representation of selected ROIs for analysis. (a) Depicts two fully contained pixels within the confines of Desert Pines High School football field, identified as a transitioned ROI, with the left displaying a grayscale image and the right showcasing the true-color image. (b) Illustrates three fully contained pixels situated within the Las Vegas Golf Club grounds, identified as a non-transitioned ROI, where the left image is grayscale, and the right reveals the natural coloration.

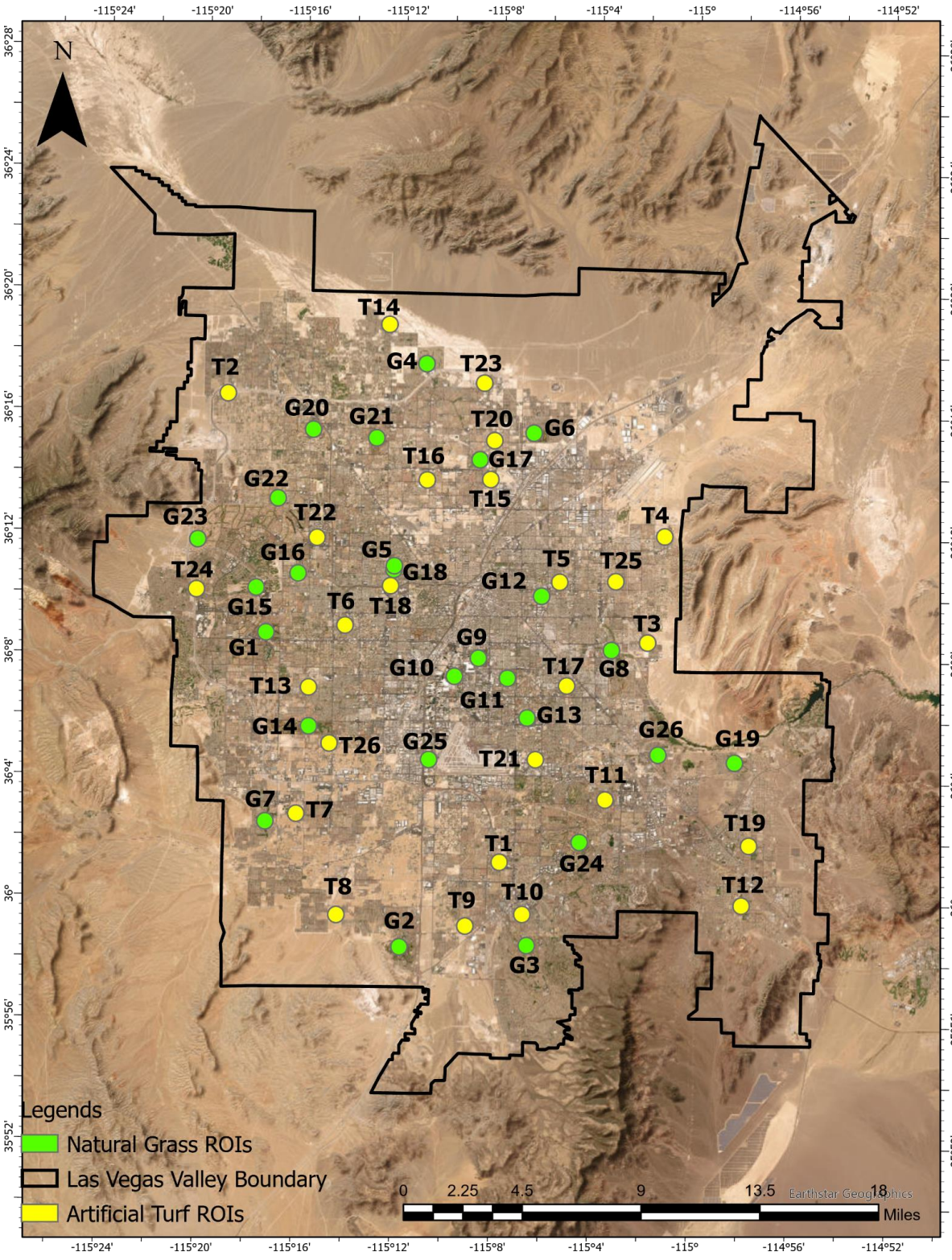

Figure 3.7: Sky Blue dots represent the ROIs converted from natural grass to artificial turf between 2018 and 2022 and green dots represent the ROIs that did not go through any conversion.

Paired T-Tests were employed to evaluate the differences in the spectral signature and NDVI of artificial turfs between 2018 and 2022. The T-Test, a statistical method, is designed to assess whether there are significant differences between two distinct groups. For Spectral Signature, the analysis was divided into two sets of T-Tests. The initial set involved conducting a T-Test for each month, resulting in a total of 12 T-Tests. For these tests, reflectance values derived from satellite imageries for each month were compared. The second set focused on identifying significant differences in reflectance values across each ROI, with a T-Test being conducted for each of the 26 ROIs. A significant threshold of 0.05 was applied to both sets of T-Tests, meaning that a P-Value below this level was required for the results to be deemed statistically significant.

Three series of Paired T-Tests were conducted to find significant differences in NDVI between 2018 and 2022 for both transitioned and non-transitioned cases. Table 3.3 gives an overview of 3 series of Paired T-Tests conducted for NDVI Analysis. The table summarizes the types of T-Tests applied, including annual, seasonal, and individual ROI assessments for both transitioned and non-transitioned ROIs, along with the count of tests conducted per category and the corresponding P-values.

Table 3.3: Summary of the types of paired T-Tests applied, the count of tests conducted in both transitioned and non-transitioned categories and the corresponding threshold values.

Paired T-Tests	Description	No of pair of T-Tests for Transitioned ROIs	No of pair of T-Tests for Non-Transitioned ROIs	Threshold P-Values
Annual T-Test	All data from all ROIs for the entire year were combined	1	1	0.05/26 = 0.002
Individual ROI	T-Tests were performed for each ROI taking all the data from the available dates	26	26	0.05 for each ROI
Combined Seasonal T-Tests	All data from all ROIs were pooled for each season to conduct T-Tests	4	4	0.05/26 = 0.002 for each season

An alpha level of 0.05 was established as the threshold for statistical significance for the second series of T-Test, indicating that any differences observed would need to be statistically significant to be considered meaningful. Bonferroni adjustment was considered for the other two series of T-Tests by adjusting the alpha level to avoid multiple testing problems.

In the context of statistical significance, if the p-value is above a predefined threshold (commonly 0.05), it is generally interpreted that there is not enough statistical evidence to reject the null hypothesis. Thus, it would be concluded that the differences between the paired samples are not statistically significant. The null hypothesis (H0) of this study posited that there were no significant differences in the reflectance values/ NDVI at different wavelengths of the EM

spectrum resulting from the turf type change between the years 2018 and 2022. Conversely, the alternative hypothesis (H1) contended that there were significant differences between the years 2018 and 2022 attributable to the conversion from natural to artificial turf.

These statistical analyses were carried out using R-Studio. In the R studio, each data set first underwent normality testing to determine if it follows a normal distribution. For data sets that do not pass the normality test, indicated by an alpha value of less than 0.05, the Mann-Whitney U test was applied.

3.4 Results and Discussions

This study aims to discuss the following topics:

1. The distinct spectral signatures associated with natural grass and artificial turf in the 26 ROIs and the way the spectral signatures of artificial turf in 2022 differ from those of natural grass in 2018 across various wavelengths.
2. The wavelengths that show the most significant differences between natural grass and artificial turf spectral signatures.
3. The way the NDVI of artificial turf differs from those of natural grass in LVV for both transitioned and non-transitioned ROIs.

3.4.1 Spectral Signature

In GEE, 45 spectral signature curves for each month of 2018 and 2022 were produced for locations that underwent a transition from natural to artificial turf between 2018 and 2022. A CSV file showing the reflectance values of all 26 ROIs at each wavelength was provided with each

curve. The data from the CSV files were compiled into an Excel sheet and were organized for analysis.

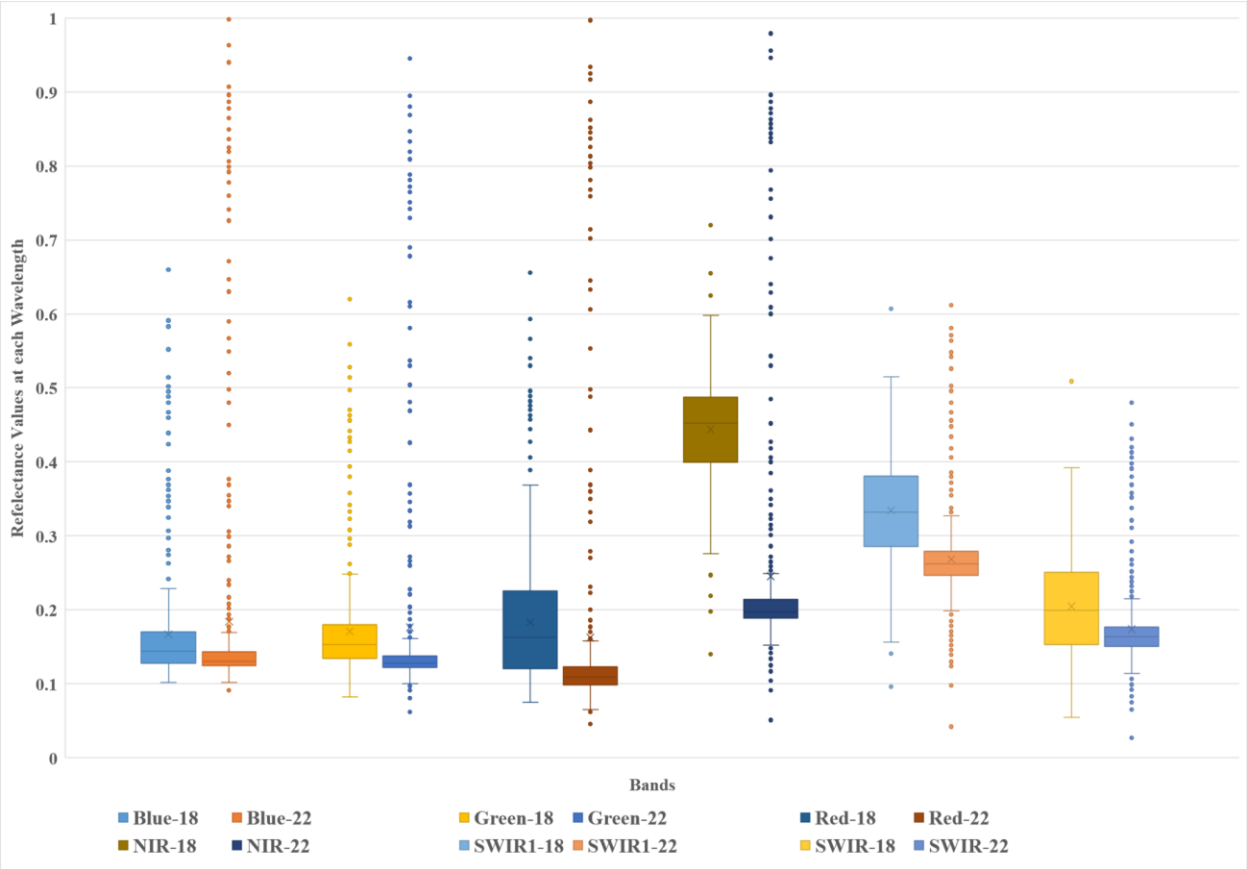

Figure 3.8: Distribution of the reflectance values from all the ROIs at each wavelength in 2018 and 2022

The box plots in figure 3.8 provide a visual comparison of reflectance values for different spectral bands of the EM spectrum between the years 2018 and 2022, taken from football fields that transitioned from natural to artificial turf. The X-axis denotes the center of the wavelengths of the EM spectrum, while the Y-axis indicates the reflectance values at each wavelength.

Box plots show the median, the interquartile range, and the overall range (the whiskers) of the reflectance values at each wavelength. An observation that deviates significantly from the rest of the data numerically is called an outlier. Outliers are indicated by dots outside the whiskers.

The plots show that the reflectance values have changed at each wavelength due to the transition from natural to artificial turf. Shifts in the median values were found for all the bands of the EM spectrum. The median values for all the bands were higher for natural grass in 2018 than those for artificial turf in 2022 (Table 3.4). A significant shift was found for the NIR band, having 0.255 difference in the median values between 2018 and 2022, which is typical as vegetation reflects more in the NIR spectrum due to the internal structure of leaves.

The spread of the data, indicated by the height of the boxes (which represent the interquartile range, or IQR), shows the middle 50% of the data for each band and year. A larger IQR suggests greater variability. The variability seemed to be greater for natural grass in 2018 compared to artificial turf in 2022. This could suggest that natural grass has more variability in how it reflects light, possibly due to the different water content, health, or density, while artificial turf was more stable.

The numbers that are the smallest and largest can be found at the end of the "whiskers" and are helpful in giving a visual representation of how the data is distributed. The ranges of the reflectance values of all the bands were found to be higher for the natural grass in 2018.

There were outliers in the data for both natural grass in 2018 and artificial turf in 2022. More numbers of outliers were found for the artificial turfs in each band. Numerous outliers may suggest that there are some areas with quite different reflectance properties compared to the rest of the ROIs.

Table 3.4: Median and Mean Reflectance Values for Various Spectral Bands in 2018 and 2022 with Corresponding Differences

Bands	Center of the Wavelength	Median Reflectance	2022-2018	Mean Reflectance	2022-2018
Blue-18	482	0.14	-0.01	0.17	0.02
Blue-22	482	0.13		0.18	
Green-18	562	0.15	-0.03	0.17	0.01
Green-22	562	0.13		0.18	
Red-18	655	0.16	-0.05	0.18	-0.02
Red-22	655	0.11		0.16	
NIR-18	865	0.45	-0.26	0.44	-0.20
NIR-22	865	0.20		0.25	
SWIR1-18	1609	0.33	-0.07	0.33	-0.07
SWIR1-22	1609	0.26		0.27	
SWIR-18	2201	0.20	-0.04	0.20	-0.03
SWIR-22	2201	0.16		0.17	

Healthy green vegetation, due to the chlorophyll pigments, absorbs substantial energy in the blue and red regions of the spectrum, resulting in low reflectance, while the leaves' internal cellular structure causes high reflectance in the NIR region (Thenkabail et al., 2000). In figure 3.8,

the spectral signature of natural grass shows higher reflectance in the NIR band compared to the visible bands (blue, green, red), which is a characteristic of healthy vegetation. The spectral signature of artificial turf is flatter and lower in reflectance, lacking the distinct peak in NIR. The difference in the spectral signatures reflect the inherent differences between the materials. Natural grass has a complex structure that interacts with light differently than more homogeneous artificial turf material.

Figure 3.9 shows the average annual reflectance values of all 26 ROIs in 2018 and 2022. In 2018, the spectral signature curves displayed characteristics typical of natural grass. Due to the internal structure and moisture content of green grass, natural grass exhibits elevated reflectance in the NIR zone, spanning from 0.7 µm to 1.3 µm (Spectral Reflectance, n.d.). The spectral signature curves obtained from each satellite image revealed that the reflectance values in this NIR zone were consistently elevated throughout 2018, with peak values surpassing 0.4 for most of the ROIs. The majority of the blue and red light is strongly absorbed by chlorophyll in healthy vegetation. A step in the process of photosynthesis is light absorption. The healthy plant reflects a large amount of infrared light and some green light. Since infrared light is invisible to human vision, healthy plants appear green to the human eyes even if they reflect more NIR radiation than visible green. This study's findings indicate that the average reflectance of red (0.183) is higher than that of green (0.171) in 2018 when there were natural grass surfaces. It may be the result of stressed or dehydrated grass which differs from healthy grass as it is not watered enough and has brown spots, whereas healthy grass is all green with no brown spots. (Kwan et al., 2020).

According to Idso et al. (1980), as plants lose chlorophyll, undergo browning, ripen, or experience the process of deterioration with age, the visible spectrum reflects these changes. Chlorophyll gives plants their green color, so its loss will significantly affect the coloration

observed in the visible spectrum. Unhealthy plants emit more visible red light. That's why as they dry up, they become reddish brown.

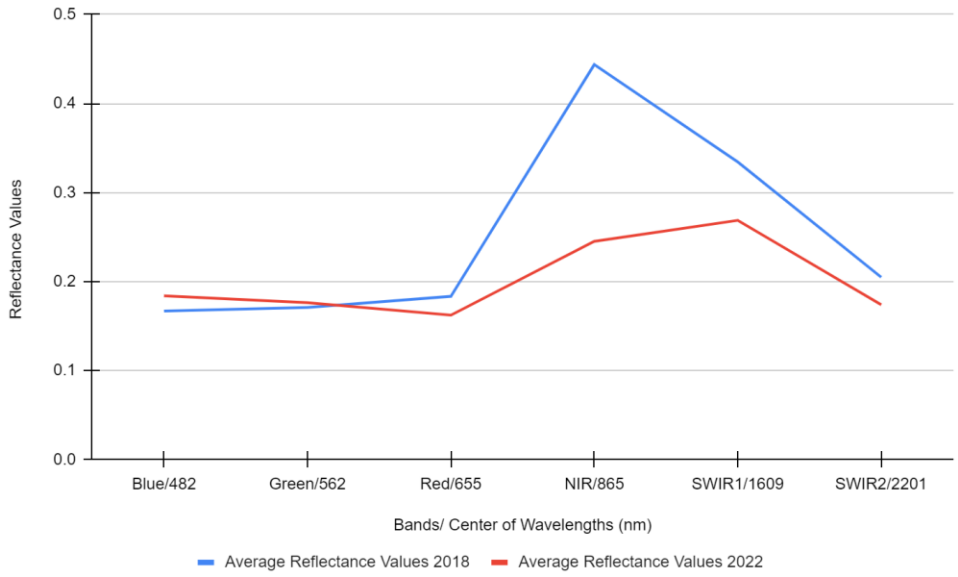

Figure 3.9: Average annual reflectance values of all 26 ROIs at each wavelength in 2018 and 2022

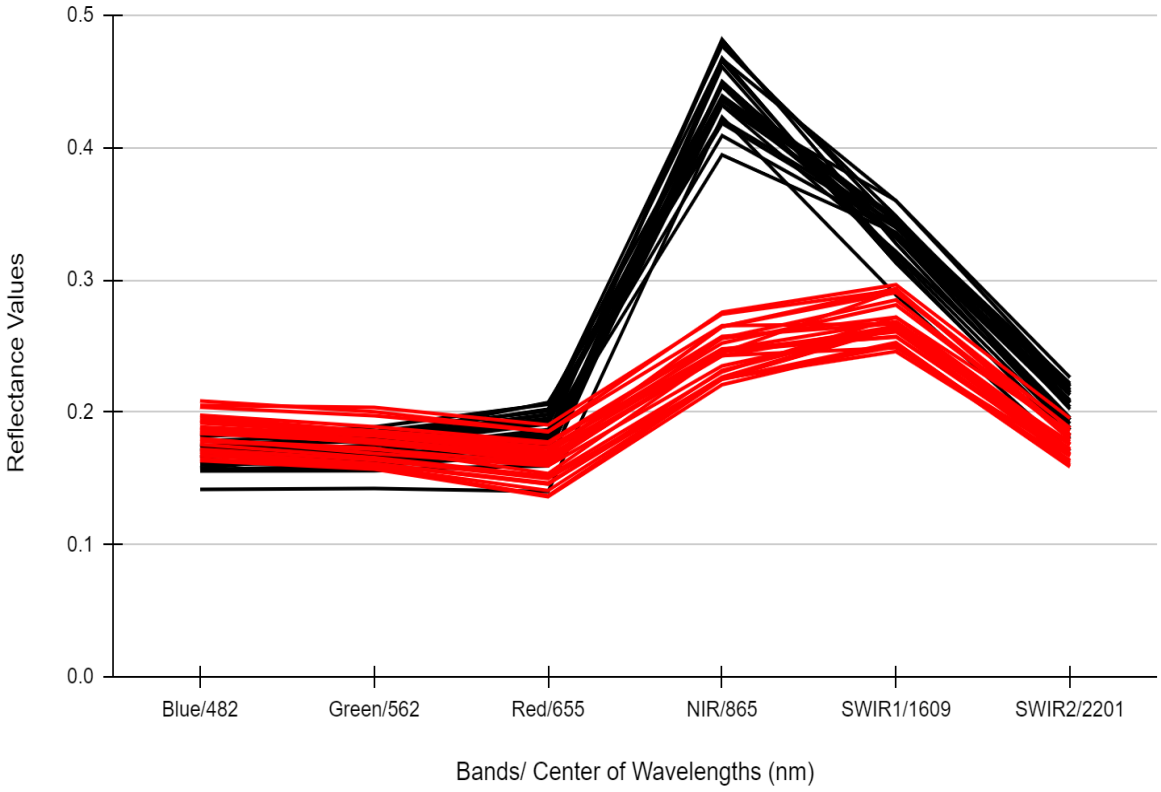

Figure 3.10: Average reflectance values of each ROI at each wavelength for 2018 and 2022. The black lines represent the spectral signatures of 26 ROIs in 2018, while the red represent the curves from 2022.

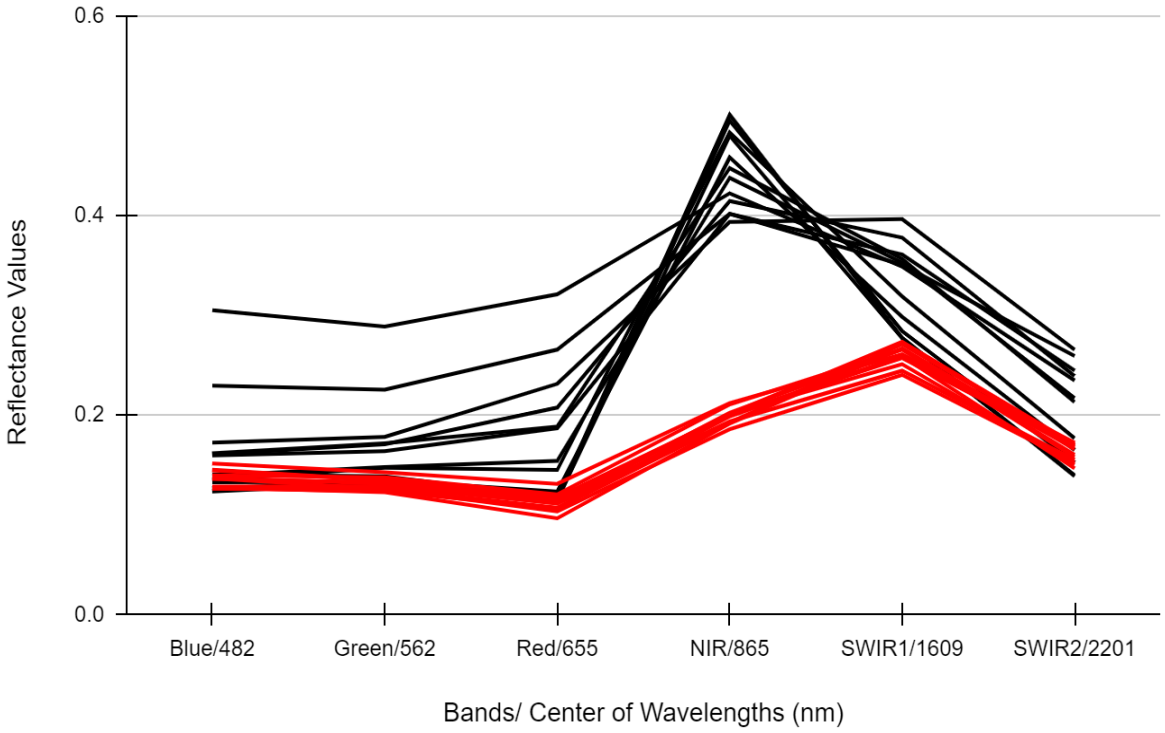

Figure 3.11: Average reflectance values of each wavelength at each month of 2018 and 2022. The black lines represent the average reflectance values for the months of 2018, while the red represent the curves from 2022.

The reflectance values were averaged for each month and figure 3.11 was plotted showing the average reflectance values of each month of 2018 and 2022 at different wavelengths of the EM spectrum. In 2022, the spectral signature curves lacked the characteristics of natural grass, given the transition from natural to artificial turfs. Except for May and June 2022, the reflectance values in the blue region were higher than those of the green region for the rest of the months. Reflectance values at blue and green regions for May (0.128173 in Blue and 0.128365 in Red) and June 2022

(0.128212 in Blue and 0.128865 in Red) were almost similar. Due to heavy cloud cover on 22nd April (81%) and 13th September (76%) data, unusual reflectance values were being obtained for April 2022 and September 2022 data. Therefore, these two images were omitted while doing monthly analysis.

The SWIR1, spanning wavelengths from 1570 to 1650 nm, exhibited a marked feature. At 1609 nm wavelength, the reflectance patterns of both natural and artificial turf displayed contrasting directions. In the first month of 2018, the SWIR1 reflectance values surpassed the values in the NIR region (Figure 3.12). However, for the subsequent months of that year, SWIR reflectance was consistently below NIR levels.

Water has a pronounced absorption property in the SWIR region, as highlighted by Moshtaghi et al. (2021) and Kim et al. (2015). Given the moisture content in natural grass, it tends to absorb more in this region, leading to SWIR reflectance values that were generally lower than NIR for 2018, except for the first month of 2018. In contrast, throughout 2022, SWIR1 reflectance consistently exceeded that in the NIR region. Artificial turf is commonly crafted from materials like nylon, polyethylene, or polypropylene, which belong to the plastic category. Each plastic type, made up of elements like carbon, hydrogen, and oxygen, exhibits distinct infrared absorption characteristics when illuminated, reflecting the vibrational movements within their polymer structures, as noted by Karaca et al. (2013). While studies by Moshtaghi et al. (2021) and Masoumi et al. (2012) identified absorption traits for various plastics, this research observed elevated reflectance in the SWIR1 zone. The increased surface temperatures from the artificial turf might account for this deviation.

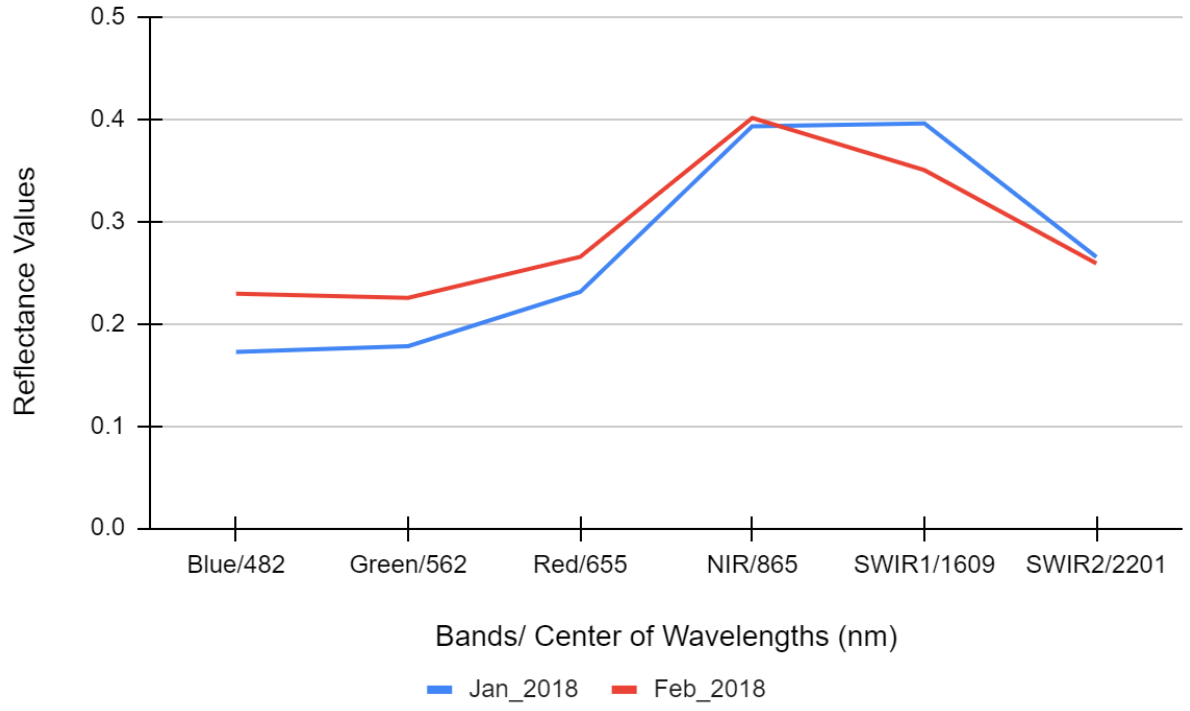

Figure 3.12: Average reflectance values at each wavelength in January 2018 and February 2018

In the subsequent analysis, the average reflectance values in the NIR region were charted for every month of 2022 to determine the reflectance of artificial turf surfaces in the NIR region (Figure 3.13). The spectral signature curves of April, May and November showed a very slight tilt between the Red and SWIR1 regions. Since the reflectance values were taken as the average of all 26 ROIs, it may suggest that a lot of ROIs might not have shown any reflectance in the NIR region during these three months. The average reflectance values of the rest of the months showed distinguishable patterns in the NIR region.

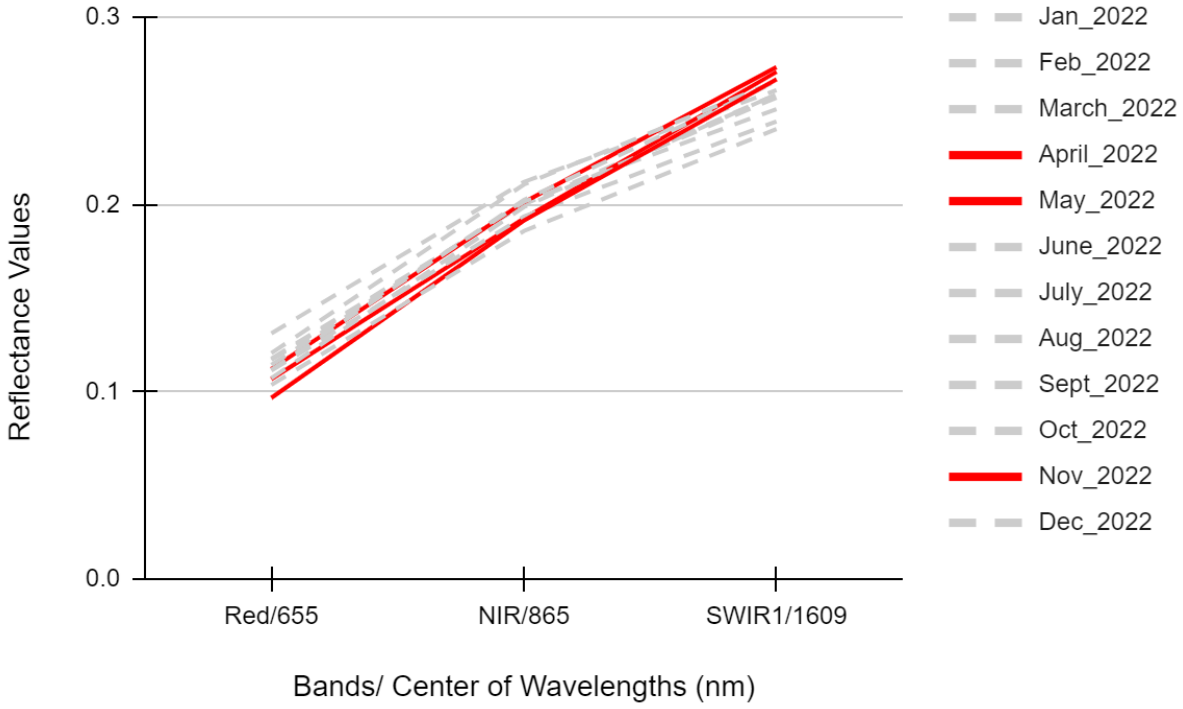

Figure 3.13: Spectral signatures of artificial turf on April 2022, May 2022 and November 2022 showing very slight reflectance values in the NIR region.

These variations in the reflectance from the NIR region in different months can come due to the following environmental and technical factors:

1. Artificial turf can be made of different materials such as polystyrene, polyethylene or nylon. Various organic or inorganic materials can be used for infill materials. Differences in material composition, age of the turf, and wear may affect NIR reflectance.

2. The reflectance properties of turf can get changed due to the accumulated dust, debris, water or snow on it. Therefore, regular maintenance of artificial turf might show higher NIR reflectance in certain months.
3. Landsat 8 collects images at 10 am. That may not be the peak time for the artificial turf to show reflection in the NIR region.
4. One or two dates from each month were chosen for the analysis. The weather on that particular date may change abruptly due to atmospheric conditions such as cloud cover or haze which, in turn, can affect the NIR reflection in some ROIs.

In contrast to the NIR region, the SWIR1 region displayed reflectance values consistently across all months of 2022 (Figure 3.11).

Subsequently, a separate graph was created to depict the reflectance values of NIR, SWIR1, and SWIR2 for each month of 2018 and 2022. The 2018 data demonstrated elevated reflectance values for NIR and SWIR1, while the 2022 data were higher for SWIR2.

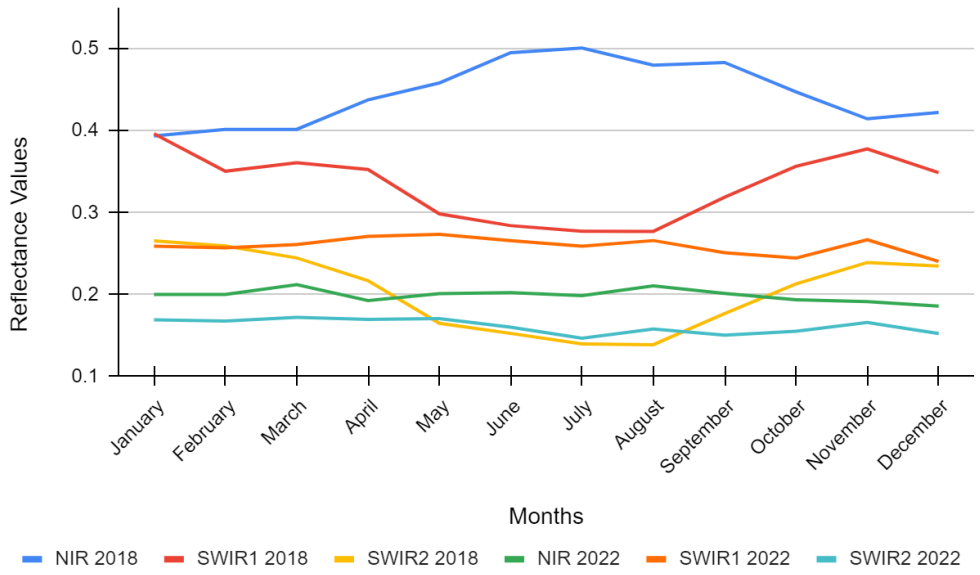

Figure 3.14: Average reflectance at the NIR, SWIR1 and SWIR2 regions in each month of 2018 and 2022

Figure 3.14 compares the average reflectance values in the NIR, SWIR1, and SWIR2 regions across the months of 2018 and 2022. The NIR and SWIR1 reflectance values in 2018 are consistently higher than in 2022. This change is likely due to the transition from natural grass in 2018 to artificial turf in 2022. In 2018, the NIR reflectance values show a seasonal pattern, peaking around the middle of the year, specifically in the hotter months, which could correspond to the growing season when vegetation is most abundant and healthy. The SWIR1 values have also shown some variability. This could be due to the SWIR1 region's sensitivity to moisture content, which can vary due to factors other than vegetation health, such as precipitation or maintenance practices. SWIR1 and SWIR2 show a similar pattern. The reflectance values for 2022 do not show the same seasonal pattern as 2018, staying relatively flat throughout the year. This lack of

seasonality is consistent with artificial turf, which does not grow or change in the same way that natural vegetation does. The NIR reflectance in 2022 is higher than the SWIR2 reflectance, and lower than the SWIR1 reflectance in 2022. However, the difference between NIR and SWIR1 reflectance is more pronounced in 2018 than in 2022, indicating that natural grass has a more distinct spectral signature compared to artificial turf. The lower reflectance values in NIR, SWIR1, and SWIR2 bands for 2022 suggest that the conversion to artificial turf could have impacted the local microclimate and ecological conditions, as these surfaces interact differently with solar radiation compared to natural vegetation.

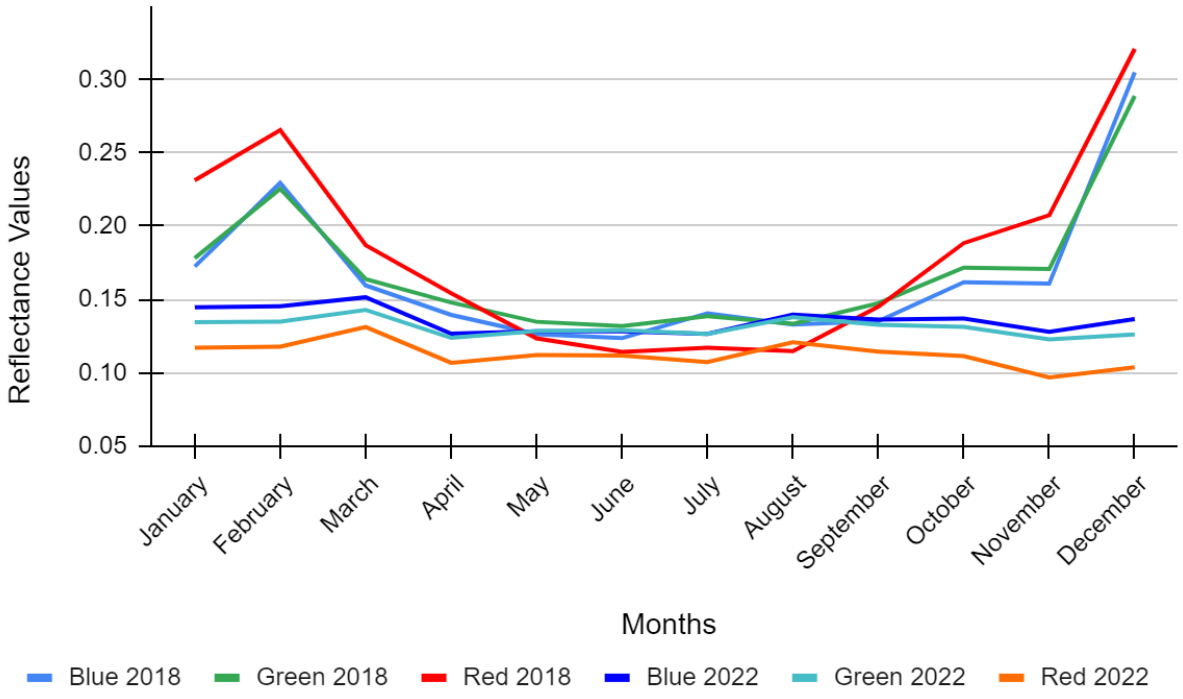

Figure 3.15: Average reflectance at the blue, green, and red regions in each month of 2018 and 2022

Figure 3.15 presents a comparative analysis of average reflectance values across the blue, green, and red regions of the EM spectrum for each month in 2018 and 2022. Green vegetation shows low reflection in the blue and red regions of the EM spectrum (Baghzouz et al., 2006) since strong absorption is done by chlorophyll in these regions and this characteristic is clearly observed in the graph. In 2018, reflectance values exhibit seasonal fluctuations, peaking during the cooler months and diminishing during the summer. The notable dips in the summer correspond to increased photosynthetic activity, during which there is substantial chlorophyll absorption in the blue and red regions. These variations are indicative of the natural growth and dormancy cycles of vegetation. Conversely, the 2022 reflectance values appear consistently uniform, lacking the seasonal variability that is typical of vegetated landscapes. This suggests a significant alteration in surface characteristics, likely attributable to the replacement of natural turf with artificial surfaces, which do not engage in photosynthesis and thus do not show the same seasonal changes in reflectance.

The T-Test is a statistical analysis that identifies any significant differences between two groups. The first series of t-tests were conducted for each month between all the reflectance data obtained from 2018 and 2022. The second series of the T-Tests were conducted considering each ROI. A significance level, or alpha value, of 0.05 was chosen for the T-Tests. The tests were performed in R-Studio. Normality tests were done for all pairs of data. The Mann Whitney U Tests were performed for the pairs that did not pass the normality tests.

12 paired sample T-tests were conducted to compare the reflectance values at each wavelength of 26 ROIs that transitioned from natural grass to artificial turf between the years 2018

and 2022. All the reflectance values of 26 ROIs were selected for each month. Table 3.5 shows the P values corresponding to each month.

Table 3.5: P Values of the T-Tests of each month of the transitioned ROI (Threshold P-Value = 0.05)

Name of the months	P Value
January	< 2.2e-16*
February	< 2.2e-16*
March	< 2.2e-16*
April	2.739e-05*
May	4.518e-14*
June	2.305e-07*
July	0.2
August	0.02*
September	0.0002*
October	< 2.2e-16*
November	< 2.2e-16*
December	< 2.2e-16*

Additional series of T-Test was performed considering the ROIs only. All the reflectance values from all the obtained satellite images were selected for each ROI. Table 3.6 shows the P-Value for each T-Test result.

Table 3.6: P-values for the T-Tests of each ROI (Threshold P-Value = 0.05)

ROIs	P-Values	ROIs	P-Values
T1	0.001*	T14	5.473e-08*
T2	6.594e-09*	T15	2.969e-06*
T3	4.248e-07*	T16	5.358e-11*
T4	5.399e-08*	T17	1.177e-06*
T5	6.255e-09*	T18	1.238e-10*
T6	3.897e-09*	T19	7.273e-09*
T7	2.786e-11*	T20	0.002231*
T8	1.512e-10*	T21	5.063e-11*
T9	1.662e-15*	T22	2.373e-05*
T10	3.535e-14*	T23	1.676e-06*
T11	5.819e-12*	T24	6.049e-11*
T12	5.581e-08*	T25	8.104e-09*
T13	2.747e-09*	T26	2.736e-10*

The first series of T-Tests, comparing reflectance values at different wavelengths between 2018 and 2022 for each ROI, revealed significant differences in all the months except July. The ROIs transitioned from natural to artificial turfs between 2018 and 2022. In the second series of T-Tests, significant differences were observed in all transitioned ROIs.

According to the results of the first series of T-Tests, the alternative hypothesis cannot be rejected for the transitioned ROIs, as significant differences were found for almost all the months. This implies that the conversion did result in statistically significant changes in spectral signature for these areas. Based on the second series of T-Tests, the null hypothesis can be rejected as well since statistically significant differences were observed for all ROIs supporting the alternative hypothesis that the conversion has affected the reflectance values in these specific areas.

Overall, T-Test results for spectral signature analysis suggest that the transition from natural to artificial turf has had a measurable impact on the spectral properties of the ROIs. Artificial turf has different reflectance properties than natural grass across the different bands of the EM spectrum due to the differences in color, texture, and the way they interact with light. Significant differences in all months also suggest that the changes are consistent throughout the year. This could indicate that the differences are not just seasonal variations but are due to the actual change in turf. So, it can be inferred that the changes in surface material have a measurable impact on the reflectance properties of any land class.

Distinctive curves have been displayed by both types of surfaces in both years due to the transition from natural to artificial turf. Artificial turf lacks the characteristics inherent to natural grass. Its spectral signature curves can vary based on factors like material composition, the infill materials used (such as sand or rubber), the turf's surface texture (e.g., the length or density of its

blades), the colors and dyes employed in its production, any contaminants, or additives present, and accumulated dirt. Unlike natural grass, the spectral signatures of artificial turf don't exhibit seasonal changes. Therefore, distinguishing between the spectral signatures of natural and artificial turf is contingent on the specific region and time of year. The materials used in the artificial turf, coupled with the ambient temperature, might account for the observed behaviors of the artificial turf.

Devitt et al. (2007) analyzed the average reflectance measured across different bands of the EM spectrum in relation to surface temperature and found that NIR reflectance significantly differed among six tested surface types and accounted for 62% of their surface temperature variance, a correlation with strong statistical significance ($p < 0.05$), establishing NIR reflectance as a reliable predictor of surface temperature. Consequently, they suggested that manufacturers of artificial turf explore modifications to increase NIR reflectance.

3.4.2 Normalized Difference Vegetation Index (NDVI)

The NDVI stands as a crucial indicator for assessing vegetation density in a specific area, derived from data collected by satellite sensors (Ceballos and Lopez, 2003). NDVI is extensively utilized to observe changes in land utilization and coverage, as well as to assess drought, land degradation, erosion, wildfires, ecological diversity and preservation, and the levels of organic carbon in soil (Kwan et al., 2020).

23 NDVI maps for 2018 and 22 NDVI maps for 2022 were generated using GEE platforms. Landsat 8 satellite was used to generate maps. The maps were then imported to ArcGIS pro, where they were clipped according to the shapefile of LVV. A ROI map showing 26 ROIs that have been switched from natural to artificial grass between 2018 and 2022, and 26 ROIs that did not go

through any transition between the time period, was used to measure the average NDVI values at these ROIs. The data were gathered on an excel sheet for further analysis. Two cases were made for the ease of the analysis:

a. Case I: 2018 (NG) vs 2022 (AT), the ROIs transitioned from natural grass to artificial turf.

b. Case II: 2018 (NG) vs 2022 (NG), the ROIs did not go through any alteration and maintained natural grass in both years.

3.4.2.1 Comparison of the NDVI of all ROIs between 2018 and 2022

NDVI values at each ROI from all the available Landsat 8 satellite images were obtained. Box plots were made to show the distribution of the NDVI values from all transitioned and non-transitioned ROIs (Figure 3.16).

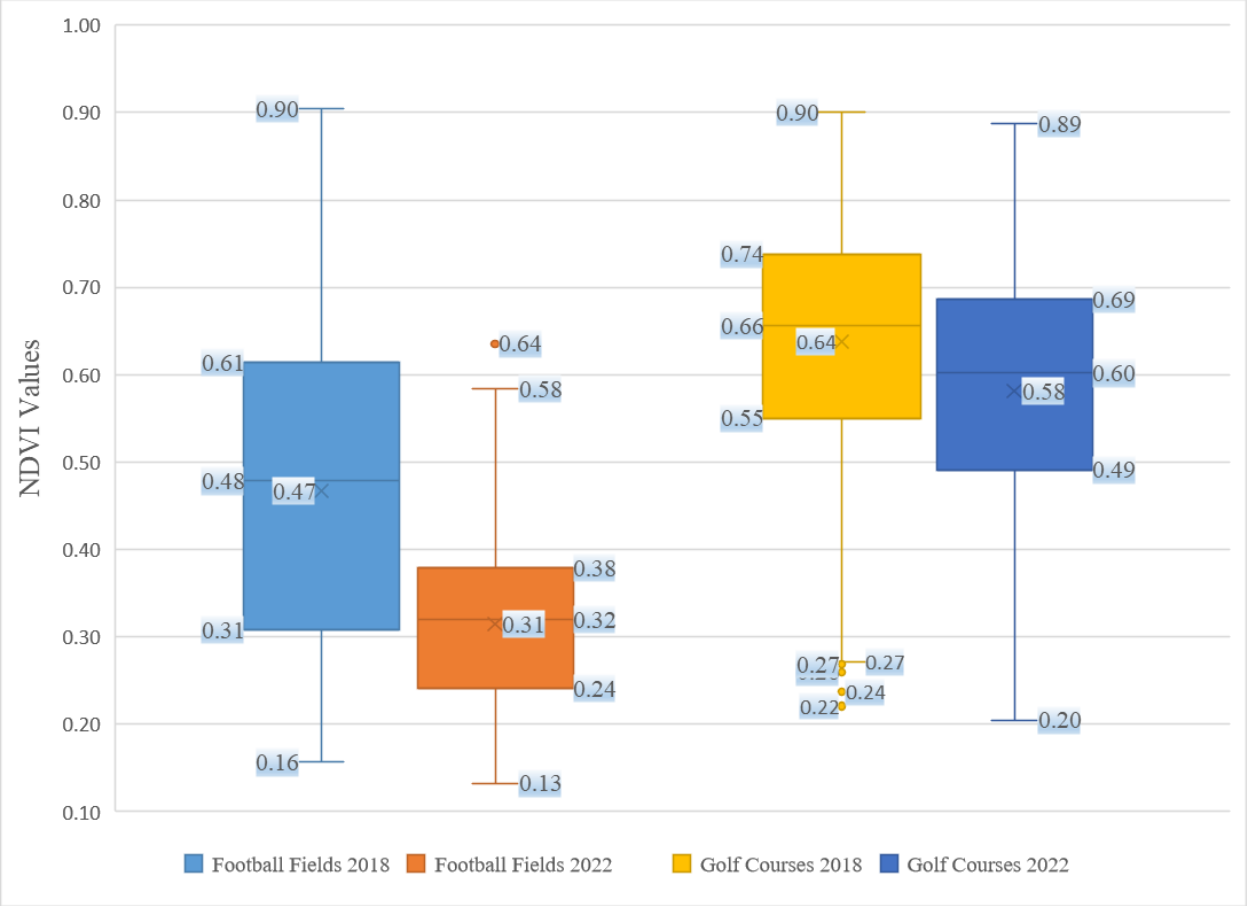

Figure 3.16: Distribution of the NDVI values from all ROIs at Transitioned (Football Fields) and non-transitioned (Golf Courses) ROIs in 2018 and 2022

The box plot illustrates the distribution of the NDVI values for transitioned and non-transitioned ROIs over two distinct years: 2018 and 2022.

For the football fields (transitioned ROIs), the NDVI values in 2018 (blue box) generally have a higher median, upper quartile, and range compared to those in 2022 (orange box), indicating that the vegetation was likely denser or healthier in 2018 than in 2022, which may be due to the transition from natural to artificial turf. Also, the transitioned ROIs showed less variability in 2022,

as indicated by the spread of the boxes, than 2018 suggesting that the NDVI became relatively uniform after the turf transition.

For the golf courses (non-transitioned ROIs), the NDVI values in 2018 and 2022 (dark and light yellow, respectively) do not show a significant difference in the median value, although the range and upper quartile are slightly lower in 2022, which suggests a slight decrease in vegetation density or health.

The differences in NDVI values between the years for the football fields might be more pronounced compared to the golf courses, potentially due to the change from natural to artificial surfaces, which does not support vegetation and thus would have lower NDVI values. The golf courses' relatively stable NDVI values suggest that no significant change in vegetation health or coverage occurred between the years.

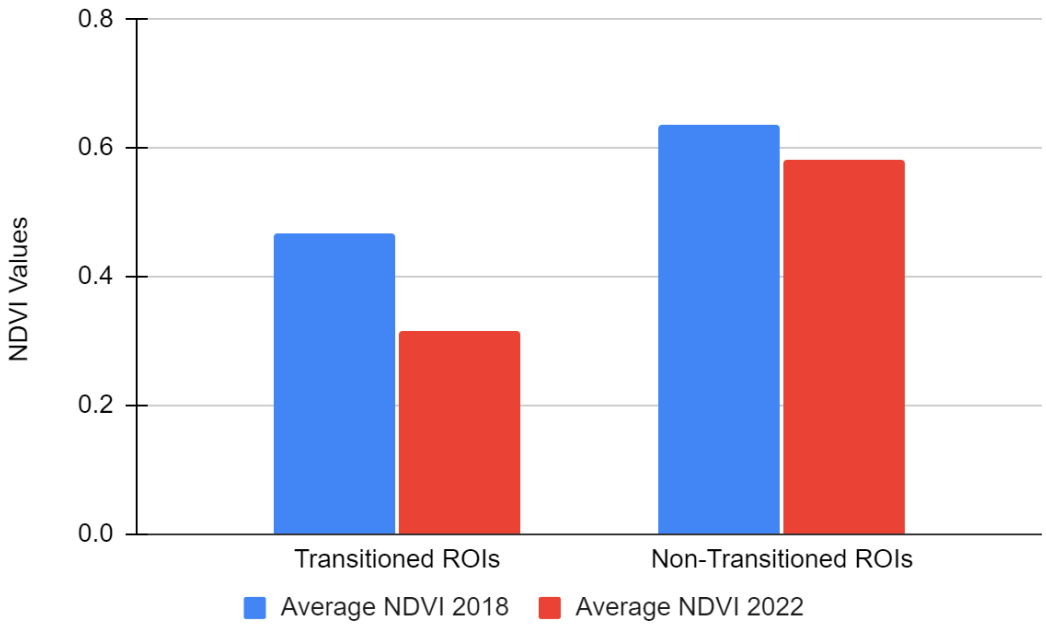

Figure 3.17: Annual average NDVI values at each transitioned and non-transitioned ROIs

Figure 3.17 shows the annual average NDVI values for both cases and both years which clearly shows the annual differences between 2018 and 2022 for both transitioned and non-transitioned ROIs. Higher NDVI values were observed for the non-transitioned ROIs, which is easily understandable since the ROIs were mostly golf courses and golf courses typically have denser grass than football fields. Generally, the denser the vegetation is, the higher the NDVI value.

Both transitioned and non-transitioned ROIs exhibited lower NDVI values in 2022. The average precipitation in 2018 was higher, at 0.17 mm, compared to 0.094 mm in 2022. This greater rainfall in 2018 likely contributed to the higher NDVI values observed that year, as the increased water availability supported healthier vegetation.

3.4.2.2 Comparison of the seasonal variabilities among the transitioned ROIs

The NDVI values of each ROI were averaged for each season, Winter, spring, summer, and Fall, to consider the seasonal variations. Box plots were made to show the distribution of the NDVI values from all transitioned and non-transitioned ROIs at each season (Figure 3.18)

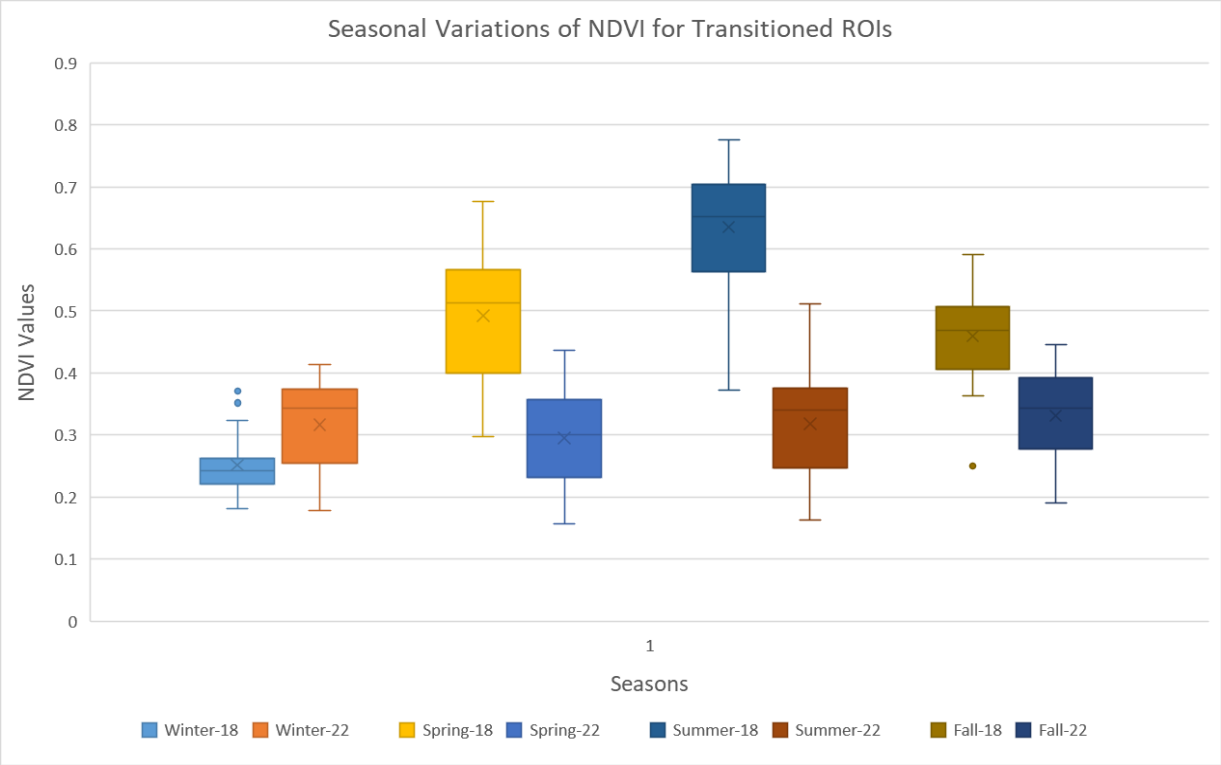

Figure 3.18: Distribution of average NDVI Values of each transitioned ROI at each season of 2018 and 2022

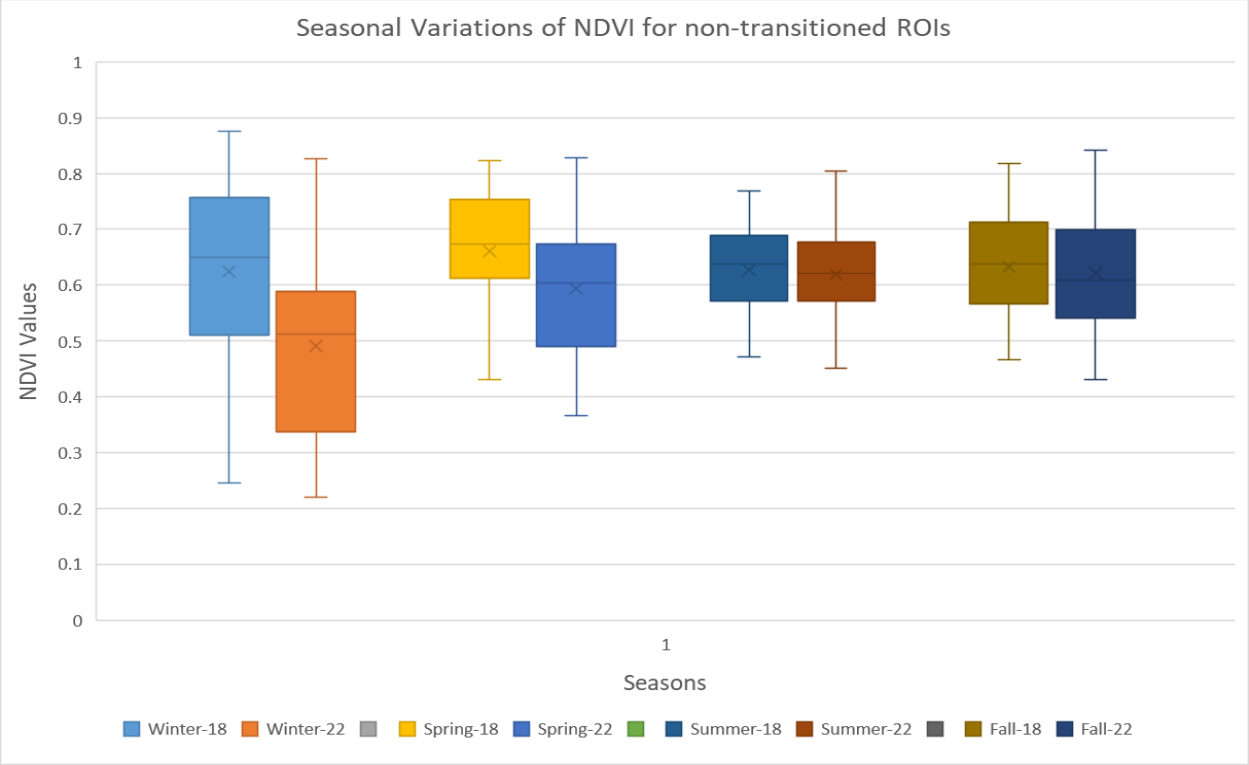

Figure 3.19: Distribution of average NDVI Values of each non-transitioned ROI at each season of 2018 and 2022

The box plots show how NDVI values change with the seasons. The seasonal representation allows for observation of growth cycles and potentially the impact of weather changes on vegetation health. The Summer, Spring and Fall 2022 values were consistently lower than those of 2018 values for both transitioned and non-transitioned ROIs. In the winter, the NDVI values for 2022 for the transitioned ROIs appear to be higher than those for 2018. During the winter season the photosynthetic process slows down or the vegetation goes dormant which can affect the NDVI values. In figure 3.18, the summer NDVI values showed the most difference between 2018 and 2022 which means the impact of replacing natural grass with artificial turf was most pronounced during the summer season. According to Way et al. (2017), photosynthetic

capacity of vegetation increases in the early summer with peak in mid-summer and then declines over the late summer and autumn. During photosynthesis, chlorophyll absorbs energy from blue- and red-light waves, and reflects green-light waves, making the plant appear green. Overall, a noticeable trend where the NDVI values in 2022 were generally lower for the transitioned ROIs, was found following the turf transition. For the non-transitioned ROIs in figure 3.19, which are the golf courses that maintained their natural grass surfaces, the changes in NDVI are very slight in all seasons suggesting that the NDVI for natural grass surfaces remains relatively stable year over year. The greater changes in NDVI values for the transitioned ROIs compared to the non-transitioned ones could be due to the difference in surface materials which indicates that converting to artificial turf can have a noticeable impact on the reflective properties of the surface.

Table 3.7: The median values in NDVI noted in different seasons for both transitioned and non-transitioned ROIs and the differences in the median values between 2018 and 2022.

Transitioned ROIs			Non-Transitioned ROIs		
Seasons	Median NDVI Values	2022-2018	Seasons	Median NDVI Values	2022-2018
Winter-18	0.24	0.10	Winter-18	0.65	-0.14
Winter-22	0.34		Winter-22	0.51	
Spring-18	0.51	-0.21	Spring-18	0.67	-0.07
Spring-22	0.30		Spring-22	0.60	
Summer-18	0.65	-0.31	Summer-18	0.64	-0.02
Summer-22	0.34		Summer-22	0.62	
Fall-18	0.47	-0.13	Fall-18	0.64	-0.03
Fall-22	0.34		Fall-22	0.61	

Table 3.7 shows that the transitioned ROIs exhibit more significant changes in median NDVI values over time, whereas non-transitioned ROIs show relatively minor changes, suggesting a more consistent vegetation condition. This implies that changes in land cover, such as transitioning from natural to artificial surfaces, have a more pronounced effect on NDVI values, which is an expected outcome considering NDVI is a measure of vegetation health and density.

3.4.2.3 NDVI Time Sequence Curve

A time sequence curve was plotted using the average NDVI values for each month for both transitioned and non-transitioned ROIs. Figure 3.20 shows the differences in the NDVI Values at each month for the studied period for both cases.

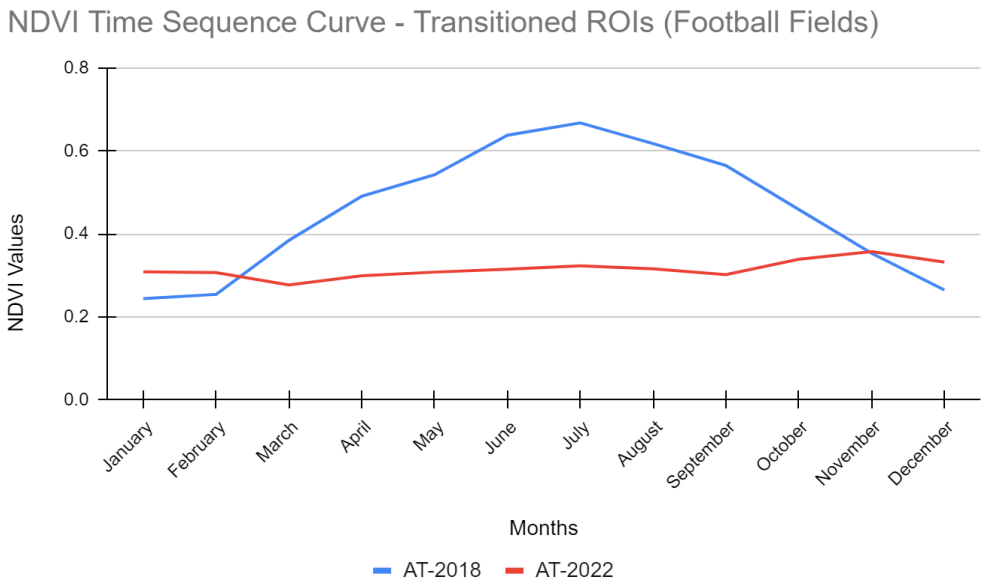

(a)

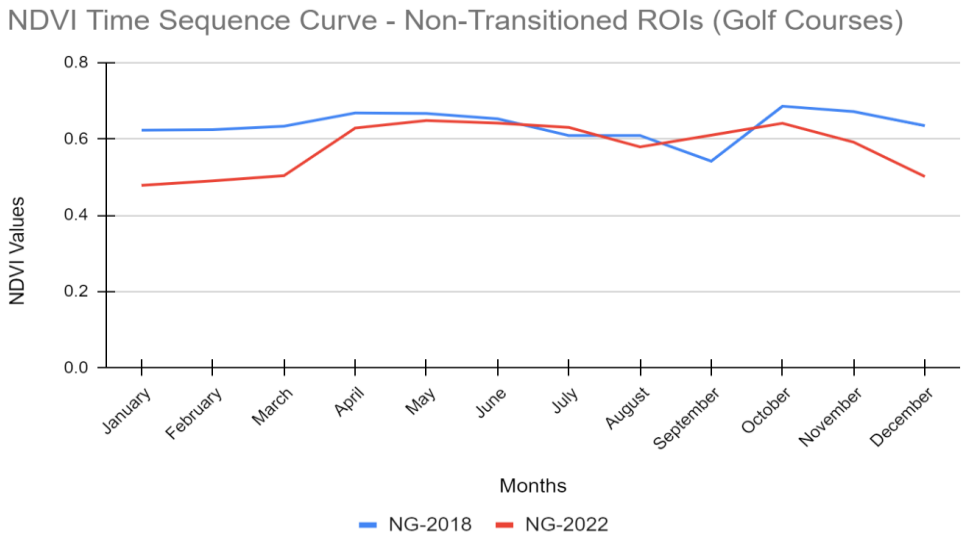

(b)

Figure 3.20: Average NDVI values for each month of 2018 and 2022 for (a) football fields and (b) golf courses

The curves illustrate a significant decline in NDVI values for football fields between 2018 and 2022, aligning with the substitution of natural grass—characterized by higher NDVI due to photosynthetically active vegetation—with artificial turf, which, lacking live vegetation, exhibits lower NDVI. Conversely, the NDVI of golf courses remained stable across both years, indicating unchanged natural grass conditions. Both football fields and golf courses exhibited seasonal patterns. NDVI increased in the spring and summer when warmer temperatures increased plant processes like photosynthesis, transpiration, and respiration, fostering vegetation growth. Conversely, NDVI dropped in autumn and winter as cooler weather slows or halts plant growth and leads to reduced transpiration rates, reflecting a period of dormancy or reduced activity in vegetation. This seasonal fluctuation in NDVI values is a reflection of the plant phenological cycle that responds to changes in the environment, such as temperature, light, and precipitation. The findings of this study on seasonal NDVI variation echo the patterns outlined by Naif et al. (2020). Golf courses, with their denser vegetation, generally exhibit higher NDVI values than football fields, indicative of the thriving, photosynthetically active plant life present. In contrast, the NDVI of football fields converted to artificial turf in 2022 remains flat throughout the year, lacking the natural seasonal variation associated with vegetative growth.

Depending on the type of vegetation land cover, NDVI value can be different Spadoni et al. (2020). Barren landscapes like rock, sand, or snow areas typically register very low NDVI values, around 0.1 or less. Lighter vegetation areas, such as those with shrubs, grasslands, or aging crops, tend to have moderate NDVI values ranging from 0.2 to 0.5. In contrast, dense vegetative areas, like those in lush forests or fields of crops at the height of their growth, often have high NDVI values between 0.6 and 0.9 (*NDVI, the Foundation for Remote Sensing Phenology | U.S.*

Geological Survey, 2018). Though Spadoni et al. (2020) concluded in their study that selecting an NDVI threshold based on data from an inappropriate time of year could lead to misclassification.

3.4.2.4 T-Tests

Three series of paired T-Tests were conducted to find any significant differences in the NDVI values between 2018 and 2022 for both transitioned and non-transitioned ROIs. The tests were performed in R-Studio. Normality tests were done for all pairs of data. The Mann Whitney U Tests were performed for the pairs that did not pass the normality tests. Table 3.3 provides an outline of the paired T-Test varieties executed, the number of tests for transitioned and non-transitioned ROIs, and their respective threshold values. The resulting p-values for each paired T-Test executed in this investigation are presented in Tables 3.8, 3.9, and 3.10.

Table 3.8: P-Values for the annual Paired T-Tests considering all LST values from all ROIs (Threshold P-Value = 0.002)

Transitioned ROIs	Non-Transitioned ROIs
3.67E-71*	1.67E-14*

Table 3.9: P-Values for the Paired T-Tests at individual ROI performed by taking all the data from the available dates (Threshold P-Value = 0.05)

Transitioned ROIs				Non-Transitioned ROIs			
ROIs	P-Values	ROIs	P-Values	ROIs	P-Values	ROIs	P-Values
T1	2.37E-06*	T14	0.005*	G1	0.2	G14	0.03*
T2	1.67E-05*	T15	0.0002*	G2	0.0006*	G15	0.1
T3	0.0009*	T16	0.03*	G3	0.001*	G16	0.45
T4	0.05*	T17	0.0002*	G4	0.006*	G17	0.006*
T5	0.03*	T18	6.90E-05*	G5	0.88	G18	0.02*
T6	0.005*	T19	0.08	G6	0.21	G19	0.02*
T7	0.006*	T20	0.001*	G7	0.52	G20	0.16
T8	0.0003*	T21	0.004*	G8	0.14	G21	0.16
T9	9.66E-05*	T22	0.01*	G9	0.25	G22	0.02*
T10	0.0002*	T23	0.0004*	G10	0.04*	G23	0.0002*
T11	0.008*	T24	0.0003*	G11	0.07	G24	0.007*
T12	0.07	T25	0.0004*	G12	0.59	G25	0.002*
T13	0.04*	T26	0.01*	G13	0.12	G26	0.26

Table 3.10: P-Values for Combined seasonal Paired T-Tests performed by taking all data from all ROIs for each season (Threshold P-Value = 0.002)

Transitioned ROIs				Non-Transitioned ROIs			
Winter	Spring	Summer	Fall	Winter	Spring	Summer	Fall
9.78E-10*	2.4E-42*	1.9E-80*	2.4E-26*	8.76E-16*	3E-09*	0.93	0.77

The first series of paired T-Test, which pooled all yearly data from all 26 ROIs, uncovered notable NDVI differences for both transitioned and non-transitioned ROIs, with p-values falling beneath the 0.002 significance level.

The second series of T-Tests, which examined each ROI individually across all collected data points, indicated significant NDVI variations for all transitioned ROIs except one and for twelve non-transitioned ROIs, achieving p-values below the 0.05 threshold. The findings from these T-Tests suggest that the shift from natural to artificial turf had a significant impact on the albedo of the transitioned ROIs during the study period.

The combined Seasonal T-Tests, which aggregated data from all ROIs by season, indicated substantial albedo differences for both transitioned and non-transitioned ROIs, with p-values below the 0.002 threshold.

According to the T-Tests results, the findings consistently demonstrate significant NDVI differentiation for ROIs that transitioned from natural grass to artificial turf, underscoring the profound influence that turf conversion has on NDVI. For these T-Tests, the alternative hypothesis

cannot be rejected for the transitioned ROIs since significant differences between the pre (2018) and post (2002) conversion were found.

3.5 Conclusions

The study focused on 26 high school football fields in LVV that transitioned from natural to artificial turf between 2018 and 2022. A total of 45 charts were produced, detailing the spectral signature curves for all the selected ROIs.

To understand the spectral characteristics of natural and artificial turfs, four distinct analyses were undertaken. Initially, box plots were created to exhibit the reflectance value distribution across all 26 ROIs in 2018 and 2022, respectively. The second approach involved averaging all reflectance readings to construct a chart displaying the mean annual reflectance, thus illustrating the spectral signatures for both years. The third method averaged reflectance values by month, resulting in a graph that detailed monthly average reflectance for 2018 and 2022 across various EM spectrum wavelengths. Lastly, a comprehensive analysis was conducted by plotting the spectral curves for the visible and infrared ranges month by month, allowing for an in-depth comparison of the spectral profiles between natural and artificial turfs.

According to the literature, healthy vegetation predominantly absorbs energy in the blue and red wavelengths of the EM spectrum, a trait attributed to chlorophyll, and reflects significantly in the NIR region with some reflectance in green as well. The box plots, along with the annual and monthly average reflectance charts, delineate spectral signatures characteristic of both natural and artificial turfs. For the year 2018, the spectral curves consistently showed pronounced absorption in the visible spectrum and marked reflection in the NIR spectrum, a pattern typical for natural

grass due to its internal structure and water content which enhances NIR reflectance. Notably, the average red reflectance exceeded that of green in 2018, possibly indicating grass under stress or lacking hydration. Artificial turf, on the other hand, demonstrated uniformly lower and more stable reflectance across all charts, reflecting its absence of the natural properties inherent to living grass.

The monthly average data also presents a distinctive spectral signature curve for each turf type. The 2018 data displayed seasonal fluctuations in reflectance within both the visible and NIR spectra, whereas the 2022 data did not show any seasonal pattern and exhibited more consistent, flatter reflectance values across the year in these regions.

Among all the wavelengths of the EM spectrum, the clearest difference between the two years was seen in the reflectance of the SWIR 1 region, where the slope for the two years moved in opposite directions. The natural grass, with its inherent moisture, typically shows greater absorption in the SWIR region, resulting in lower SWIR reflectance compared to the NIR in 2018. However, in 2022, the SWIR1 reflectance values consistently surpassed those in the NIR region. Notably, the artificial turf, despite being made of plastic, showed elevated reflectance in the SWIR 1 region, which could be attributed to the influence of surface temperature.

The variation in spectral signatures highlights the fundamental disparities between the two materials. The intricate architecture of natural grass engages with light in a manner distinct from the more uniform composition of artificial turf.

Upon concluding the analysis, two sets of T-Tests were performed. The initial series of tests compared the monthly reflectance data between 2018 and 2022. The subsequent series focused on each specific ROI. For these tests, a significant threshold (alpha value) was set at 0.05. The first series of T-Tests, which examined the reflectance variations across different wavelengths

between the two years for each ROI, identified notable differences for all months except July. In the second set of T-Tests, notable discrepancies were found in all the ROIs that underwent the transition, with only one exception. The outcomes of the T-Tests indicate that changing from natural to artificial turf significantly altered the spectral characteristics of the ROIs.

Additionally, NDVI values were determined for ROIs that switched from natural to artificial turfs between 2018 and 2022, as well as for ROIs that retained natural grass, serving as a control group. Initially, box plots were created to show the distribution of the NDVI values from all ROIs in 2018 and 2022. While NDVI values decreased in both scenarios, the drop was notably more substantial in the ROIs that had transitioned. A further analysis segmented the NDVI data of the transitioned ROIs by season, revealing significant differences, particularly during the summer. Lastly, a NDVI time series curve plotted the monthly average NDVI for both sets of ROIs, showing a marked reduction in NDVI for football fields that transitioned to artificial turf. Conversely, the natural grass areas exhibited consistent seasonal fluctuations in NDVI values. Three sets of paired T-Tests were conducted to detect significant changes in NDVI values for the transitioned ROIs from 2018 to 2022. Each set revealed significant alterations, highlighting the impact of changes in surface materials on NDVI readings. NDVI measurements can provide valuable insights into the environmental and ecological dynamics of artificial turf and natural grass in arid urban areas like Las Vegas, supporting more sustainable urban development and conservation strategies.

The GEE was instrumental in assessing the spectral signatures and the NDVI of the turfs, offering insights on reflectance values for each wavelength. The GEE Code Editor streamlined the process, allowing easy access to the API (Application programming interface) for analytical tasks. It efficiently generated spectral signature charts, and the entire undertaking was cost-free. While the Landsat imagery available in GEE wasn't of the highest spatial resolution for this detailed

analysis, the platform's capabilities surpassed other geoprocessing software, especially when conducted on less robust systems (Liss et al., 2017).

The results obtained from this study could be used by policymakers and environmental planners to understand the impact of replacing natural turf with artificial alternatives, potentially guiding future decisions regarding urban planning and environmental conservation.

3.6 Limitations and Recommendations

3.6.1 Limitations

- Since the equatorial crossing time of Landsat 8 satellite is 10:00 am +/- 15 minutes (European Space Agency, 2022), the remote sensing images are taken at 10am local time. Hence, the recorded temperature gives a snapshot of the surface conditions specifically at that time (Black et al., 2019). The reflectance might not be the peak at this time.
- Some external factors, such as changes in surrounding infrastructure, shade availability, irrigation practices, and other management changes can affect the accuracy of spectral data and NDVI calculations.
- The temporal resolution of the Landsat 8 satellite is 16 days. So only one or two images were found each month. The data from this one image can be impacted by atmospheric conditions like cloud, haze, precipitation, pollution etc.
- At 30 meters per pixel, Landsat 8 may not capture fine-scale variations in urban landscapes, where a single pixel can contain a mix of natural and artificial materials.
- The spectral signature and NDVI values can be seasonally dependent. Variations in sun angle, weather conditions, and plant life cycles throughout the year can introduce variability in the data.

- The spectral bands of Landsat 8 might not be sufficient to capture all the nuances necessary for distinguishing certain types of surfaces or conditions.
- Different brands or types of artificial turf may have unique spectral signatures, and GEE's ability to generalize across these variations could be a concern.
- The study compared the NDVI differences in football fields with the golf courses which have varying topography, grass characteristics, surrounding structures etc. For enhanced accuracy, a comparison should be made between football fields that have transitioned and those that have remained unchanged.

3.6.2 Recommendations for the Future Studies

- Combining remote sensing with ground-truthing to validate the classification would help better understand the context of the spectral signatures.
- The research utilized the GEE platform, a freely available tool, to execute the entire project. While Landsat 8 satellites lack the multitude of bands found in hyperspectral images from commercial satellites, similar analyses could be conducted using hyperspectral images or data fusion methods and then compared with the results of this study.
- Understanding the specific turf materials utilized at each site could provide important information on their seasonal performance variations. This knowledge could serve as a critical component for future research, guiding more tailored and effective strategies for turf management and selection based on regional climate conditions and usage needs.
- Additional research can be undertaken to identify areas within the valley that have shifted from natural to artificial turf providing deeper insights into the effectiveness of the lawn transition initiatives.

- Future studies can consider the use of thermal infrared data to provide additional insights into the heat characteristics of different surfaces.
- Alongside NDVI, future studies could include additional vegetation indices or thermal data to provide a more comprehensive view of vegetation health and surface temperatures.

3.6.3 Recommendations for the Policy Makers and Urban Planners

- Since the approach suggested by this study has been proven successful to locate artificial turf surfaces within a large area, the urban policy makers can employ this method to get the spectral signature of any object from a larger area at completely free of cost, without using any powerful tool or expensive satellite.
- Urban planners can locate artificial turf in LVV with the aid of spectral signature identification.
- Since artificial turf has been found to have lower surface albedo values, identifying ways to make these surfaces more reflective, or incorporating higher albedo materials in the vicinity can reduce the overall thermal effect.
- Urban planners can increase the use of natural vegetation in urban planning to enhance the NDVI and provide cooling through evapotranspiration.
- Continuous monitoring of urban areas with artificial turf is recommended to further understand long-term impacts on local microclimates and to assess whether adjustments in urban planning policies might be needed.
- Developing policies that require the consideration of spectral and thermal characteristics in the selection of urban materials should be encouraged.

- The community should be engaged in understanding the importance of NDVI and green spaces for urban quality of life.
- Urban planners can use a combination of NDVI data, local climate patterns, and water usage studies to make informed decisions about urban landscape planning.

REFERENCES

Akwensi, P. H., Kang, Z., & Wang, R. (2023). Hyperspectral image-aided LiDAR point cloud labeling via spatio-spectral feature representation learning. International Journal of Applied Earth Observation and Geoinformation, 120, 103302. https://doi.org/10.1016/j.jag.2023.103302

Baghzouz, M., Devitt, D. A., & Morris, R. L. (2006). Evaluating temporal variability in the spectral reflectance response of annual ryegrass to changes in nitrogen applications and leaching fractions. *International Journal of Remote Sensing*, *27*(19), 4137–4157. https://doi.org/10.1080/01431160600851843

Becker, W. R., Ló, T. B., Johann, J. A., & Mercante, E. (2021). Statistical features for land use and land cover classification in Google Earth Engine. Remote Sensing Applications, 21, 100459. https://doi.org/10.1016/j.rsase.2020.100459

Black, A., Ahmad, S., & Stephen, H. (2019). Urban heat island intensity mapping of Las Vegas using Landsat thermal infrared data. *World Environmental and Water Resources Congress 2019: Groundwater, Sustainability, Hydro-Climate/Climate Change, and Environmental Engineering - Selected Papers from the World Environmental and Water Resources Congress 2019, 397–409.* https://doi.org/10.1061/9780784482346.040

Brandt, J. (2008, November). Locating turf and water features in the Las Vegas valley, Nevada, using remote sensing techniques and GIS. In *American Society for Photogrammetry and Remote Sensing*.

Brelsford, C., & Abbott, J. K. (2017). Growing into Water Conservation? Decomposing the Drivers of Reduced Water Consumption in Las Vegas, NV. Ecological Economics, 133, 99–110. https://doi.org/10.1016/j.ecolecon.2016.10.012

Carvalho, H. D. R., B. Chang, K. J. McInnes, J. L. Heilman, B. Wherley, and J. A. Aitkenhead-Peterson. 2021. "Energy balance and temperature regime of different materials used in urban landscaping." *Urban Climate*, 37. https://doi.org/10.1016/j.uclim.2021.100854.

Ceballos-Silva, A., & López-Blanco, J. (2003). Delineation of suitable areas for crops using a Multi-Criteria Evaluation approach and land use/cover mapping: a case study in Central Mexico. *Agricultural Systems*, *77*(2), 117–136. https://doi.org/10.1016/S0308-521X(02)00103-8

Chen, Y., Wang, Q., Wang, Y., Duan, S. B., Xu, M., & Li, Z. L. (2016). A spectral signature shape-based algorithm for landsat image classification. *ISPRS International Journal of Geo-Information,* 5(9), 154–154. https://doi.org/10.3390/ijgi5090154

Cheng, H., Y. Hu, and M. Reinhard. 2014. "Environmental and health impacts of artificial turf: A review." *Environ. Sci. Technol.* 48 (4): 2114–2129.

Cities with low humidity in US - current results. *(n.d.)*. https://www.currentresults.com/Weather-Extremes/US/low-humidity-cities.php

Crawford, C. J., Roy, D. P., Arab, S., Barnes, C., Vermote, E., Hulley, G., Gerace, A., Choate, M., Engebretson, C., Micijevic, E., Schmidt, G., Anderson, C., Anderson, M., Bouchard, M., Cook, B., Dittmeier, R., Howard, D., Jenkerson, C., Kim, M., … Zahn, S. (2023). The 50-year Landsat collection 2 archive. Science of Remote Sensing, 8, 100103. https://doi.org/10.1016/j.srs.2023.100103

Devitt, D. A., Young, M. H., Baghzouz, M., Bird, B. M., & Devittl, B. D. A. (2007). Surface temperature, heat loading and spectral reflectance of artificial turfgrass. *J Turfgrass Sports Surf Sci*, *83*, 68-82.

Duble, R. L. (1993). Water management on turfgrasses. https://aggiehort.tamu.edu/plantanswers/turf/publications/water.html#:~:text=Grasses%20with%20poor%20drought%20resistance,depth%20of%20rootzone%20and%20slope.

Gorelick, N., Hancher, M., Dixon, M., Ilyushchenko, S., Thau, D., & Moore, R. (2017). Google Earth Engine: Planetary-scale geospatial analysis for everyone. Remote Sensing of Environment, 202, 18–27. https://doi.org/10.1016/j.rse.2017.06.031

Google Earth Engine. (n.d.). https://www.google.com/earth/education/tools/google-earth-engine/#:~:text=Google%20Earth%20Engine%20is%20a,natural%20resource%20management%2C%20and%20more

Gupta, D. K., Prashar, S., Singh, S., Srivastava, P. K., & Prasad, R. (2022). Chapter 1 - Introduction to RADAR remote sensing. In *Radar Remote Sensing* (pp. 3–27). Elsevier Inc. https://doi.org/10.1016/B978-0-12-823457-0.00018-5

Idso, S. B., Pinter, P. J., Jackson, R. D., & Reginato, R. J. (1980). Estimation of grain yields by remote sensing of crop senescence rates. *Remote Sensing of Environment*, *9*(1), 87–91. https://doi.org/10.1016/0034-4257(80)90049-8

Jastifer, J. R., A. S. McNitt, C. D. Mack, R. W. Kent, K. A. McCullough, M. J. Coughlin, and R. B. Anderson. 2019. "Synthetic Turf: History, Design, Maintenance, and Athlete Safety." *Sports Health*. https://doi.org/10.1177/19417381187933

Jensen, J. R. (2009). *Remote sensing of the environment: An earth resource perspective 2/e*. Pearson Education India.

Jim, C. Y. 2016. "Solar-terrestrial radiant-energy regimes and temperature anomalies of natural and artificial turfs." *Applied Energy*, 173. https://doi.org/10.1016/j.apenergy.2016.04.072.

Kachhwaha, T. (1983). Spectral signatures obtained from Landsat digital data for forest vegetation and land-use mapping in India. Photogrammetric Engineering and Remote Sensing, 49(5), 685–689.

Karaca, A. C., Erturk, A., Gullu, M. K., Elmas, M., & Erturk, S. (2013). Automatic waste sorting using shortwave infrared hyperspectral imaging system. 2013 5th Workshop on Hyperspectral Image and Signal Processing: Evolution in Remote Sensing (WHISPERS), 1–4. https://doi.org/10.1109/WHISPERS.2013.8080744

Kwan, C., Gribben, D., Ayhan, B., Li, J., Bernabe, S., & Plaza, A. (2020). An Accurate Vegetation and Non-Vegetation Differentiation Approach Based on Land Cover Classification. Remote Sensing (Basel, Switzerland), 12(23), 3880. https://doi.org/10.3390/rs12233880

Kim, D. M., Zhang, H., Zhou, H., Du, T., Wu, Q., Mockler, T. C., & Berezin, M. Y. (2015). Highly sensitive image-derived indices of water-stressed plants using hyperspectral imaging in SWIR and histogram analysis. Scientific Reports, 5(1), 15919–15919. https://doi.org/10.1038/srep15919

Kim, A. M., Kruse, F. A., & Olsen, R. C. (2016, May). Integrated analysis of light detection and ranging (LiDAR) and hyperspectral imagery (HSI) data. In *Laser Radar Technology and Applications XXI* (Vol. 9832, pp. 271-285). SPIE.

Kriegler, F.J., Malila, W.A., Nalepka, R.F. and Richardson, W., 1969, Preprocessing transformations and their effect on multispectral recognition, in: Proceedings of the sixth International Symposium on Remote Sensing of Environment, University of Michigan, Ann Arbor, MI, pp. 97-131

Kirkpatrick, M., Stewart, D., Bridges, C., Crear, C., Gibson, J., Jones, J., & Lee, J. (2019). Joint Water Conservation Plan. https://www.snwa.com/assets/pdf/reports-conservation-plan-2019.pdf

Kruse, F. A., Kim, A. M., Runyon, S. C., Carlisle, S. C., Clasen, C. C., Esterline, C. H., ... & Olsen, R. C. (2014, June). Multispectral, hyperspectral, and LiDAR remote sensing and geographic information fusion for improved earthquake response. In *Algorithms and Technologies for Multispectral, Hyperspectral, and Ultraspectral Imagery XX* (Vol. 9088, pp. 132-145). SPIE.

Lavorgna, J., Song, J., Beattie, W., Riley, M., Beil, C., Levchenko, K., & Shofar, S. (2011). A Review of Benefits and Issues Associated with Natural Grass and Artificial Turf Rectangular Stadium Fields Final Report. *Montgomery County Council: Rockville, MD*.

Liu, Z., and C. Y. Jim. 2021. "Playing on natural or artificial turf sports field? Assessing heat stress of children, young athletes, and adults in Hong Kong." *Sustainable Cities and Society*, 75. https://doi.org/10.1016/j.scs.2021.103271.

Liss, B., Howland, M. D., & Levy, T. E. (2017). Testing Google Earth Engine for the automatic identification and vectorization of archaeological features: A case study from Faynan, Jordan.

Masoumi, H., Safavi, S. M., & Khani, Z. (2012). Identification and classification of plastic resins using near infrared reflectance. *Int. J. Mech. Ind. Eng*, *6*, 213-220.

Moshtaghi, M., Knaeps, E., Sterckx, S., Garaba, S., & Meire, D. (2021). Spectral reflectance of marine macroplastics in the VNIR and SWIR measured in a controlled environment. Scientific Reports, 11(1), 5436–5436. https://doi.org/10.1038/s41598-021-84867-6

Mei, A., Bassani, C., Fontinovo, G., Salvatori, R., & Allegrini, A. (2016). The use of suitable pseudo-invariant targets for MIVIS data calibration by the empirical line method. *ISPRS Journal of Photogrammetry and Remote Sensing*, *114*, 102–114. https://doi.org/10.1016/j.isprsjprs.2016.01.016

Morris, Devitt, D. A., Crites, A. M., Borden, G., & Allen, L. N. (1997). Urbanization and water conservation in Las Vegas Valley, Nevada. Journal of Water Resources Planning and Management, 123(3), 189–195. https://doi.org/10.1061/(ASCE)0733-9496(1997)123:3(189)

Naif, S., Mahmood, D. & Al-Jiboori, M. (2020). Seasonal normalized difference vegetation index responses to air temperature and precipitation in Baghdad. *Open Agriculture*, *5*(1), 631-637. https://doi.org/10.1515/opag-2020-0065

NDVI, The Foundation for Remote Sensing Phenology | U.S. Geological Survey. (2018, November 29). https://www.usgs.gov/special-topics/remote-sensing-phenology/science/ndvi-foundation-remote-sensing-phenology#overview

NOAA's National Weather Service. (n.d.). *Climate*. https://www.weather.gov/wrh/climate?wfo=vef

Priem, F., & Canters, F. (2016). Synergistic use of LiDAR and APEX hyperspectral data for high-resolution urban land cover mapping. Remote Sensing (Basel, Switzerland), 8(10), 787–787. https://doi.org/10.3390/rs8100787

Salvador, P., Sanz, J., Rodriguez, J., Molina, V., & JL, C. A Hand Goniometer For Ads Spectroradiometer: Application To Brdf Sentinel 2 Bands Over Urban Surfaces.

Seeman, M. (2020, July 16). *Artificial turf to replace grass fields at 29 Southern Nevada schools*. KSNV. https://news3lv.com/news/local/artificial-turf-to-replace-grass-fields-at-29-southern-nevada-schools

Southern Nevada Water Authority. (n.d.). https://www.snwa.com/water-resources/conservation-initiatives/index.html

Spadoni, G. L., Cavalli, A., Congedo, L., & Munafò, M. (2020). Analysis of Normalized Difference Vegetation Index (NDVI) multi-temporal series for the production of forest cartography. Remote Sensing Applications, 20, 100419. https://doi.org/10.1016/j.rsase.2020.100419

Spectral reflectance. (n.d.). https://gsp.humboldt.edu/olm/Courses/GSP_216/lessons/reflectance.html#:~:text=Chlorophyll%20strongly%20absorbs%20light%20at,between%200.7%20and%201.3%20%C2%B5m

Tamiminia, H., Salehi, B., Mahdianpari, M., Quackenbush, L., Adeli, S., & Brisco, B. (2020). Google Earth Engine for geo-big data applications: A meta-analysis and systematic review. *ISPRS Journal of Photogrammetry and Remote Sensing*, *164*, 152-170.

Thenkabail, P. S., Smith, R. B., & De Pauw, E. (2000). Hyperspectral Vegetation Indices and Their Relationships with Agricultural Crop Characteristics. *Remote Sensing of Environment*, *71*(2), 158–182. https://doi.org/10.1016/S0034-4257(99)00067-X

Understand laws & ordinances. (n.d.). https://www.snwa.com/conservation/understand-laws-ordinances/index.html#:~:text=Grass%20restrictions&text=A%20law%20enacted%20by%20the,nonfunctional%20grass%2C%20beginning%20in%202027

Water Smart Landscapes Rebate. (n.d.-b). https://www.snwa.com/rebates/wsl/index.html#process

Wynne, T., & Devitt, D. (2020). Evapotranspiration of Urban Landscape Trees and Turfgrass in an Arid Environment: Potential Trade-offs in the Landscape.

Weather averages Las Vegas, Nevada. (n.d.). US Climate Data. https://www.usclimatedata.com/climate/las-vegas/nevada/united-states/usnv0049

Wetherley, E. B., Roberts, D. A., & McFadden, J. P. (2017). Mapping spectrally similar urban materials at sub-pixel scales. Remote Sensing of Environment, 195, 170–183. https://doi.org/10.1016/j.rse.2017.04.013

CHAPTER 4: HEALTH AND ENVIRONMENTAL IMPLICATIONS OF ARTIFICIAL TURF

4.1 Introduction

Synthetic grass is becoming popular due to its aesthetic appeal, comfort, low maintenance requirements, and the fact that it doesn't need watering, making it an ideal option in regions facing drought or water scarcity. The market for artificial turf was estimated at $8.10 billion in 2021 and is projected to expand to $12.68 billion by 2027. It is anticipated that by 2027, sales will encompass approximately 2863.6 million square feet of artificial turf (Arizton Advisory & Intelligence, 2022). Many sports authorities view artificial turf as a viable alternative to natural grass worldwide, highlighting its importance in providing a reliable and safe playing field in various weather conditions (Charalambous et al., 2023). Artificial turf is used not only in sports fields like soccer, golf, field hockey, and rugby but also in many other areas. This includes places like playgrounds, lawns at homes and in public spaces, rooftops, gardens, and gyms. It's also used in business settings for decoration and in small businesses, among other uses (De Haan et al., 2023).

Artificial turf has emerged as a notable contributor to primary plastic pollution in the environment (De Haan et al., 2023). The current third-generation artificial turf systems comprise three principal components: synthetic grass fibers, infill, and backing layers. The synthetic grass, made from materials like nylon, polypropylene, or polyethylene, mimics the appearance and feel of natural grass (Murphy et al., 2022). Infill, typically a combination of sand and rubber or just rubber, is spread across the turf to a depth of around 4 cm to support the blades and provide stability (Ruffino et al., 2013; Cheng et al., 2014). Crumb rubber, derived from ground-up recycled tires and resembling coarse-grain sand, is favored for infill due to its cost-effectiveness and accounts for about 90% of the field's composition (Schiliro et al., 2013; Donald et al., 2019). The backing

material secures the fibers in place and facilitates water drainage, often made from polypropylene, polyamide-6, polyolefins, or polyurethane, and can be either perforated for better irrigation or non-perforated for weed control (Cheng et al., 2014). Additional plastic components like shock-absorbing layers, drainage sheets, and pipes, typically made from materials such as styrene-butadiene rubber (SBR) or polyurethane for the shock pads and polypropylene or Ethylene Propylene Diene Monomer (EPDM) for the drainage systems, are installed below the turf's surface to enhance its functionality, as discussed in research by Hann et al. (2018), Nilsson et al. (2008), and Ramboll (2020).

The installation of artificial turf surfaces has sparked significant health and environmental debates owing to the components involved in their fabrication. These issues have been widely explored in a range of academic studies. Figure 4.1 shows the structure of artificial turf and Table 4.1 and 4.2 present a range of health and environmental concerns associated with artificial turf as highlighted in existing studies, which are extensively reviewed in a subsequent section.

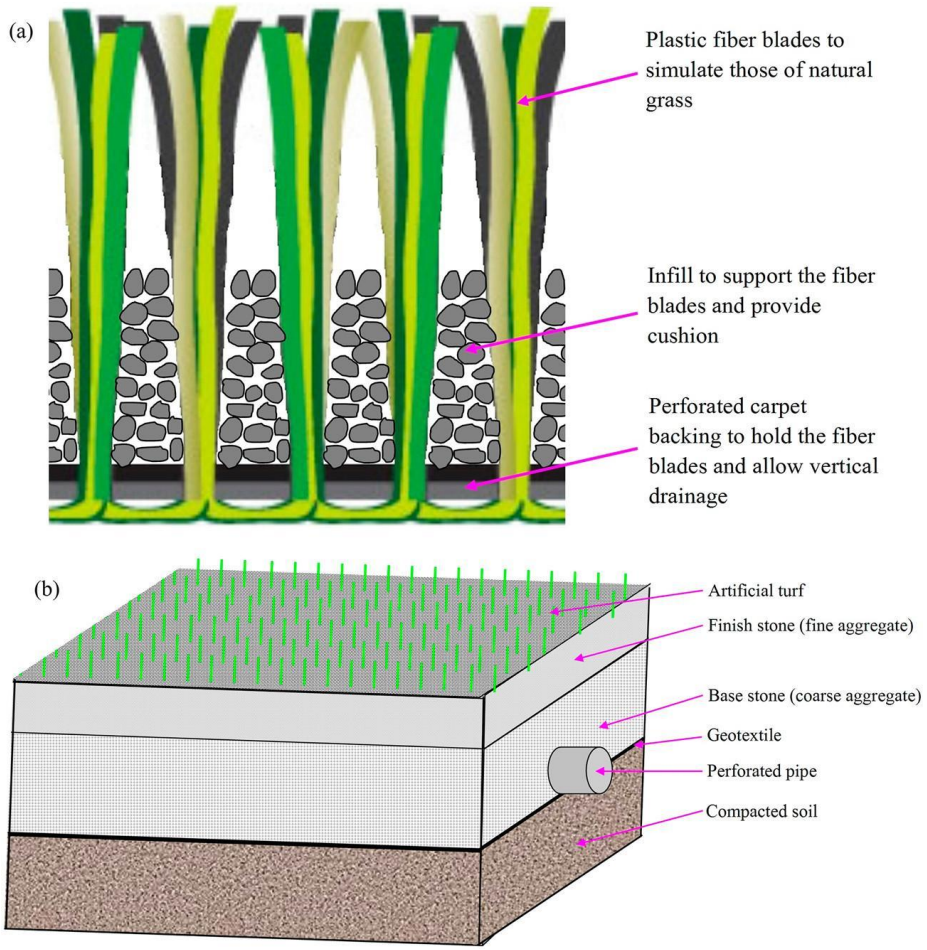

Figure 4.1: Schematic illustrations of the makeup of a typical artificial turf field: (a) the major components of artificial turf, and (b) the built-in drainage system (Cheng et al., 2014)

Table 4.1: Artificial Turf Materials and their associated health impacts

Materials	**Health Impacts**
Crumb Tire Rubber	Blister formation on individuals
	Increased air pollution
	Adverse effect on human fertility.
	Head, neck, ankle injuries among athletes
	Concussions, skin infections, respiratory issues, and potential carcinogenic risks
Microplastics	Inflammation in tissues
	Genetic damage
	Cellular oxidative stress
Artificial turf fibers	Risk of MRSA infection among athletes

Table 4.2: Artificial Turf Materials and their associated Environmental Impacts

Materials	**Environmental Impacts**
Crumb Rubber tire	Release of heavy metals and toxic chemical substances in the air and rainwater around artificial playfields.
	Runoff emanating from artificial fields
	Rise in surface temperature of artificial turf.
	Adverse effects on benthic invertebrates
	Diminished ground infiltration
	Heightened risk of flooding in city areas
Artificial turf fibers	Plastic pollution when washed away by rainwater runoff.
	Plastic contamination in natural water bodies.

4.2 Health Impacts of Artificial Turf

Various health concerns have been raised about the use of artificial turfs in urban areas due to their composition of various plastics and their ability to conduct heat. Health impacts due to artificial turf are explained in the following sections.

4.2.1 Use of recycled tire crumb as infill material

Notably, crumb rubber, which is derived from recycled tires and commonly used in these turfs for its widespread availability, has been cited as a primary concern in these discussions (Schilirò et al., 2013).

A variety of research studies have been undertaken to assess the possible health hazards linked to the incorporation of tire crumbs in artificial turf surfaces. Research by Schiliro et al. (2013) and Cheng et al. (2014) has addressed how these crumbs may enter the human body and the resultant effects. Potential exposure methods include ingestion, oral contact, skin contact, and respiratory inhalation. However, these studies have not identified any considerable health risks via these exposure pathways. Conversely, Murphy and Warner (2022) have highlighted concerns about the presence of hazardous chemicals within crumb rubber, including substances that are carcinogenic, neurotoxic, and endocrine-disrupting chemicals.

Negev et al. (2022) presented their concerns about infants and toddlers who are at a high risk of being exposed to the harmful chemicals released by artificial turf, which could potentially harm their health. The authors mentioned that the recycled crumb rubber may carry toxic metals like Pb, Cd, Cr, Zn, Al, as well as volatile organic compounds, polycyclic aromatic hydrocarbons, and ortho-phthalate esters (Larsans, n.d.) which can be transferred into the environment or can be at a risk level in the surroundings of synthetic grass surfaces. Ulirsch et al. (2010) highlighted that children engaging in play on synthetic turf might encounter dust infused with lead at concentrations potentially hazardous to their health. Given the absence of a definitive safe limit for lead exposure, even minimal amounts could negatively impact neurodevelopment and behavior (Lanphear et al., 2005).

Though the literature indicates that the bio accessibility of heavy metals found in tire crumb rubber, when exposed to saliva, sweat, and gastric fluids, is minimal (Thomas et al., 2019). This suggests that artificial turf may not significantly contribute to children's exposure to heavy metals. The disintegration of artificial grass can increase the number of heavy metals in rainwater runoff

and nearby soil. This may lead to a higher risk of children coming into contact with these harmful substances (Cheng and Reinhard, 2014; Celeieo et al., 2014).

Artificial turf containing crumb rubber infill can reach a high temperature of 78°C, which has the potential to cause blisters on human skin in less than 3 seconds (ISO 13732-3:2005(en)), emitting longwave radiation (heat) at approximately 675Wm^{-2}. This emission is greater than the one from dark asphalt, which is about 600Wm^{-2} (Wardenaar et al., 2023).

According to Henryk et al. (2023), artificial turf contributes to higher air pollution levels due to the wear of the granules it contains. This pollution, which includes harmful chemical substances, adversely affects the health of football players.

4.2.2 Incorporation of microplastics in artificial playing surfaces

Murphy and Warner (2022), along with Mehmood and Peng (2022), have raised issues regarding microplastics, a growing concern for both health and the environment. Particles smaller than 5 millimeters in diameter qualify as microplastics. Human exposure to these particles can occur through inhaling dust, consuming foods, or eating marine organisms that have ingested microplastics from their aquatic habitats. The common installation of artificial turf, particularly in cities, has been recognized as a possible origin of microplastics. This is because numerous infill substances are made from recycled materials, which tend to break down more easily. Environmental factors, such as extreme temperatures, scarce rainfall, humidity, sunlight exposure, and saline conditions, can accelerate the deterioration of these materials, causing them to disintegrate into smaller fragments. These particles may then enter the environment when infill materials are washed away or when they cling to the apparel and footwear of athletes.

Mehmood and Peng (2022) also detailed several health hazards stemming from microplastic ingestion:

- Preemptive cellular reaction due to the penetration of microplastics in the pulmonary or gastrointestinal epithelium.
- Inflammation in tissues that come into contact with microplastics.
- Risks to reproductive health and potential mutagenic and cancer-causing effects following microplastic consumption.
- Genetic damage from toxic substances carried by microplastics into the body.
- Cellular oxidative stress is due to the introduction of oxidizing agents by microplastics.
- Lung inflammation resulting from inhaling microplastic particles.

4.2.3 Dye and material composition of synthetic turf fibers

Encapsulated lead chromate pigment, a heavy metal, was previously used in the plastic fibers of older artificial turf fields. According to Cheng et al. (2014), such heavy metal can be harmful to the users. Given the risks associated with even low levels of lead exposure in children, it is advised either to limit or completely avoid non-critical applications of lead. (Centers for Disease Control Prevention, 2005)

4.2.4 Release of reproductive toxins from tire crumb leachate

Murphy and Warner (2022) identified several phthalates released from synthetic turf fibers as reproductive toxins that could negatively impact human reproductive capabilities.

4.2.5 Risk of MRSA infection among athletes

Artificial turf contributes to a higher risk of Methicillin-Resistant Staphylococcus Aureus (MRSA) infection in players, (Schneider & Hypes, 2014) as the bacteria thrive in the fibers and infill of the turf, fostered by the accumulation of waste. (Shi & Jim, 2021)

4.2.6 Increased likelihood of heat-related illness

The combined effect of direct sunlight and radiated heat from the surface, alongside intense heat transfer from the components of artificial turf, may adversely affect athletes' health and performance. This heat dynamic can increase stress levels past safe limits, as discussed by Jim (2017).

4.2.7 Athletic injuries sustained

The utilization of artificial turf in sports has triggered discussions about its implications for athlete injury occurrences. Studies suggest that although the overall incidence of injuries on artificial and natural grass surfaces is comparable, the types of injuries differ between the two (Charalambous et al., 2016; Dragoo & Braun, 2010).

Research by Dragoo and Braun (2010) compared the injury patterns on artificial and natural turf fields. According to the authors, there tends to be a higher occurrence of head and neck injuries, cuts, abrasions, and ankle sprains on artificial turfs. Gould et al. (2022) found that the overall rate of injuries, as well as knee-specific injuries, were comparable for artificial turf and natural grass. However, injuries to the foot and ankle were more commonly reported on artificial turf than on natural grass. Drakos et al. (2013) identified a range of injuries associated with artificial turf such as injuries related to the foot, ankle, and knee. They also highlighted several non-orthopedic injuries that can occur on artificial turf, including concussions, skin infections, respiratory issues, and potential carcinogenic risks due to the crumb rubber used in the third generation of artificial turf fields.

Charalambous et al. (2023) assessed how the temperature of artificial turf affects its mechanical characteristics and the movement dynamics related to sports played on turf. The research indicated that the temperature of the turf surface impacts its mechanical characteristics.

Notably, the study observed that a colder surface temperature range of 1.8°C to 2.4°C resulted in a noticeably "firmer" and more rigid turf. Such alterations in the turf's mechanical properties could influence an athlete's movements during landing and sprinting, potentially affecting their performance and increasing the risk of injuries, especially in colder environments where artificial turf is used for sports activities.

According to Villacañas et al. (2017), manufacturers have consistently enhanced artificial turf to mimic the features and qualities of natural grass. Despite these advancements, artificial turf still tends to heat up more than natural grass, leading to user dissatisfaction, diminished performance, and an increased risk of heat-induced injuries.

Research in various sports disciplines has shown that excessive heat can affect an athlete's performance by raising body temperature, which may lead to an elevated sense of exertion among athletes (Nybo, 2008; Galloway and Maughan, 1997). Buskirk et al. (1971) suggested that the elevated temperatures associated with artificial turf could contribute to physiological stress among athletes.

Wardenaar et al. (2023) described that despite receiving less solar radiation than natural grass during practice times, artificial turf’s higher surface temperature led to greater emission of longwave radiation, thus increasing the heat radiated back to athletes. This, coupled with the elevated air temperature on artificial turf, which impedes convective heat dissipation, resulted in a greater heat burden on players. Consequently, athletes on artificial turf reported significantly higher skin temperatures and perceived heat stress. These factors diminished when players engaged in activities under cooler conditions, with natural grass being cooler than artificial turf providing the lowest heat load.

The performance of athletes on artificial turf fields can significantly vary based on the field's design and the materials used in its construction (Fleming, 2011). Factors such as the type of fibers, infill material, the sub-base, and the presence of an elastic layer can all influence the mechanical properties of the turf (Alcantara et al., 2006; Burillo et al., 2014).

Drakos et al. (2013) mentioned that the modern third generation artificial turf fields show lower association with injuries. Introduced in 1998, the third generation of artificial turf features longer fibers, measuring 60-65 mm, compared to the shorter fibers of the first and second generations, and utilizes a mix of rubber and sand for the infill layer, which is 40 mm thick, instead of just sand (Aoki, 2011). William and Pulley (2002) mentioned that in hot weather, third-generation artificial turf can become up to 3°C hotter than asphalt and 30°C warmer than natural grass. Furthermore, a 2008 report by the New York City Department of Health and Mental Hygiene (Denly et al., 2008) highlighted that the primary health concern with third-generation artificial turf is the high surface temperatures it can reach. The surface temperature of artificial turf can significantly increase when ambient temperatures exceed 32.2°C, elevating the risk of heat-related issues like heatstroke, blisters, and dehydration (Nybo, 2008).

4.3 Environmental Impacts

The use of artificial turf contributes to various detrimental environmental effects, particularly in cities where it can cause a significant rise in ground temperature, leading to heat-related health issues. The environmental impacts of artificial turf are detailed in the following sections.

4.3.1 Elevated temperatures of playing surface

Artificial turf's thermal properties can lead to an increase in surface temperatures, which may sometimes surpass safe levels. A study by Twomey et al. (2016) analyzed how different

factors, including ambient temperature, humidity, cloudiness, and wind velocity, affect the surface temperatures of both natural and artificial grass. The findings indicated that higher ambient temperatures and direct sunlight are the primary contributors to the rise in surface temperature of artificial turf. There was an observed negative correlation between humidity and the surface temperature of artificial turf, while wind speed's impact was inconsistent across various fields.

According to Villacañas et al. (2017), altering the shape and structure of the artificial turf fibers should be considered, as their design can contribute to lowering the surface temperature of artificial turf.

4.3.2 Concerns about the environment stemming from tire crumbs

Prior research has highlighted the concern over heavy metals like Cd, Cr, and Pb transferring to the air and rainwater around artificial playfields. The environmental hazard is underscored by the incineration of rubber tire crumbs, which has shown a marked increase in the quantity and toxicity of dangerous chemicals released (Celeiro et al., 2018; Armada et al., 2022). Under The Safe Drinking Water and Toxic Enforcement Act of 1986, California established a limit of 50 mg/kg for lead content in artificial turf. (Brown et al., n.d.).

A study from Yale University discovered that the crumb rubber infill contains at least 306 different chemicals, with as many as 197 identified as carcinogens (Perkins et al., 2019). Environmental harm can result from the runoff emanating from artificial fields containing crumb rubber, as this runoff may include hydrocarbons, organic substances, and metals (Pochron et al., 2017).

Kole et al. (2023) identified the different routes through which infill material exits an artificial turf football field and estimated the amount of infill material leaving the turf through each of these routes. The authors calculated an annual loss of 948 kg of tire granulate from the turf

through known pathways, excluding snow removal. Considering snow removal an additional 830 kg of granulate per year would be lost, resulting in a total loss ranging from 1778 kg/year to 5030 kg/year. On average, these fields are replenished with 3312 kilograms of rubber granulate each year. To mitigate the effects of surface hardening, the authors have recommended adding an average of 1260 kilograms of rubber granulate annually. Figure 4.2 shows the pathways and corresponding amount of rubber granules leaving an artificial turf football field according to Kole et al. (2023).

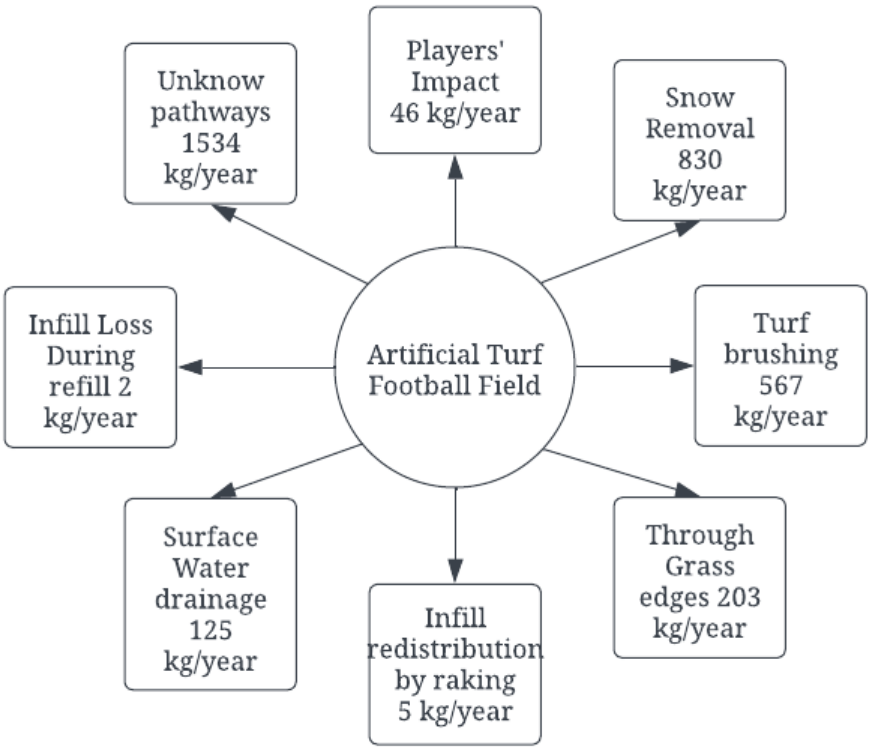

Figure 4.2: The routes and corresponding quantities of rubber granulate used as infill for an artificial turf football field (adapted from Kole et al., 2023)

4.3.3 Release of heavy metals into the environment

Cheng et al. (2014) and Murphy and Warner (2022) have both reported that heavy metals and organic pollutants can leach out from the rubber crumbs of tires used in artificial turf as rainwater percolates through the infill layer. The levels of these leached substances differ among various types of infill materials. Magnusson and Macsik (2017) found detectable levels of zinc, chloride, fluoride, sulfate, distillable phenols, and Dissolved Organic Compounds (DOCs) in the leachates from different types of infill materials. Additionally, Schilirò et al. (2013) found that zinc and Polycyclic Aromatic Hydrocarbons (PAHs) were commonly present in the leachate from crumb rubber.

Trace amounts of lead and other heavy metals are deliberately added to artificial turf components to maintain their color brightness over an extended period (Brown et al., n.d.) which, over time, can leach out from artificial turf.

Aoki (2011) mentioned that the leaching of heavy metals into the environment increases as the acidity of solutions, mimicking acid rain, rises.

4.3.4 Harm to ecosystems caused by toxic substances

Cheng et al. (2014) highlighted the potential ecological toxicity stemming from runoff from synthetic sports fields, which tend to contain elevated levels of zinc that could harm aquatic ecosystems.

The use of tire granulate as infill for artificial turf is often perceived as a troubling method for disposing of old tires because of its loose application on the surface, leading to inevitable dispersion into the surrounding environment (Kole et al., 2023). Research conducted by Khan et

al. (2019) and Halle et al. (2021) highlighted that not only can leachate from tires be problematic, but ingested tire particles can also have adverse effects on benthic invertebrates.

4.3.5 Increased potential for flooding

Substituting natural grass with synthetic turf might lead to adverse environmental and hydrological consequences, including challenges with urban drainage systems, such as increased surface runoff, diminished ground infiltration, and a heightened risk of flooding in city areas (Simpson & Francis, 2021).

4.3.6 Contribution to plastic pollution in the environment

The issue of plastic pollution, impacting both land and sea environments worldwide, is exacerbated by artificial turf, as identified by Simpson & Francis (2021). Their research found that artificial turf lawns shed plastic materials, such as fibers and thatch, which then contribute to pollution when washed away by rainwater runoff.

Plastic pollution is widely acknowledged as a significant human-induced problem in aquatic ecosystems. De Haan et al. (2023) examined the presence of artificial turf fibers in rivers and oceans, which serve as significant pathways for plastic debris carried by runoff. Their investigation revealed that artificial turf fibers can make up over 15% of mesoplastics and macro plastics, suggesting a notable contribution to plastic pollution. The authors also mentioned that up to 20,000 fibers are observed in river flow, and nearshore sea surfaces everyday containing up to 213,200 fibers per square kilometer. They concluded that in addition to impacting urban biodiversity, water runoff, heat absorption, and chemical discharge, artificial turf is becoming a significant contributor to plastic contamination in natural water bodies. The concentration of artificial turf-derived plastics is particularly pronounced in coastal areas and regions close to

human settlements, especially during the rainy season when runoff into aquatic environments is heightened (De Haan et al., 2023).

4.4 Appropriateness for Artificial Turf Usage

Artificial turf serves as a practical option for areas where harsh climates impede the growth of natural grass or where upkeep is prohibitively expensive. However, it should not be regarded as a complete replacement for natural grass pitches, as it does not suit all climatic conditions. Table 4.2 presents the appropriateness of using artificial turf explored by Shi and Jim (2021) and Jim (2016) in their respective research.

Table 4.3: Appropriateness for artificial turf usage

Recommended applications for artificial turf	Situations where using artificial turf is discouraged
In conditions with cloudy or overcast weather, which diminish the intensity of direct sunlight and overall solar radiation.	In areas that receive intense direct sunlight, which can elevate the risk of heat-related stress.
Indoor sports arenas that are equipped with adequate air circulation systems.	For activities that involve intense physical exertion under direct sun exposure, due to the increased risk of heat stress.

In the United States, northern regions typically experience dry conditions with cold winters and hot summers, whereas the southern areas are characterized by a humid subtropical climate. Schneider and Hypes (2014) suggest that in northern states, where natural grass only experiences

optimal growth for about three months, artificial turf fields might be a more suitable option. Conversely, in the southern states, where conditions are more favorable for the year-round growth of natural grass, it is recommended to opt for natural turf over artificial alternatives due to the inherent advantages that natural grass offers, which artificial turf cannot replicate.

Charalambous et al. (2023) suggested the manufacturers and researchers should explore the appropriateness of artificial turf for colder settings. The authors also mentioned that artificial turf fields should be certified before use, to ensure they do not negatively impact the game or player safety. Henryk et al. (2023) mentioned that maintaining artificial turf playing fields involves not just the evaluation of certified cushioning materials (such as top-grade rubber granulate) but also the routine substitution of the worn products.

4.5 Conclusions

Despite the health and environmental issues associated with artificial turf, the incorporation of recycled tire crumbs into these surfaces offers several advantages. According to Schiliro et al. (2013), using crumb rubber in football fields can lead to a reduction in sports-related injuries. Furthermore, the process of creating tire crumbs repurposes a substantial quantity of used tires (Cheng et al., 2014). Murphy and Warner (2022) noted that a professional-sized sports field typically requires between 20,000 to 40,000 tires to produce the necessary crumb rubber. While crumb rubber can also be made from virgin rubber, utilizing recycled tires lowers the overall cost of producing artificial turf.

The decision to install artificial turf must be tailored to the specific characteristics and needs of each location. Factors to consider include the surface's longevity, total lifecycle expenses, its propensity to retain heat, potential exposure to harmful substances, environmental effects, and

aesthetic qualities (Schneider & Hypes 2014). Shi and Jim (2021) recommended conducting an assessment of a site's solar exposure before deciding on the installation of artificial turf. Installing artificial turf in areas exposed to direct sunlight is not recommended due to the potential for heat-related health risks. To mitigate the danger of heat stress for athletes on warmer days, it is advisable to organize games and training sessions during nighttime hours. Twomey et al. (2016) argue that artificial turf's ability to withstand harsh weather conditions and provide a consistent playing surface makes it an appealing choice. However, its tendency to heat up more than natural grass is a concern that needs to be managed effectively.

In conclusion, it's crucial to have a well-rounded understanding of both the beneficial and adverse effects of artificial turf before proceeding with its installation. While artificial turf may serve aesthetic purposes well, architects and urban planners should also consider its long-term impacts on urban settings.

4.5.1 Challenges

- Recycled crumb rubber is favored over other, less damaging infill options primarily because it lowers production expenses. However, these recycled materials may deteriorate more rapidly in extreme weather, leading to environmental concerns.
- Various methodologies are employed to assess the effects of artificial turf on human health and the environment, yet the scarcity of experimental data challenges the validation of model-generated information.
- The absence of consistent, long-term data collection also complicates the creation of time-series analyses.

- The limited availability of studies on health risks and toxicological impacts hampers the comprehensive understanding of the health implications associated with artificial turf.
- The potential for microplastic pollution, the heat island effect increasing local temperatures, and the loss of natural habitat contribute to the growing list of challenges associated with the use of artificial turf.

4.5.2 Opportunities

- It is important to conduct life cycle assessments for various artificial turf materials, such as nylon, polyethylene, and polypropylene, to evaluate and compare their environmental footprints.
- Apart from crumb rubber, other artificial turf components, like the fibers and backing materials made from different polymers, should also be studied to measure their overall impact.
- Future investigations should also delve into the fate and toxicity of contaminants found in crumb rubber, such as heavy metals and organic pollutants, to better understand their environmental consequences.
- Exploring the various ways in which crumb rubber particles might enter the human body through detailed modeling could illuminate their potential health effects.
- Comparative studies on the health impacts of recycled versus virgin infill materials are needed, as well as research on the leachates from crumb rubber that may contaminate groundwater with harmful chemicals like phthalates.
- Recycling facilities for synthetic turf materials should be developed to prevent landfill disposal at the end of their lifecycle.

- Finally, the design parameters like the height and density of the artificial turf fibers, along with the choice of infill materials, play a crucial role in influencing hydrological processes and should be selected with care to mitigate adverse impacts, as highlighted by Simpson and Francis (2021).

REFERENCES

Alcantara, E., Rosa, D., Gamez, J., Martinez, A., Comin, M., Such, M. J., Vera, P., & Prat, J. (2006). Analysis of the influence of rubber infill on the mechanical performance of artificial turf surfaces for soccer. *Sports Engineering*, *9*(2), 107–107
.

Arizton Advisory & Intelligence. (2022). Artificial turf market demand, size analysis, forecast report [WWW document]. Arizton advisory & intelligence. URL. https://www.arizton.com/market-reports/artificial-turf-market.

Armada, D., Llompart, M., Celeiro, M., Garcia-Castro, P., Ratola, N., Dagnac, T., & de Boer, J. (2022). Global evaluation of the chemical hazard of recycled tire crumb rubber employed on worldwide synthetic turf football pitches. *The Science of the Total Environment*, *812*, 152542–152542. https://doi.org/10.1016/j.scitotenv.2021.152542

Brown, E. G., JR., Rodriquez, J. M., Alex, K., Weil, E. G., Ragen, D. A., Los Angeles City Attorney, Thomas, E. E., Bilgin, P., Ruden, E., Minassian, V., Paulson, D. W., Gonzalez, C. B., Superior Court of California for the County of Alameda, People of the State of California. ex rel. Edmund G. Brown, JR., Attorney General, Carmen A. Trutanich, Los Angeles City Attorney, David W. Paulson, Solano County District Attorney, Beaulieu Group, LLC, et al., & Astroturf, LLC. (n.d.). *Consent Judgement as to Defendant Astroturf*. https://oag.ca.gov/system/files/attachments/press_releases/n1782_astroturf_cj%2C_final-signed.pdf

Burillo, P., Gallardo, L., Felipe, J. L., & Gallardo, A. M. (2014). Artificial turf surfaces: Perception of safety, sporting feature, satisfaction and preference of football users. *European Journal of Sport Science*, *14*(sup1), S437–S447. https://doi.org/10.1080/17461391.2012.713005

Buskirk, E. R., McLaughlin, E. R., & Loomis, J. L. (1971). Microclimate over Artificial Turf. *Journal of Health, Physical Education, Recreation*, *42*(9), 29–30. https://doi.org/10.1080/00221473.1971.10617177

Charalambous, L., von Lieres und Wilkau, H. C., Potthast, W., & Irwin, G. (2016). The effects of artificial surface temperature on mechanical properties and player kinematics during landing and acceleration. *Journal of Sport and Health Science*, *5*(3), 355–360. https://doi.org/10.1016/j.jshs.2015.01.013

Cheng, H., Hu, Y., & Reinhard, M. (2014). Environmental and Health Impacts of Artificial Turf: A Review. *Environmental Science & Technology*, *48*(4), 2114–2129. https://doi.org/10.1021/es4044193

Celeiro, M., Lamas, J. P., Garcia-Jares, C., Dagnac, T., Ramos, L., & Llompart, M. (2014). Investigation of PAH and other hazardous contaminant occurrence in recycled tyre rubber surfaces. Case-study: restaurant playground in an indoor shopping centre. *International*

Journal of Environmental Analytical Chemistry, *94*(12), 1264–1271. https://doi.org/10.1080/03067319.2014.930847

Celeiro, M., Dagnac, T., & Llompart, M. (2018). Determination of priority and other hazardous substances in football fields of synthetic turf by gas chromatography-mass spectrometry: A health and environmental concern. *Chemosphere (Oxford)*, *195*, 201–211. https://doi.org/10.1016/j.chemosphere.2017.12.063

Centers for Disease Control Prevention. (2005). *Preventing lead poisoning in young children a statement by the Centers for Disease Control and Prevention* ([5th rev.].). U.S. Dept. of Health and Human Services, Centers for Disease Control and Prevention.

Dragoo, J. L., & Braun, H. J. (2010). The Effect of Playing Surface on Injury Rate: A Review of the Current Literature. *Sports Medicine (Auckland)*, *40*(11), 981–990. https://doi.org/10.2165/11535910-000000000-00000

Drakos, M. C., Taylor, S. A., Fabricant, P. D., & Haleem, A. M. (2013). Synthetic Playing Surfaces and Athlete Health. *Journal of the American Academy of Orthopaedic Surgeons*, *21*(5), 293–302. https://doi.org/10.5435/JAAOS-21-05-293

Denly, E., Rutkowski, K., & Vetrano, K. M., Ph. D. (2008). A review of the potential health and safety risks from synthetic turf fields containing crumb rubber infill. In New York City Department of Health and Mental Hygiene & TRC, *New York City Department of Health and Mental Hygiene*. https://www.nyc.gov/assets/doh/downloads/pdf/eode/turf_report_05-08.pdf

Fleming, P. (2011). Maintenance best practice and recent research. *Proceedings of the Institution of Mechanical Engineers, Part P: Journal of Sports Engineering and Technology*, *225*(3), 159-170.

Gould, H. P., Lostetter, S. J., Samuelson, E. R., & Guyton, G. P. (2022). Lower Extremity Injury Rates on Artificial Turf and Natural Grass Playing Surfaces: A Systematic Review. *Foot & Ankle Orthopaedics*, *7*(1), 2473011421S00217. https://doi.org/10.1177/2473011421S00217

Galloway, S. D. R., & Maughan, R. J. (1997). Effects of ambient temperature on the capacity to perform prolonged cycle exercise in man. *Medicine and Science in Sports and Exercise*, *29*(9), 1240–1249. https://doi.org/10.1097/00005768-199709000-00018

Hann, S., Sherrington, C., Jamieson, O., Hickman, M., Kershaw, P., Bapasola, A., & Cole, G. (2018). Investigating options for reducing releases in the aquatic environment of microplastics emitted by (but not intentionally added in) products. *Report for DG Environment of the European Commission*, *335*.

Halle, L. L., Palmqvist, A., Kampmann, K., Jensen, A., Hansen, T., & Khan, F. R. (2021). Tire

wear particle and leachate exposures from a pristine and road-worn tire to Hyalella azteca: Comparison of chemical content and biological effects. *Aquatic Toxicology*, *232*, 105769. https://doi.org/10.1016/j.aquatox.2021.105769

Henryk Duda, Łukasz Rydzik, Andrzej Soroka, & Kamil Sokołowski. (2023). Rationalization of soccer training in terms of health effects of metropolitan smog and activity on the artificial turf. *Zeszyty Naukowe Wyższej Szkoły Finansów i Prawa w Bielsku-Białej*, *27*(4). https://doi.org/10.19192/wsfip.sj4.2023.10

ISO 13732-3:2005(en), Ergonomics of the thermal environment — Methods for the assessment of human responses to contact with surfaces — Part 3: Cold surfaces.https://www.iso.org/obp/ui/#iso:std:iso:13732:-3:ed-1:v1:en (accessed 20 March 2024).

Jim, C. Y. (2016). Solar–terrestrial radiant-energy regimes and temperature anomalies of natural and artificial turfs. *Applied Energy*, *173*, 520–534. https://doi.org/10.1016/j.apenergy.2016.04.072

Jim, C. Y. (2017). Intense summer heat fluxes in artificial turf harm people and environment. *Landscape and Urban Planning*, *157*, 561–576. https://doi.org/10.1016/j.landurbplan.2016.09.012

Khan, F. R., Halle, L. L., & Palmqvist, A. (2019). Acute and long-term toxicity of micronized car tire wear particles to Hyalella azteca. *Aquatic Toxicology*, *213*, 105216–105216. https://doi.org/10.1016/j.aquatox.2019.05.018

Larsans. (2020). An Evaluation of the Possible Health Risks of Recycled Rubber Granules Used as Infill in Synthetic Turf Sports Fields – *all sports recycled*. https://www.allsportsrecycled.com/an-evaluation-of-the-possible-health-risks-of-recycled-rubber-granules-used-as-infill-in-synthetic-turf-sports-fields/

Lanphear, B. P., Hornung, R., Khoury, J., Yolton, K., Baghurst, P., Bellinger, D. C., Canfield, R. L., Dietrich, K. N., Bornschein, R., Greene, T., Rothenberg, S. J., Needleman, H. L., Schnaas, L., Wasserman, G., Graziano, J., & Roberts, R. (2005). Low-Level Environmental Lead Exposure and Children's Intellectual Function: An International Pooled Analysis. *Environmental Health Perspectives*, *113*(7), 894–899. https://doi.org/10.1289/ehp.7688

Murphy, M., & Warner, G. R. (2022). Health impacts of artificial turf: Toxicity studies, challenges, and future directions. *Environmental Pollution (1987)*, *310*, 119841–119841. https://doi.org/10.1016/j.envpol.2022.119841

Mehmood, T., & Peng, L. (2022). Polyethylene scaffold net and synthetic grass fragmentation: a source of microplastics in the atmosphere? *Journal of Hazardous Materials*, *429*, 128391–128391. https://doi.org/10.1016/j.jhazmat.2022.128391

Nilsson, N. H., Malmgren-Hansen, B., Thomsen, U. S., & Teknologisk Institut. (2008). Mapping, emissions and environmental and health assessment of chemical substances in artificial turf. Copenhagen, Denmark: Danish Environmental Protection Agency.

Nybo, L. (2008). Hyperthermia and fatigue. *Journal of Applied Physiology (1985)*, *104*(3), 871–878. https://doi.org/10.1152/japplphysiol.00910.2007

Olshammar, M., Graae, L., Robijn, A., & Nilsson, F. (2021). Microplastic fromcast rubber granulate andgranulate-free artificial grass surfaces.

Perkins, A. N., Inayat-Hussain, S. H., Deziel, N. C., Johnson, C. H., Ferguson, S. S., Garcia-Milian, R., Thompson, D. C., & Vasiliou, V. (2019). Evaluation of potential carcinogenicity of organic chemicals in synthetic turf crumb rubber. *Environmental Research*, *169*, 163–172. https://doi.org/10.1016/j.envres.2018.10.018

Pochron, S. T., Fiorenza, A., Sperl, C., Ledda, B., Lawrence Patterson, C., Tucker, C. C., Tucker, W., Ho, Y. L., & Panico, N. (2017). The response of earthworms (Eisenia fetida) and soil microbes to the crumb rubber material used in artificial turf fields. *Chemosphere (Oxford)*, *173*, 557–562. https://doi.org/10.1016/j.chemosphere.2017.01.091

Ramboll. (2020). Comparative Analysis of Major Companies within Artificial Turf Recycling and Treatment. Nordic Alpha Partners. https://bekogr.se/wp-content/uploads/2020/09/NAP_comparative-analysis-ATR_30-4-2020-1.pdf

Ruffino, B., Fiore, S., & Zanetti, M. C. (2013). Environmental–sanitary risk analysis procedure applied to artificial turf sports fields. *Environmental Science and Pollution Research International*, *20*(7), 4980–4992. https://doi.org/10.1007/s11356-012-1390-2

Russo, C., Cappelletti, G. M., & Nicoletti, G. M. (2022). The product environmental footprint approach to compare the environmental performances of artificial and natural turf. *Environmental Impact Assessment Review*, *95*, 106800. https://doi.org/10.1016/j.eiar.2022.106800

Safe Drinking Water & Toxic Enforcement Act of 1986 (Proposition 65), California Environmental Protection Agency, Office of Environmental Health Hazard Assessment, San Francisco, CA. (1999). *Journal of Toxicology. Cutaneous and Ocular Toxicology*, *18*(2), 149–150. https://doi.org/10.3109/15569529909037565

Schilirò, T., Traversi, D., Degan, R., Pignata, C., Alessandria, L., Scozia, D., Bono, R., & Gilli, G. (2013). Artificial Turf Football Fields: Environmental and Mutagenicity Assessment. *Archives of Environmental Contamination and Toxicology*, *64*(1), 1–11. https://doi.org/10.1007/s00244-012-9792-1

Schneider, D., Hypes, J. A., & Hypes, M. G. (2014). Synthetic Turf vs. Natural Grass. *Journal of Facility Planning, Design, and Management*, *2*(2), np–np.

Shi, Y., & Jim, C. Y. (2022). Developing a thermal suitability index to assess artificial turf applications for various site-weather and user-activity scenarios. *Landscape and Urban Planning*, *217*, 104276. https://doi.org/10.1016/j.landurbplan.2021.104276

Simpson, T. J., & Francis, R. A. (2021). Artificial lawns exhibit increased runoff and decreased water retention compared to living lawns following controlled rainfall experiments. *Urban Forestry & Urban Greening*, *63*, 127232. https://doi.org/10.1016/j.ufug.2021.127232

Thomas, K., E. Irvin-Barnwell, A. Guiseppi-Elie, A. Ragin-Wilson, AND J. Zambrana. Synthetic Turf Field Recycled Tire Crumb Rubber Research Under the Federal Research Action Plan: Final Report Part 1 - Tire Crumb Rubber Characterization Appendices Volume 2. U.S. Environmental Protection Agency, Washington, DC, EPA/600/R-19/051.2, (2019). https://cfpub.epa.gov/si/si_public_record_report.cfm?Lab=NERL&dirEntryId=346618

Twomey, D. M., Petrass, L. A., Harvey, J. T., Otago, L., & Le Rossignol, P. (2016). Selection and Management of Sports Grounds: Does Surface Heat Matter? *Journal of Facility Planning, Design, and Management*, *4*(1). https://doi.org/10.18666/JFPDM-2016-V4-I1-6507

Van Ulirsch, G., Gleason, K., Gerstenberger, S., Moffett, D. B., Pulliam, G., Ahmed, T., & Fagliano, J. (2010). Evaluating and Regulating Lead in Synthetic Turf. *Environmental Health Perspectives*, *118*(10), 1345–1349. https://doi.org/10.1289/ehp.1002239

Williams, C. F., & Pulley, G. E. (2002). Synthetic surface heat studies. Brigham Young University.

CHAPTER 5: CONTRIBUTIONS AND RECOMMENDATIONS

5.1 Summary

This thesis presents a comprehensive analysis of the thermal and spectral characteristics of Las Vegas Valley. This first objective examines the effects of artificial turf on the urban thermal environment in the LVV. To assess this impact, LST and surface albedo were analyzed at 26 ROIs that transitioned from natural to artificial turf, alongside another 26 ROIs that remained unchanged between 2018 and 2022. The data for this analysis was obtained from all available Landsat 8 satellite imagery for the respective years. The transitioned ROIs comprised high school football fields, while the non-transitioned ROIs, primarily golf courses, served as a control group in this research. The entire analysis was conducted using GEE and ArcGIS Pro, with statistical assessments carried out in R-Studio.

This study investigated the effect of artificial turf on LST in the LVV from 2018 to 2022, focusing on 26 ROIs where turf transitioned from natural to artificial. These were compared with 26 control ROIs that retained their natural turf. Initial analyses involved comparing LST for each ROI across the two years, revealing that artificial turf tended to elevate surface temperatures during warmer months, while cooler months saw a reduction in LST for transitioned ROIs. The control group, however, showed minimal changes, with a slight increase in LST during summer in a few ROIs. Further analysis examined average LST changes per ROI, identifying an increase in 7 transitioned ROIs but a decrease or no change in the rest. Conversely, the control ROIs largely maintained their average LST, with only one showing an increase. Annual average comparisons indicated a general decrease in surface temperature for both groups in 2022. Seasonal variability was also assessed, showing a significant summer LST increase in all transitioned ROIs, whereas

the control ROIs presented mixed results. T-Tests were conducted to assess the significance of these changes. The T-Tests results which combined the data revealed substantial impact of turf transition on LST for transitioned ROIs, and stability within the control group across the study period.

The average discrepancy between the 10 am temperatures and the daily peaks for specific dates rose marginally from 5.83°C in 2018 to 6.23°C in 2022. The LST readings taken at 10 am using Landsat 8 satellites are likely a few degrees Celsius below the true peak LST, which could be captured during the hottest part of the day. To obtain the actual peak LST, an on-site infrared radiometer can be employed, rather than relying on satellite-based remote sensing data.

Several analyses were performed to assess the effect of switching to artificial turf on the surface albedo within the LVV over the period from 2018 to 2022, focusing on 26 ROIs that underwent this transition. These findings were then compared with those from another 26 ROIs that maintained their natural turf, serving as a control group for this investigation. Initial assessments involved comparing the surface albedo for each ROI across the two years through scatter plots. A significant decline in albedo values was noted in 2022 for the ROIs that had transitioned, with these values remaining relatively stable throughout the year, in contrast to the seasonal variability observed in 2018. The average albedo for all transitioned ROIs decreased in 2022 where the albedo values decreased at 8 non-transitioned ROIs and increased in the rest. Seasonal analysis indicated a reduction in albedo for nearly all transitioned ROIs during the summer, except for two. In contrast, the non-transitioned ROIs displayed a seasonal trend of decreasing albedo from winter to fall. The T-Tests revealed marked differences in surface albedo

between 2018 and 2022 for the transitioned ROIs, whereas the non-transitioned ROIs mostly showed no significant change.

In the comprehensive comparison of ROIs over the two years in question, it was observed that transitioning to artificial turf correlated with elevated surface temperatures, but only during the warmer months. The paired T-Test results that combined annual and seasonal data showed significant differences on LST between 2018 and 2022 for the transitioned ROIs. The albedo values for ROIs with natural grass remained relatively unchanged between the two years. Conversely, a notable decrease in albedo was observed in most ROIs that transitioned to artificial turf. The T-Tests revealed significant differences in albedo between 2018 and 2022 for these transitioned ROIs, whereas the non-transitioned ROIs showed no significant changes.

The second objective focused on 26 high school football fields in the valley that transitioned from natural to artificial turf between 2018 and 2022. A total of 48 charts were produced, detailing the spectral signature curves for all the selected regions. The 2018 curves had features indicative of natural grass, while the 2022 curves did not show these traits. Some areas and months did not exhibit NIR reflection. The most evident distinction was in the SWIR 1 region's reflectance, with opposing slope directions in the two years. Interestingly, despite being plastic, the synthetic turf exhibited increased reflectance in the SWIR 1 region, possibly due to surface temperature effects. Average reflectance values of all 26 ROIs of each month of 2018 and 2022 at each wavelength displayed distinct curves for each year. Additionally, NDVI values were determined for ROIs that switched from natural to artificial turfs between 2018 and 2022, as well as for ROIs that retained natural grass, serving as a control group. Distinct NDVI values and curves

were obtained for artificial turf. T-Test results also confirm significant differences in NDVI for the transitioned ROIs between 2018 and 2022.

The GEE was instrumental in assessing the spectral signatures of the turfs, offering insights on reflectance values for each wavelength. The GEE Code Editor streamlined the process, allowing easy access to the API (Application programming interface) for analytical tasks. It efficiently generated spectral signature charts, and the entire undertaking was cost-free. While the Landsat imagery available in GEE wasn't of the highest spatial resolution for this detailed analysis, the platform's capabilities surpassed other geoprocessing software, especially when conducted on less robust systems (Liss et al., 2017).

This thesis includes an additional chapter that examines the health and environmental effects of artificial turf. It covers issues such as the use of recycled tire crumb as infill, the presence of microplastics in turf components, and the composition of turf fibers. It also addresses health risks like MRSA infections, heat-related illnesses, and various injuries that athletes might suffer on artificial playing surfaces. On the environmental side, the focus is on the higher temperatures of turf surfaces, ecological damage from toxic substances, and a greater risk of flooding. The thesis suggests that the decision to install artificial turf should be tailored to the unique conditions and requirements of each location.

Artificial turf is often utilized as a water-saving substitute for natural grass in arid regions like the LVV, where water conservation is a major concern. Artificial turf can raise local temperatures, therefore it's important to balance the advantages of water conservation against any potential thermal effects. Elevated surface temperatures have the potential to negatively impact public health, cause discomfort, and raise the risk of heat-related illnesses. Artificial turf should not be considered as a full replacement for natural grass. Its suitability varies with different weather

conditions. Shi and Jim (2022) suggested avoiding artificial turf in areas that receive direct sunlight, as it can increase the risk of heat stress, and particularly in situations involving intense physical activities under direct sun exposure. Therefore, studying the impact of artificial turf on the urban thermal environment of LVV is essential for informed urban planning and policymaking, aimed at creating a healthy and comfortable urban environment, especially considering the unique climate challenges of the region.

5.2 Contributions

In this research, the potential of GEE and ArcGIS Pro were explored to ascertain the LST, surface Albedo and spectral signature of natural grass and artificial turf in the LVV. These tools offer a cost-free method for acquiring LST, albedo, and spectral data without the need for sophisticated equipment or costly satellite imagery. No previous research has employed these technologies to gather data on LST, albedo, or spectral reflectance. Unlike prior research that primarily focused on summer periods to evaluate the impact of artificial turf on urban heat, this study expanded its analysis to include all months of the years 2018 and 2022, capturing seasonal fluctuations in surface temperatures of both turf types. Most of the previous studies spanned for only two days, while this research stands out by examining data from all the days of 2018 and 2022 when the satellite images were available. In total, 48 Landsat 8 satellite images from 2018 and 2022 were downloaded to carry out a comprehensive analysis. The study encompassed 26 ROIs that transitioned from natural to artificial turf during this period, alongside a control group of 26 ROIs that retained natural grass, enabling a detailed comparison of surface temperatures, albedo, and spectral signatures of both types of turf throughout the entire LVV. This approach of covering an extensive number of regions over a prolonged time frame is unique in the field. This

research examined the transformation of 26 high school football fields from natural grass to artificial turf over the period from 2018 to 2022, in contrast to earlier studies that only analyzed data from a single point in time.

5.3 Limitations

- Since the equatorial crossing time of Landsat 8 satellite is 10:00 am +/- 15 minutes (European Space Agency, 2022), the remote sensing images are taken at 10am local time. Hence, the recorded temperature gives a snapshot of the surface conditions specifically at that time (Black et al., 2019). The LST of the reflectance might not be the peak at this time.
- Some external factors, such as changes in surrounding infrastructure, shade availability, irrigation practices, and other management changes can affect the accuracy of LST, albedo readings, spectral data and NDVI calculations.
- The temporal resolution of the Landsat 8 satellite is 16 days. So only one or two images were found each month. The data from this one image can be impacted by atmospheric conditions like cloud, haze, precipitation, pollution etc.
- Freely available Landsat 8 dataset was used in this study, which has coarser spatial resolution. Finer resolution data could give better results.
- The data can be seasonally dependent. Variations in sun angle, weather conditions, and plant life cycles throughout the year can introduce variability in the data.
- The absence of consistent, long-term data collection complicates the creation of time-series analyses for health and environmental implications of artificial turf.
- The limited availability of studies on health risks and toxicological impacts hampers the comprehensive understanding of the health implications associated with artificial turf.

5.4 Recommendations for the Future Studies

- Subsequent research could employ high-resolution satellite imagery from commercial satellites. Companies like Maxar Technologies, Planet Labs, 21st Century Aerospace Technology, and Airbus Defense and Space, which operate in the commercial satellite sector, provide the public with access to some of the most detailed satellite imagery. They supply images with resolutions reaching up to 30 centimeters (about 11.8 inches) per pixel, allowing for the identification of ground objects as small as 30 centimeters in the imagery. (GeoWGS, 2024)
- Investigating the parameters across various natural grass types (such as Bermuda, Bent, and Rye) and artificial turfs made from diverse materials like polyethylene, polypropylene, and nylon would facilitate a comparative study.
- Given that temperature fluctuations are natural from year to year, extending the analysis over multiple years would enhance the comparative aspect of the study.
- To mitigate the limitations of solely focusing on football fields, it might be beneficial to include a more diverse range of sites and consider additional variables that could influence the studied parameters for future studies.
- Future studies could extend to measuring the night-time temperatures of artificial turf in addition to daytime readings. Monitoring the 24-hour diurnal cycle could reveal nocturnal heat exchanges, which play a crucial role in the overall energy balance.
- Verifying the outcomes of this study through ground truthing with suitable measurement tools can help ascertain the accuracy of the findings.
- Understanding the specific turf materials utilized at each site could provide important information on their seasonal performance variations. This knowledge could serve as a

critical component for future research, guiding more tailored and effective strategies for turf management and selection based on regional climate conditions and usage needs.

- Additional research can be undertaken to identify areas within the valley that have shifted from natural to artificial turf, providing deeper insights into the effectiveness of the lawn transition initiatives.
- Alongside NDVI, future studies could include additional vegetation indices or thermal data to provide a more comprehensive view of vegetation health and surface temperatures.
- It is important to conduct life cycle assessments for various artificial turf materials, such as nylon, polyethylene, and polypropylene, to evaluate and compare their environmental footprints.
- While there is a wealth of research focusing on the use of recycled crumb rubber as an infill material due to its associated health and environmental risks, the other components of artificial turfs, like the fibers and backing materials made from different polymers, warrant similar scrutiny to gauge their overall impact.
- Future investigations should also delve into the fate and toxicity of contaminants found in crumb rubber, such as heavy metals and organic pollutants, to better understand their environmental consequences.
- The study compared the LST/ Albedo/ NDVI differences in football fields with the golf courses which have varying topography, grass characteristics, surrounding structures etc. For enhanced accuracy, a comparison should be made between football fields that have transitioned and those that have remained unchanged.

5.5 Recommendations for the Policy Makers and Urban Planners

- The study indicates that artificial turf elevates surface temperatures in the summer, highlighting the need for policymakers and urban planners to consider this factor in their summer construction and landscaping plans.
- Given the substantial water required to lower temperatures on artificial turf fields during hotter months, water resource management should be tailored to accommodate this demand.
- The strategic placement of artificial turf around the valley is essential to prevent any single area from having an excessive concentration, which could result in elevated surface temperatures compared to other areas.
- In areas with artificial turf, adding shade structures, water features, or incorporating cooling materials into the surrounding landscapes are some examples of heat mitigation measures that can be used to mitigate the increase of heat during summer season.
- Given that increased surface albedo can significantly lower maximum surface temperatures (Gustin et al., 2018), urban planners are advised to incorporate urban elements with higher albedo values to help reduce surface temperatures.
- The choice of fiber height and density, along with the type of infill used in artificial turf, can impact water drainage and retention, as highlighted by Simpson & Francis (2021). These elements should be meticulously considered during the selection process prior to installing artificial turf to ensure optimal hydrological performance. In their research, Petrass et al. (2014) found that products using Thermoplastic Elastomer (TPE) as infill exhibited significantly cooler surface temperatures compared to those using organic or

Styrene-butadiene Rubber (SBR) infill. Villacañas et al. (2017) suggested the use of thermoplastic rubber and monofilament fibers to reduce the turf surface temperature.

- The urban policy makers can employ the approach studied in this thesis to get the spectral signature of any object from a larger area at completely free of cost, without using any powerful tool or expensive satellite.
- Urban planners can use a combination of NDVI data, local climate patterns, and water usage studies to make informed decisions about urban landscape planning.
- Alternatives to traditional recycled crumb rubber, such as organic or natural infill materials derived from coconut shells, walnut shells, rice husks, and renewable corks, could offer a solution, albeit at a higher cost.
- Installing artificial turf in areas exposed to direct sunlight is discouraged to prevent heat-related health concerns among individuals. To mitigate the risk of heat stress among athletes on warmer days, it is advisable to schedule games and practice sessions during nighttime.
- Charalambous et al. (2016) suggested the manufacturers and researchers should explore the appropriateness of artificial turf for colder settings. The authors also mentioned that artificial turf fields should be certified before use, to ensure they do not negatively impact the game or player safety. Henryk et al. (2023) mentioned that maintaining artificial turf playing fields involves not just the evaluation of certified cushioning materials (such as top-grade rubber granulate) but also the routine substitution of the worn products.
- Developing policies that require the consideration of spectral and thermal characteristics in the selection of urban materials should be encouraged.

- Continuous monitoring of urban areas with artificial turf is recommended to further understand long-term impacts on local microclimates and to assess whether adjustments in urban planning policies might be needed.
- According to the SNWA conservation plan 2019 existing building regulations limit the installation of turf in new developments. It should be maintained strictly by the urban planners to prevent water wastage on non-functional turf. (Joint Water Conservation Plan, 2019)

APPENDIX A

Appendix A.1: Comparative Analysis of LST for 26 transitioned ROIs in 2018 (Blue) and 2022 (Orange)

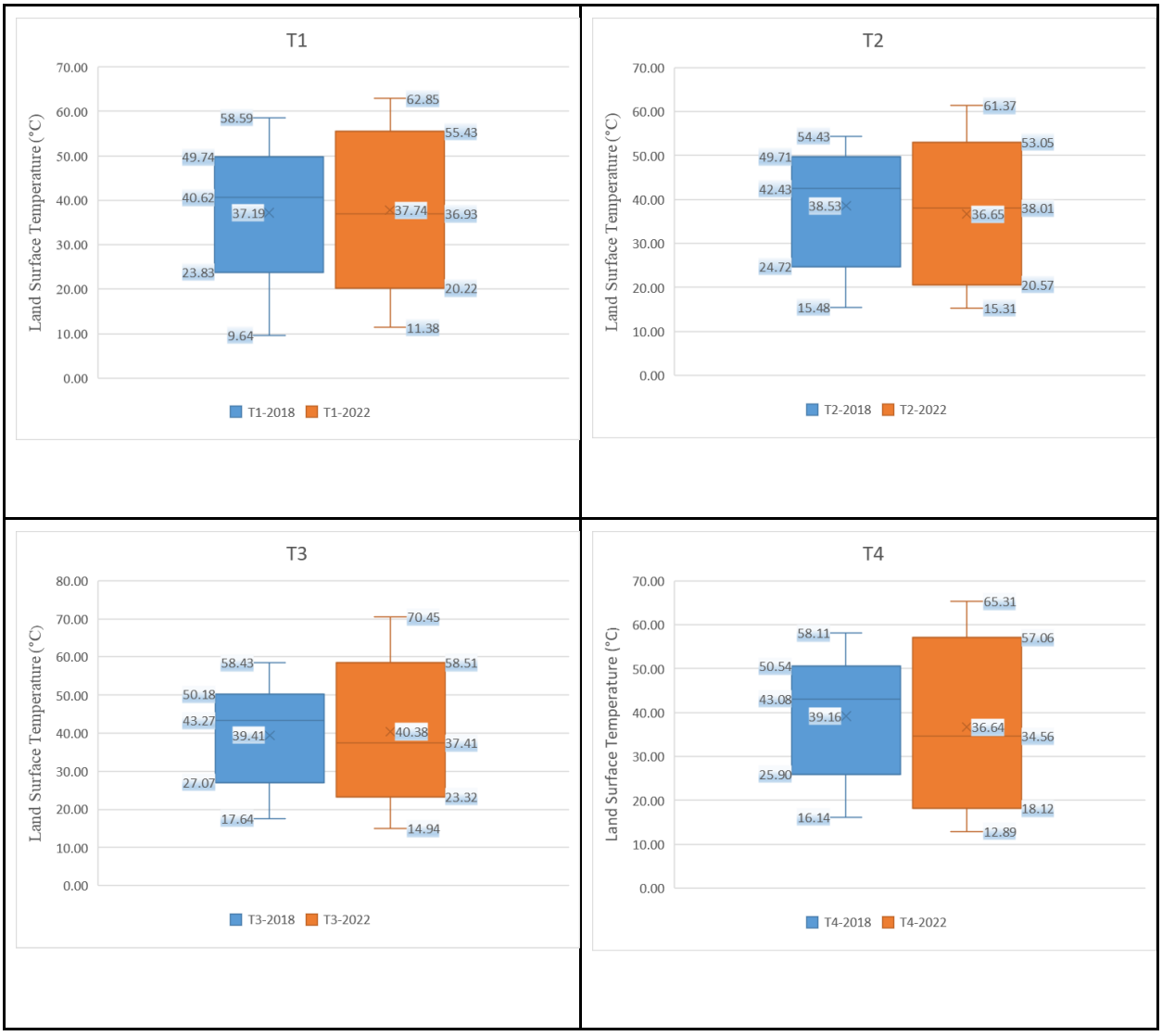

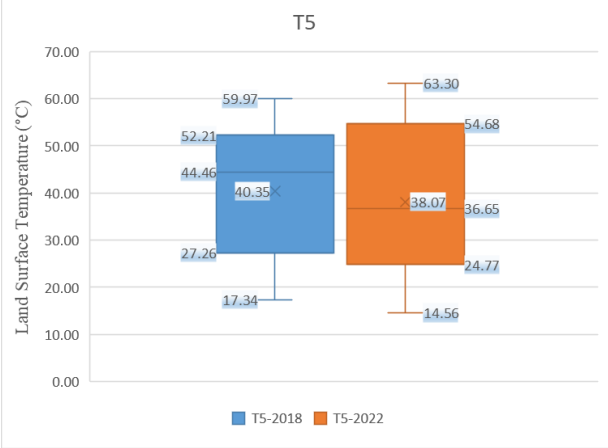
T5
Land Surface Temperature (°C)
70.00
60.00
50.00
40.00
30.00
20.00
10.00
0.00
59.97
52.21
44.46
40.35
27.26
17.34
63.30
54.68
38.07
36.65
24.77
14.56
T5-2018
T5-2022

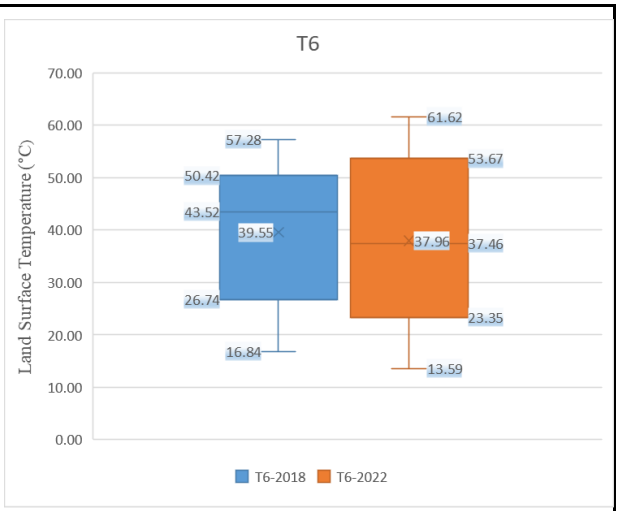
T6
Land Surface Temperature (°C)
70.00
60.00
50.00
40.00
30.00
20.00
10.00
0.00
57.28
50.42
43.52
39.55
26.74
16.84
61.62
53.67
37.96
37.46
23.35
13.59
T6-2018
T6-2022

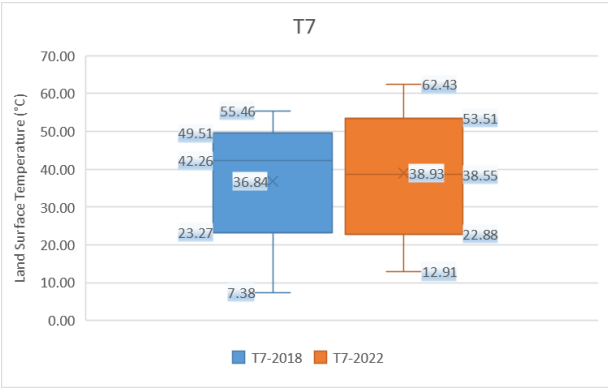
T7
Land Surface Temperature (°C)
70.00
60.00
50.00
40.00
30.00
20.00
10.00
0.00
55.46
49.51
42.26
36.84
23.27
7.38
62.43
53.51
38.93
38.55
22.88
12.91
T7-2018
T7-2022

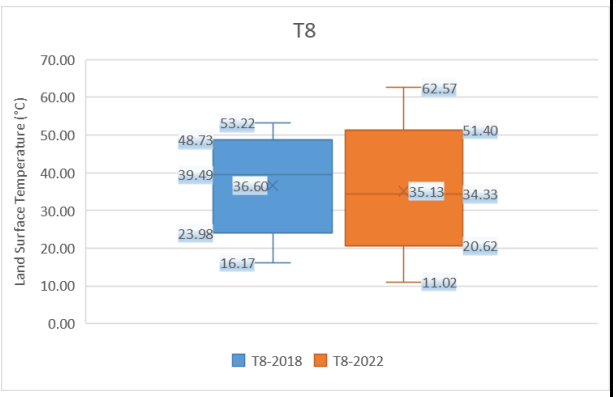
T8
Land Surface Temperature (°C)
70.00
60.00
50.00
40.00
30.00
20.00
10.00
0.00
53.22
48.73
39.49
36.60
23.98
16.17
62.57
51.40
35.13
34.33
20.62
11.02
T8-2018
T8-2022

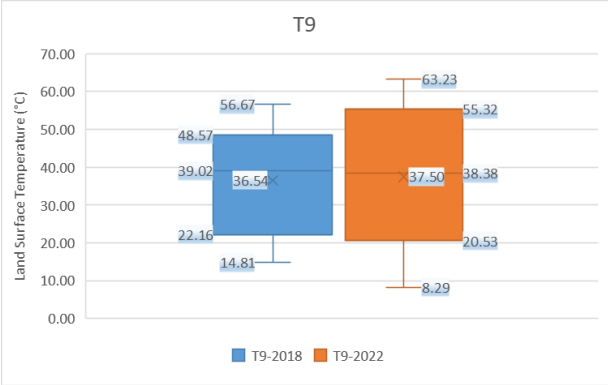
T9
Land Surface Temperature (°C)
70.00
60.00
50.00
40.00
30.00
20.00
10.00
0.00
56.67
48.57
39.02
36.54
22.16
14.81
63.23
55.32
37.50
38.38
20.53
8.29
T9-2018
T9-2022

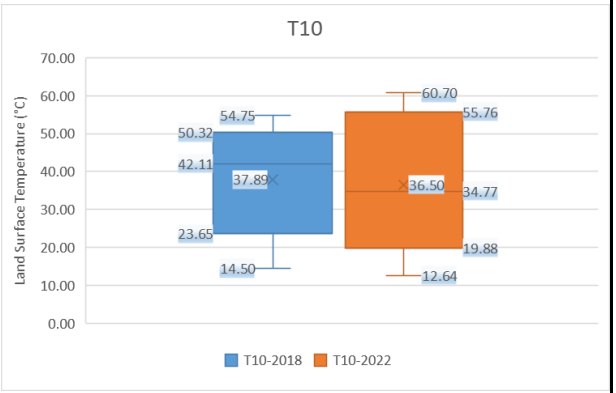
T10
Land Surface Temperature (°C)
70.00
60.00
50.00
40.00
30.00
20.00
10.00
0.00
54.75
50.32
42.11
37.89
23.65
14.50
60.70
55.76
36.50
34.77
19.88
12.64
T10-2018
T10-2022

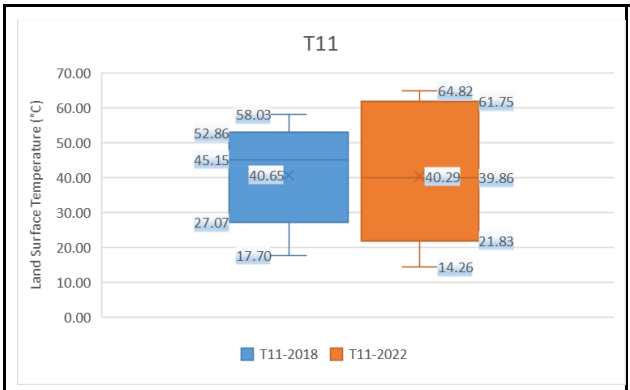
T11
Land Surface Temperature (°C)
70.00
60.00
50.00
40.00
30.00
20.00
10.00
0.00
58.03
52.86
45.15
40.65
27.07
17.70
64.82
61.75
40.29
39.86
21.83
14.26
T11-2018
T11-2022

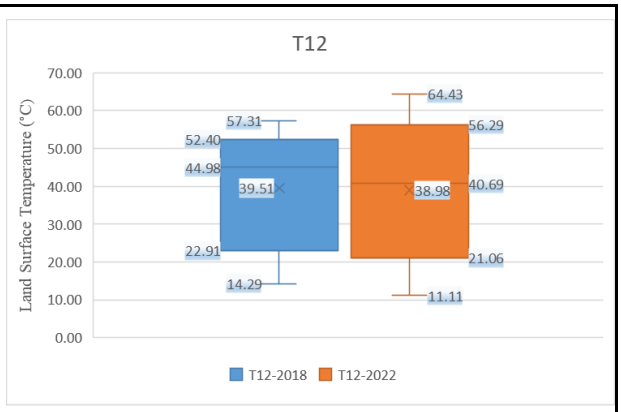
T12
Land Surface Temperature (°C)
70.00
60.00
50.00
40.00
30.00
20.00
10.00
0.00
57.31
52.40
44.98
39.51
22.91
14.29
64.43
56.29
38.98
40.69
21.06
11.11
T12-2018
T12-2022

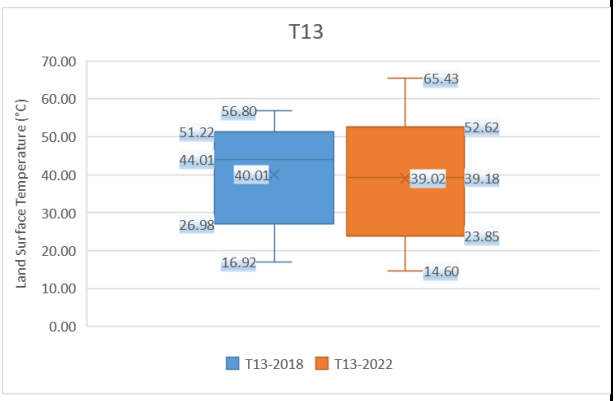
T13
Land Surface Temperature (°C)
70.00
60.00
50.00
40.00
30.00
20.00
10.00
0.00
56.80
51.22
44.01
40.01
26.98
16.92
65.43
52.62
39.02
39.18
23.85
14.60
T13-2018
T13-2022

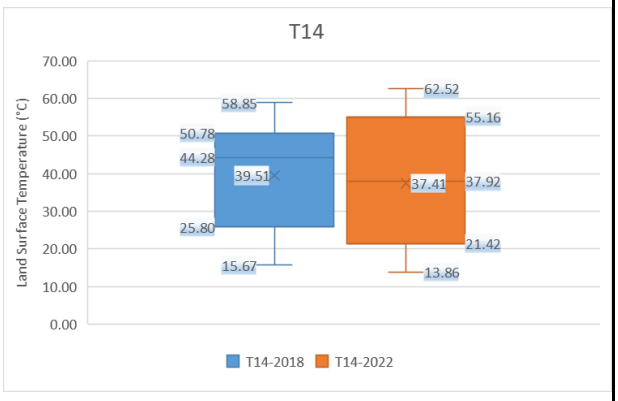
T14
Land Surface Temperature (°C)
70.00
60.00
50.00
40.00
30.00
20.00
10.00
0.00
58.85
50.78
44.28
39.51
25.80
15.67
62.52
55.16
37.41
37.92
21.42
13.86
T14-2018
T14-2022

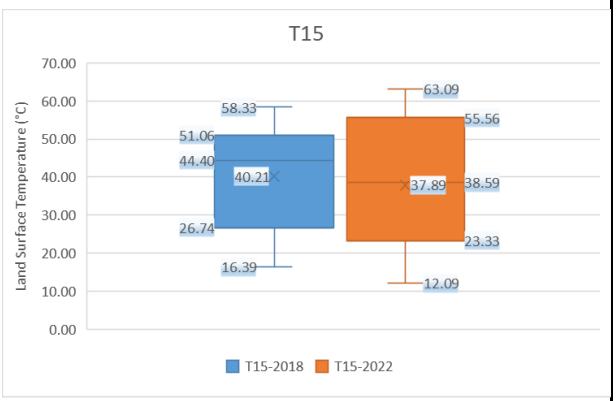
T15
Land Surface Temperature (°C)
70.00
60.00
50.00
40.00
30.00
20.00
10.00
0.00
58.33
51.06
44.40
40.21
26.74
16.39
63.09
55.56
37.89
38.59
23.33
12.09
T15-2018
T15-2022

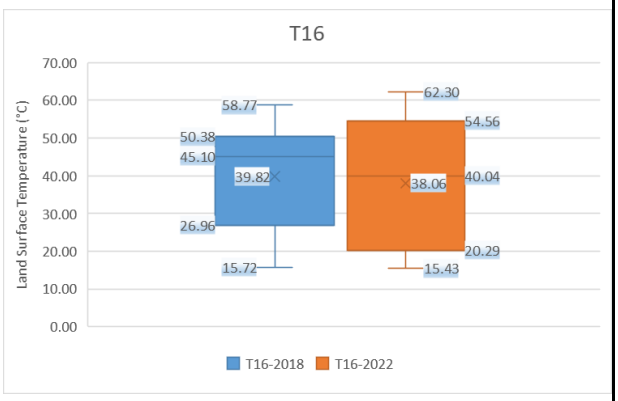
T16
Land Surface Temperature (°C)
70.00
60.00
50.00
40.00
30.00
20.00
10.00
0.00
58.77
50.38
45.10
39.82
26.96
15.72
62.30
54.56
38.06
40.04
20.29
15.43
T16-2018
T16-2022

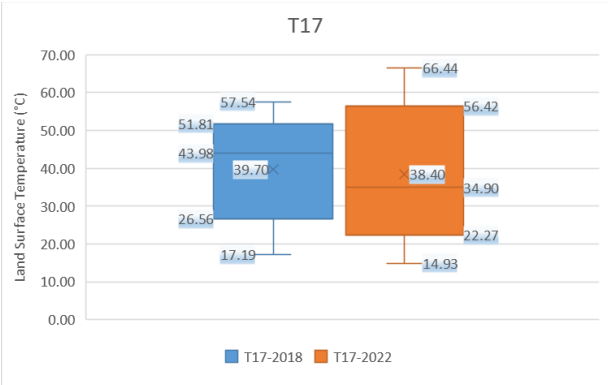
T17
Land Surface Temperature (°C)
70.00
60.00
50.00
40.00
30.00
20.00
10.00
0.00
66.44
57.54
56.42
51.81
43.98
39.70
38.40
34.90
26.56
22.27
17.19
14.93
T17-2018
T17-2022

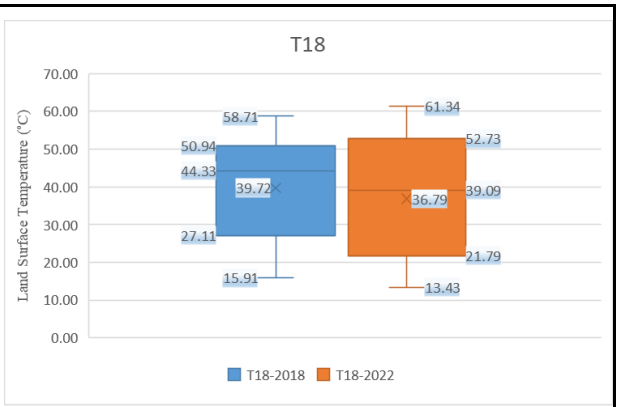
T18
Land Surface Temperature (°C)
70.00
60.00
50.00
40.00
30.00
20.00
10.00
0.00
61.34
58.71
52.73
50.94
44.33
39.72
36.79
39.09
27.11
21.79
15.91
13.43
T18-2018
T18-2022

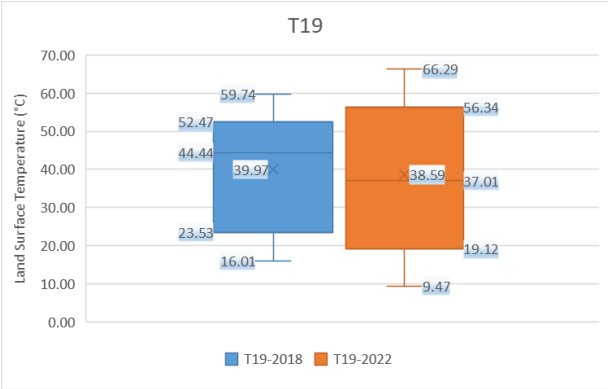
T19
Land Surface Temperature (°C)
70.00
60.00
50.00
40.00
30.00
20.00
10.00
0.00
66.29
59.74
56.34
52.47
44.44
39.97
38.59
37.01
23.53
19.12
16.01
9.47
T19-2018
T19-2022

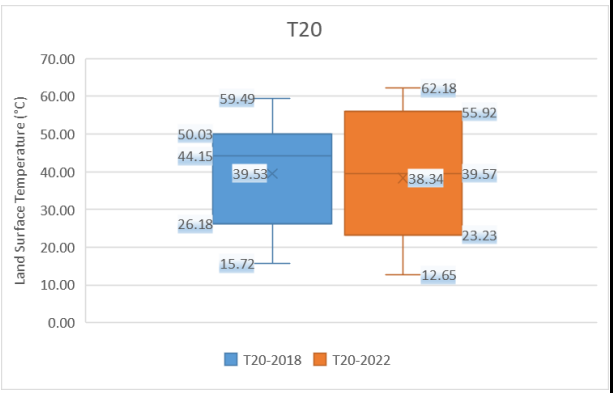
T20
Land Surface Temperature (°C)
70.00
60.00
50.00
40.00
30.00
20.00
10.00
0.00
62.18
59.49
55.92
50.03
44.15
39.53
38.34
39.57
26.18
23.23
15.72
12.65
T20-2018
T20-2022

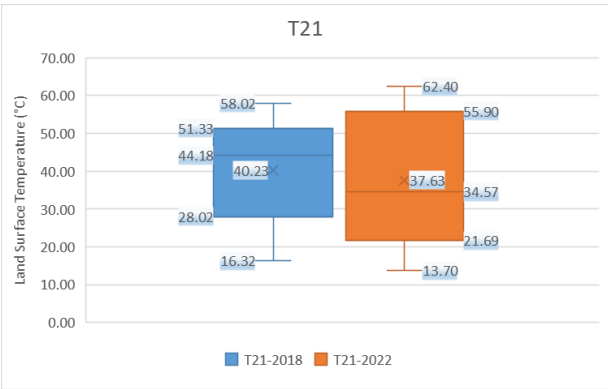
T21
Land Surface Temperature (°C)
70.00
60.00
50.00
40.00
30.00
20.00
10.00
0.00
62.40
58.02
55.90
51.33
44.18
40.23
37.63
34.57
28.02
21.69
16.32
13.70
T21-2018
T21-2022

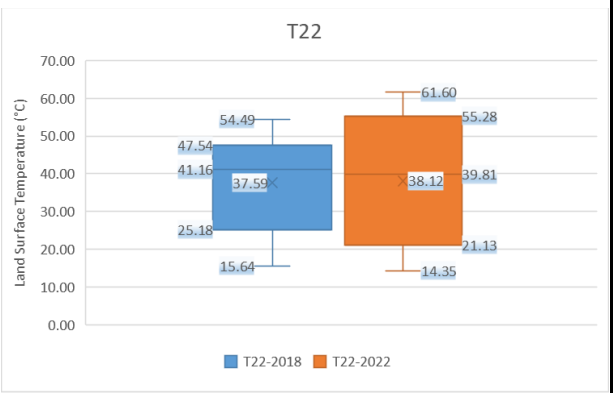
T22
Land Surface Temperature (°C)
70.00
60.00
50.00
40.00
30.00
20.00
10.00
0.00
61.60
54.49
55.28
47.54
41.16
37.59
38.12
39.81
25.18
21.13
15.64
14.35
T22-2018
T22-2022

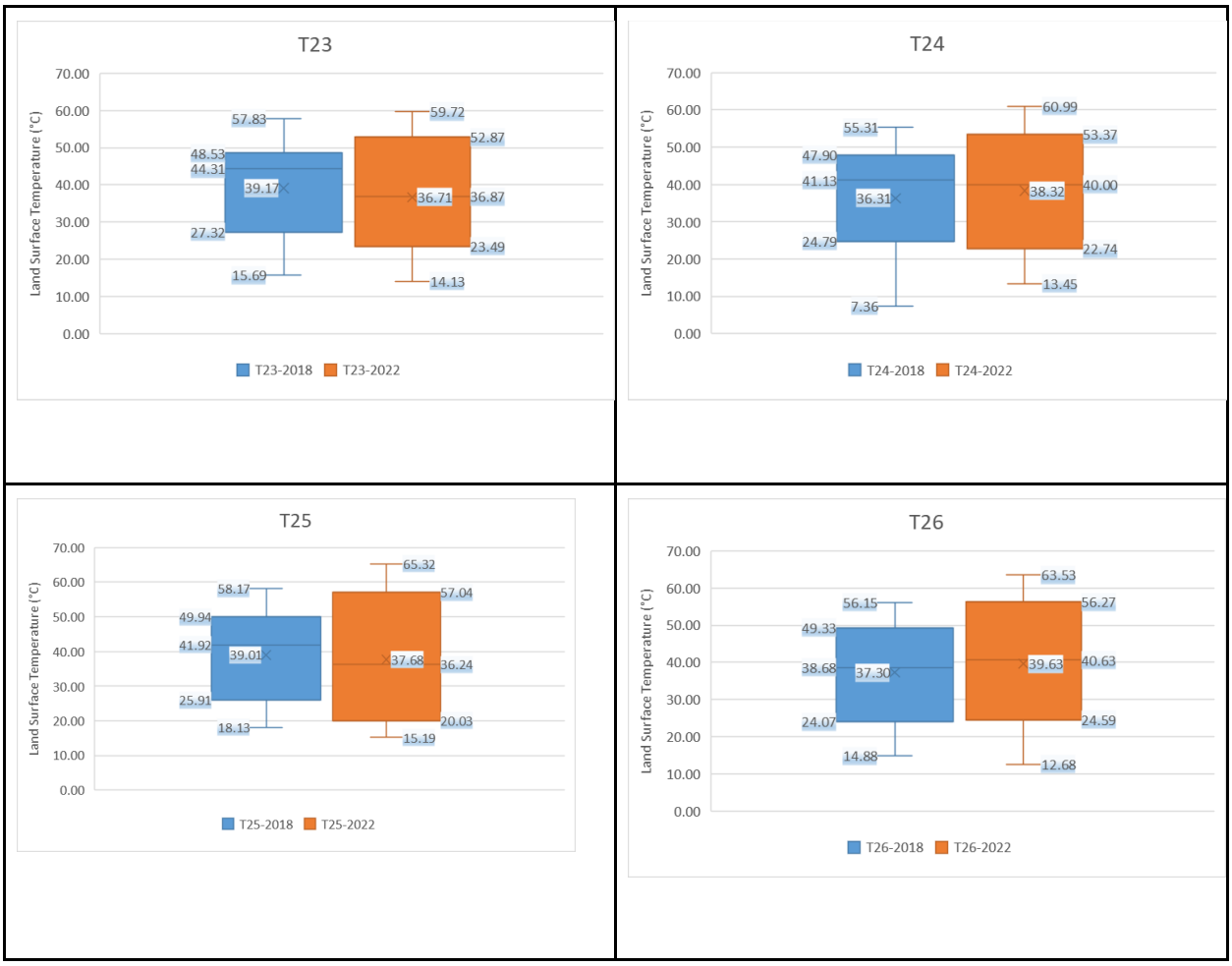

Figure A.1: Comparative Analysis of LST for 26 transitioned ROIs in 2018 (Blue) and 2022 (Orange)

Appendix A.1: Comparative Analysis of LST for 26 non-transitioned ROIs in 2018 (Blue) and 2022 (Orange)

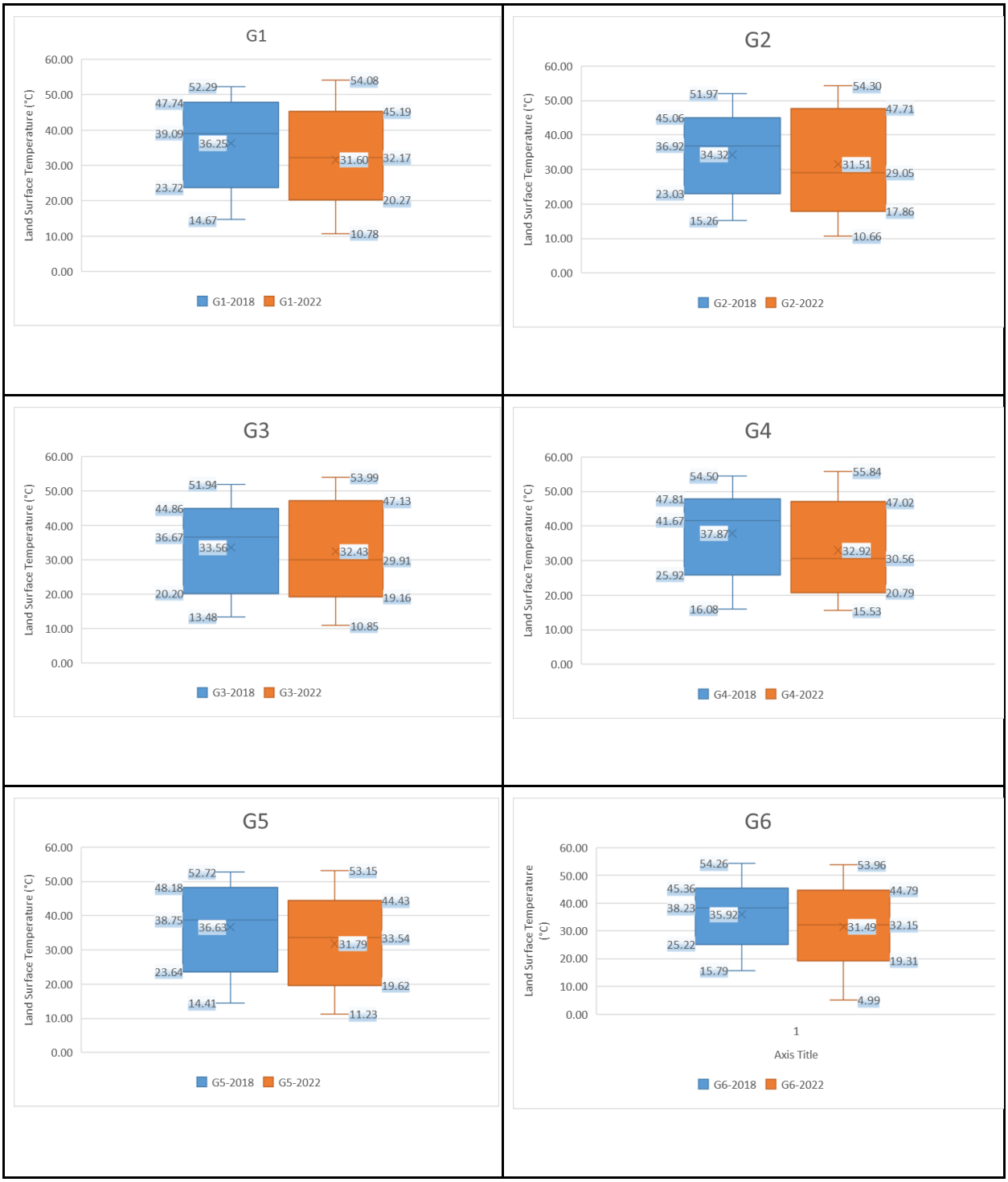

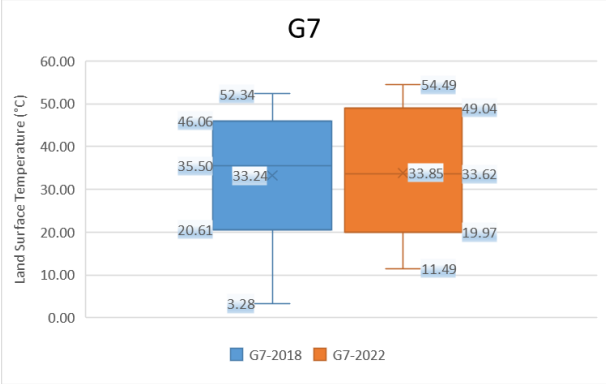
G7
Land Surface Temperature (°C)
60.00
50.00
40.00
30.00
20.00
10.00
0.00
52.34
46.06
35.50
33.24
20.61
3.28
54.49
49.04
33.85
33.62
19.97
11.49
G7-2018
G7-2022

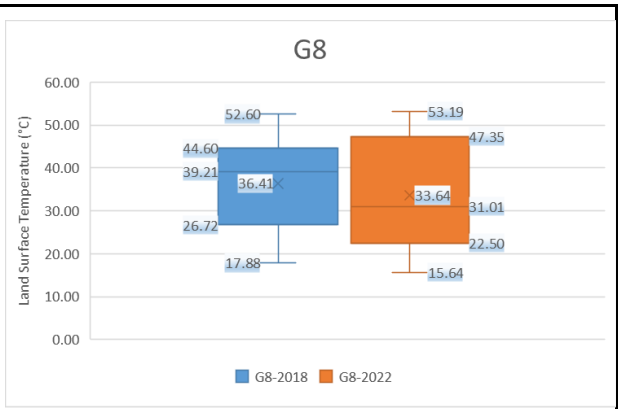
G8
Land Surface Temperature (°C)
60.00
50.00
40.00
30.00
20.00
10.00
0.00
52.60
44.60
39.21
36.41
26.72
17.88
53.19
47.35
33.64
31.01
22.50
15.64
G8-2018
G8-2022

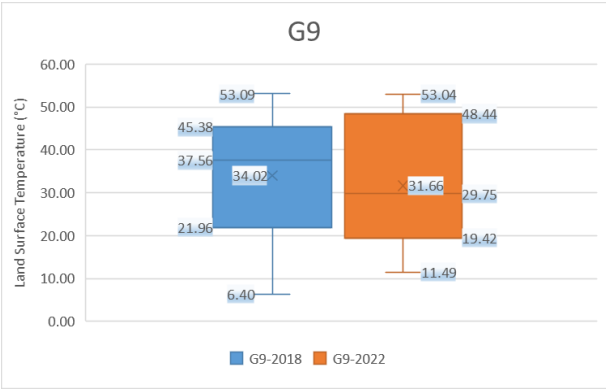
G9
Land Surface Temperature (°C)
60.00
50.00
40.00
30.00
20.00
10.00
0.00
53.09
45.38
37.56
34.02
21.96
6.40
53.04
48.44
31.66
29.75
19.42
11.49
G9-2018
G9-2022

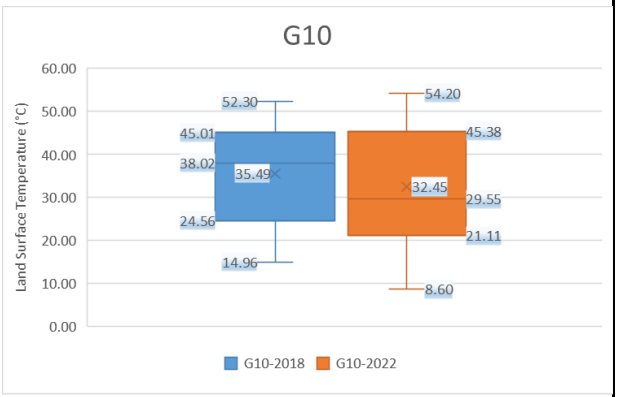
G10
Land Surface Temperature (°C)
60.00
50.00
40.00
30.00
20.00
10.00
0.00
52.30
45.01
38.02
35.49
24.56
14.96
54.20
45.38
32.45
29.55
21.11
8.60
G10-2018
G10-2022

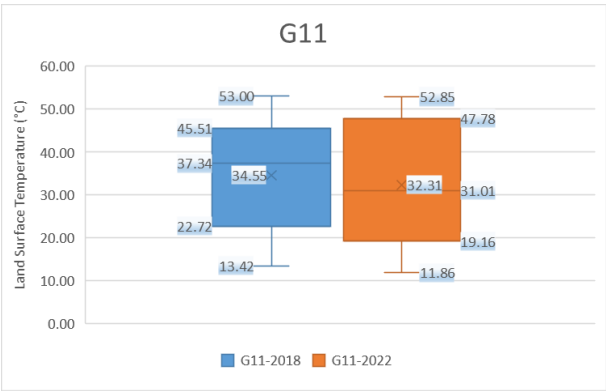
G11
Land Surface Temperature (°C)
60.00
50.00
40.00
30.00
20.00
10.00
0.00
53.00
45.51
37.34
34.55
22.72
13.42
52.85
47.78
32.31
31.01
19.16
11.86
G11-2018
G11-2022

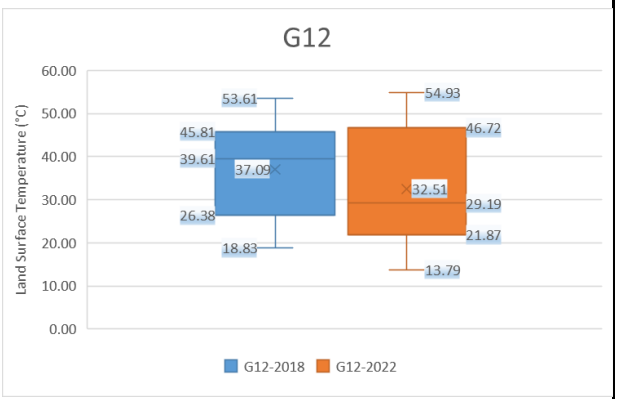
G12
Land Surface Temperature (°C)
60.00
50.00
40.00
30.00
20.00
10.00
0.00
53.61
45.81
39.61
37.09
26.38
18.83
54.93
46.72
32.51
29.19
21.87
13.79
G12-2018
G12-2022

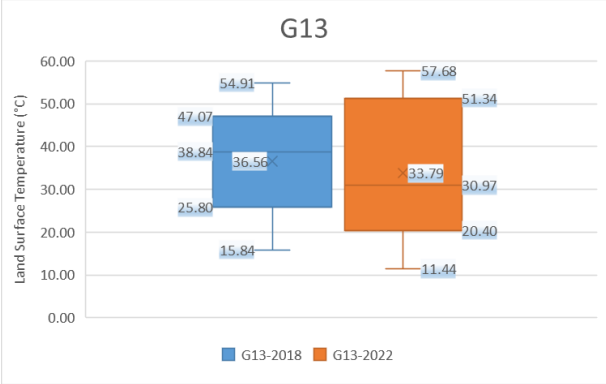
G13
Land Surface Temperature (°C)
60.00
50.00
40.00
30.00
20.00
10.00
0.00
54.91
47.07
38.84
36.56
25.80
15.84
57.68
51.34
33.79
30.97
20.40
11.44
G13-2018
G13-2022

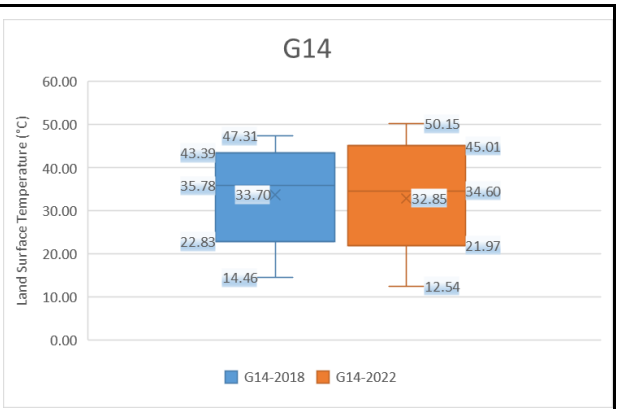
G14
Land Surface Temperature (°C)
60.00
50.00
40.00
30.00
20.00
10.00
0.00
47.31
43.39
35.78
33.70
22.83
14.46
50.15
45.01
34.60
32.85
21.97
12.54
G14-2018
G14-2022

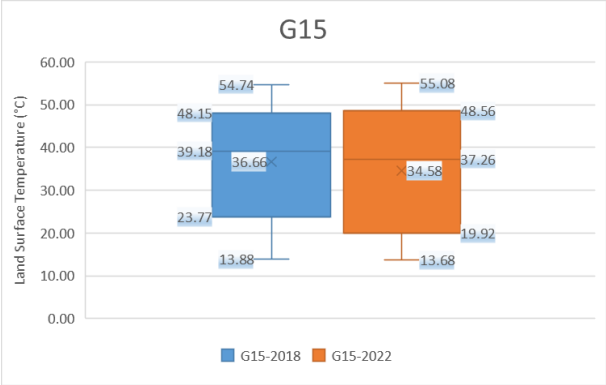
G15
Land Surface Temperature (°C)
60.00
50.00
40.00
30.00
20.00
10.00
0.00
54.74
48.15
39.18
36.66
23.77
13.88
55.08
48.56
37.26
34.58
19.92
13.68
G15-2018
G15-2022

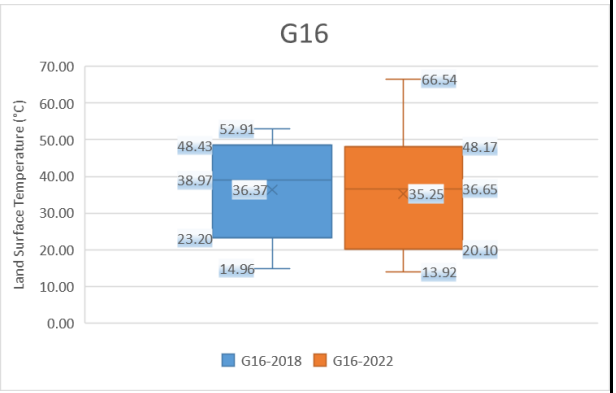
G16
Land Surface Temperature (°C)
70.00
60.00
50.00
40.00
30.00
20.00
10.00
0.00
52.91
48.43
38.97
36.37
23.20
14.96
66.54
48.17
36.65
35.25
20.10
13.92
G16-2018
G16-2022

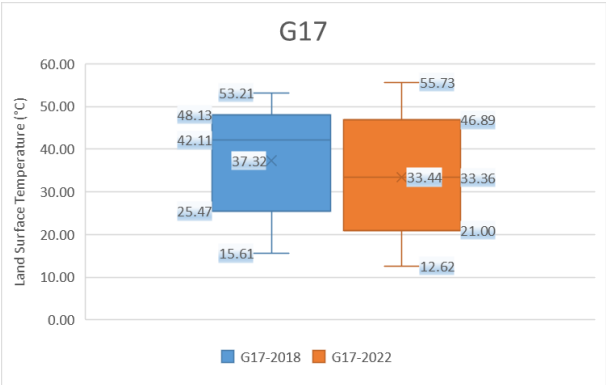
G17
Land Surface Temperature (°C)
60.00
50.00
40.00
30.00
20.00
10.00
0.00
53.21
48.13
42.11
37.32
25.47
15.61
55.73
46.89
33.36
33.44
21.00
12.62
G17-2018
G17-2022

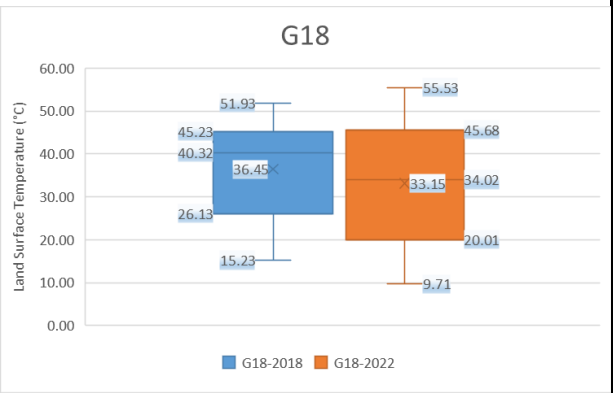
G18
Land Surface Temperature (°C)
60.00
50.00
40.00
30.00
20.00
10.00
0.00
51.93
45.23
40.32
36.45
26.13
15.23
55.53
45.68
34.02
33.15
20.01
9.71
G18-2018
G18-2022

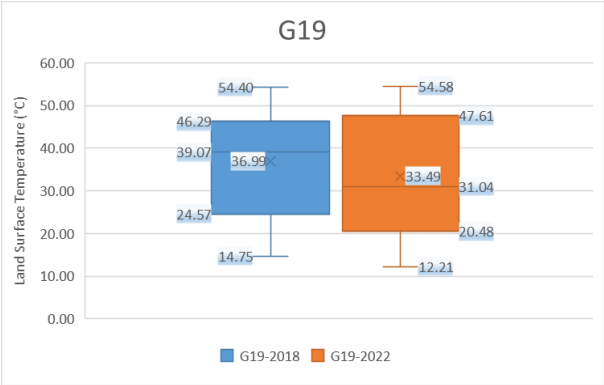
G19
Land Surface Temperature (°C)
60.00
50.00
40.00
30.00
20.00
10.00
0.00
54.40
46.29
39.07
36.99
24.57
14.75
54.58
47.61
33.49
31.04
20.48
12.21
G19-2018
G19-2022

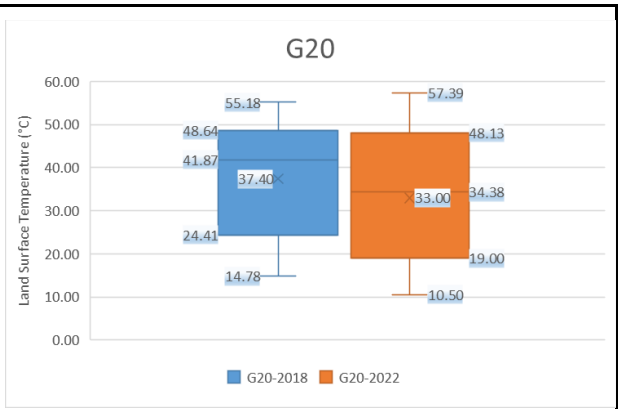
G20
Land Surface Temperature (°C)
60.00
50.00
40.00
30.00
20.00
10.00
0.00
55.18
48.64
41.87
37.40
24.41
14.78
57.39
48.13
33.00
34.38
19.00
10.50
G20-2018
G20-2022

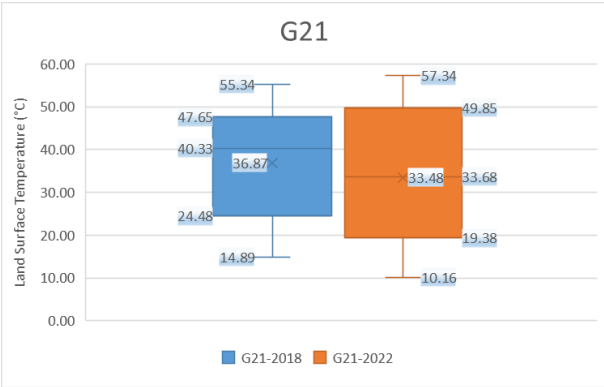
G21
Land Surface Temperature (°C)
60.00
50.00
40.00
30.00
20.00
10.00
0.00
55.34
47.65
40.33
36.87
24.48
14.89
57.34
49.85
33.48
33.68
19.38
10.16
G21-2018
G21-2022

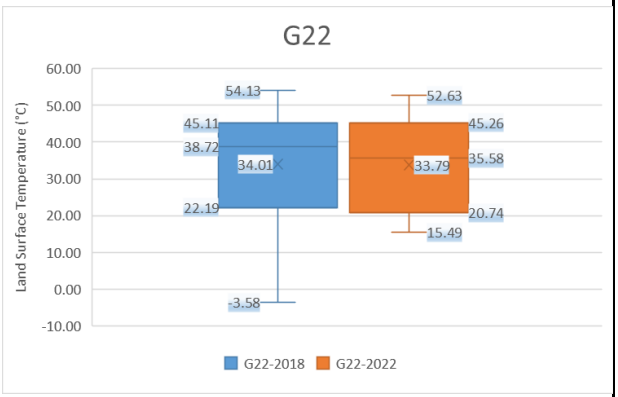
G22
Land Surface Temperature (°C)
60.00
50.00
40.00
30.00
20.00
10.00
0.00
-10.00
54.13
45.11
38.72
34.01
22.19
-3.58
52.63
45.26
33.79
35.58
20.74
15.49
G22-2018
G22-2022

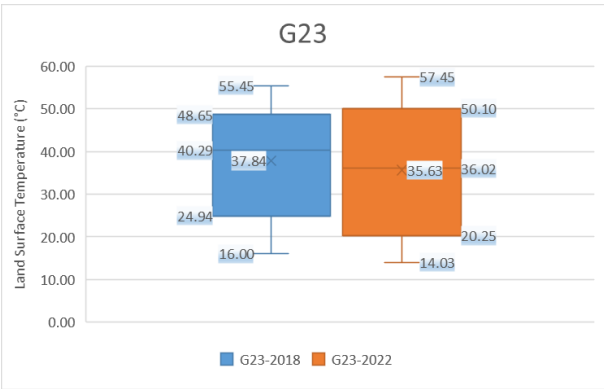
G23
Land Surface Temperature (°C)
60.00
50.00
40.00
30.00
20.00
10.00
0.00
55.45
48.65
40.29
37.84
24.94
16.00
57.45
50.10
35.63
36.02
20.25
14.03
G23-2018
G23-2022

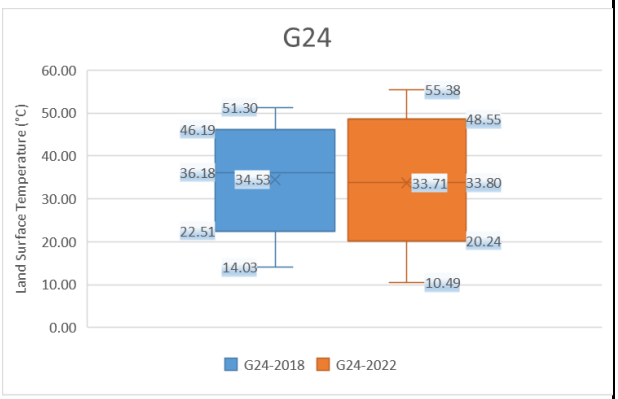
G24
Land Surface Temperature (°C)
60.00
50.00
40.00
30.00
20.00
10.00
0.00
51.30
46.19
36.18
34.53
22.51
14.03
55.38
48.55
33.71
33.80
20.24
10.49
G24-2018
G24-2022

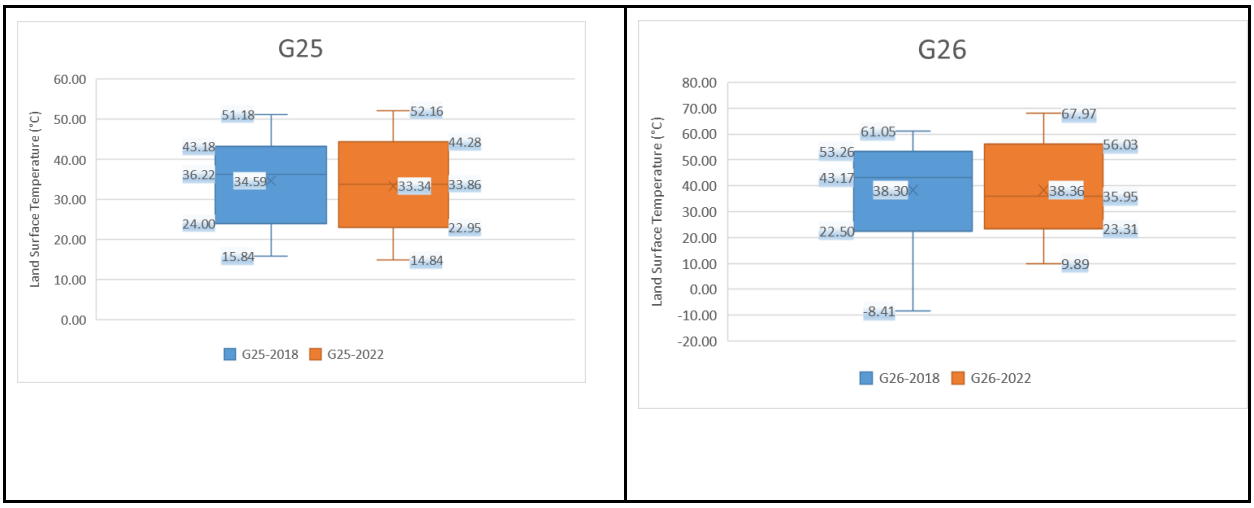

Figure A.2: Comparative Analysis of LST for 26 non-transitioned ROIs in 2018 (Blue) and 2022 (Orange)

Appendix A.2: Comparative Analysis of Surface Albedo for 26 transitioned ROIs in 2018 (Blue) and 2022 (Orange)

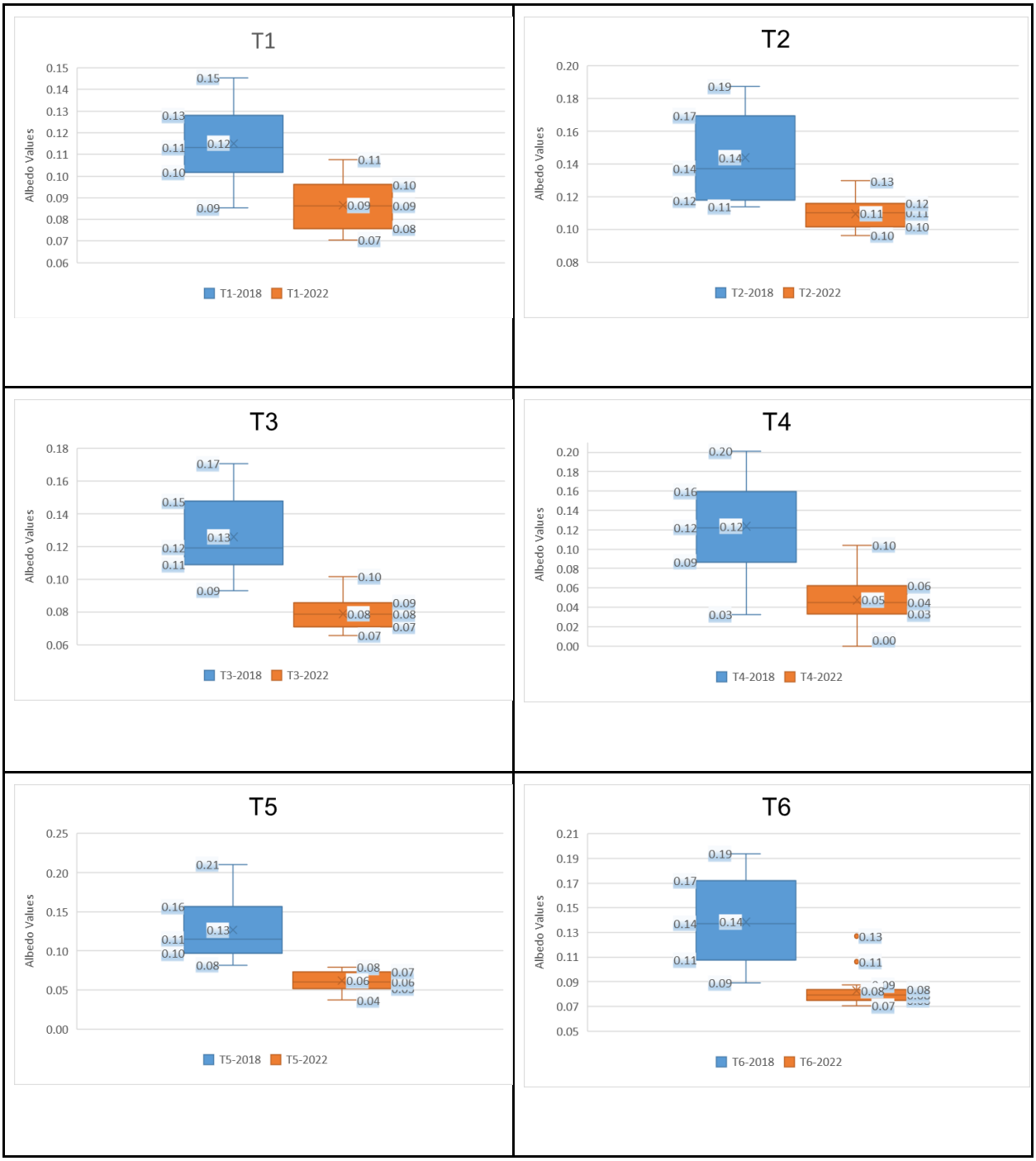

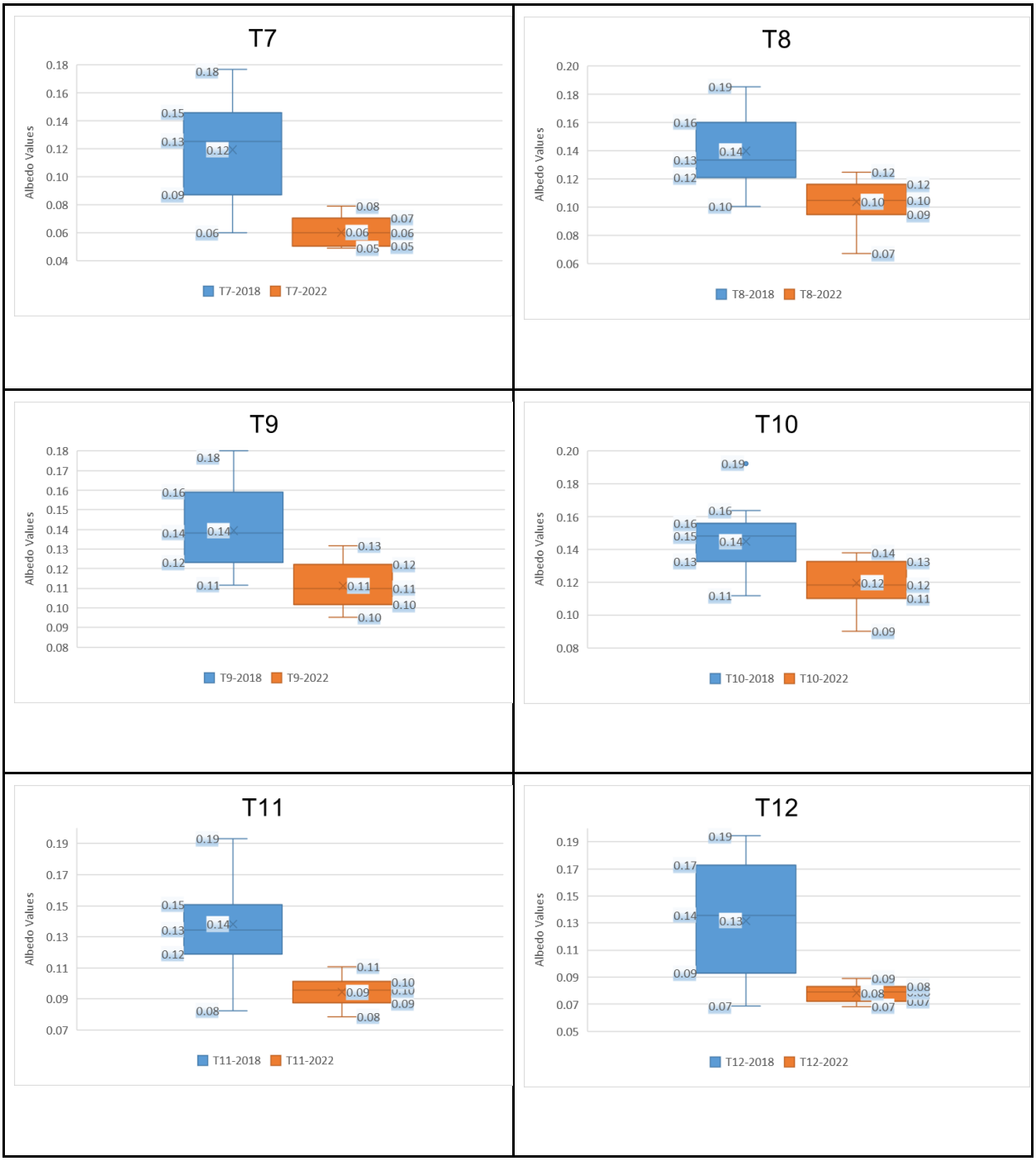
T7
Albedo Values
0.18
0.16
0.14
0.12
0.10
0.08
0.06
0.04
0.18
0.15
0.13
0.12
0.09
0.06
0.08
0.07
0.06
0.06
0.05
0.05
T7-2018
T7-2022
T8
Albedo Values
0.20
0.18
0.16
0.14
0.12
0.10
0.08
0.06
0.19
0.16
0.14
0.13
0.12
0.10
0.12
0.12
0.10
0.10
0.09
0.07
T8-2018
T8-2022
T9
Albedo Values
0.18
0.17
0.16
0.15
0.14
0.13
0.12
0.11
0.10
0.09
0.08
0.18
0.16
0.14
0.14
0.12
0.11
0.13
0.12
0.11
0.11
0.10
0.10
T9-2018
T9-2022
T10
Albedo Values
0.20
0.18
0.16
0.14
0.12
0.10
0.08
0.19
0.16
0.16
0.15
0.14
0.13
0.11
0.14
0.13
0.12
0.12
0.11
0.09
T10-2018
T10-2022
T11
Albedo Values
0.19
0.17
0.15
0.13
0.11
0.09
0.07
0.19
0.15
0.14
0.13
0.12
0.08
0.11
0.09
0.10
0.09
0.08
T11-2018
T11-2022
T12
Albedo Values
0.19
0.17
0.15
0.13
0.11
0.09
0.07
0.05
0.19
0.17
0.14
0.13
0.09
0.07
0.09
0.08
0.07
0.08
T12-2018
T12-2022

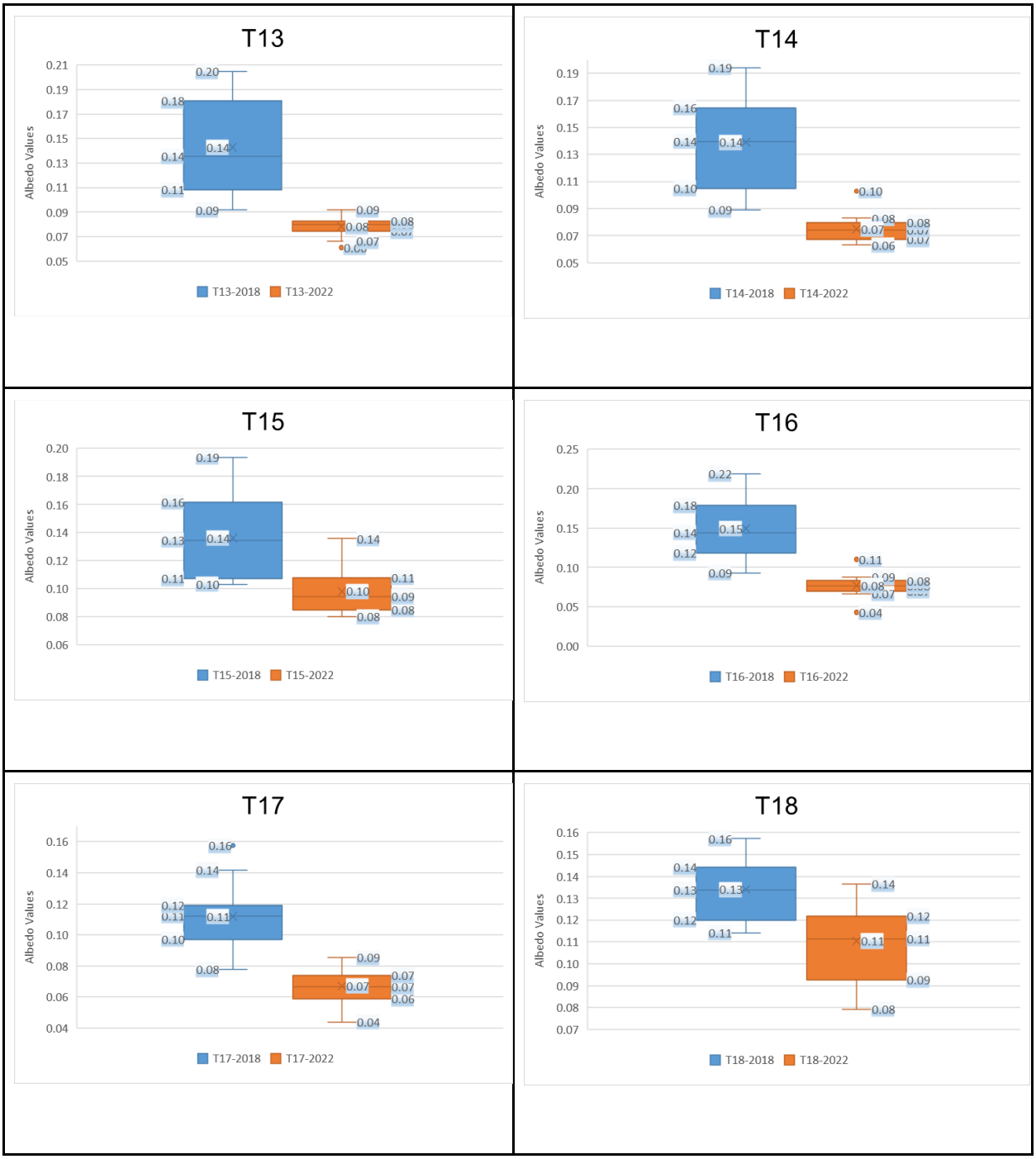
T13
Albedo Values
T13-2018
T13-2022
T14
Albedo Values
T14-2018
T14-2022
T15
Albedo Values
T15-2018
T15-2022
T16
Albedo Values
T16-2018
T16-2022
T17
Albedo Values
T17-2018
T17-2022
T18
Albedo Values
T18-2018
T18-2022

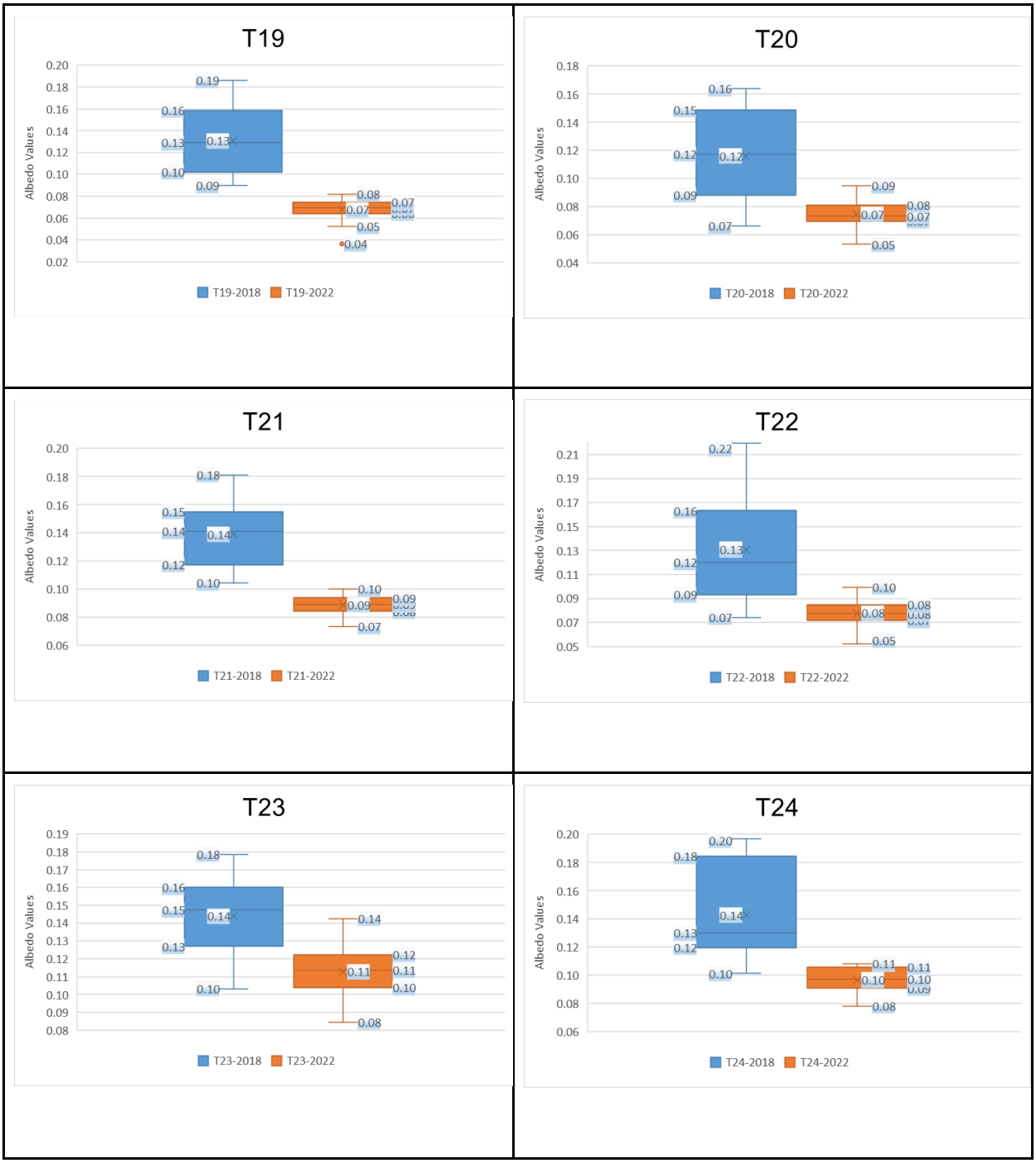
T19
Albedo Values
T19-2018
T19-2022
T20
Albedo Values
T20-2018
T20-2022
T21
Albedo Values
T21-2018
T21-2022
T22
Albedo Values
T22-2018
T22-2022
T23
Albedo Values
T23-2018
T23-2022
T24
Albedo Values
T24-2018
T24-2022

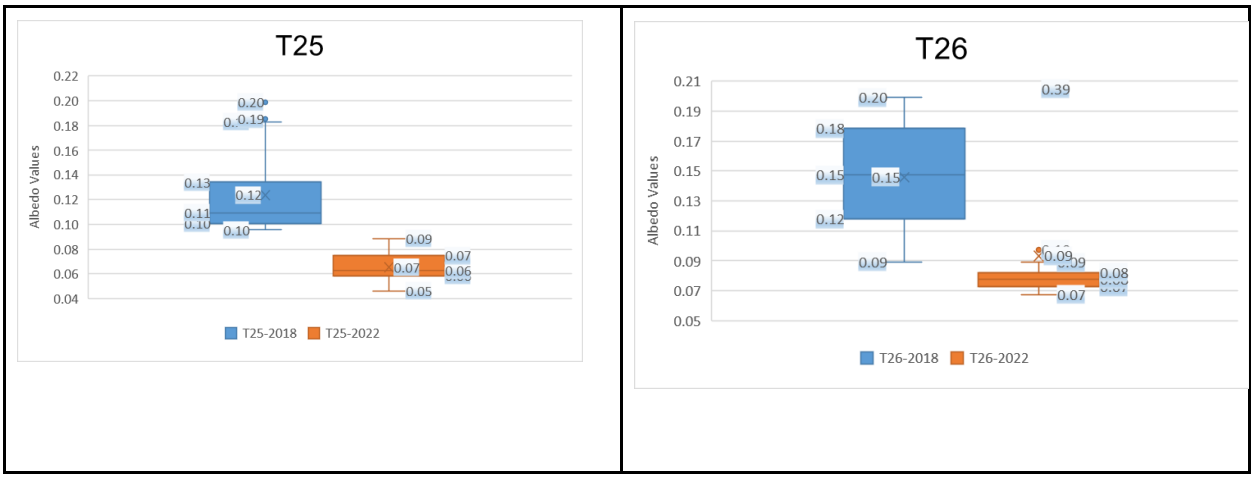

Figure A.3: Comparative Analysis of Surface Albedo for 26 transitioned ROIs in 2018 (Blue) and 2022 (Orange)

Appendix A.3: Comparative Analysis of Surface Albedo for 26 non-transitioned ROIs in 2018 (Blue) and 2022 (Orange)

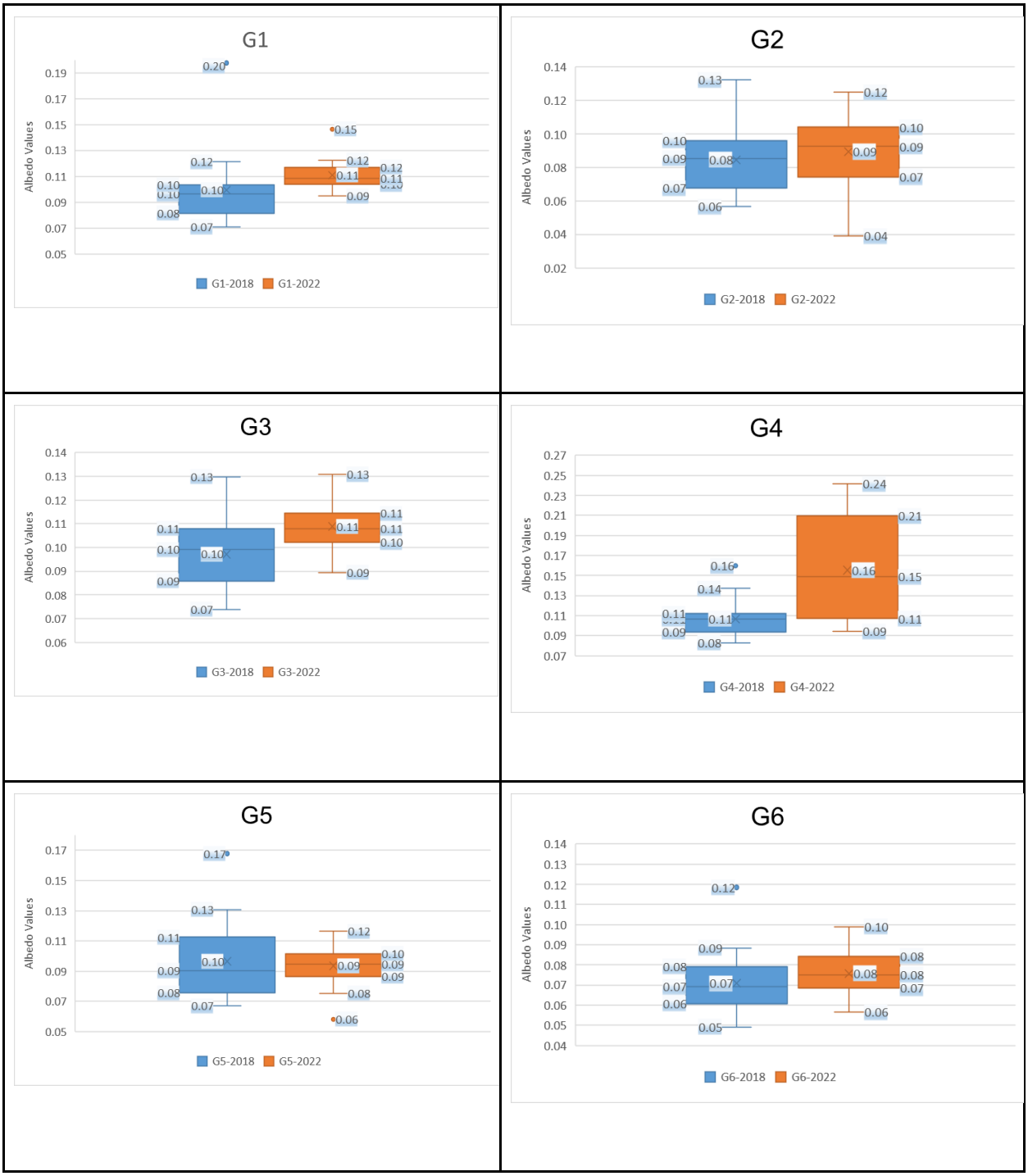

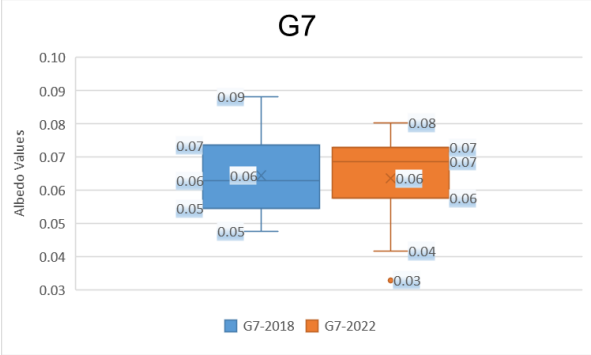
G7
Albedo Values
G7-2018
G7-2022

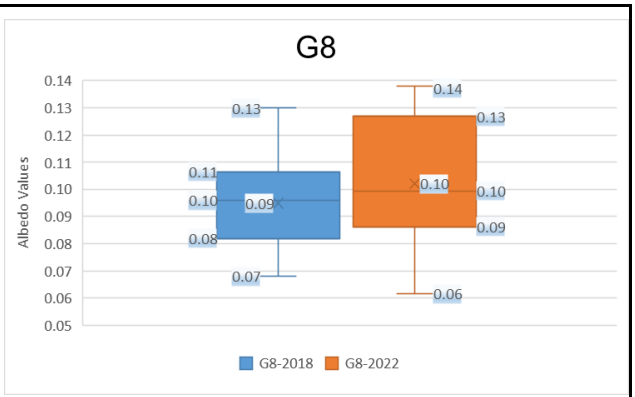
G8
Albedo Values
G8-2018
G8-2022

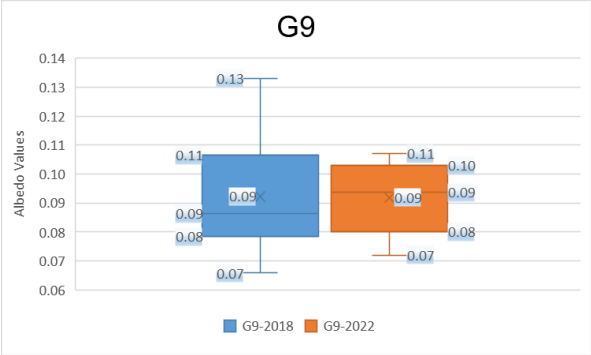
G9
Albedo Values
G9-2018
G9-2022

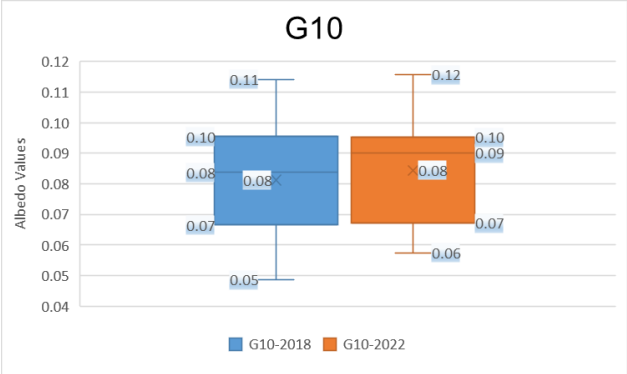
G10
Albedo Values
G10-2018
G10-2022

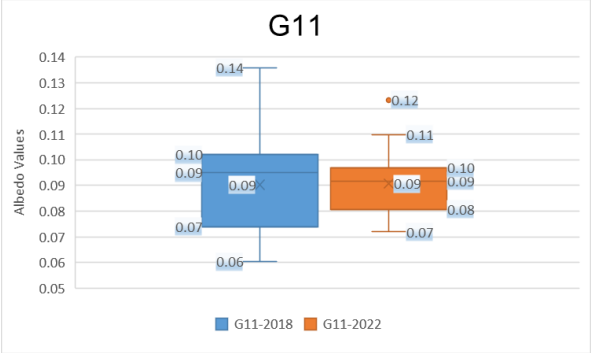
G11
Albedo Values
G11-2018
G11-2022

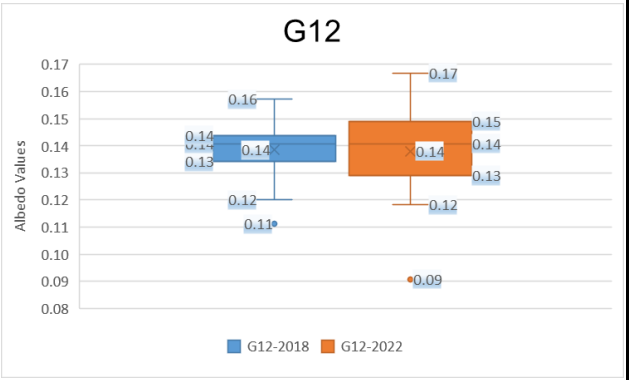
G12
Albedo Values
G12-2018
G12-2022

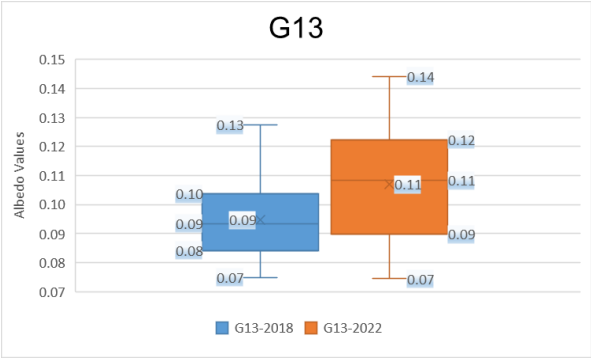
G13
Albedo Values
G13-2018
G13-2022

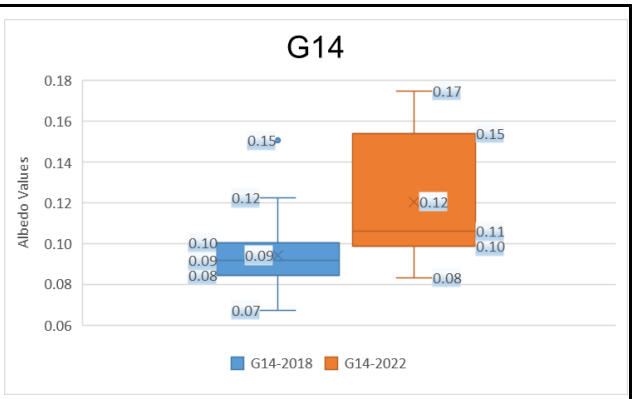
G14
Albedo Values
G14-2018
G14-2022

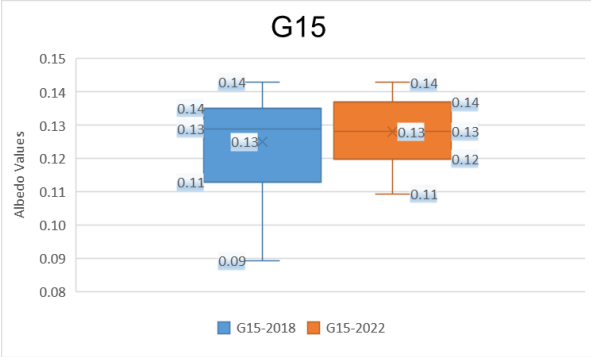
G15
Albedo Values
G15-2018
G15-2022

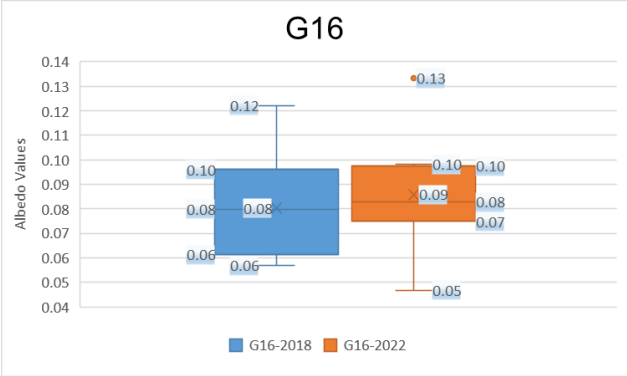
G16
Albedo Values
G16-2018
G16-2022

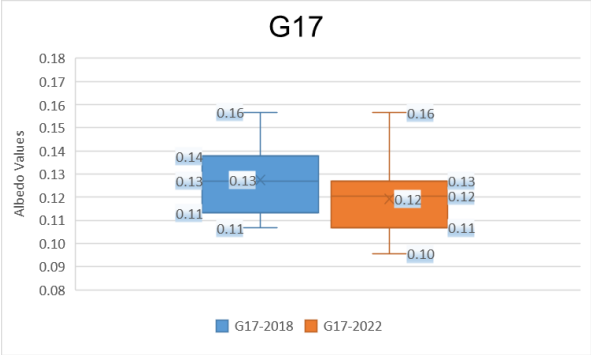
G17
Albedo Values
G17-2018
G17-2022

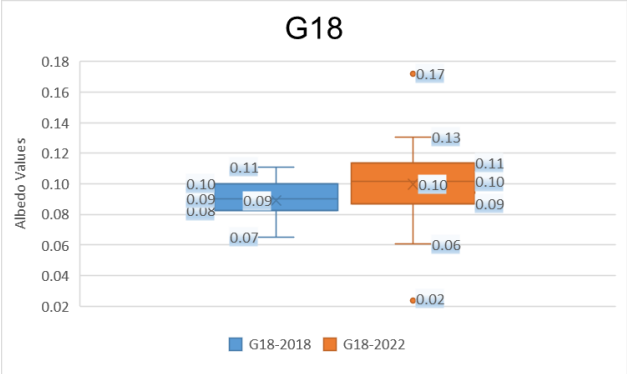
G18
Albedo Values
G18-2018
G18-2022

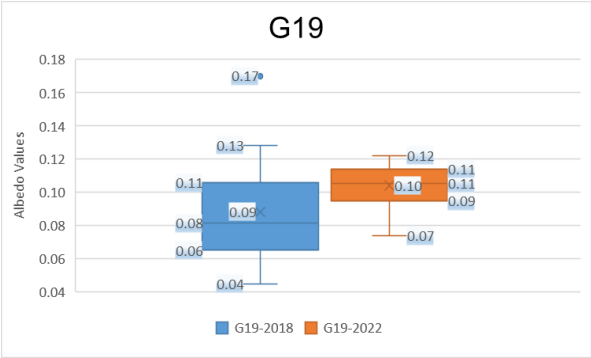
G19
Albedo Values
G19-2018
G19-2022

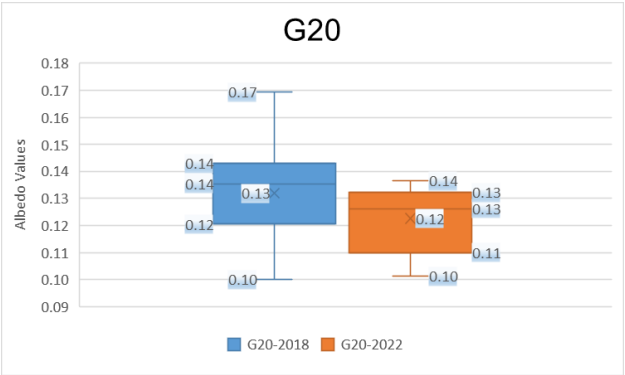
G20
Albedo Values
G20-2018
G20-2022

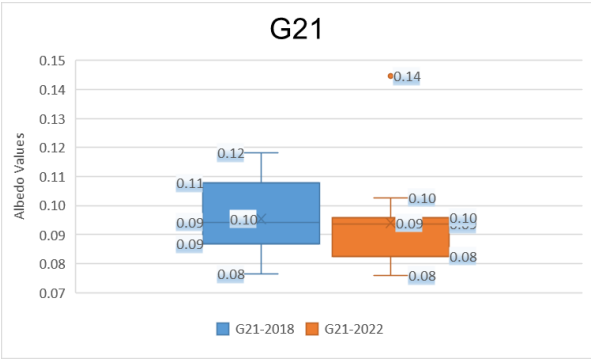
G21
Albedo Values
G21-2018
G21-2022

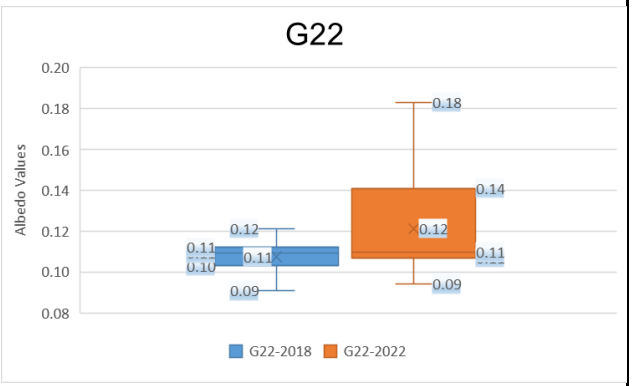
G22
Albedo Values
G22-2018
G22-2022

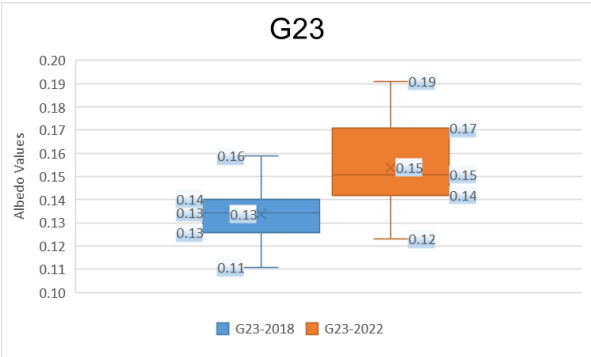
G23
Albedo Values
G23-2018
G23-2022

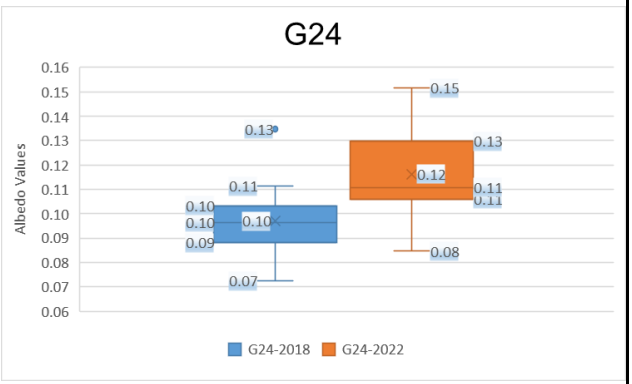
G24
Albedo Values
G24-2018
G24-2022

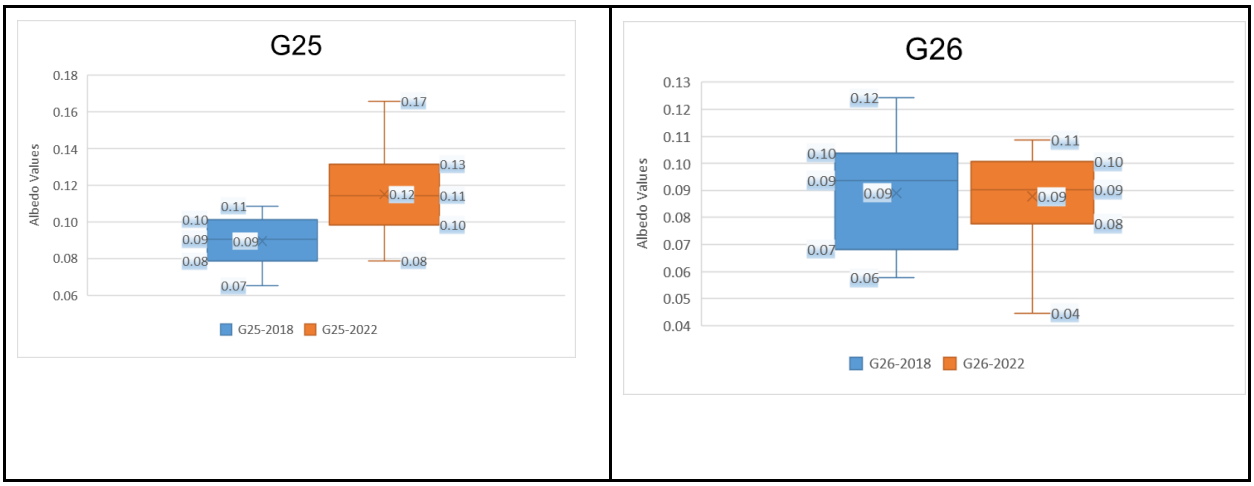

Figure A.4: Comparative Analysis of Surface Albedo for 26 non-transitioned ROIs in 2018 (Blue) and 2022 (Orange)

Appendix A.4: LST 18 Inverse Distance Row

Spatial Autocorrelation Report

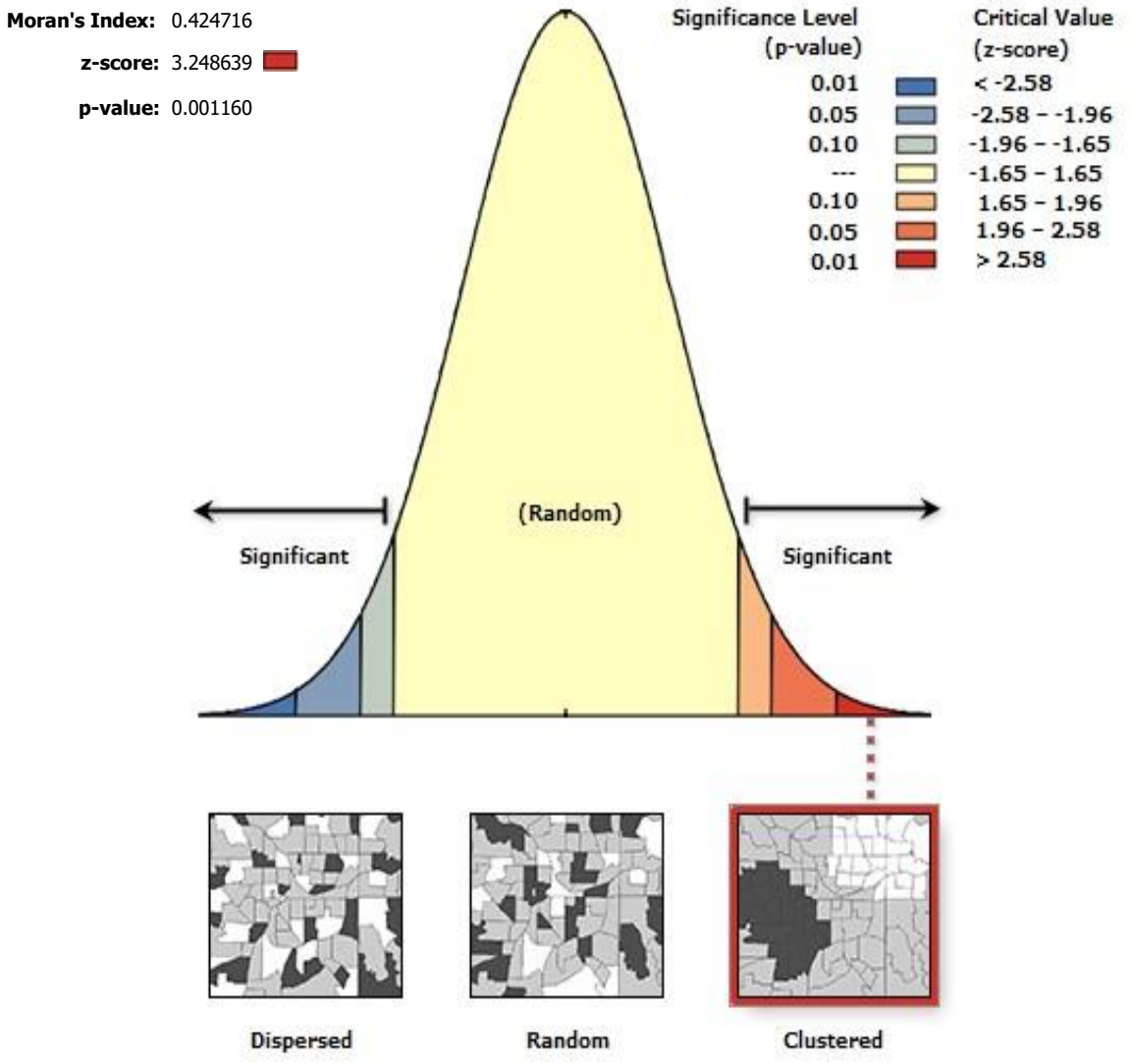

Given the z-score of 3.248639, there is a less than 1% likelihood that this clustered pattern could be the result of random chance.

Global Moran's I Summary

Moran's Index:	0.424716
Expected Index:	-0.040000
Variance:	0.020463
z-score:	3.248639
p-value:	0.001160

Dataset Information

Input Feature Class:	FullPixels_AT_SpatialJoin1
Input Field:	LST18
Conceptualization:	INVERSE_DISTANCE
Distance Method:	EUCLIDEAN
Row Standardization:	True
Distance Threshold:	10301.8266 Meters
Weights Matrix File:	None
Selection Set:	False

Appendix A.5: LST 18 KNN Row 8

Spatial Autocorrelation Report

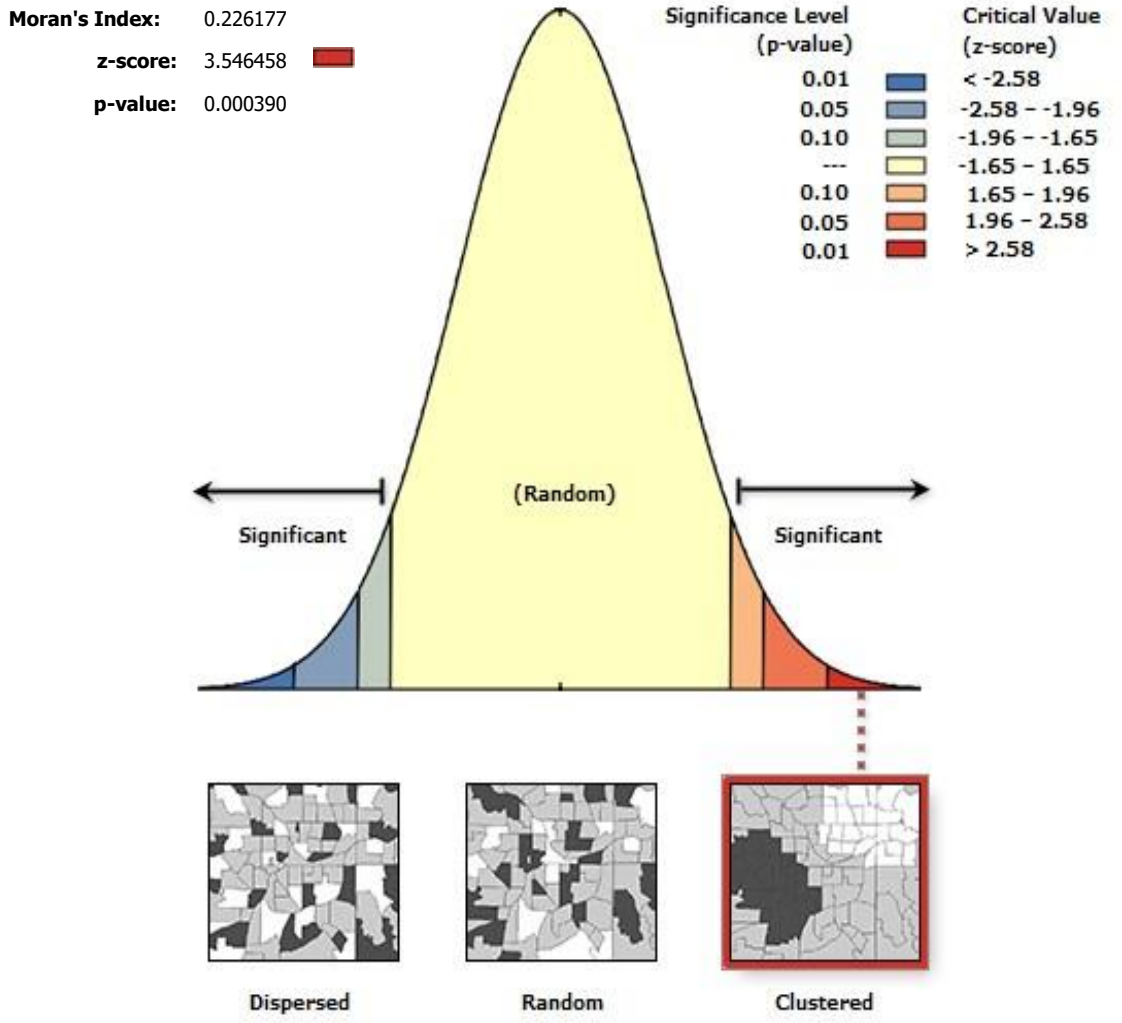

Given the z-score of 3.546458, there is a less than 1% likelihood that this clustered pattern could be the result of random chance.

Global Moran's I Summary

Moran's Index:	0.226177
Expected Index:	-0.040000
Variance:	0.005633
z-score:	3.546458
p-value:	0.000390

Dataset Information

Input Feature Class:	FullPixels_AT_SpatialJoin1
Input Field:	LST18
Conceptualization:	K_NEAREST_NEIGHBORS
Distance Method:	EUCLIDEAN
Row Standardization:	True
Distance Threshold:	None
Weights Matrix File:	None
Selection Set:	False

Appendix A.6: LST 22 Inverse Distance Row

Spatial Autocorrelation Report

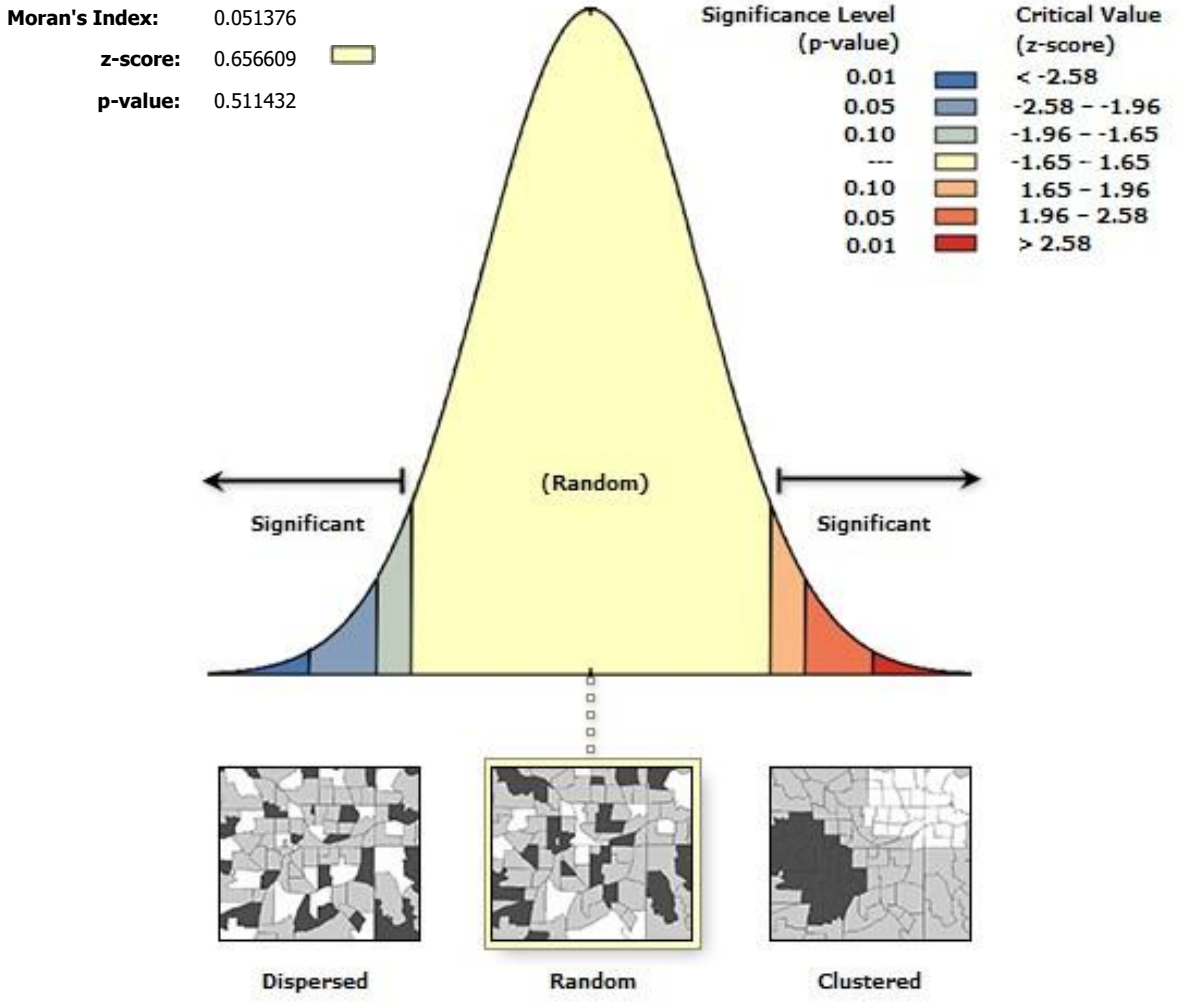

Given the z-score of 0.656609, the pattern does not appear to be significantly different than random.

Global Moran's I Summary

Moran's Index:	0.051376
Expected Index:	-0.040000
Variance:	0.019366
z-score:	0.656609
p-value:	0.511432

Dataset Information

Input Feature Class:	FullPixels_AT_SpatialJoin1
Input Field:	LST22
Conceptualization:	INVERSE_DISTANCE
Distance Method:	EUCLIDEAN
Row Standardization:	True
Distance Threshold:	10301.8266 Meters
Weights Matrix File:	None
Selection Set:	False

Appendix A.7: LST 22 KNN Row 8

Spatial Autocorrelation Report

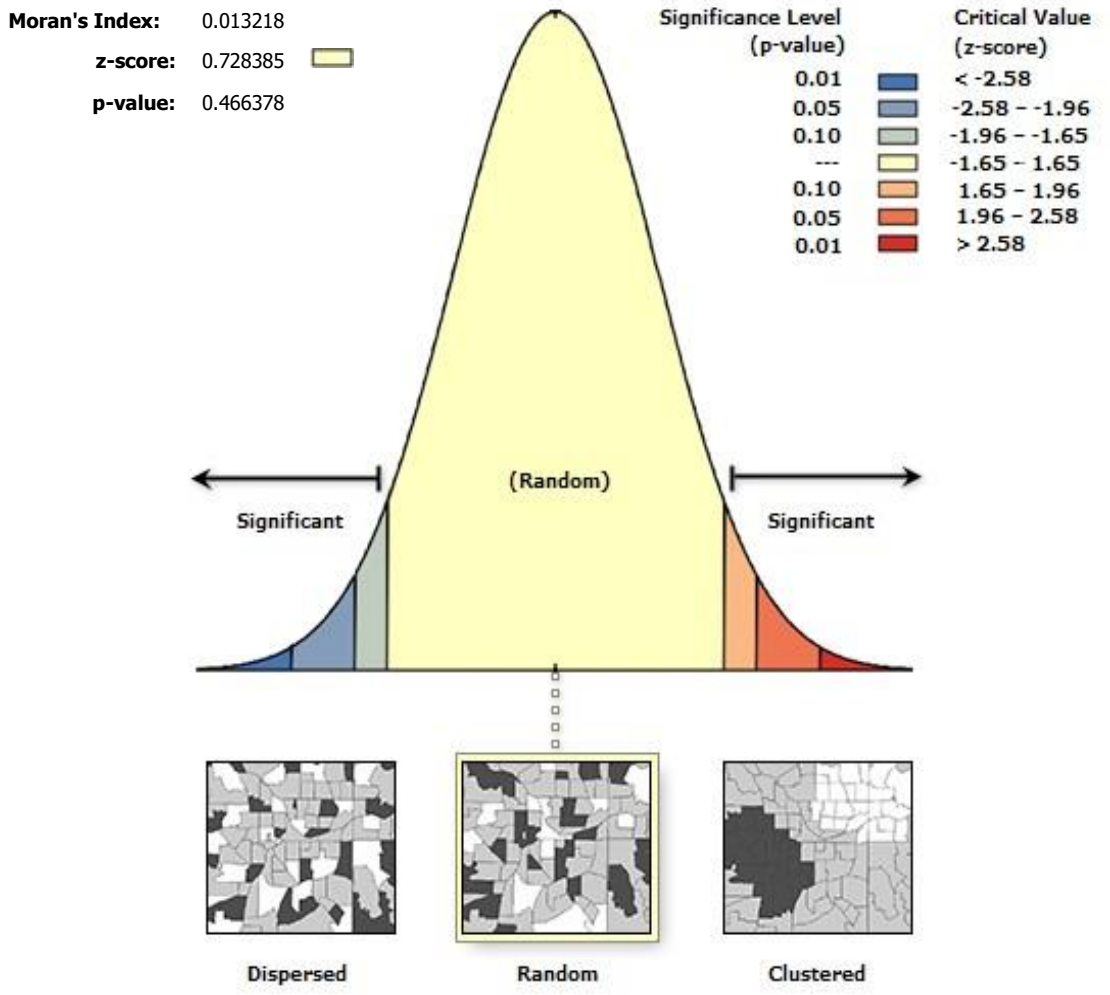

Given the z-score of 0.728385, the pattern does not appear to be significantly different than random.

Global Moran's I Summary

Moran's Index:	0.013218
Expected Index:	-0.040000
Variance:	0.005338
z-score:	0.728385
p-value:	0.466378

Dataset Information

Input Feature Class:	FullPixels_AT_SpatialJoin1
Input Field:	LST22
Conceptualization:	K_NEAREST_NEIGHBORS
Distance Method:	EUCLIDEAN
Row Standardization:	True
Distance Threshold:	None
Weights Matrix File:	None
Selection Set:	False

REFERENCES

Akwensi, P. H., Kang, Z., & Wang, R. (2023). Hyperspectral image-aided LiDAR point cloud labeling via spatio-spectral feature representation learning. *International Journal of Applied Earth Observation and Geoinformation, 120*, 103302. https://doi.org/10.1016/j.jag.2023.103302

Alcantara, E., Rosa, D., Gamez, J., Martinez, A., Comin, M., Such, M. J., Vera, P., & Prat, J. (2006). Analysis of the influence of rubber infill on the mechanical performance of artificial turf surfaces for soccer. *Sports Engineering*, *9*(2), 107–107.

Aoki, T. (2009). Effect of solar illuminance and albedo on surface temperature of outdoor sport surfaces. *Nat. Environ.* 11, 40–48.

Arizton Advisory & Intelligence. (2022). Artificial turf market demand, size analysis, forecast report [WWW document]. Arizton advisory & intelligence. URL. https://www.arizton.com/market-reports/artificial-turf-market.

Armada, D., Llompart, M., Celeiro, M., Garcia-Castro, P., Ratola, N., Dagnac, T., & de Boer, J. (2022). Global evaluation of the chemical hazard of recycled tire crumb rubber employed on worldwide synthetic turf football pitches. *The Science of the Total Environment*, *812*, 152542–152542. https://doi.org/10.1016/j.scitotenv.2021.152542

Baghzouz, M., Devitt, D. A., & Morris, R. L. (2006). Evaluating temporal variability in the spectral reflectance response of annual ryegrass to changes in nitrogen applications and leaching fractions. *International Journal of Remote Sensing*, *27*(19), 4137–4157. https://doi.org/10.1080/01431160600851843

Bala, R., Prasad, R., Yadav, V. P., & Sharma, J. (2018). A Comparative Study of Land Surface Temperature With Different Indices on Heterogeneous Land Cover Using Landsat 8 Data. *International Archives of the Photogrammetry, Remote Sensing and Spatial Information Sciences.*, *XLII-5*, 389–394. https://doi.org/10.5194/isprs-archives-XLII-5-389-2018

Becker, W. R., Ló, T. B., Johann, J. A., & Mercante, E. (2021). Statistical features for land use and land cover classification in Google Earth Engine. *Remote Sensing Applications, 21*, 100459. https://doi.org/10.1016/j.rsase.2020.100459

Biran, I., Bravdo, B., Bushkin-Harav, I., & Rawitz, E. (1981). Water consumption and growth rate of 11 turfgrasses as affected by mowing height, irrigation frequency, and soil moisture 1. *Agronomy Journal*, *73*(1), 85-90. https://doi.org/10.2134/agronj1981.00021962007300010020x

Black, A., Ahmad, S., & Stephen, H. (2019). Urban heat island intensity mapping of Las Vegas using Landsat thermal infrared data. *World Environmental and Water Resources Congress 2019: Groundwater, Sustainability, Hydro-Climate/Climate Change, and Environmental*

Engineering - Selected Papers from the World Environmental and Water Resources Congress 2019, 397–409. https://doi.org/10.1061/9780784482346.040

Bonfils, C., de Noblet-Ducoudré, N., Braconnot, P., & Joussaume, S. (2001). Hot Desert Albedo and Climate Change: Mid-Holocene Monsoon in North Africa. *Journal of Climate*, *14*(17), 3724–3737. https://doi.org/10.1175/1520-0442(2001)014<3724:HDAACC>2.0.CO;2

Brandt, J. (2008). Locating turf and water features in the Las Vegas valley, Nevada, using remote sensing techniques and GIS. In *American Society for Photogrammetry and Remote Sensing*.

Brelsford, C., & Abbott, J. K. (2017). Growing into Water Conservation? Decomposing the Drivers of Reduced Water Consumption in Las Vegas, NV. *Ecological Economics*, *133*, 99–110. https://doi.org/10.1016/j.ecolecon.2016.10.012

Brown, E. G., JR., Rodriquez, J. M., Alex, K., Weil, E. G., Ragen, D. A., Los Angeles City Attorney, Thomas, E. E., Bilgin, P., Ruden, E., Minassian, V., Paulson, D. W., Gonzalez, C. B., Superior Court of California for the County of Alameda, People of the State of California. ex rel. Edmund G. Brown, JR., Attorney General, Carmen A. Trutanich, Los Angeles City Attorney, David W. Paulson, Solano County District Attorney, Beaulieu Group, LLC, et al., & Astroturf, LLC. (n.d.). *Consent Judgement as to Defendant Astroturf.* https://oag.ca.gov/system/files/attachments/press_releases/n1782_astroturf_cj%2C_final-signed.pdf

Burillo, P., Gallardo, L., Felipe, J. L., & Gallardo, A. M. (2014). Artificial turf surfaces: Perception of safety, sporting feature, satisfaction and preference of football users. *European Journal of Sport Science*, *14*(sup1), S437–S447. https://doi.org/10.1080/17461391.2012.713005

Buskirk, E. R., McLaughlin, E. R., & Loomis, J. L. (1971). Microclimate over Artificial Turf. *Journal of Health, Physical Education, Recreation*, *42*(9), 29–30. https://doi.org/10.1080/00221473.1971.10617177

Carvalho, H. D. R., Chang, B., McInnes, K. J., Heilman, J. L., Wherley, B., & Aitkenhead-Peterson, J. A. (2021). Energy balance and temperature regime of different materials used in urban landscaping. *Urban Climate*, *37*, 100854. https://doi.org/10.1016/j.uclim.2021.100854

Ceballos-Silva, A., & López-Blanco, J. (2003). Delineation of suitable areas for crops using a Multi-Criteria Evaluation approach and land use/cover mapping: a case study in Central Mexico. *Agricultural Systems*, *77*(2), 117–136. https://doi.org/10.1016/S0308-521X(02)00103-8

Celeiro, M., Lamas, J. P., Garcia-Jares, C., Dagnac, T., Ramos, L., & Llompart, M. (2014). Investigation of PAH and other hazardous contaminant occurrence in recycled tyre rubber surfaces. Case-study: restaurant playground in an indoor shopping center. *International*

Journal of Environmental Analytical Chemistry, *94*(12), 1264–1271. https://doi.org/10.1080/03067319.2014.930847

Celeiro, M., Dagnac, T., & Llompart, M. (2018). Determination of priority and other hazardous substances in football fields of synthetic turf by gas chromatography-mass spectrometry: A health and environmental concern. *Chemosphere (Oxford)*, *195*, 201–211. https://doi.org/10.1016/j.chemosphere.2017.12.063

Centers for Disease Control Prevention. (2005). *Preventing lead poisoning in young children a statement by the Centers for Disease Control and Prevention* ([5th rev.].). U.S. Dept. of Health and Human Services, Centers for Disease Control and Prevention.

Charalambous, L., von Lieres und Wilkau, H. C., Potthast, W., & Irwin, G. (2016). The effects of artificial surface temperature on mechanical properties and player kinematics during landing and acceleration. *Journal of Sport and Health Science*, *5*(3), 355–360. https://doi.org/10.1016/j.jshs.2015.01.013

Chen, Y., Wang, Q., Wang, Y., Duan, S. B., Xu, M., & Li, Z. L. (2016). A spectral signature shape-based algorithm for landsat image classification. *ISPRS International Journal of Geo-Information*, 5(9), 154–154. https://doi.org/10.3390/ijgi5090154

Cheng, H., Hu, Y., & Reinhard, M. (2014). Environmental and Health Impacts of Artificial Turf: A Review. *Environmental Science & Technology*, *48*(4), 2114–2129. https://doi.org/10.1021/es4044193

Cities with low humidity in US - current results. (n.d.). https://www.currentresults.com/Weather-Extremes/US/low-humidity-cities.php

Crawford, C. J., Roy, D. P., Arab, S., Barnes, C., Vermote, E., Hulley, G., Gerace, A., Choate, M., Engebretson, C., Micijevic, E., Schmidt, G., Anderson, C., Anderson, M., Bouchard, M., Cook, B., Dittmeier, R., Howard, D., Jenkerson, C., Kim, M., … Zahn, S. (2023). The 50-year Landsat collection 2 archive. *Science of Remote Sensing*, *8*, 100103. https://doi.org/10.1016/j.srs.2023.100103

Denly, E., Rutkowski, K., & Vetrano, K. M., Ph. D. (2008). A Review of the Potential Health and Safety Risks from Synthetic Turf Fields Containing Crumb Rubber Infill. In New York City Department of Health and Mental Hygiene & TRC, *New York City Department of Health and Mental Hygiene*. https://www.nyc.gov/assets/doh/downloads/pdf/eode/turf_report_05-08.pdf

Devitt, D. A., Young, M. H., Baghzouz, M., Bird, B. M., & Devittl, B. D. A. (2007). Surface temperature, heat loading and spectral reflectance of artificial turfgrass. *J Turfgrass Sports Surf Sci*, *83*, 68-82.

Dickinson, R. E. (1983). Land Surface Processes and Climate—Surface Albedos and Energy Balance. In *Advances in Geophysics* (Vol. 25, pp. 305–353). Elsevier Science & Technology. https://doi.org/10.1016/S0065-2687(08)60176-4

Duble, R. L. (1993). Water management on turfgrasses. https://aggie-hort.tamu.edu/plantanswers/turf/publications/water.html#:~:text=Grasses%20with%20poor%20drought%20resistance,depth%20of%20rootzone%20and%20slope.

Dragoo, J. L., & Braun, H. J. (2010). The Effect of Playing Surface on Injury Rate: A Review of the Current Literature. *Sports Medicine (Auckland)*, *40*(11), 981–990. https://doi.org/10.2165/11535910-000000000-00000

Drakos, M. C., Taylor, S. A., Fabricant, P. D., & Haleem, A. M. (2013). Synthetic Playing Surfaces and Athlete Health. *Journal of the American Academy of Orthopaedic Surgeons*, *21*(5), 293–302. https://doi.org/10.5435/JAAOS-21-05-293

Drought and conservation measures. (2024). *Las Vegas Valley Water District*. https://www.lvvwd.com/conservation/measures/index.html

Elhinnawy, T. S. (2004). Tools To Investigate Building Envelope Thermal Behaviour For Urban Heat Island Mitigation (UHIM). Eng. Res. J.

European Space Agency. (2022, December 6). *Landsat-8*. Earth Online. https://earth.esa.int/eogateway/missions/landsat-8

Fleming, P. (2011). Maintenance best practice and recent research. *Proceedings of the Institution of Mechanical Engineers, Part P: Journal of Sports Engineering and Technology*, *225*(3), 159-170.

Galloway, S. D. R., & Maughan, R. J. (1997). Effects of ambient temperature on the capacity to perform prolonged cycle exercise in man. *Medicine and Science in Sports and Exercise*, *29*(9), 1240–1249. https://doi.org/10.1097/00005768-199709000-00018

Garai, A., & Kleissl, J. (2011). Air and Surface Temperature Coupling in the Convective Atmospheric Boundary Layer. *Journal of the Atmospheric Sciences*, *68*(12), 2945–2954. https://doi.org/10.1175/JAS-D-11-057.1

GeoWGS. (2024, January 19). What is the highest resolution satellite imagery available? *GeoWGS84*. https://www.geowgs84.com/post/what-is-the-highest-resolution-satellite-imagery available#:~:text=As%20of%20January%202024%2C%20commercial,imagery%20available%20to%20the%20public .

Google Earth Engine. (n.d.). https://www.google.com/earth/education/tools/google-earth-engine/#:~:text=Google%20Earth%20Engine%20is%20a,natural%20resource%20management%2C%20and%20more

Gorelick, N., Hancher, M., Dixon, M., Ilyushchenko, S., Thau, D., & Moore, R. (2017). Google Earth Engine: Planetary-scale geospatial analysis for everyone. *Remote Sensing of Environment, 202*, 18–27. https://doi.org/10.1016/j.rse.2017.06.031

Gould, H. P., Lostetter, S. J., Samuelson, E. R., & Guyton, G. P. (2022). Lower Extremity Injury Rates on Artificial Turf and Natural Grass Playing Surfaces: A Systematic Review. *Foot & Ankle Orthopaedics*, *7*(1), 2473011421S00217. https://doi.org/10.1177/2473011421S00217

Gupta, D. K., Prashar, S., Singh, S., Srivastava, P. K., & Prasad, R. (2022). Chapter 1 - Introduction to RADAR remote sensing. In *Radar Remote Sensing* (pp. 3–27). Elsevier Inc. https://doi.org/10.1016/B978-0-12-823457-0.00018-5

Gustin, M., P. R. Fleming, D. Allinson, & S. Watson. (2018). Modelling Surface Temperatures on 3G Artificial Turf. *Proceedings*, *2*(6), 279. https://doi.org/10.3390/proceedings2060279

Guyer, H., Georgescu, M., Hondula, D. M., Wardenaar, F., & Vanos, J. (2021). Identifying the need for locally-observed wet bulb globe temperature across outdoor athletic venues for current and future climates in a desert environment. *Environmental Research Letters, 16(12)*, 124042. https://doi.org/10.1088/1748-9326/ac32fb

Halle, L. L., Palmqvist, A., Kampmann, K., Jensen, A., Hansen, T., & Khan, F. R. (2021). Tire wear particle and leachate exposures from a pristine and road-worn tire to Hyalella azteca: Comparison of chemical content and biological effects. *Aquatic Toxicology*, *232,* 105769. https://doi.org/10.1016/j.aquatox.2021.105769

Hann, S., Sherrington, C., Jamieson, O., Hickman, M., Kershaw, P., Bapasola, A., & Cole, G. (2018). Investigating options for reducing releases in the aquatic environment of microplastics emitted by (but not intentionally added in) products. *Report for DG Environment of the European Commission*, *335*. https://bmbf-plastik.de/sites/default/files/2018-04/microplastics_final_report_v5_full.pdf

Hara, K., Liu, W., Yamazaki, F., Suzuki, K., & Maruyama, Y. (2013). Spectral Characteristics And Classification Of Urban Land-Cover Based On Airborne Hyperspectral Data. *Proceedings of ACRS* 2013http://ares.tu.chiba-u.jp/yamazaki/pdf/proceeding/2013ACRS_Hara.pdf

Henderson, J. J., Rogers III, J. N., & Crum, J. R. (2003). Athletic Field Systems Study 2000-2003. https://canr.msu.edu/uploads/236/68628/MSU_Athletic_Field_Systems_Performance_Study.pdf

Henryk Duda, Łukasz Rydzik, Andrzej Soroka, & Kamil Sokołowski. (2023). Rationalization of soccer training in terms of health effects of metropolitan smog and activity on the artificial turf. *Zeszyty Naukowe Wyższej Szkoły Finansów i Prawa w Bielsku-Białej*, *27*(4). https://doi.org/10.19192/wsfip.sj4.2023.10

Huang, B. (2008). Turfgrass water requirements and factors affecting water usage. *Water quality and quantity issues for turfgrass in urban landscapes. Council Agr. Sci. Technol. Spec. Publ*, *27*, 193-205. https://www.usga.org/content/dam/usga/pdf/Water%20Resource%20Center/turfgrass-water-requirements.pdf

Hydrochill | Shaw Sports Turf. (n.d.). https://www.shawsportsturf.com/hydrochill/

Idso, S. B., Pinter, P. J., Jackson, R. D., & Reginato, R. J. (1980). Estimation of grain yields by remote sensing of crop senescence rates. *Remote Sensing of Environment*, *9*(1), 87–91. https://doi.org/10.1016/0034-4257(80)90049-8

ISO 13732-3:2005(en), Ergonomics of the thermal environment — Methods for the assessment of human responses to contact with surfaces — Part 3: Cold surfaces. https://www.iso.org/obp/ui/#iso:std:iso:13732:-3:ed-1:v1:en (accessed 20 March 2024).

Khan, F. R., Halle, L. L., & Palmqvist, A. (2019). Acute and long-term toxicity of micronized car tire wear particles to Hyalella azteca. *Aquatic Toxicology*, *213*, 105216–105216. https://doi.org/10.1016/j.aquatox.2019.05.018

Jastifer, J. R., McNitt, A. S., Mack, C. D., Kent, R. W., McCullough, K. A., Coughlin, M. J., & Anderson, R. B. (2019). Synthetic Turf: History, Design, Maintenance, and Athlete Safety. *Sports Health*, *11*(1), 84–90. https://doi.org/10.1177/1941738118793378

Jensen, J. R. (2009). *Remote sensing of the environment: An earth resource perspective 2/e*. Pearson Education India.

Jim, C. Y. (2016). Solar–terrestrial radiant-energy regimes and temperature anomalies of natural and artificial turfs. *Applied Energy*, *173*, 520–534. https://doi.org/10.1016/j.apenergy.2016.04.072

Jim, C. Y. (2017). Intense summer heat fluxes in artificial turf harm people and the environment. *Landscape and Urban Planning*, *157*, 561–576. https://doi.org/10.1016/j.landurbplan.2016.09.012

Kachhwaha, T. (1983). Spectral signatures obtained from Landsat digital data for forest vegetation and land-use mapping in India. *Photogrammetric Engineering and Remote Sensing, 49(5)*, 685–689. https://www.asprs.org/wp-content/uploads/pers/1983journal/may/1983_may_685-689.pdf

Kanaan, A., Sevostianova, E., Leinauer, B., & Sevostianov, I. (2020). Water Requirements for Cooling Artificial Turf. *Journal of Irrigation and Drainage Engineering*, *146*(10). https://doi.org/10.1061/(ASCE)IR.1943-4774.0001506

Kandelin, W. W. (1976). Athletic field microclimates and heat stress. *Journal of Safety Research, 8(3)*, 106–111. https://www.researchgate.net/profile/Gary-Krahenbuhl/publication/303457417_Athletic_Fields_and_Heat_Stress/links/5be1cb2f299bf1124fbf1701/Athletic-Fields-and-Heat-Stress.pdf

Karaca, A. C., Erturk, A., Gullu, M. K., Elmas, M., & Erturk, S. (2013). Automatic waste sorting using shortwave infrared hyperspectral imaging system. *2013 5th Workshop on Hyperspectral Image and Signal Processing: Evolution in Remote Sensing (WHISPERS)*, 1–4. https://doi.org/10.1109/WHISPERS.2013.8080744

Kim, D. M., Zhang, H., Zhou, H., Du, T., Wu, Q., Mockler, T. C., & Berezin, M. Y. (2015). Highly sensitive image-derived indices of water-stressed plants using hyperspectral imaging in SWIR and histogram analysis. *Scientific Reports, 5(1)*, 15919–15919. https://doi.org/10.1038/srep15919

Kim, A. M., Kruse, F. A., & Olsen, R. C. (2016). Integrated analysis of light detection and ranging (LiDAR) and hyperspectral imagery (HSI) data. In *Laser Radar Technology and Applications XXI* (Vol. 9832, pp. 271-285). SPIE. https://www.spiedigitallibrary.org/conference-proceedings-of-spie/9832/98320W/Integrated-analysis-of-light-detection-and-ranging-LiDAR-and-hyperspectral/10.1117/12.2223041.short

Konopacki, S., & Akbari, H. (2001). Measured energy savings and demand reduction from a reflective roof membrane on a large retail store in Austin. *Lawrence Berkeley National Laboratory*. Retrieved from https://escholarship.org/uc/item/7gw9f9sc

Kriegler, F. J. (1969). Preprocessing transformations and their effects on multispectral recognition. *In Proceedings of the Sixth International Symposium on Remote Sensing of Environment* (pp. 97-131).

Kirkpatrick, M., Stewart, D., Bridges, C., Crear, C., Gibson, J., Jones, J., & Lee, J. (2019). Joint Water Conservation Plan. https://www.snwa.com/assets/pdf/reports-conservation-plan-2019.pdf

Kruse, F. A., Kim, A. M., Runyon, S. C., Carlisle, S. C., Clasen, C. C., Esterline, C. H., ... & Olsen, R. C. (2014). Multispectral, hyperspectral, and LiDAR remote sensing and geographic information fusion for improved earthquake response. In *Algorithms and Technologies for Multispectral, Hyperspectral, and Ultraspectral Imagery XX* (Vol. 9088, pp. 132-145). SPIE.

https://www.spiedigitallibrary.org/conference-proceedings-of-spie/9088/90880K/Multispectral-hyperspectral-and-LiDAR-remote-sensing-and-geographic-information-fusion/10.1117/12.2049725.short#_=_

Kwan, C., Gribben, D., Ayhan, B., Li, J., Bernabe, S., & Plaza, A. (2020). An Accurate Vegetation and Non-Vegetation Differentiation Approach Based on Land Cover Classification. Remote Sensing (Basel, Switzerland), *Remote Sens. 2020, 12(23), 3880;* https://doi.org/10.3390/rs12233880

Lanphear, B. P., Hornung, R., Khoury, J., Yolton, K., Baghurst, P., Bellinger, D. C., Canfield, R. L., Dietrich, K. N., Bornschein, R., Greene, T., Rothenberg, S. J., Needleman, H. L., Schnaas, L., Wasserman, G., Graziano, J., & Roberts, R. (2005). Low-Level Environmental Lead Exposure and Children's Intellectual Function: An International Pooled Analysis. *Environmental Health Perspectives*, *113*(7), 894–899. https://doi.org/10.1289/ehp.7688

Larsans. (2020). An Evaluation Of The Possible Health Risks Of Recycled Rubber Granules Used As Infill In Synthetic Turf Sports Fields – *all sports recycled*. https://www.allsportsrecycled.com/an-evaluation-of-the-possible-health-risks-of-recycled-rubber-granules-used-as-infill-in-synthetic-turf-sports-fields/

Lavorgna, J., Song, J., Beattie, W., Riley, M., Beil, C., Levchenko, K., & Shofar, S. (2011). A Review of Benefits and Issues Associated with Natural Grass and Artificial Turf Rectangular Stadium Fields Final Report. *Montgomery County Council: Rockville, MD*.

Lee, S., Moon, H., Choi, Y., & Yoon, D. K. (2018). Analyzing thermal characteristics of urban streets using a thermal imaging camera: A case study on commercial streets in Seoul, Korea. *Sustainability (Basel, Switzerland), 10(2)*, 519. https://doi.org/10.3390/su10020519

Li, D. (2008). Managing field surface temperature. In *Field Science* [Journal-article]. https://sturf.lib.msu.edu/article/2008apr14.pdf

Liu, Z., & Jim, C. Y. (2021). Playing on natural or artificial turf sports field? Assessing heat stress of children, young athletes, and adults in Hong Kong. *Sustainable Cities and Society*, *75*, 103271. https://doi.org/10.1016/j.scs.2021.103271

Liss, B., Howland, M. D., & Levy, T. E. (2017). Testing Google Earth Engine for the automatic identification and vectorization of archaeological features: A case study from Faynan, Jordan. *Journal of Archaeological Science*: Reports, 15, 299-304.

Lopez-Cabeza, V. P., Alzate-Gaviria, S., Diz-Mellado, E., Rivera-Gomez, C., & Galan-Marin, C. (2022). Albedo influences the microclimate and thermal comfort of courtyards under Mediterranean hot summer climate conditions. *Sustainable Cities and Society*, *81*, 103872. https://doi.org/10.1016/j.scs.2022.103872

Loveday, J., Loveday, G., Byrne, J. J., Boon-lay Ong, & Morrison, G. M. (2019). Seasonal and diurnal surface temperatures of urban landscape elements. *Sustainability*, *11*(19), 5280. doi:https://doi.org/10.3390/su11195280

Masoumi, H., Safavi, S. M., & Khani, Z. (2012). Identification and classification of plastic resins using near infrared reflectance. *Int. J. Mech. Ind. Eng*, *6*, 213-220. https://www.researchgate.net/profile/Hamed-Masoumi/publication/285330830_Identification_and_classification_of_plastic_resins_using_near_infrared_reflectance_spectroscopy/links/572af79808aef7c7e2c5026d/Identification-and-classification-of-plastic-resins-using-near-infrared-reflectance-spectroscopy.pdf

Mehmood, T., & Peng, L. (2022). Polyethylene scaffold net and synthetic grass fragmentation: a source of microplastics in the atmosphere? *Journal of Hazardous Materials*, *429*, 128391–128391. https://doi.org/10.1016/j.jhazmat.2022.128391

Mei, A., Bassani, C., Fontinovo, G., Salvatori, R., & Allegrini, A. (2016). The use of suitable pseudo-invariant targets for MIVIS data calibration by the empirical line method. *ISPRS Journal of Photogrammetry and Remote Sensing*, *114*, 102–114. https://doi.org/10.1016/j.isprsjprs.2016.01.016

Mediterranean hot summer climate conditions. *Sustainable Cities and Society*, *81*, 103872. https://doi.org/10.1016/j.scs.2022.103872

McNitt, A., Petrunak, D., & Serensits, T. (2008). Temperature Amelioration Of Synthetic Turf Surfaces Through Irrigation. *Acta Horticulturae*, *783(Jun)*, 573–582. https://doi.org/10.17660/ActaHortic.2008.783.59

Morris, R. L., Devitt, D. A., Crites, A. M., Borden, G., & Allen, L. N. (1997). Urbanization and Water Conservation in Las Vegas Valley, Nevada. *Journal of Water Resources Planning and Management*, *123*(3), 189–195. https://doi.org/10.1061/(ASCE)0733-9496(1997)123:3(189)

Moshtaghi, M., Knaeps, E., Sterckx, S., Garaba, S., & Meire, D. (2021). Spectral reflectance of marine macroplastics in the VNIR and SWIR measured in a controlled environment. *Scientific Reports*, *11(1)*, 5436–5436. https://doi.org/10.1038/s41598-021-84867-6

Murphy, M., & Warner, G. R. (2022). Health impacts of artificial turf: Toxicity studies, challenges, and future directions. *Environmental Pollution (1987)*, *310*, 119841–119841. https://doi.org/10.1016/j.envpol.2022.119841

Mutanga, O., & Kumar, L. (2019). Google Earth Engine Applications. *Remote Sensing (Basel, Switzerland)*, *11*(5), 591. https://doi.org/10.3390/rs11050591

Myers, V. I., & Allen, W. A. (1968). Electro Optical remote sensing methods as nondestructive testing and measuring techniques in agriculture. *Applied Optics (2004)*, *7*(9), 1819–1838. https://doi.org/10.1364/AO.7.001819

Naif, S., Mahmood, D. & Al-Jiboori, M. (2020). Seasonal normalized difference vegetation index responses to air temperature and precipitation in Baghdad. *Open Agriculture, 5*(1), 631-637. https://doi.org/10.1515/opag-2020-0065

NDVI, The Foundation for Remote Sensing Phenology | *U.S. Geological Survey*. (2018, November 29). https://www.usgs.gov/special-topics/remote-sensing-phenology/science/ndvi-foundation-remote-sensing-phenology#overview

Nilsson, N. H., Malmgren-Hansen, B., Thomsen, U. S., & Teknologisk Institut. (2008). Mapping, emissions and environmental and health assessment of chemical substances in artificial turf. Copenhagen, *Denmark: Danish Environmental Protection Agency.* https://www.researchgate.net/profile/Nils-Nilsson-3/publication/242241995_Mapping_emissions_and_environmental_and_health_assessment_of_chemical_substances_in_artificial_turf/links/54114c5f0cf2df04e75d763e/Mapping-emissions-and-environmental-and-health-assessment-of-chemical-substances-in-artificial-turf.pdf

NOAA's National Weather Service. (n.d.). *Climate*. https://www.weather.gov/wrh/climate?wfo=vef

NORTH LAS VEGAS, NV Weather History | *Weather Underground. (n.d.).* https://www.wunderground.com/history/monthly/us/nv/north-las-vegas/KVGT/date/2018-4

Nybo, L. (2008). Hyperthermia and fatigue. *Journal of Applied Physiology (1985), 104*(3), 871–878. https://doi.org/10.1152/japplphysiol.00910.2007

Olshammar, M., Graae, L., Robijn, A., & Nilsson, F. (2021). Microplastic fromcast rubber granulate and granulate-free artificial grass surfaces. *Swedish Environmental Protection Agency* https://www.diva-portal.org/smash/record.jsf?pid=diva2%3A1663995&dswid=-8119

Perkins, A. N., Inayat-Hussain, S. H., Deziel, N. C., Johnson, C. H., Ferguson, S. S., Garcia-Milian, R., Thompson, D. C., & Vasiliou, V. (2019). Evaluation of potential carcinogenicity of organic chemicals in synthetic turf crumb rubber. *Environmental Research, 169*, 163–172. https://doi.org/10.1016/j.envres.2018.10.018

Petrass, L. A., Twomey, D. M., & Harvey, J. T. (2014). Understanding how the Components of a Synthetic Turf System Contribute to Increased Surface Temperature. *Procedia Engineering, 72*, 943–948. https://doi.org/10.1016/j.proeng.2014.06.159

Petrass, L. A., Twomey, D. M., Harvey, J. T., Otago, L., & LeRossignol, P. (2015). Comparison of surface temperatures of different synthetic turf systems and natural grass: Have advances in synthetic turf technology made a difference. *Proceedings of the Institution of Mechanical Engineers, Part P: Journal of Sports Engineering and Technology, 229*(1), 10-16. https://doi.org/10.1177/1754337114553692

Ponce, V. M., Lohani, A. K., & Huston, P. T. (1997). Surface Albedo and Water Resources: Hydroclimatological Impact of Human Activities. *Journal of Hydrologic Engineering*, *2*(4), 197–203. https://doi.org/10.1061/(ASCE)1084-0699(1997)2:4(197)

Pochron, S. T., Fiorenza, A., Sperl, C., Ledda, B., Lawrence Patterson, C., Tucker, C. C., Tucker, W., Ho, Y. L., & Panico, N. (2017). The response of earthworms (Eisenia fetida) and soil microbes to the crumb rubber material used in artificial turf fields. *Chemosphere (Oxford)*, *173*, 557–562. https://doi.org/10.1016/j.chemosphere.2017.01.091

Priem, F., & Canters, F. (2016). Synergistic use of LiDAR and APEX hyperspectral data for high-resolution urban land cover mapping. *Remote Sensing (Basel, Switzerland)*, *8(10)*, 787–787. https://doi.org/10.3390/rs8100787

Safe Drinking Water & Toxic Enforcement Act of 1986 (Proposition 65), California Environmental Protection Agency, Office of Environmental Health Hazard Assessment, San Francisco, CA. (1999). *Journal of Toxicology. Cutaneous and Ocular Toxicology*, *18*(2), 149–150. https://doi.org/10.3109/15569529909037565

Salvador, P., Sanz, J., Rodriguez, J., Molina, V., & JL, C. A. (2014). Hand Goniometer For Ads Spectroradiometer: Application To Brdf Sentinel 2 Bands Over Urban Surfaces. *International Journal of Geosciences and Geomatics, Vol. 2, Issue 2,* 2014,ISSN:2052-5591 https://arsgiso-org.mapping-solutions.co.uk/publications/2014_2_2_SalvadorCasanov_A%20Han.pdf

Schilirò, T., Traversi, D., Degan, R., Pignata, C., Alessandria, L., Scozia, D., Bono, R., & Gilli, G. (2013). Artificial Turf Football Fields: Environmental and Mutagenicity Assessment. *Archives of Environmental Contamination and Toxicology*, *64*(1), 1–11. https://doi.org/10.1007/s00244-012-9792-1

Schneider, D., Hypes, J. A., & Hypes, M. G. (2014). Synthetic Turf vs. Natural Grass. *Journal of Facility Planning, Design, and Management*, *2*(2), np–np.

Seeman, M. (2020, July 16). *Artificial turf to replace grass fields at 29 Southern Nevada schools*. KSNV. https://news3lv.com/news/local/artificial-turf-to-replace-grass-fields-at-29-southern-nevada-schools

Shi, Y., & Jim, C. Y. (2022). Developing a thermal suitability index to assess artificial turf applications for various site-weather and user-activity scenarios. *Landscape and Urban Planning*, *217*, 104276. https://doi.org/10.1016/j.landurbplan.2021.104276

Simpson, T. J., & Francis, R. A. (2021). Artificial lawns exhibit increased runoff and decreased water retention compared to living lawns following controlled rainfall experiments. *Urban Forestry & Urban Greening*, *63*, 127232. https://doi.org/10.1016/j.ufug.2021.127232

Southern Nevada Water Authority. (n.d.). https://www.snwa.com/water-resources/conservation-initiatives/index.html

Spadoni, G. L., Cavalli, A., Congedo, L., & Munafò, M. (2020). Analysis of Normalized Difference Vegetation Index (NDVI) multi-temporal series for the production of forest cartography. Remote Sensing Applications, 20, 100419. https://doi.org/10.1016/j.rsase.2020.100419

Spectral reflectance. (n.d.). https://gsp.humboldt.edu/olm/Courses/GSP_216/lessons/reflectance.html#:~:text=Chlorophyll%20strongly%20absorbs%20light%20at,between%200.7%20and%201.3%20%C2%B5m

Ramboll (2020). Comparative Analysis of Major Companies within Artificial Turf Recycling and Treatment. *Report for Nordic Alpha Partners*. https://bekogr.se/wp-content/uploads/2020/09/NAP_comparative-analysis-ATR_30-4-2020-1.pdf

Ramsey, J. D. (1982). Environmental Heat from Synthetic and Natural Turf. *Research Quarterly for Exercise and Sport, 53(1),* 82–85. https://doi.org/10.1080/02701367.1982.10605230

Ruffino, B., Fiore, S., & Zanetti, M. C. (2013). Environmental–sanitary risk analysis procedure applied to artificial turf sports fields. *Environmental Science and Pollution Research International*, *20*(7), 4980–4992. https://doi.org/10.1007/s11356-012-1390-2

Russo, C., Cappelletti, G. M., & Nicoletti, G. M. (2022). The product environmental footprint approach to compare the environmental performances of artificial and natural turf. *Environmental Impact Assessment Review*, *95*, 106800. https://doi.org/10.1016/j.eiar.2022.106800

Tamiminia, H., Salehi, B., Mahdianpari, M., Quackenbush, L., Adeli, S., & Brisco, B. (2020). Google Earth Engine for geo-big data applications: A meta-analysis and systematic review. *ISPRS Journal of Photogrammetry and Remote Sensing*, *164*, 152–170. https://doi.org/10.1016/j.isprsjprs.2020.04.001

Thenkabail, P. S., Smith, R. B., & De Pauw, E. (2000). Hyperspectral Vegetation Indices and Their Relationships with Agricultural Crop Characteristics. *Remote Sensing of Environment*, *71*(2), 158–182. https://doi.org/10.1016/S0034-4257(99)00067-X

Thomas, K., E. Irvin-Barnwell, A. Guiseppi-Elie, A. Ragin-Wilson, AND J. Zambrana. Synthetic Turf Field Recycled Tire Crumb Rubber Research Under the Federal Research Action Plan: Final Report Part 1 - Tire Crumb Rubber Characterization Appendices Volume 2. *U.S. Environmental Protection Agency, Washington, DC, EPA/600/R-19/051.2*, 2019. https://cfpub.epa.gov/si/si_public_record_report.cfm?Lab=NERL&dirEntryId=346618

Tian, L., Zhang, Y., & Zhu, J. (2014). Decreased surface albedo driven by denser vegetation on the Tibetan Plateau. *Environmental Research Letters*, *9*(10), 104001. https://doi.org/10.1088/1748-9326/9/10/104001

Twomey, D., Petrass, L., Harvey, J., Otago, L., & LeRossignol, P. (2014). Heat experienced on synthetic turf surfaces: An inevitable or preventable risk? *Journal of Science and Medicine in Sport, Suppl.Supplement 1, 18*, e119-e120. doi: https://doi.org/10.1016/j.jsams.2014.11.086

Twomey, D. M., Petrass, L. A., Harvey, J. T., Otago, L., & Le Rossignol, P. (2016). Selection and Management of Sports Grounds: Does Surface Heat Matter? *Journal of Facility Planning, Design, and Management*, *4*(1). https://doi.org/10.18666/JFPDM-2016-V4-I1-6507

Understand laws & ordinances. (n.d.). https://www.snwa.com/conservation/understand-laws-ordinances/index.html#:~:text=Grass%20restrictions&text=A%20law%20enacted%20by%20the,nonfunctional%20grass%2C%20beginning%20in%202027

USGS Landsat 8 Level 2, Collection 2, Tier 1. (n.d.). Google for Developers. https://developers.google.com/earth-engine/datasets/catalog/LANDSAT_LC08_C02_T1_L2#:~:text=These%20images%20contain%205%20visible,processed%20to%20orthorectified%20surface%20temperature

Van Ulirsch, G., Gleason, K., Gerstenberger, S., Moffett, D. B., Pulliam, G., Ahmed, T., & Fagliano, J. (2010). Evaluating and Regulating Lead in Synthetic Turf. *Environmental Health Perspectives*, *118*(10), 1345–1349. https://doi.org/10.1289/ehp.1002239

Villacañas, V., Sánchez-Sánchez, J., García-Unanue, J., López, J., & Gallardo, L. (2017). The influence of various types of artificial turfs on football fields and their effects on the thermal profile of surfaces. *Proceedings of the Institution of Mechanical Engineers, Part P: Journal of Sports Engineering and Technology*, *231*(1), 21-32.

Waleed, M., & Sajjad, M. (2022). Leveraging cloud-based computing and spatial modeling approaches for land surface temperature disparities in response to land cover change: Evidence from Pakistan. *Remote Sensing Applications*, *25*, 100665. https://doi.org/10.1016/j.rsase.2021.100665

Water Smart Landscapes Rebate. (n.d.-b). https://www.snwa.com/rebates/wsl/index.html#process

Water Smart Landscapes Rebate Program https://www.usbr.gov/watersmart/weeg/docs/2022/Southern_Nevada_Water_Authority_FGII_FY22WEEG_508.pdf

Way, D. A., Stinziano, J. R., Berghoff, H., & Oren, R. (2017). How well do growing season dynamics of photosynthetic capacity correlate with leaf biochemistry and climate fluctuations? *Tree Physiology*, 37(7), 879–888. https://doi.org/10.1093/treephys/tpx086

Weather averages Las Vegas, Nevada. (n.d.). US Climate Data. https://www.usclimatedata.com/climate/las-vegas/nevada/united-states/usnv0049

Wetherley, E. B., Roberts, D. A., & McFadden, J. P. (2017). Mapping spectrally similar urban materials at sub-pixel scales. *Remote Sensing of Environment, 195*, 170–183. https://doi.org/10.1016/j.rse.2017.04.013

What We're Doing to Conserve. (2024). *Southern Nevada Water Authority*. https://www.snwa.com/water-resources/conservation-initiatives/index.html#:~:text=The%20Southern%20Nevada%20Water%20Authority%20offers%20a%20variety%20of%20programs,technologies%3B%20and%20the%20Water%20Upon

Wickham, J., Nash, M. S., & Barnes, C. A. (2016). Effect of land cover change on snow free surface albedo across the continental United States. *Global and Planetary Change, 146, 1–9.* https://doi.org/10.1016/j.gloplacha.2016.09.005

Williams, C. F., & Pulley, G. E. (2002). Synthetic surface heat studies. Brigham Young University.

Wynne, T., & Devitt, D. (2020). Evapotranspiration of Urban Landscape Trees and Turfgrass in an Arid Environment: Potential Trade-offs in the Landscape. *HortScience, 55*(10), 1558–1566. https://doi.org/10.21273/HORTSCI15027-20

Xian, G. and Crane, M. (2006). An analysis of urban thermal characteristics and associated land cover in Tampa Bay and Las Vegas using Landsat satellite data. *Remote Sensing of Environment*, 104(2), 147–156. https://doi.org/10.1016/j.rse.2005.09.023

Xiao, Y. Q., & Cao, Y. X. (2013). Study on thermal environment of sports field in different materials. *Applied Mechanics and Materials, 361-363*, 538. doi: https://doi.org/10.4028/www.scientific.net/AMM.361-363.538

Yaghoobian, N., Kleissl, J., & Krayenhoff, E. S. (2010). Modeling the Thermal Effects of Artificial Turf on the Urban Environment. *Journal of Applied Meteorology and Climatology*, *49*(3), 332–345. https://doi.org/10.1175/2009JAMC2198.1

Yu, Y., Liu, Y., Yu, P., Liu, Y., & Yu, P. (2018). 5.12 - Land Surface Temperature Product Development for JPSS and GOES-R Missions. In *Comprehensive Remote Sensing* (pp. 284–303). Elsevier Inc. https://doi.org/10.1016/B978-0-12-409548-9.10522-6

CURRICULUM VITAE

Tarannum Kalam Khandoker

University of Nevada, Las Vegas

Department of Civil and Environmental Engineering and Construction

Email address: tarannumkalam26@gmail.com

EDUCATION

Bachelor of Science, Civil Engineering, Ahsanullah University of Science and Technology, Dhaka, Bangladesh

RESEARCH EXPERIENCE

Master's Research Work

University of Nevada Las Vegas (UNLV)
Thesis Title: "Analyses of Thermal and Spectral Characteristics of Artificial Turf and Natural Grass in Las Vegas Valley"
Research supervisors: Dr. Sajjad Ahmad and Dr. Haroon Sahotra

Undergraduate Research Work

Ahsanullah University of Science and Technology
Thesis Title: "Assessment of spatio-temporal pattern of land use and land cover changes of Savar Upazilla using remote sensing technologies"
Research supervisor: Dr. Afzal Ahmed

PUBLICATIONS

Khandoker, T., Yusufzai, A., Ahmad, S., Stephen, H., 2023. Artificial Turf on Urban Landscapes: An Overview. In: Henderson, Nevada, World Environmental and Water Resources Congress 2023: Adaptive Planning and Design in an Age of Risk and Uncertainty (pp. 740–754). DOI:10.1061/9780784484852. American Society of Civil Engineers.

POSTER PRESENTATION

Khandoker, T., Ahmad, S., Stephen, H., 2023. Temperature Difference in 20 years: A Comparison of Artificial Turf and Natural Grass Surfaces. Poster presented at: Graduate Symposium Poster Event; 2023 March 28; UNLV, Las Vegas, Nevada.

Khandoker, T., Yusufzai, A., Ahmad, S., Stephen, H., 2023. Artificial Turf on Urban Landscapes: An Overview. Poster presented at: World Environmental and Water Resources Congress 2023; 22nd to 25th May 2023; Henderson, Nevada.

Khandoker, T., Ahmad, S., Stephen, H., 2024. Artificial Turf And Urban Thermal Environment: Analyses of the Changes In Land Surface Temperature And Surface Albedo In Las Vegas Valley. Poster presented at: Graduate Symposium Poster Event; 2024 March 26; UNLV, Las Vegas, Nevada.

Khandoker, T., Ahmad, S., Stephen, H., 2023. Detection and Analysis of the Spectral Signatures and NDVI of Artificial Turf And Natural Grass In Las Vegas Valley. Poster presented at: 26th Annual Graduate & Professional Student Research Forum; 2024 April 06; UNLV, Las Vegas, Nevada.